Rockefeller University
Digital Commons @ RU

Student Theses and Dissertations

2015

A Reductionist Approach to Modeling Human Corticogenesis

Mohammad Zeeshan Ozair

Follow this and additional works at: https://digitalcommons.rockefeller.edu/student_theses_and_dissertations

 Part of the Life Sciences Commons

Recommended Citation
Ozair, Mohammad Zeeshan, "A Reductionist Approach to Modeling Human Corticogenesis" (2015). *Student Theses and Dissertations*. 493.
https://digitalcommons.rockefeller.edu/student_theses_and_dissertations/493

This Thesis is brought to you for free and open access by Digital Commons @ RU. It has been accepted for inclusion in Student Theses and Dissertations by an authorized administrator of Digital Commons @ RU. For more information, please contact nilovao@rockefeller.edu.

A REDUCTIONIST APPROACH TO MODELING HUMAN CORTICOGENESIS

A Thesis Presented to the Faculty of

The Rockefeller University

in Partial Fulfillment of the Requirements for

the degree of Doctor of Philosophy

by

Mohammad Zeeshan Ozair

June 2015

© Copyright by Mohammad Zeeshan Ozair 2015

A REDUCTIONIST APPROACH TO MODELING HUMAN CORTICOGENESIS

Mohammad Zeeshan Ozair, PhD, MD

The Rockefeller University 2015

The formation of the mammalian cerebral cortex is a complex multi-tiered process that involves three major milestones: 1) neural induction and folding of the neuroepithelium, 2) areal patterning and generation of various progenitor types, and 3) corticogenesis. Our current understanding of the molecular and cellular basis of cortical development comes largely from mouse studies due to the genetic tractability of this model system. However, as primate studies have shown, the primate brain is unique in terms of its progenitor and neuronal composition, cortical areas, scale, and gene expression. Limitations in the availability of non-human primate and human fetal material, the longer timescale of developmental processes, as well as the ethical considerations involved preclude direct experimental observations in both these organisms. However, human pluripotent stem cells (hPSCs) allow a window into early human fetal development and permit experimental manipulation of developmental events, thereby enabling molecular and cellular dissection of corticogenesis.

The default model of neural induction, described originally in amphibians, posits that induction of telencephalic (forebrain) fate in an embryo requires elimination of TGFβ signaling. Using transgenic hPSCs, we show that inducible expression of a cell-intrinsic inhibitor of canonical TGFβ signaling – SMAD7 – is sufficient to directly convert hPSCs to forebrain fate as seen by gene expression and immunocytochemical analysis of several

transcription factors. Moreover, this conversion is direct and does not involve induction of non-neural fates. Our findings suggest a conservation of the default model in humans. Additionally, we also show that FGF-MEK signaling has no direct role in hPSC neural induction, thereby resolving an existing debate in the field.

We were able to derive neuroepithelium from PSCs of multiple species (mouse, primates, and human) with small molecule inhibitors of TGFβ signaling. In order to demonstrate that *in vitro* generated neuroepithelium is comparable to the *in vivo* germinal zone of an embryo, we utilized transgenic lines expressing FUCCI (fluorescently ubiquitination cell cycle indicators). Together with single-cell analysis, we were able to demonstrate self-organization in radial progenitors, interkinetic nuclear migration, as well as requirement for Notch signaling for progenitor maintenance, all of which are hallmarks of human neural progenitors *in vivo*. Region-specific marker analysis, we conclude that *in vitro* hPSC-derived neural progenitors are similar to their *in vivo* counterparts based on several measurements.

Within telencephalic territory generated by TGFβ inhibition, we demonstrate that the *in vitro* derived neuroepithelium can be patterned on the rostrocaudal axis by manipulating WNT signaling. Small molecule inhibitors of WNT signaling promoted expression of frontal markers; conversely, small molecule activators of WNT promoted expression of occipitotemporal markers. Importantly, WNT activation had to be moderate; higher levels of WNT activation resulted in switch of neuroepithelial identity from forebrain to midbrain. This finding provides insights into arealization in the mammalian cortex and

suggests that exposure to different levels of WNT signaling early on may act as a selector between generation of a six-layered neocortex or a three-layered archicortex.

Lastly, we utilize our reductionist *in vitro* corticogenesis model to establish that neural progenitors can be differentiated into various classes of projection neurons. By utilizing genome modification strategies in hPSCs, we observe that single neural progenitors possess the capacity to give rise to callosal projection neurons (CPNs) and subcortical projection neurons (SCPNs), thereby lending support to the "Progressive Restriction" model of corticogenesis. Additionally, based on analysis of human fetal tissue at various stages, and further confirmation with BrdU labeling studies during *in vitro* differentiation, we propose that progressive progenitor restriction manifests during corticogenesis as a progressive limitation in the ability of their daughter neurons to express various projection neuron class-determinants over time. Co-expression of CPN and SCPN fate determinants is rarely observed during mouse development, even though recent mouse studies clearly show the requirement of CPN genes in SCPN formation. This suggests that neuronal restriction may be evolutionary conserved and this may have implications for diseases such as autism where laminar differentiation is affected. Neuronal restriction provides a conceptual link between how defects in progenitors could affect laminar development and neuronal hodology, which in turn underlies neuronal circuit formation. Finally, by lineage-tracing CUX2 positive progenitors in transgenic hPSC-derived neuroepithelium, we show that a small fraction of CPNs in our *in vitro* corticogenesis paradigm may be derived from lineage-restricted progenitors. Given the large numbers of progenitors that display multi-laminar differentiation ability, we conclude that lineage-

restricted progenitors are not a major source of CPNs in our system, but may represent a transient population derived from multipotential progenitors.

Thus, by combining human genome modification technologies with the default model of neural induction, we are now able to probe fundamental questions of human corticogenesis. Using genetic tools, we have established that hPSC-derived neural progenitors retain most characteristics of their *in vivo* mammalian counterparts and have begun to uncover mechanistic principles for generation of the cortical projection neuron classes. Together, our findings open new avenues for study of human brain development, disease modelling, and drug screening using hPSCs. Moreover, the genetic and analytical tools we describe here can be used for *in vitro* studies of cell cycle dynamics, self-organization, lineage tracing, and live imaging of multiple PSC-derived tissue types.

This thesis is dedicated to my late mother, Meraj un-Nisa Ozair, for giving me the courage to swim against the tide and pursue my scientific ambitions; for willing to support and believe in me unreservedly; and for teaching me about strength in all its manifestations, right until the end of her illness. Completion of this thesis was our shared dream, one that encapsulated the two things closest to her: knowledge and hard work. *Ammi's* singular love made me a better person, and her resolute nurture made me a better intellect.

ACKNOWLEDGEMENTS

I would like to extend my foremost gratitude to my mentor and thesis advisor, Ali Brivanlou. It has been an honor for me to carry the flame that he lit with his seminal discoveries on brain development, which laid the foundations for my thesis. As a mentor, Ali always found a way to push my scientific and aesthetic abilities through a balance of tough love, provision of resources, and generous appreciation. His inclination to ask the big questions and staying away from uninspired ones is an enduring lesson that I learnt during my time in the lab. I greatly admire his leadership skills and his ability to create a primed environment for quality science by bringing together people from varied scientific backgrounds. Another of Ali's many talents is hiring fantastic, diverse, and perennially helpful people in the lab, whom I relied on for advice, training, and critic over the years. These include past members (Alessandro Rosa, Brigitte Arduini, Joanna Krzyspiak, Aryeh Warmflash, Alin Vonica, Benoit Paire, Ismail Ismailoglu, Sacha Hacker, Saad Chiguer, and Frada Berentshyn), as well as current ones (Albert Ruzo, Christoph Kirst, Fred Etoc, Gist Croft, Michael Heke, Alessia D'eglincerti, Melissa Popowski, Qixiang Zhang, Shu Li, Lauren Pietila, Lauren Gerber, Corbyn Nchako, and Danielle Little). I count many of them as close friends and they are a big part of the memories I will cherish during my time in the Brivanlou lab.

I was privileged to have three very illustrious neuroscientists and phenomenal people on my committee: Professors Jim Hudspeth (chair), Cori Bargmann, and Nat Heintz. Their curiosity, ingenuity, and landmark discoveries have shaped modern neuroscience, and my

meetings with them were a regular source of inspiration for me. They motivated me to stay focused and do better. Growing up where science was not a career option, it was but a distant dream to be in the same room with these intellects, let alone discuss my work with them; I consider that to be fulfilled. I hope that towards the end of my career, I will possess a fraction of Jim's eloquence and the meticulousness that permeates all aspects of his work; of Cori's poise and her limitless pool of knowledge and intellect; and of Nat's grand vision and incisive mind.

My deep appreciation and acknowledgment for the contributions of Christoph Kirst, an independent fellow at the Center for Studies in Physics and Biology. Christoph's prodigious computational skills and enthusiasm were invaluable for data analysis in parts of this thesis. I consider myself fortunate to have access to his abilities, and even more so to count him as one of my close friends. I am also indebted to several Rockefeller faculty members who shared their insights with me from time to time: Mary Hynes and Mary Beth Hatten – whom our lab shares a floor with, as well as Eric Siggia, whom our lab collaborates with very closely.

That I was able to work with so many extraordinary people is a testament to how special a place The Rockefeller University is. As a student, not only did it give me the platform and the freedom to pursue novel ideas, but also provided the ecosystem and the mentality to do impactful science. I would like to acknowledge the people at the helm of the graduate program who have fostered this environment for the students: Dean Sid Strickland and Associate Dean Emily Harms. I would also like to extend my gratitude to

other members of the Dean's Office: Kristen Cullen, Marta Delgado, and Cris Rosario. Together, their genuine willingness to help out with day-to-day problems as well as during personal issues was without equal; I am greatly touched by their gesture. I would also like to thank Professor Jean Hébert from the Albert Einstein College of Medicine for kindly accepting to be my external examiner.

Before graduate school, I had the serendipity of being exposed to exemplary mentors who stoked the flames of curiosity in my mind. I am grateful to them for sharing their wisdom with me and contributing to my evolution as a scientist. Dr. HR Ahmad (Professor of Physiology at The Aga Khan University) introduced to me the intricate beauty of neuroscience and got me started on my scientific journey. Prof. Richard Sidman (Emeritus Professor at Harvard Medical School) gave me a one-of-a-kind opportunity to work with him and introduced me to fundamental principles of brain development. My thesis work was inspired by his original observations on cortical lamination, made over 50 years ago. Evan Snyder (Associate Professor at Harvard Medical School) was my co-mentor with Professor Sidman; he introduced me to stem cell biology and gave me an appreciation for understanding developmental processes before their clinical applications. Both Evan and Dr. Sidman went out of their way to nurture my interest in developmental neurobiology and were key figures in my decision to apply to graduate school. Dr. Philippe Frossard (Professor and head of the department of Biological and Biomedical Sciences at AKU) provided me with immense support, first as a medical student, and subsequently as a teaching assistant. His enthusiasm and encouragement buoyed me through many a setback.

Having remarkably compassionate and supportive human beings for a family contributed tremendously to my graduate life. They were my emotional bedrocks, especially through personal lows. I cannot thank my sister Nausheen, Nani, Razia aunty, and Mamma enough for being there for me and enriching my upbringing. Together, they taught me about kindness and unconditional love. And to my father, Ozair ul-Haque, for indulging my curiosity and showing me how to take apart things and put them back together. Even though he passed away when I was 9, it was him who introduced to me to the possibility of a career in science; in many ways this thesis is a materialization of the idea that he seeded in my head all those years ago.

Finally, I would like to acknowledge the gracious generosity, patience, and friendship of the people who have been closest to me over the past several years: Joanna Krzyspiak, Siddarth Venkatesh, Kiri Mackersey, Danish Saleheen, Ali Kazmi, Enam ur-Rehman, Yoav Litvin, Albert Ruzo, Christoph Kirst, Fred Etoc, Thomas Hsiao, and Harvir Singh. They were my intellectual bedrocks, discussion partners, confidantes, and anything I needed them to be through the vicissitudes of graduate life. Their willingness to lend an ear, a shoulder, a hug, their brains, and sometimes a boot in the back was always appreciated and will be remembered. Each of them taught me something new about science, humanities, or being a better version of myself; and for this I remain in their debt.

STATEMENT OF CONTRIBUTIONS

Parts of Chapter 1 are adapted and modified from a published manuscript that was co-written with Ali Brivanlou and Chris Kintner. Analysis of images in Chapters 3 and 4 was carried out in collaboration with Christoph Kirst and Aryeh Warmflash. The SMAD7-EGFP lines described in Chapters 2 and 3 were made by Scott Noggle, while the TALENs used to engineer the CUX2-CreER^{T2} lines in Chapters 2 and 4 were made by Albert Ruzo. Joanna Krzyspiak provided technical support for several experiments in Chapters 2-4.

TABLE OF CONTENTS

LIST OF FIGURES

LIST OF TABLES

LIST OF ABBREVIATIONS

AAVS1	Adeno-Associated Virus Integration Site
ALK4	Activin receptor type-1B
A-P	Antero-posterior
aPKC	Atypical protein kinase C
ApoER2	Apolipoprotein E receptor
ARHGAP11B	Rho GTPase activating protein 11B
ASCL1	Achaete-scute homolog
ASPM	Abnormal spindle protein homolog
AVE	Anterior visceral endoderm
BAMBI	BMP and activin membrane-bound inhibitor
bFGF	Basic fibroblast growth factor
BG	Basal ganglia
β-gal	beta-galactosidase
bHLH	Basic helix loop helix
BLBP	Brain lipid-binding protein
BMP	Bone morphogenetic protein
BrdU	Bromodeoxyuridine
bRG	Basal radial glia
BRN2	Brain-Specific Homeobox/POU Domain Protein
CASC5	Cancer susceptibility candidate
Cb	Cerberus
CBF1	C-promoter binding factor

CDK4	Cyclin-dependent kinase
CDK5RAP2	CDK5 Regulatory subunit-associated protein
CDX	Caudal type homeobox
CDT1	Chromatin licensing and DNA replication factor
CFP	Cyan or Cerulean fluorescent protein
CG	Cement gland
Chd	Chordin
CM	Conditioned media
cMYC	V-myc avian myelocytomatosis viral oncogene homolog
CNS	Central nervous system
CP	Cortical plate
CPN	Callosal projection neuron
CR	Cajal-Retzius (cells)
Cre	Cre recombinase
CThPN	Corticothalamic projection neuron
CTIP2	Chicken ovalbumin upstream promoter transcription factor-interacting protein
CUX(1/2)	Cut-like homeobox
DCX	Doublecortin
DMEM	Dulbecco's Modified Eagle's medium
DMNT	DNA (cytosine-5-)-methyltransferase
DMRT3	Doublesex and mab-3 related transcription factor
DNA	Deoxyribonucleic acid
DN-ActRIIB	Dominant negative Activin receptor
DOX	Doxycycline

Dpp	Decapentaplegic
DRAGONbow	Doxycycline Regulated Auto-excisable Genetic-labeling Of Neurons Based On brainboW
D-V	Dorsal-ventral
EB	Embryoid body
ECM	Extracellular matrix
EGR1	Early growth response protein
EMX(1/2)	Empty spiracles homeobox
EP	Epidermis
EOMES	Eomesodermin
EpiSCs	Epiblast stem cells
ER81	Ets-Related Protein
ER^{T2}	Estrogen receptor domain
ETS	E26 transformation-specific
ESCs	Human embryonic stem cells
FEZF2	FEZ family zinc finger
FGF	Fibroblast growth factor
FOS	FBJ murine osteosarcoma viral oncogene homolog
FOXG1	Forkhead box G1
FUCCI	Fluorescently ubiquitination cell cycle indicator
FZD8	Frizzled class receptor
GABA	γ-aminobutyric acid
Gem	Geminin
GDF	Growth differentiation factor
GPR56	G protein-coupled receptors

H2B	Histone 2B
^{3}H	Tritiated
HAR	Human accelerated region
HES(1/3/5)	Hes family bHLH transcription factor
Hyg	Hygromycin
IF	Immunofluorescence
IPs	Intermediate progenitor cells
ISVZ	Inner subventricular zone
ITR	Inverted terminal repeats
IZ	Intermediate zone
Kb	Kilobase
KLF4	Kruppel-like factor
KIF18A	Kinesin family member 18A
LAM	Laminin
LHX2	LIM homeobox
LIF	Leukemia inhibitory factor
MADM	Mosaic analysis of double markers
MAPK	Mitogen-activated protein kinase
MCS	Multiple cloning site
MEFs	Mouse embryonic fibroblasts
MEF2C	Myocyte enhancer factor-2
MEK	Mitogen/Extracellular signal-regulated Kinase
MIB1	Mindbomb
M-L	Medial-lateral

mRNA	Messenger ribonucleic acid
MZ	Marginal zone
NC	Neural crest
N-CAD	Neural cadherin
NCAM	Neural cell adhesion molecule
NCX	Neocortex
NEO	Neomycin
Neurog(1/2)	Neurogenin
NHP	Non-human primate
Ng	Noggin
NICD	Notch intracellular domain
NMD	Nonsense mediated decay
NP	Neural plate
NR2F1	Nuclear receptor subfamily 2, group F, member 1
NT3	Neurotrophin
NURR1	Nuclear receptor related protein
OCT4	Octamer-binding transcription factor
OSVZ	Outer subventricular zone
OTX2	Orthodenticle homeobox 2
PAR(3/6)	Protease activated receptor
PAX6	Paired box
PBS	Phosphate-buffered saline
PCR	Polymerase chain reaction
PCW	Post conception week

PDGFD	Platelet derived growth factor D
PFA	Paraformaldehyde
PGK	Phosphoglycerate kinase 1
PI3K	Phosphoinositide 3-kinase
PLCF	Polyornithine/laminin/collagen/fibronectin
PLZF	Promyelocytic leukaemia zinc finger
polyA	Polyadenylation
POU5F1	POU class 5 homeobox 1
PSC	Pluripotent stem cells
PUΔTK	Puromycin delta thymidine kinase
PURO	Puromycin
RA	Retinoic acid
RFP	Red fluorescent protein
RGs	Radial glial cells
RNA	Ribonucleic acid
RNA-seq	Ribonucleic acid sequencing
RNF12	Ring finger protein
ROCK-I	Rho-associated protein kinase inhibitor
R-SMADs	Receptor-associated SMAD
rTA-M2	Reverse transactivator
RT-PCR	Reverse transcription polymerase chain reaction
RUES(1/2)	Rockefeller University embryonic stem cells
RVDs	Repeat variable dinucleotides
SATB2	Special AT-rich sequence-binding protein

SB/LDN	SB431542 and LDN193189
SCPN	Subcortical projection neuron
SDS	Sodium dodecyl sulfate
SFRP2	Secreted frizzled-related protein
SHH	Sonic hedgehog
SMAD	Small body size Mothers against decapentaplegic
Sog	Short gastrulation
SOX(1/2/5)	Sex determining region Y-box
SP8	Specificity protein
SP	Subplate
SPN	Subplate neuron
SPAG5	Sperm associated antigen
STAT	Signal transducers and activators of transcription
SVZ	Subventricular zone
T2A	Thoseaasigna virus 2A
TBR(1/2)	T-box, brain
TBS-T	Tris-Buffered Saline and Tween 20
TFAP2C	Transcription Factor AP-2 Gamma
TGFβ	Transforming growth factor beta
Thal	Thalamus
TLE4	Transducin-like enhancer of split
TRE	Tetracycline response element
TRNP1	TMF1-regulated nuclear protein
TxFs	Transcription factors

UTR	Untranslated region
VLDLR	Very-low-density-lipoprotein receptor
v/v	Volume/volume
VZ	Ventricular Zone
WM	White matter
WNT	Wingless-Type MMTV integration site family, member
w/v	Weight/volume
ZEB2	Zinc finger E-box binding homeobox
ZO1	Zona Occludens

CHAPTER 1: INTRODUCTION

The development of the cerebral cortex in all mammals can be broadly divided into three overlapping phases: 1) neural induction and folding of the neuroepithelium, 2) forebrain patterning, and establishment of various progenitors in the radial plane, and lastly 3) corticogenesis (Figure 1.1). Neural induction from the embryonic epiblast is the first step in the development of the central nervous system (CNS) in all vertebrate embryos. The resulting neuroepithelium will roll into a fluid-filled tube and separate from the overlying epidermis. This process of neural tube formation is referred to as neurulation. The neural tube is now surrounded by a layer of neuroepithelium that will mature further into the various progenitors during radial patterning. These progenitors will subsequently give rise to the entire repertoire of neurons found in the CNS during the corticogenesis phase. Corticogenesis itself encompasses several events: neurogenesis, axonal guidance and synaptogenesis, and gliogenesis. Neurogenesis involves generation of neurons to populate the various cortical layers, while axonal guidance and synaptogenesis occur in tandem and will enable local and long distance circuit formation in the CNS. Gliogenesis follows neurogenesis and leads to generation of astrocytes and oligodendrocytes, which support maturation of the circuits and conduction of action potentials, respectively.

In human embryos, neural induction occurs over a two week period (Days 5-19 in Figure 1.1), while neural tube closure occurs between Days 22-24. Areal and radial patterning of the neuroepithelium initiates around this time and will continue for the rest of the first trimester and early part of the second trimester. Corticogenesis, specifically

neurogenesis, starts downstream of the conversion of the neuroepithelium into radial glial cells around post conception week (PCW) 6. Axonal pathfinding initiates after PCW10 and continues till the beginning of the third trimester. Synaptogenesis and gliogenesis continue well into postnatal life.

In this chapter, I will focus on the molecular and cellular basis of neural induction, the patterning events occurring during corticogenesis, and cortical progenitors and their cellular diversity. I will also present a brief overview of embryonic stem cells to facilitate an understanding of the model system I am using for my experiments. Together, these ideas form the basis for this thesis. I will discuss them in the context of mammalian embryonic development, with evolutionary examples where they are instructive.

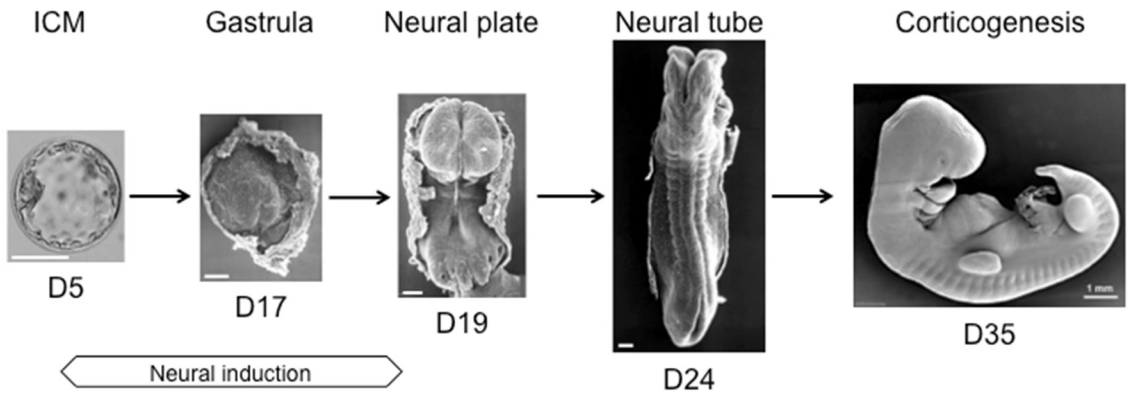

Figure 1.1: Morphological changes in a human embryo from blastula to the initiation of corticogenesis. From the Carnegie Collection. Scale bars: 1mm for corticogenesis, 200µm for others.

NEURAL INDUCTION AND EARLY PATTERNING IN VERTEBRATES

The molecular mechanisms and developmental milestones associated with neural induction are largely conserved across the evolutionary tree (Levine and Brivanlou, 2007; Muguruma and Sasai, 2012). In amphibians – where it was originally described – neural induction initiates after the fertilized egg undergoes a series of divisions to generate a fluid filled mass of cells called a blastula (blastocyst in mammals). Three different territories emerge in the blastula: ectoderm, mesoderm, and endoderm, which are collectively referred to as germ layers, while the process by which they arise is called gastrulation. Each germ layer is fated to generate different tissues as the embryo matures. The primitive ectoderm (epiblast in mammals) covers the outside of the embryo and forms different tissue derivatives depending on its position along the embryonic dorsal-ventral (D-V) axis. During gastrulation, neural induction occurs in the most dorsal region of the ectoderm, and morphologically manifests as thickening of the ectoderm into a flat, raised structure called the neural plate. The neural plate will undergo neurulation as described above and will form the brain at the anterior end and the spinal cord at the posterior end. Hence the entire CNS of the amphibian embryo is derived from the dorsal ectoderm.

The ventral region of the ectoderm follows a different fate: it will form the epidermis, which gives rise to skin and its derivatives. The neural crest forms at the junction of the dorsal and ventral boundaries, which correspond to the edge of the neural plate. Neural crest cells are highly migratory in nature and invade the developing embryo where they

will eventually give rise to the peripheral and enteric nervous system, craniofacial cartilage and bone, pigmented melanocytes, as well as smooth muscle cells. Ectodermal cells at the most anterior edge of the neural-epidermal boundary give rise to placodal areas that will form sensory organs – such as the ear, nose, and eyes – as well as some cranial sensory ganglia (Figure 1.2). At the start of gastrulation, cells from any part of the ectoderm can still develop as either epidermis or neural tissue, but by the end of gastrulation commitment has occurred (Holtfreter, 1955).

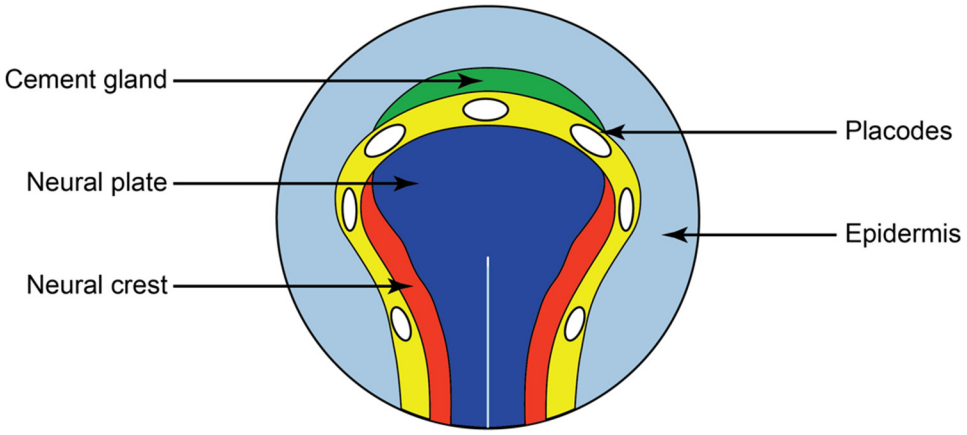

Figure 1.2: Fate map of the anterior border of the neural plate in Xenopus embryos.

These events described above are characteristic of all vertebrates, although the actual timing and topology may vary in different species. Thus, neural induction is an evolutionarily conserved requirement in the establishment of the nervous system in vertebrates and partitions the primitive ectoderm into epidermal and neural primordia upon gastrulation. But how does a mass of uncommitted cells become committed to a neural fate versus epidermal or mesendodermal fate? What are the molecular mechanisms that contribute to this commitment? Clues to these answers arose from the classic transplantation experiments of Hilde Mangold and Hans Spemann and

subsequently from *in vitro* explants of the dorsal ectoderm in the presence or absence of specific growth factors.

NEURAL INDUCTION: FROM EXPERIMENTAL EMBRYOLOGY TO THE DEFAULT MODEL

The Mangold-Spemann experiments and animal cap assays

The fundamental insight into how the neural plate is established came from the famous observations of Hilde Mangold and Hans Spemann in the newt (*Triturus*) (Spemann and Mangold, 1924). In their experiment, tissue from the dorsal mesoderm of an early newt gastrula was grafted to the ventral side of a second embryo. The host embryo developed a second set of dorsal axial structures on the ventral side, including a well-organized second nervous system. This experiment suggested that signals from the dorsal mesodermal region were responsible for diverting nearby ectoderm to a neural fate (Figure 1.6B). This region became known to amphibian embryologists as "Spemann's organizer". In normal development, cells of the organizer involute into the embryo during gastrulation, giving rise to dorsal structures in the mesoderm such as muscle and the notochord that underlie the future neural plate. Lineage-tracing experiments revealed that while the entire mesoderm of the secondary axis was derived from the progeny of the grafted cells, the entire CNS, was derived from the host, with the exception of the floor plate (Gimlich and Cooke, 1983). This suggests that signals from the organizer caused ventral ectodermal cells – that normally would have given rise to the epidermis – to convert instead to a neural fate. Similar findings are also observed in fish, where grafting

pieces of organizer (called the shield in fish) induces a secondary axis in the host fish (Oppenheimer, 1936; Oppenheimer, 1953). Grafting experiments carried out in the chick and mouse embryos (where the organizer is called the node) show similar results (Waddington, 1952; Beddington, 1994), highlighting the evolutionary conservation of the "organizer" as source of signal(s) that is sufficient to generate the entire nervous system.

To probe the mechanism by which organizer grafts were giving rise to a secondary axis, the ectoderm of the amphibian blastula (called the animal cap) can be grown as explants in pond water. By itself, the isolated animal cap only forms epidermal tissue (Holtfreter, 1955), but when recombined with explants derived from another portion of the embryo, the same explant can generate other cell types. For instance, mesodermal derivatives arise in explants exposed to early endoderm while neural tissue can be induced after exposure to dorsal mesoderm (including the organizer) (Nieuwkoop, 1951; Slack and Forman, 1980). This demonstrates the potential of animal cap cells to form both mesodermal and ectodermal derivatives, depending on the inductive interactions that were encountered over the course of early development. Since isolated animal cap explants were observed to undergo epidermal differentiation, it reinforced the view from the Spemann-Mangold experiments that the ectoderm forms epidermis as a default state. More surprising was the fact that simple cell dissociations of the animal cap led to conversion of cells from epidermal to neural fate *directly*, without previous or concomitant induction of mesoderm (Godsave and Slack, 1989; Sato and Sargent, 1989). To explain these results, neural inducers were proposed to be widely distributed and

under negative control in the animal cap by factors that could be lost by dissociation (Sato and Sargent, 1989), but the nature of either the inducer or its inhibitor remained elusive.

The role of TGFβ family members in embryonic differentiation

The field of embryology benefited from the introduction of modern molecular techniques to complement classical experimental embryology in the clawed African frog *Xenopus*. These approaches soon led to the discovery that physiological amounts of polypeptide growth factors of the fibroblast growth factor (FGF) and transforming growth factor beta (TGFβ) family were sufficient to impose mesodermal fates in animal caps. For example, when treated with increasing thresholds of Activin, a member of the TGFβ family, animal caps respond by forming ventral, lateral and dorsal mesoderm (including the organizer) (Kurth et al., 2005). Work in a variety of vertebrate model systems has established the pivotal role of these growth factors in the formation of mesodermal and organizer tissues in the embryo (Schier, 2009). Of note, animal caps also undergo some degree of neural induction when treated with high concentrations of a mesodermal inducer such as Activin, suggesting that neural tissue is also induced by growth factor action. Experimentally, the difference between *indirect* versus *direct* neural induction can be assessed by examining tissue specific markers, where direct induction is characterized by the expression of neural markers (*NCAM*) in the *absence* of mesodermal/organizer-specific molecular markers (*brachyury, goosecoid*). Expression of both markers, however, is a strong indication of an indirect cascade where one signaling factor induces responding cells to release additional inducing factors. In Activin-induced neural induction of the

animal cap, both mesoderm and neural markers are found, suggesting that neural induction in this instance is likely to be secondary to the inductive effect of the organizer. It was during the studies of the Activin receptor, one of the first TGFβ family receptors cloned in mammals (Mathews and Vale, 1991) and in *Xenopus*, that the nature of direct neural inducers began to emerge.

The TGFβ pathway

There are two major branches of the TGFβ superfamily: the Activin/Nodal branch and BMP branch (Figure 1.3). On binding of ligands to their cognate receptors, signaling is induced by ligand-dependent dimerization of type II receptors with type I receptors through serine-threonine kinase activity. The type I receptor in turn induces signaling by either the canonical pathway, via receptor-associated SMAD proteins (R-SMADs), or by the non-canonical pathway which involves MAPK and NF-κB pathway components (Taylor and Wrana, 2008; Poorgholi Belverdi et al., 2012). The Activin/Nodal branch utilizes SMAD2/3 as its receptor SMAD, while the BMP branch utilizes SMAD1/5/8. For both classes of receptor SMADs, SMAD4 is an essential cofactor (referred to as co-SMAD) for their translocation into the nucleus. There are also multiple ligands and inhibitors of each branch in the extracellular space as shown in Figure 1.3; a few of them will be discussed in the following sections. In addition to extracellular inhibitors, there are also two intracellular inhibitors of signaling (inhibitory SMADs): SMAD6 and SMAD7. SMAD6 inhibits the BMP-SMAD1/5/8 branch as well as the non-canonical branches of signaling,

while SMAD7 is a specific inhibitor of the canonical branches of both pathways (Yan et al., 2009; Jung et al., 2013).

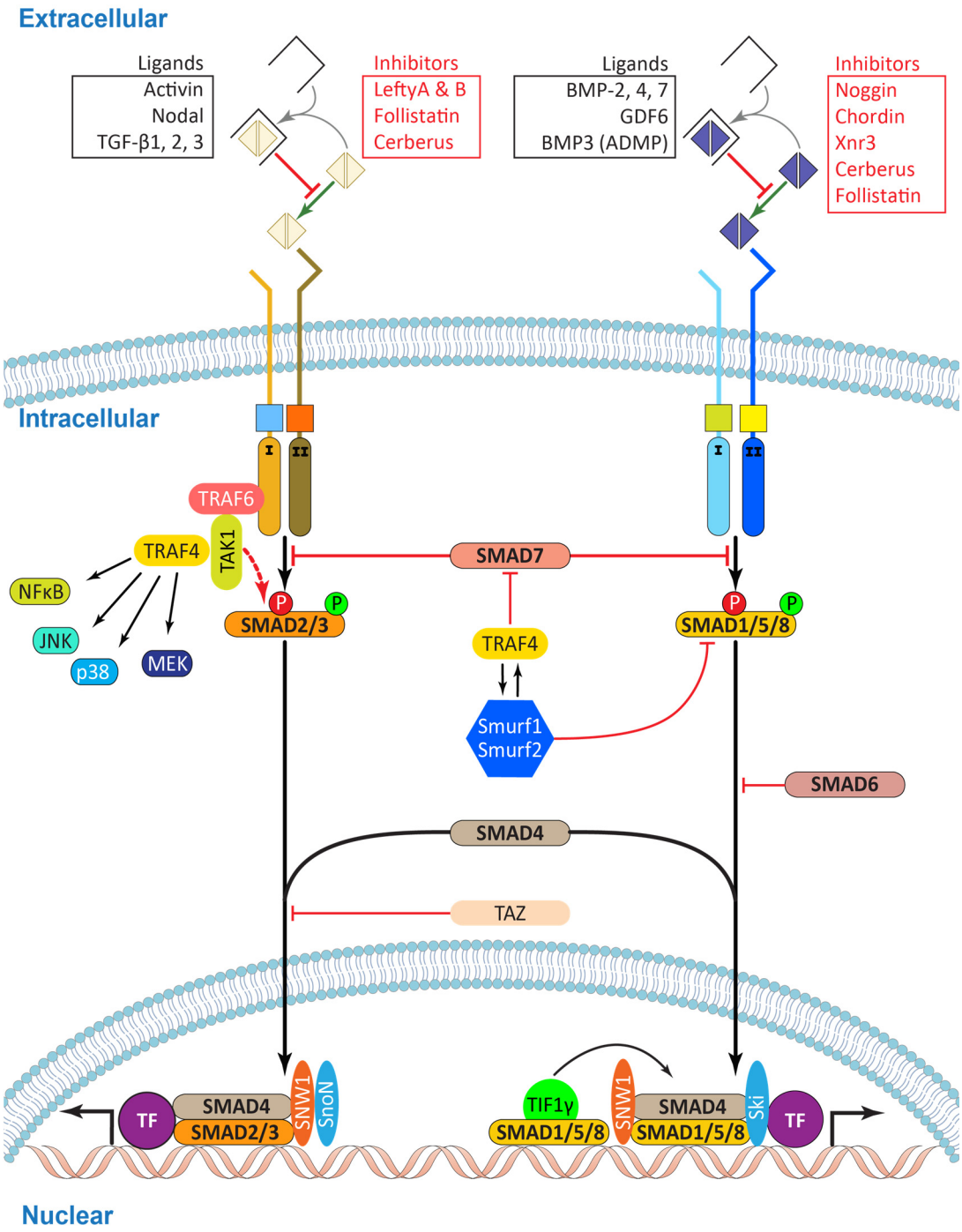

Figure 1.3: Schematic showing the two main TGFβ pathways: the Activin/Nodal and the BMP branches.

The molecular basis of neural induction

Serendipitously, a role for TGFβ signaling in neural induction was suggested by studies of mesodermal induction in *Xenopus*. In order to determine if Activin signaling is necessary for mesoderm induction *in vivo*, a dominant negative Activin receptor (DN-ActRIIB) was injected into a 2-cell stage embryo to challenge the inducing activity of Activin (Figure 1.4) (Hemmati-Brivanlou and Melton, 1992). Like many dominant-negative mutants, DN-ActRIIB is known to be broad acting and capable of blocking all TGFβ ligands, including Nodals, BMPs, and GDFs. When expressed in early embryos, DN-ActRIIB completely inhibits endogenous mesoderm induction, in line with the idea that TGFβ signaling through the ActRIIB receptor is necessary for mesoderm induction *in vivo*. DN-ActRIIB expression in animal caps also completely blocks mesoderm induction by Activin. Unexpectedly, however, when expressed alone in control animal caps in pond water (i.e. not exposed to any ligand), it leads to a strong conversion of fate directly from epidermal to neural, in the absence of neural-inducing signals from Spemann's organizer (Figure 1.4). Furthermore, it was subsequently shown that the neural cells induced by DN-ActRIIB are of forebrain identity, but not of hindbrain or spinal cord (Chang and Harland, 2007), suggesting that TGFβ inhibition has the dual effect of determining the lineage choice of the animal cap as well as its antero-posterior (A-P) identity. These precepts would give rise to a new model of neural induction: the default model.

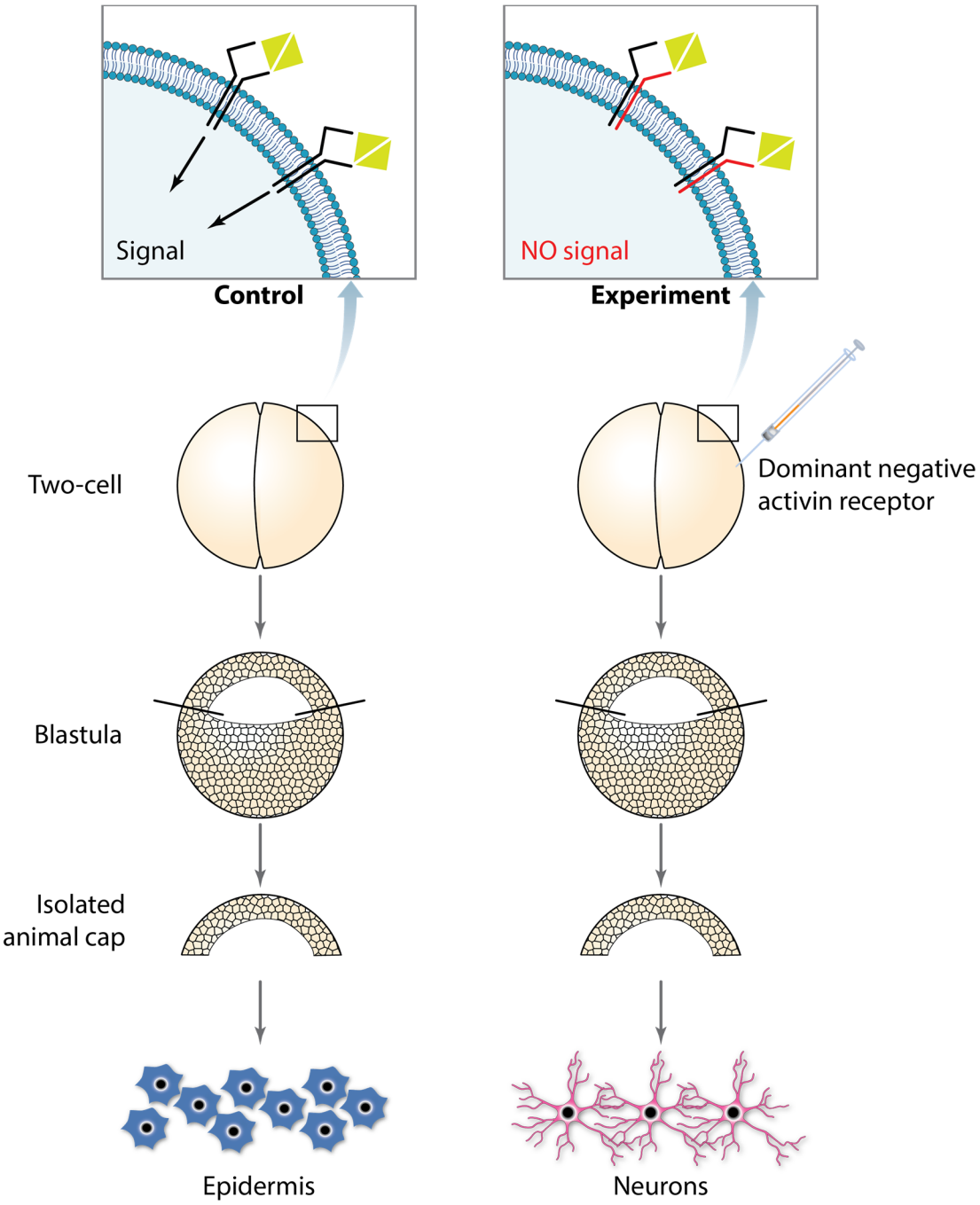

Figure 1.4: Injection of dominant-negative activin receptor (which blocks all TGFβ signaling) in two-cell stage Xenopus embryos converts prospective epidermal tissue into neural tissue. Modified from Sanes et al. (Sanes et al., 2012).

The "Default Model" of neural induction

That neural tissue could be induced by cell dissociation or by expression of a dominant negative Activin receptor were distinct observations with one common denominator: they both made sense if traditional thinking about neural induction was inverted. In this revised view, the default fate for animal caps would not be epidermal, but neural. Ongoing signals in the explants repress the natural tendency of the cells to become neural by inducing the epidermal fate. When this signaling is interrupted (by either expression of DN-ActRIIB or by cell dissociation), cells assume a neural fate. This became known as the default model of neural induction (Hemmati-Brivanlou and Melton, 1992, 1994). The implication of this model is that vertebrate embryonic cells will become forebrain tissue unless told otherwise (see next section) (Hemmati-Brivanlou and Melton, 1997).

Although the default model was based partially on over-expression of an artificial dominant negative receptor, one of its predictions is the presence of endogenous epidermal-inducing signal(s) as well as an organizer-derived inhibitor(s) of this signal. In this scenario, neural inducers from the organizer locally antagonize these epidermal inducing signals, allowing the dorsal ectoderm to follow its “default” neural fate. Indeed, these endogenous signals and their inhibitors were found in subsequent studies described below, as predicted by the model.

Neural tissue induced by TGFβ inhibition is forebrain by default

The early neural plate is already specified to form different parts of the nervous system immediately downstream of neural induction. As discussed above, the anterior end of the embryo will form forebrain, midbrain, and hindbrain in succession, while the posterior end will form the spinal cord. This is a property conserved in all vertebrates studied (Rallu et al., 2002). Working with Axolotl explants, Nieuwkoop was the first to observe that newly formed neuroepithelium adopts an anterior identity by default ("activation"), while generation of posterior neural tissues required caudalization of this anterior neuroepithelium ("transformation") (Nieuwkoop and Nigtevecht, 1954). This "activation-transformation" model thus predicts that "activation" by direct neural inducers should give rise to neural tissue with an anterior identity. Indeed, it has now been shown in multiple contexts that all direct neural inducers that inhibit TGFβ signaling induce neural tissue of anterior (forebrain) character. Thus the default model provides a molecular explanation to the "activation" aspect of Nieuwkoop's model.

We now know that "transformation" involves a complex set of inductive signals generated by the extra-embryonic endoderm, the axial mesoderm (notochord), non-neural ectoderm, and paraxial mesoderm that will pattern the neural plate into different regions along the embryonic axes. These signals include BMPs and Sonic Hedgehog (Shh) in the D-V axis, and WNTs, FGFs, and Retinoic acid (RA) in the A-P axis (Chizhikov and Millen, 2004; Kurth et al., 2005; Liu and Niswander, 2005; Fuccillo et al., 2006).

Epidermal induction

To dissect the identity of epidermal inducing signals, dissociated animal cap can be subjected to purified proteins, and the fate of the cells determined with molecular markers (Wilson and Hemmati-Brivanlou, 1995). Since animal cap cells are neuralized upon dissociation, candidate factors can be tested for the ability to suppress neuralization and restore epidermal specification, thus replacing endogenous signals lost on dispersion. As expected, treating these cells with Activin blocks neuralization by inducing mesoderm. Another member of the TGFβ superfamily, BMP4, not only suppresses neuralization, but is also a potent epidermal inducer (Wilson and Hemmati-Brivanlou, 1995). Significantly, the dominant-negative Activin receptor not only blocks signaling by BMP4, but also by BMP2 and BMP7, which are epidermal inducers in this assay (Suzuki et al., 1997). Indeed, the expression pattern of BMPs is in accord with their proposed role as neural inhibitors: BMP4 RNA is found throughout the ectoderm at the start of gastrulation, subsequently disappearing from the prospective neural plate (Figure 1.5) (Fainsod et al., 1994; Hemmati-Brivanlou and Thomsen, 1995; Schmidt et al., 1995). Epidermal differentiation is also blocked in animal caps after inhibiting endogenous BMP signaling using dominant-negative BMP receptors (Sasai et al., 1995; Schmidt et al., 1995; Xu et al., 1995), dominant negative BMP4 or BMP7 ligands (Hawley et al., 1995), or antisense BMP4 RNA (Sasai et al., 1995), suggesting further that the BMP family are essential epidermal inducing factors *in vivo*. The requirement of BMP signaling in epidermal induction and blocking neural induction has now been validated in both mouse and humans ESCs (Coraux et al., 2003;

Metallo et al., 2008) as well as mouse embryos (Davis et al., 2004; Di-Gregorio et al., 2007).

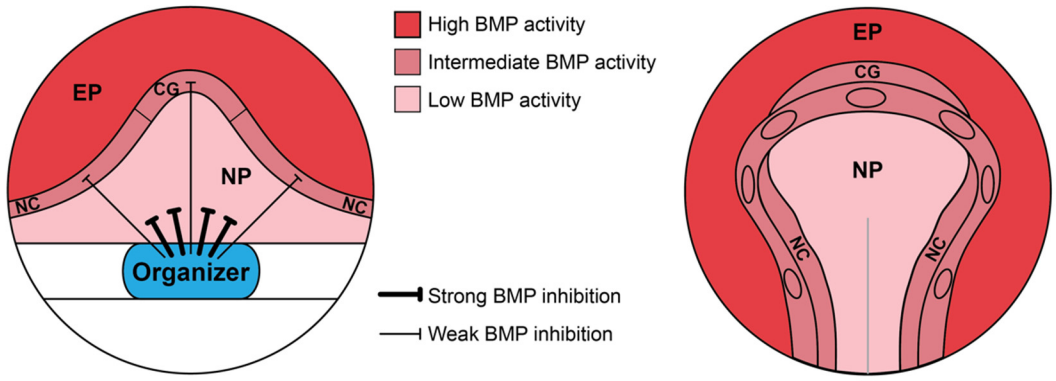

Figure 1.5: Schematic of graded BMP activity in the gastrula and neurula ectoderm in the Xenopus embryo. A schematic fate map of the early gastrula shows the approximate positions of the future neural plate (NP), border region, and epidermis, viewed from the dorsal side. Diffusible antagonists produced in the organizer region of the mesoderm result in a graded distribution of BMP signaling in the neighboring ectoderm. The relative positions of epidermis (EP), NP, organizer, cement gland (CG), and neural crest (NC) are shown. Sensory placodes form at various positions in the border region. Dorsal view of the neurula fate map with BMP activity levels superimposed.

INDUCERS OF NEURAL FATE *IN VIVO*

Endogenous neural inducers are inhibitors of TGFβ signaling and are expressed in the organizer and primordial endoderm

Independent approaches in *Xenopus* led to the identification of the endogenous neural inducers. Screening of cDNA libraries for embryonic inducing activity led to the discovery of noggin, the first endogenous direct neural inducer (Smith and Harland, 1992). The second involved isolating organizer-specific genes. This led to the identification of chordin

(Sasai et al., 1994). Finally, testing the activity of candidate TGFβ inhibitors led to the characterization of follistatin (Hemmati-Brivanlou et al., 1994). All three genes are secreted proteins, specifically expressed in the organizer, and with direct neural-inducing ability (Figure 1.6A). Together, they confirm that the organizer is indeed the major source of signals that induces neural tissue *in vivo*.

Biochemical characterization of noggin, chordin, and follistatin have established that they are potent extracellular inhibitors of BMP signaling (Figure 1.3). They bind with high affinity to the ligands, thus preventing them from activating their cognate receptors (Piccolo et al., 1996; Zimmerman and Mathews, 1996). In *Xenopus*, a high gradient of BMP signaling on the ventral side of the ectoderm promotes epidermal fate, whereas on the dorsal side BMP signaling is kept low by organizer generated BMP inhibitors, thus promoting a neural fate (Figure 1.5). There is now an extensive list of secreted BMP inhibitors, with many that are expressed in the organizer (node in mammals). Nearly all of these that have been tested in the animal cap assay have been shown to act as a direct neural inducer. Together, BMP ligands and their inhibitors establish a gradient of BMP-SMAD1/5/8 activity in the developing embryo that will result in distinct fates within the ectoderm. Hence high levels of BMP will induce epidermis, while low levels are permissive for neural fate. Intermediate levels of BMP activity at the border of the neural plate and the epidermis will induce neural crest and neural placodal fates (Figures 1.2 and 1.5).

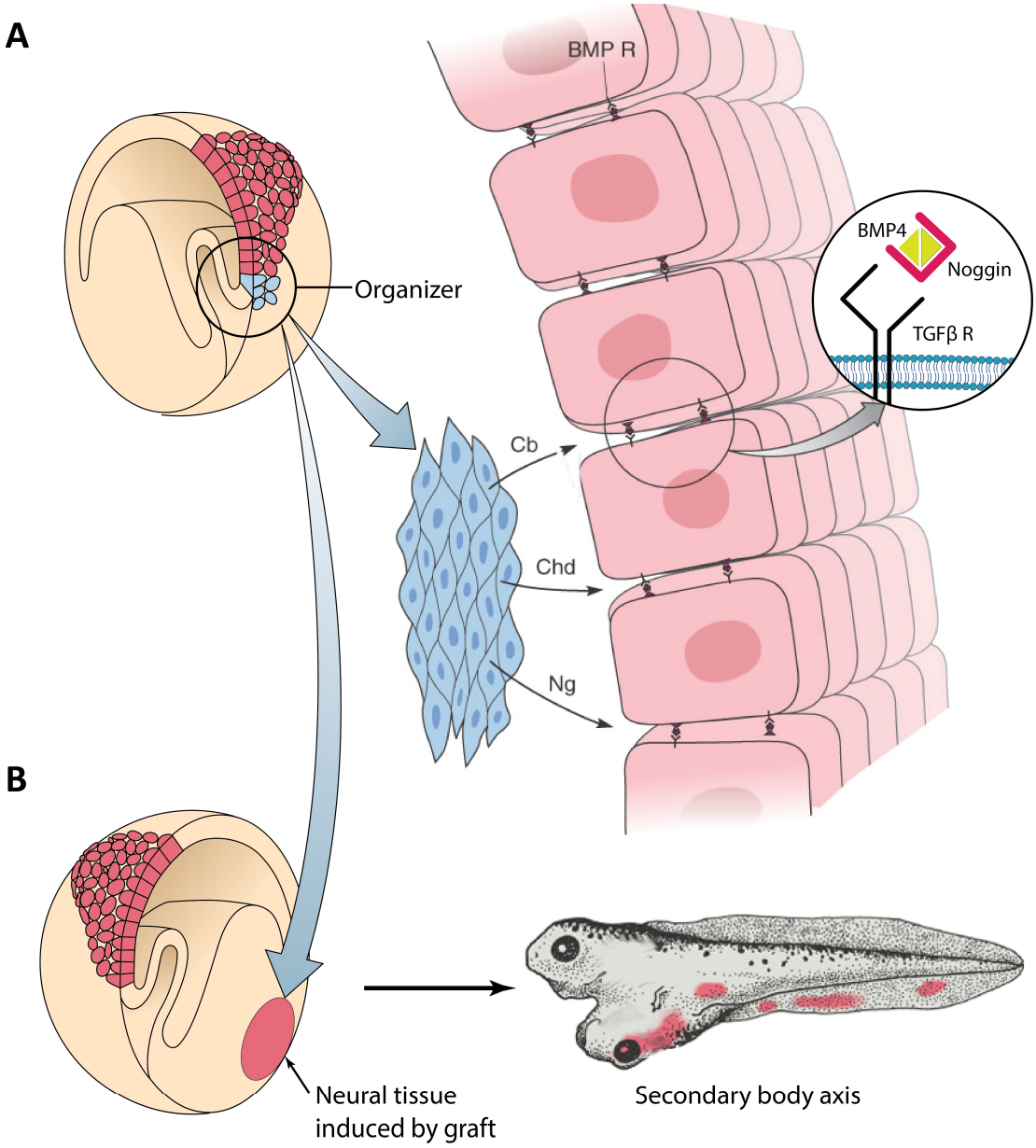

Figure 1.6: The organizer acts as a neural inducer by releasing TGFβ inhibitors. A) Cross-section through the Xenopus embryo at gastrula stage showing the organizer (blue cells). TGFβ inhibitors released by the organizer induces neural fate (in red) in the overlying ectoderm. Transplantation of the organizer into the ventral side of a host embryo gives rise to a duplication of the body axes due to the inductive activity of the organizer. This was essentially the experiment carried out by Spemann and Mangold in Newt embryos. Cb: Cerberus, Chd: Chordin, Ng: Noggin. Modified from Sanes et al. (Sanes et al., 2012).

Following the discovery of endogenous BMP inhibitors, another class of neural inducers was also found in prospective endoderm of Xenopus embryos, away from the classical organizer. This head inducer was identified in a differential screen for cDNAs enriched in the dorsal region of *Xenopus* embryos and named Cerberus (Bouwmeester et al., 1996). Cerberus is an inhibitor of the Nodal, BMP and WNT pathways in *Xenopus*, but is predominantly a Nodal inhibitor in mouse (Piccolo et al., 1999; Perea-Gomez et al., 2002). Two other neural inducers, Lefty1 and Lefty2 were initially identified based on their homology to TGFβ ligands and later identified as Nodal inhibitors that were found to have neural inducing activity in *Xenopus* animal caps (Meno et al., 1997; Hamada et al., 2002). Homologues of both Lefty and Cerberus have also been found in *Xenopus*, zebrafish, chicken, and mouse in analogous expression patterns (Shen, 2007). Unlike Cerberus, *Xenopus* lefty (called xantivin) is not expressed in the organizer and does not appear to have neural inducing activity in neural caps by itself (Cheng et al., 2000). However, knock-down of endogenous lefty with morpholinos in the embryo leads to a strong reduction in forebrain markers (Tanegashima et al., 2004). In mouse embryos, both Lefty1 and Cerberus-like are released by an extra-embryonic structure called the anterior visceral endoderm (AVE); this is in contrast to BMP inhibitors, which are released by the organizer/node. In addition to promoting neural induction, Nodal inhibitors also have a conserved and well-studied role in left-right patterning of the embryo (Shen, 2007).

Xenopus animal cap cells pass through a competence phase when they respond to Activin/Nodal signaling by forming mesendodermal derivatives, followed by a second phase when they become epidermis in response to BMP signaling. In the default model

therefore, a neural fate ensues only when animal cap cells avoid both mesoderm and epidermal inducing signals. This explains why co-inhibition of both BMP-SMAD1/5/8 and Activin/Nodal-SMAD2/3 branches of the TGFβ pathway induces a neural fate more potently than each alone (Chang and Harland, 2007) in a manner similar to DN-ActRIIB, which interferes with both Activin/Nodal and BMP signaling. In addition to these endogenous inhibitors, small molecules that block the different branches of the TGFβ signaling have also been characterized. As with endogenous inhibitors, they have now been shown to act as direct neural inducers when tested in the context of animal cap explants or in mammalian pluripotent stem cells (PSCs), as will be discussed later.

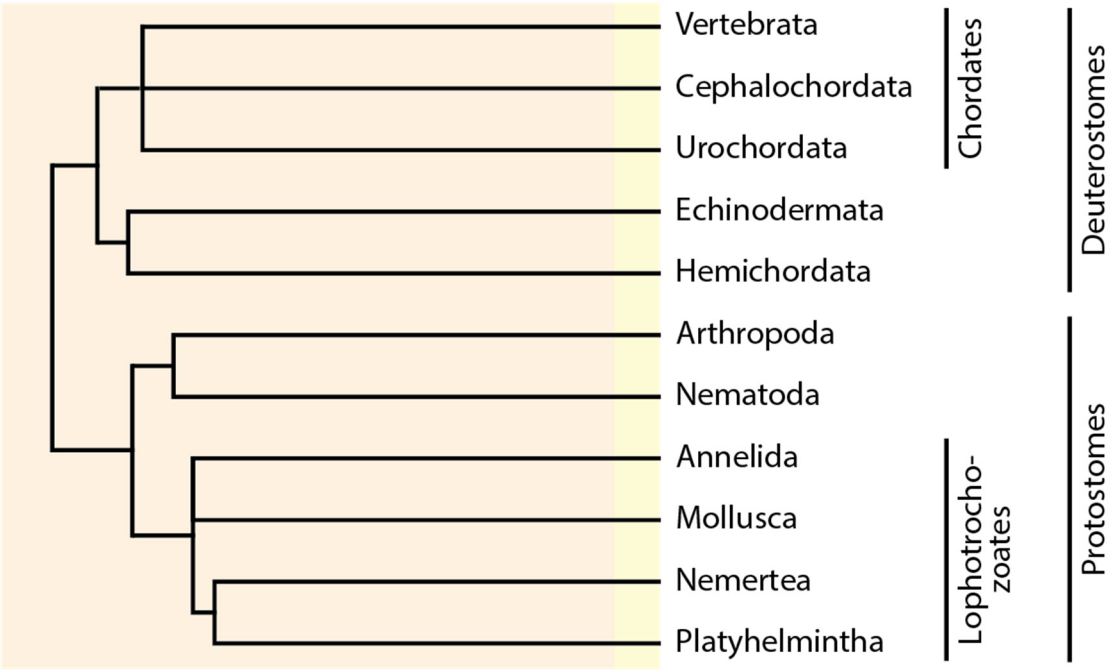

Figure 1.7: Taxonomy of the bilaterian group of animals. As the name suggests, bilaterians have bilateral symmetry, with an anterior-posterior, dorsoventral and left-right axis. Adapted from Hedges and Kumar (Hedges and Kumar, 2009).

Evolutionary conservation of the requirement of TGFβ inhibition for neural commitment

Inhibition of ongoing TGFβ signaling to delineate neural and non-neural ectoderm is a commonly utilized module during evolution in bilaterian animals (Figure 1.7) (Hartenstein and Stollewerk, 2015). In the fruitfly *Drosophila* (anthropoda) for example, *short gastrulation* (*sog*) is a homolog of the organizer-specific BMP-inhibitor *chordin*. *Sog* was identified in a systematic screen for genes involved in patterning the *Drosophila* embryo along the D-V axis (Zusman et al., 1988). As in vertebrates, the dorsal and ventral regions of the ectoderm of the *Drosophila* embryos generate different fates. However, as the embryonic axis is flipped in arthropods compared to chordates, the epidermis forms in the dorsal regions, while neural tissue arises ventrally. Nonetheless, the molecular circuitry involving inhibition of BMP in segregating dorsal from ventral ectoderm operates precisely in the same manner as in vertebrates (Holley et al., 1995; Eldar et al., 2002). *Drosophila* correlates of BMP signaling, including ligands, receptors and inhibitors such as *Sog* generate an activity gradient of *Dpp*, a BMP-like ligand, from high dorsal to low ventral, thus specifying epidermal and neural tissue, respectively (Mizutani et al., 2005). Indeed, *Sog* has been shown to directly promote neuroectoderm specification in blastoderm drosophila embryos by inhibiting the anti-neurogenic and dorsalizing activity of *Dpp* (Biehs et al., 1996). This activity of *Sog* is also shared by other arthropods, such as spider and beetles (Mizutani and Bier, 2008). Similarly, inhibition of HrBMPb, the ascidian homolog of BMP, is required for induction of rostral neural lineages in sea squirts (a representative of urochordates) and BMP overexpression results in a fate switch of the presumptive neural cells to epidermal lineages (Miya et al., 1997). Similarly, lancelets

(which are cephalochordates) have been shown to possess a ventral-high dorsal-low gradient of BMPs, and addition of exogenous BMPs ventralizes the embryo while preventing expression of neural markers (Yu et al., 2007b). Likewise, in annelids (which are lophotrochozoates) inhibition of BMP signaling is required to specify neuroectodermal fate, which lies in the ventral territory (Kuo and Weisblat, 2011). A notable exception to this rule is found in hemichordates, which lack an organized CNS and do not have segregation of the ectoderm into neurogenic and epidermal territories. Exposure of these embryos to exogenous BMPs does not repress neural markers, and conversely, BMP knockdown does not promote neuralization, even though it has a role in D-V patterning in these embryos (Lowe et al., 2006). Neural fate choice in nematodes is also not reliant on BMP inhibition, since they have a fixed lineage map at the onset of embryogenesis (Hartenstein and Stollewerk, 2015). Taken together, these observations suggest that D-V patterning by the BMP pathway is an ancient mechanism that evolved early in bilaterians and was subsequently utilized by many members of protostomes and deuterostomes as a means of establishing segregating neural-epidermal fates in the early embryo (Figure 1.7) (Mizutani and Bier, 2008; Hartenstein and Stollewerk, 2015). The requirement for TGFβ inhibition in neural induction has remained highly conserved across hundreds of millions of years of evolution in vertebrates as well, and has been demonstrated in mouse embryos as well as human and non-human primate (NHP) embryonic stem cells. I will focus on mammals in the sections below.

TGFβ inhibition is required for neural induction in vivo in mammals, and there is significant redundancy among TGFβ inhibitors

As stated previously, a requirement for inhibition of both branches of the TGFβ pathway (i.e. Nodal and BMP branches) has been shown *in vivo* in *Xenopus* (Chang and Harland, 2007). In mouse embryos, knockout of both branches has not been reported, presumably due to the severe embryonic malformations of the mutations. However, mutant embryos that have lower activity of only one branch give a phenotype consistent with the predictions of the default model. For example, knockout of the predominant BMP receptor in the mouse epiblast, Bmpr1a, results in expansion of the neural domain to cover nearly the entire epiblast. This neuralized epiblast expresses several markers of forebrain territory (Figure 1.8A) (Di-Gregorio et al., 2007). Moreover, the expression of Nodal is completely lost in these embryos, as is the expression of mesodermal markers. In early mouse embryos, Nodal is the predominant ligand for the Activin/Nodal pathway. This suggests that the anterior neural fate conversion in the epiblast is direct and due to inhibition of both branches of TGFβ.

Conversely, knockout of Nodal in mouse embryos results in severe gastrulation defects. The mesendoderm fails to be specified, along with the AVE, which secretes Nodal inhibitors such as Lefty1 and Cerberus-like (Shen, 2007). Nevertheless, the epiblast undergoes a precocious, near-complete neural conversion and expresses several markers of forebrain fate, suggesting a direct conversion (Brennan et al., 2001; Camus et al., 2006).

Cripto (also called TDGF1 in humans) is an essential co-receptor for Nodal signaling and increases its binding affinity to its primary receptor ALK4 (Yeo and Whitman, 2001). As with Nodal knockouts, Cripto knockout embryos also have severe gastrulation defects; unlike nodal knockouts, mesendodermal markers are specified but displaced to the proximal epiblast while the AVE is also present (Ding et al., 1998; Liguori et al., 2003). Notably, the distal epiblast in Cripto knockout consists mostly of neuroectoderm, with expression of several markers of forebrain identity. Since Nodal is required for maintenance of BMP expression in the gastrulating embryo (Shen, 2007), both TGFβ branches are effectively repressed in Nodal and Cripto knockouts.

There is a robust functional redundancy in Nodal and BMP ligands and their inhibitors that mediate neural induction. Hence, mutations that eliminate only one inhibitor tend to have mild to no phenotypes on their own. For example, a loss-of-function mutation in Zebrafish *chordin* (the *chordino* mutant), a BMP inhibitor, causes only a reduction in the size of the neural plate (Schulte-Merker et al., 1997). Similarly, mouse embryos that lack just one of the BMP antagonists, *chordin* or *noggin* by knockout mutations have a relatively normal nervous system (McMahon et al., 1998; Bachiller et al., 2000). However, the full consequence of unopposed BMP signaling becomes apparent when several inhibitors are removed at the same time. For instance, a complete loss of neural tissue is observed when all three BMP antagonists - i.e. *chordin*, *follistatin* and *noggin* - are simultaneously targeted using morpholinos both in *Xenopus* (Khokha et al., 2005) and zebrafish (Dal-Pra et al., 2006). Likewise, the mouse double *noggin/chordin* mutants lacks all anterior neural structures (Figure 1.8B) (Bachiller et al., 2000). Conversely, multiple

BMP ligands are required for epidermal differentiation: at least three of the four BMPs, BMP2/4/7, need to be disrupted in *Xenopus* embryos to expand the neural plate, but even then, some ventral epidermal tissue remains. Taken together, the Bmpr1a, Nodal, Cripto, and Noggin/Chordin mouse knockouts provide strong evidence for the necessity of TGFβ inhibition and applicability of the default model of neural induction *in vivo*.

Multiple inhibitors of the Nodal pathway are also found in the anterior half of mouse embryos, of which Lefty1 and Cerberus-like are the best studied. Unlike BMP inhibitors, which are released by the node, both these inhibitors are released by the AVE. Here they promote anterior neural development by protecting the overlying forebrain from mesendodermal inducing Nodal signals (Shen, 2007). As with BMP inhibitors, Nodal inhibitors also appear to be redundant, as deletion of Cerberus-like alone has no effect on anterior neural development (Belo et al., 2000). Likewise, depletion of Cerberus in *Xenopus* with morpholinos is not sufficient to prevent head formation by itself (Silva et al., 2003). In mice, double knockout of Cerberus-like and Lefty1 are embryonic-lethal and associated with severe defects, including expansion of the extra-embryonic endoderm, patterning of the mesoderm, and multiple primitive streaks (Perea-Gomez et al., 2002). The effect on neural fate in these embryos has not been explored systematically yet.

Thus, neural induction *in vivo* probably depends on multiple ligands and inhibitors as a means to fine-tune TGFβ signals during patterning of the early embryo.

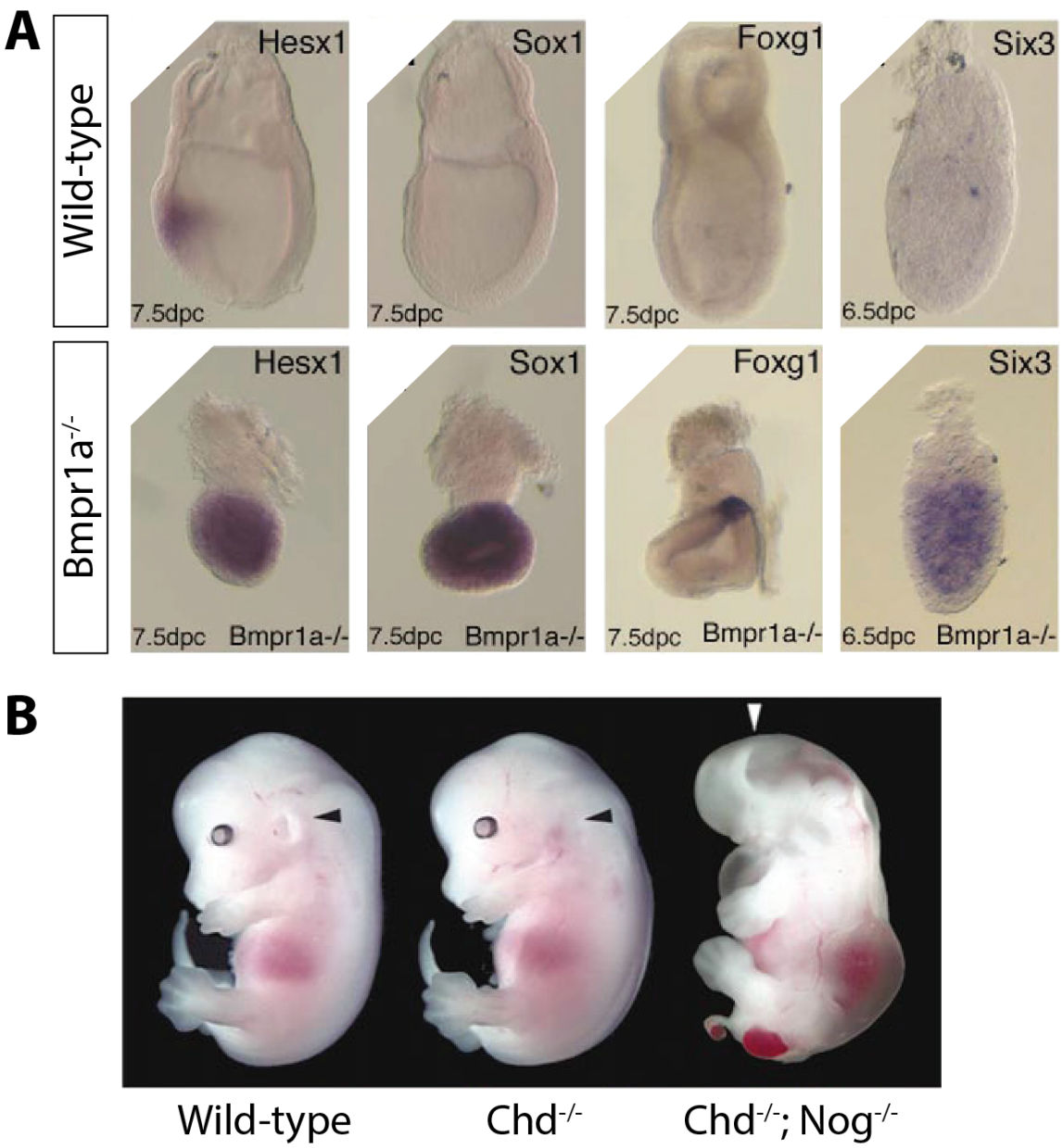

Figure 1.8: Absence of BMP signaling promotes forebrain fates in mouse embryos while excessive BMP signaling prevents forebrain induction. A) Bmpr1a$^{-/-}$ mice display premature expression of TxF dilineating forebrain territory including Hesx1, Foxg1, and Six3. Sox1 is a general neural marker. B) Chordin and noggin double knockout mouse embryos, but not chordin knockouts alone, fail to form forebrain and midbrain structures. Adapted from Bachiller et al. and Di-Gregorio et al. (Bachiller et al., 2000; Di-Gregorio et al., 2007).

FGF signaling and neural induction

Differential TGFβ signaling provides an instructive mechanism for restricting neural tissue to one part of the embryo on A-P axis (Levine and Brivanlou, 2007). The default model, however, leaves open the possibility that other factors are involved in neural induction, including those that operate in a more permissive fashion to grant the nascent ectoderm (epiblast in chick and mammals) competence to respond to TGFβ inhibition. The best evidence for a factor in this category are ligands of the FGF and IGF family, both of which bind to tyrosine kinase receptors and signal via the MAPK cascade. FGF signaling has been shown to inhibit BMP signaling in the Xenopus embryo by several mechanisms: for instance, FGF signaling through MAPK can promote phosphorylation of the linker domain and degradation of SMAD1, thereby functionally reducing BMP signaling (Pera et al., 2003). In addition, FGFs can also inhibit BMP activity indirectly, by inducing the expression of a protein called Zeb2 (also known as SIP1/Zfhx1b), a zinc-finger homeodomain protein that binds to and represses the transcriptional activity of the SMAD protein (Sheng et al., 2003). For much of the neural plate, the role of FGF signaling is likely to be minor, since neural induction by the BMP inhibitors occurs readily in *Xenopus* in the absence of FGF signaling (Wills et al., 2010). As discussed below, this has now been shown to be the case in mammalian PSCs.

The strongest argument for a role of FGF signaling in neural induction has come from studies in the chick embryo, where inhibition of FGF represses expression of neural markers even in the presence of BMP inhibitors (Stern, 2005). It has been suggested that in chick, BMP inhibition is more important for *maintenance* of neural markers in the

neural plate rather than their *initial* induction. Based on our current understanding, there are two important caveats to these observations: first, these studies were carried out before the differences in signaling pathways naïve and primed pluripotent cells were recognized in mouse and human embryos. As will be discussed below, it is now appreciated that FGF signaling promotes the transition of "naïve" inner cell mass cells to "primed" epiblast cells, which possess the competence to generate neuroectoderm upon TGFβ inhibition. Therefore it remains possible that FGF plays an important but permissive role, rather than an instructive role in chick neural induction as well. This is consistent with the observation that exposure 5 hours of FGFs is sufficient to make the chick epiblast competent to respond to BMP inhibitors and promote neural fate (Streit et al., 1998). Whether the pre-FGF chick epiblast resembles a naïve pluripotent state is not currently known. The second caveat in nearly all chick neural induction studies is that BMP signaling inhibition is not accompanied with concurrent Activin/Nodal inhibition (Wilson et al., 2000; Wilson et al., 2001; Linker and Stern, 2004). Co-inhibition of both BMP and Activin/Nodal branches is synergistic and required for inducing anterior neural fate (Chang and Harland, 2007). While it remains plausible that in chick the neural induction circuitry is wired to favor FGF signaling over TGFβ inhibition, a role for FGF signaling in promoting progression of an epiblast fate, followed by TGFβ inhibition for neuralization intuitively explains many of the observations and resolves many contradictions in chick neural induction experiments. Hence, studies specifically addressing these issues are required to clarify the role of FGF signaling in chick neural induction.

NEURAL INDUCTION IN MAMMALIAN EMBRYONIC STEM CELLS

Mouse and Human Pluripotent Stem Cells (PSCs)

About thirty years ago, mouse embryonic stem cells (mESCs) were derived from the blastocysts of the pre-implantation mouse embryo (Evans and Kaufman, 1981; Martin, 1981). These cells provided the functional definition of ESCs: unlimited proliferation with the ability to differentiate into cells from each of the three embryonic germ layers - ectoderm, mesoderm, and endoderm. These properties of ESCs are referred to as self-renewal and pluripotency, respectively. While self-renewal is a purely *in vitro* property, pluripotency has now been definitively demonstrated by the ability of ESCs to contribute to all tissues (including the germ cells) in developing embryos. In this assay, called morula aggregation, labeled mESCs are introduced into a wild type morula and allowed to develop normally; the resulting embryo is thus a chimera of two different starting cell populations (Bradley et al., 1984). Even more stringently, mESCs have been shown to generate entire mice in the tetraploid embryo complementation assay (Nagy et al., 1993). In this assay, tetraploid host cells are generated by application of an electric current. When cultured mESCs are mixed together with the tetraploid cells, the resulting embryo is derived exclusively from the diploid mESCs, whereas the tetraploid cells contribute exclusively to extra-embryonic tissue. This advance has enabled manipulation of the mouse germline.

Following the discovery of mESCs, NHP and human embryonic stem cells (hESCs) were subsequently derived from blastocysts (Thomson et al., 1998). Like mESCs, hESCs

demonstrate the hallmark characteristics of self-renewal and pluripotency. While the gold standard pluripotency assays of morula aggregation or tetraploid embryo complementation are ethically infeasible using human cells, hESCs have passed several standard tests for pluripotency including embryoid body differentiation and teratoma formation assays.

Over the past decade, somatic cells from both mouse and humans have also been reprogrammed to a pluripotent state (Takahashi and Yamanaka, 2006; Takahashi et al., 2007). The reprogrammed cells are called induced pluripotent stem cells (IPSCs) and were first generated by overexpression of a combination of four transcription factors (TxFs): POU5F1, SOX2, cMYC and KLF4 in the appropriate culture conditions. They display properties largely indistinguishable from their mouse and human ESC counterparts including pluripotency, self-renewal, teratoma formation, and the ability to contribute to germ layers on tetraploid complementation in the case of mouse IPSCs (Kang et al., 2009; Hanna et al., 2010).

The principal promise of stem cell biology is their utilization for novel *in vitro* models of poorly understood diseases and for cell replacement strategies in translational medicine. From a developmental perspective however, mouse and human PSCs provide an *in vitro* platform to test hypotheses and investigate mechanisms controlling embryonic fate determination. For the mouse system, ESCs serve to complement *in vivo* approaches, but for humans, ESCs constitute the only experimental window into early human embryogenesis.

Similarities and differences in the pluripotent state of mouse and human ESCs

Both mouse and human ESCs express identical embryonic TxFs such as OCT4 (POU5F1), SOX2 and NANOG during pluripotency, and form teratomas when grafted into adult mice (Hanna et al., 2010). However, there are also important differences between the two, including: signaling requirements, X-chromosome status, and growth characteristics. These differences are due to the fact that mESCs represent an earlier stage of development than hESCs as described below.

Mouse ESCs require LIF, BMP, and WNTs for the maintenance of a naïve (or "ground") state of pluripotency (Figure 1.9A) (Ying et al., 2008). Treatment of these cells with FGFs and Activin, and/or WNT inhibition induces a rapid conversion of mESCs to epiblast stem cells (EpiSCs) that self-renew and maintain pluripotency, but acquire the gene expression signature of post-implantation epiblast cells (Guo et al., 2009; ten Berge et al., 2011). This suggests that these signaling pathways also contribute to the transition from naïve to primed pluripotency *in vivo*. Mouse EpiSCs have distinct signaling requirements—Activin/Nodal and FGF—compared to mESCs (Hanna et al., 2010) and display and can also be derived directly from both pre- and post-implantation embryos (Brons et al., 2007).

Unlike mESCs, hESCs are dependent on Activin/Nodal, FGF, and Insulin signaling for maintenance of pluripotency (Figure 1.9B) (James et al., 2005; Vallier et al., 2005; Bendall et al., 2007; Vallier et al., 2009b; Vallier et al., 2009c; Singh et al., 2012). This property is similar to mEpiSCs, even though hESCs are derived from an equivalent embryonic source

as mESCs: the inner cell mass of pre-implantation blastocysts. It is thought that the derivation process accelerates the transition of hESCs to a more advanced stage of pluripotency than mESCs (Vallier et al., 2009a; Hanna et al., 2010). They are closer to the aforementioned EpiSCs in their developmental potential as well as their exclusive reliance on aerobic glycolysis, unlike mESCs (Zhou et al., 2012). Based on functional assays, it seems likely - though not formally proven - that the pluripotent cells of *Xenopus* animal caps are closer to the primed pluripotent state of mEpiSCs and hESCs than to the naïve state of mESCs since they can give rise to all the germ layer derivatives in the absence of priming (Dixon et al., 2010; Theunissen et al., 2011; Scerbo et al., 2012). It has been shown that NHP PSCs, such as from cynomolgus monkeys (*Macacca fascicularis*) also have similar signaling requirements as their human counterparts and exist in a primed state of differentiation (Ono et al., 2014). IPSCs derived from mouse, NHPs, and humans share identical signaling properties for maintenance and differentiation to the ESCs of the species from which they were derived. Hence, mouse IPSCs require LIF, BMPs and WNTs for maintaining pluripotency, while human and NHP IPSCs require Activin/Nodal, FGF and Insulin signaling (Yu et al., 2007a; Liu et al., 2008; Nakagawa et al., 2008; Park et al., 2008).

More recently, several groups have isolated “naïve” hESCs that resemble mESCs more closely in terms of growth characteristics, morphology, dependence on LIF and WNT signaling, gene expression patterns, and epigenetic characteristics (Chan et al., 2013; Gafni et al., 2013; Theunissen et al., 2014; Ware et al., 2014). Similar cells have been isolated from monkey ESCs as well (Fang et al., 2014). Whether these cells are correlates of an *in vivo* population or a synthetically stabilized *in vitro* state of pluripotency is not

clear at present. It is also unknown if the different naïve hESCs generated by the various groups represent different pluripotent states of the same cell type, or different cell types altogether.

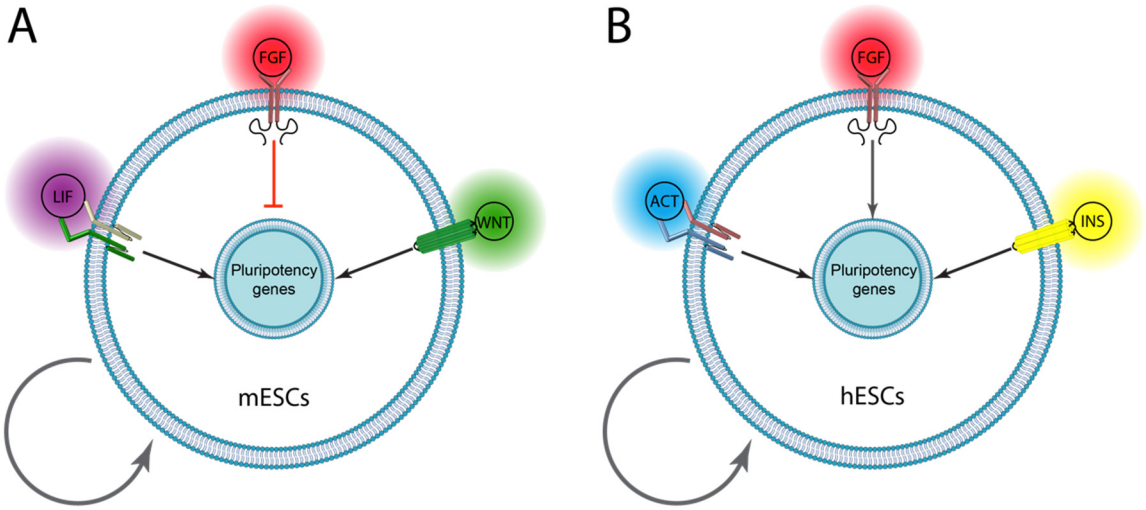

Figure 1.9: Signaling pathways are different between mouse and human PSCs. A) Mouse PSCs depend on LIF-STAT, canonical WNT, and inhibition of FGF-MEK signaling for self-renewal. B) human PSCs are dependent on FGF-MEK, INSULIN-PI3K, and ACTIVIN/NODAL-SMAD2/3 signaling for self-renewal. Once mouse PSCs convert to EpiSCs, they share the same pathways as hESCs, suggesting that hESCs represent a later stage of development compared to mESCs.

Neural induction in mouse ESCs/EpiSCs and the role of FGF signaling

Neural induction paradigms in mESCs have evolved over the past decade from culturing ESCs as EBs in serum- and RA- containing medium to co-culturing ESCs with cell lines possessing neural-inducing activity, and now to defined culture conditions utilizing some combinations of growth factors or small molecules. Here I will focus on the role of RA in neural differentiation, as it is well characterized and informative with respect to the

default model and address the controversy surrounding the role of FGF signaling in mouse neural induction.

A role for FGF in neuralization of mESCs had been suggested early on in many independent studies of neural differentiation in mESCs (Tropepe et al., 2001; Ying et al., 2003). Most of these studies, however, did not address whether FGF was acting directly or indirectly as a neuralizing factor. We now know that mESCs require FGF signaling to progress from a naïve to primed state of pluripotency i.e. the epiblast-like EpiSC state (also referred to as 'primitive ectoderm' in some of these studies), before they are competent to undergo neural induction (Kunath et al., 2007; Stavridis et al., 2007; Guo et al., 2009). Hence, as with chick embryos, it remains possible that the observed requirement for FGF signaling will be related to its role in priming mESCs for germ layer differentiation, rather than neural induction *per se*. This is supported by the fact that FGF signaling inhibits, rather than promotes neural induction in EpiSCs (Stavridis et al., 2007; Engberg et al., 2010; Greber et al., 2010; Sterneckert et al., 2010). Furthermore, small molecule inhibition of FGF signaling in ex vivo cultures of epiblast stage embryos accelerates anterior neural induction in control embryos (Di-Gregorio et al., 2007). In the EpiSC state, inhibition of Activin/Nodal and BMP signaling can induce anterior neural commitment from this cell type, thus revealing the default pathway of neural induction in this cellular context (Najm et al., 2011). It is worth noting that FGF signaling can also directly inhibit SMAD signaling by promoting the degradation of SMAD1 via linker phosphorylation in Xenopus animal caps, but this activity has not been demonstrated in mammalian PSCs (Pera et al., 2003; LaVaute et al., 2009). Thus, the requirements for FGF

can be explained by its role in the transition of mESCs to EpiSCs, which are then primed for differentiation and resemble human ESCs more closely.

It has been established for a long time that retinoic acid can direct the differentiation of mESCs and teratocarcinoma cells into a neural fate (Jones-Villeneuve et al., 1982; Strubing et al., 1995). While BMP4 can inhibit this neural inducing activity of RA (Finley et al., 1999; Engberg et al., 2010), it was unknown until recently whether RA acts through a separate parallel pathway to promote neural fate in mESCs or if it promotes transition to an EpiSC fate. RA acts via a bimodal mechanism to a) repress the pluripotency signaling pathways in mESCs and b) subsequently promote a neural fate. First, RA accelerates the transition of ESCs to EpiSCs by upregulation of Fgf8-MEK signaling and concurrent inhibition of WNT signaling (Engberg et al., 2010; Stavridis et al., 2010). Once the cells are in an EpiSC state, RA represses expression of Fgf4 as well as Nodal to promote a neural fate; the latter is achieved via inhibition of WNT signaling through a yet unknown cross-interaction (Engberg et al., 2010; Stavridis et al., 2010). It is worth noting that it has been previously shown that RA inhibits WNT signaling in mESCs/EpiSCs through induction of an extracellular inhibitor of WNTs, Sfrp2 (Aubert et al., 2002; Glaser and Brustle, 2005). Hence, the mechanistic studies of RA function also support the requirement of FGF signaling in transition from mESCs to mEpiSCs rather than in neural induction. Additionally, they also reveal the absolute requirement of inhibition of TGFβ signaling in EpiSCs for acquisition of neural fate.

Other protocols have also been developed for neural induction from mESCs that involve acceleration of transition of mESCs to EpiSCs. For example, differentiation of mESC aggregates (called “embryoid bodies”) with small molecule inhibitors of TGFβ and WNT signaling can also recapitulate major spatial and temporal milestones of cortical development and generated functional neurons with forebrain identities (Watanabe et al., 2005; Eiraku et al., 2008). The WNT inhibitor in this paradigm facilitates the transition of mESCs to EpiSCs initially, as discussed above; indeed, inhibition of endogenous WNT signaling in mESCs has been shown to readily promote their conversion to EpiSCs (ten Berge et al., 2011). Subsequently, WNT inhibitors serve to prevent the WNT-like posteriorizing activity of an undefined, albumin-rich component of the culture medium (Fasano et al., 2010; Menendez et al., 2011; Blauwkamp et al., 2012; Nakano et al., 2012). Interestingly, exogenous BMP4 completely abolishes neural induction in this setting (Kamiya et al., 2011). Taken together in light of emerging concepts, studies of mESC neural differentiation strongly support the relevance of the default model in mouse EpiSCs.

Neural induction in hPSCs

Many of the same protocols that have been used for neural induction in mESCs have also been adapted for neural differentiation of hESCs. Since hESCs do not survive as single cells, most early studies used cell aggregation approaches in the absence of exogenous factors to achieve differentiation. These so-called ‘embryoid bodies’ can be differentiated into anterior (forebrain) neural derivatives, expressing the neural determinant TxF PAX6 (Zhang et al., 2001; Pankratz et al., 2007). This could be interpreted to imitate a default

pathway of differentiation in the absence of exogenous signaling. Indeed differentiating cells in these paradigms display low levels of BMP-SMAD1/5/8 signaling, presumably due to the high-level expression of several soluble BMP antagonists such as Noggin, Follistatin, and Gremlin as well as intracellular inhibitors of BMP signaling such SMAD6. Several other differentiation protocols regularly include Noggin in serum-free medium to promote neuralization of hESCs (Itsykson et al., 2005; Yao et al., 2006). Hence these studies suggest that in the absence of exogenous morphogens or in the presence of BMP inhibitors, hESC aggregates take on an anterior neural fate.

Separately, inhibition of Activin/Nodal-SMAD2/3 signaling has also been shown to be a prerequisite for neuroectodermal differentiation in hESC cultures (Vallier et al., 2004; Patani et al., 2009; Vallier et al., 2009b; Chng et al., 2010). Combining the classical observations made in *Xenopus* animal cap explants with these studies in hESCs, Chambers et al. utilized small molecule inhibitors of Activin/Nodal and BMP signaling to demonstrate conversion of hPSCs to a neural fate (Chambers et al., 2009). As would be expected from the default model, the neuralized cells are of anterior identity, expressing the forebrain TxF OTX2. The primitive neuroepithelium generated from this protocol can be subsequently patterned into multiple regional CNS derivatives, including ventral telencephalon, hypothalamus, cranial placodes, midbrain, floor plate, and spinal cord in the presence of appropriate signaling cues (Christopher et al., 2010; Kriks et al., 2011; Dincer et al., 2013; Maroof et al., 2013; Maury et al., 2015). This paradigm provides support for the “activation-transformation” model of Nieuwkoop discussed above (Figure 1.10).

A role for endogenous FGF signaling has been as a requirement for neural induction in some studies, since small molecule inhibitors of FGF signaling reduce the number of cells expressing PAX6 (Zeng et al., 2010; Yoo et al., 2011). However, in these studies FGF or FGF inhibitors were added at late stages of differentiation, a time point at which the cells have already initiated the neural program (Zhang et al., 2001; LaVaute et al., 2009; Yoo et al., 2011). This suggests that FGF signaling does not directly promote neural induction in these experiments, but rather has a proliferative role for the early neuroepithelium. In support of this idea, exogenous FGF increases the size of neural colonies without changing the efficiency of neural induction (Pankratz et al., 2007). Indeed, it has since been shown that FGF signaling directly inhibits induction of PAX6 in hESCs and prevents neuroepithelial differentiation (Greber et al., 2011). This is in line with the inhibitory role of FGF in neural induction of EpiSCs derived from mouse embryos (Greber et al., 2010). Together, the available evidence suggests that FGF has no role in neural induction of hESCs in the presence of TGFβ inhibitors. It is worth noting that FGF does play a role in areal specification of the neuroepithelium, as it does *in vivo*. For instance, FGF8 promotes expression of anterior telencephalic areal TxFs in neuralized hESCs, while FGF2 upregulates expression of spinal cord markers (Patani et al., 2009; Chng et al., 2010; Lupo et al., 2013).

More recent studies have shown that neuroectoderm generated by TGFβ inhibition in hESCs/hIPSCs that can also recapitulate many aspects of corticogenesis, including human specific aspects which will be discussed in sections below (Shi et al., 2012; Kadoshima et al., 2013). The serum free embryoid body protocol involves aggregation of hESCs followed

by inhibition of Activin/Nodal and WNT (Kadoshima et al., 2013). WNT inhibitors in this system serve to prevent mesendodermal and neural crest differentiation in the initial phases, and subsequently block the effect of WNT-like posteriorizing signals in the culture medium.

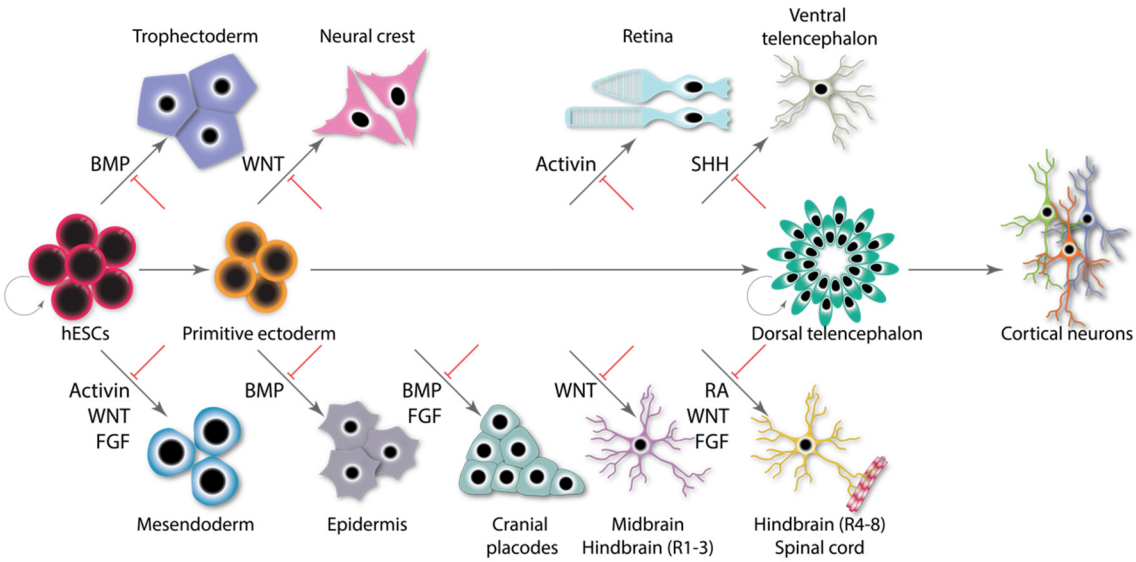

Figure 1.10: Schematic of induction of anterior neural fate (dorsal telencephalic) in hESCs by a "default mechanism". Inhibition of TGFβ in the absence of other growth factors or morphogens is sufficient to recapitulate the developmental trajectory uptil early neuroepithelium by blocking all alternative fates.

In summary, work in hESCs provides the strongest evidence so far of the conservation of molecular mechanisms underlying neural fate specification from *Xenopus* to humans and conforms to the predictions of the default model (Figure 1.10).

PATTERNING AND PROGENITOR DIVERSITY DURING MAMMALIAN CORTICOGENESIS

Neural tube closure and establishment of the telencephalic territory

In mammalian embryos, as in *Xenopus*, the origins of the CNS can be traced to gastrulation, where the inhibitors released by the node and AVE coordinately induce the earliest neuroectodermal cells in anterior part of the embryo that forms the neural plate. These neuroectodermal cells possess epithelial characteristics and display an apical-basal polarity – hence they are referred to as neuroepithelium. As stated above, the first neural specific TxF expressed by these cells differs between mice and NHPs: mouse neuroepithelium expresses Sox1, while the NHP neuroepithelium expresses PAX6 (Zhang et al., 2010). Under the influence of local signaling centers, the neuroepithelium undergoes spatial patterning in the antero-posterior (AP) axis; the anterior most part of the neural plate will assume a forebrain (prosencephalon) identity, and subsequent segments will be patterned into midbrain (mesencephalon), hindbrain and spinal cord (together called rhombencephalon). The signals patterning the neural tube in the AP axis include FGF8 for forebrain (originating in the anterior neural ridge), WNT3A for midbrain (isthmic organizer), WNT3A and retinoic acid (RA) for hindbrain (arising in the isthmic organizer and somitic mesoderm respectively), and WNT, FGF2 and RA (somitic mesoderm) for the spinal cord (Murielle et al., 2002). At the end of neural tube closure (E8.5 in the mouse, PCD22-24 in human), the prosencephalon, mesencephalon, and rhombencephalic segments each form visible brain vesicles. The walls of the forebrain evaginate to generate the neural folds comprising the telencephalic (anterior) and diencephalic (posterior) vesicles (at E9-E10 in mouse, PCW5 in human) (Figure 1.11).

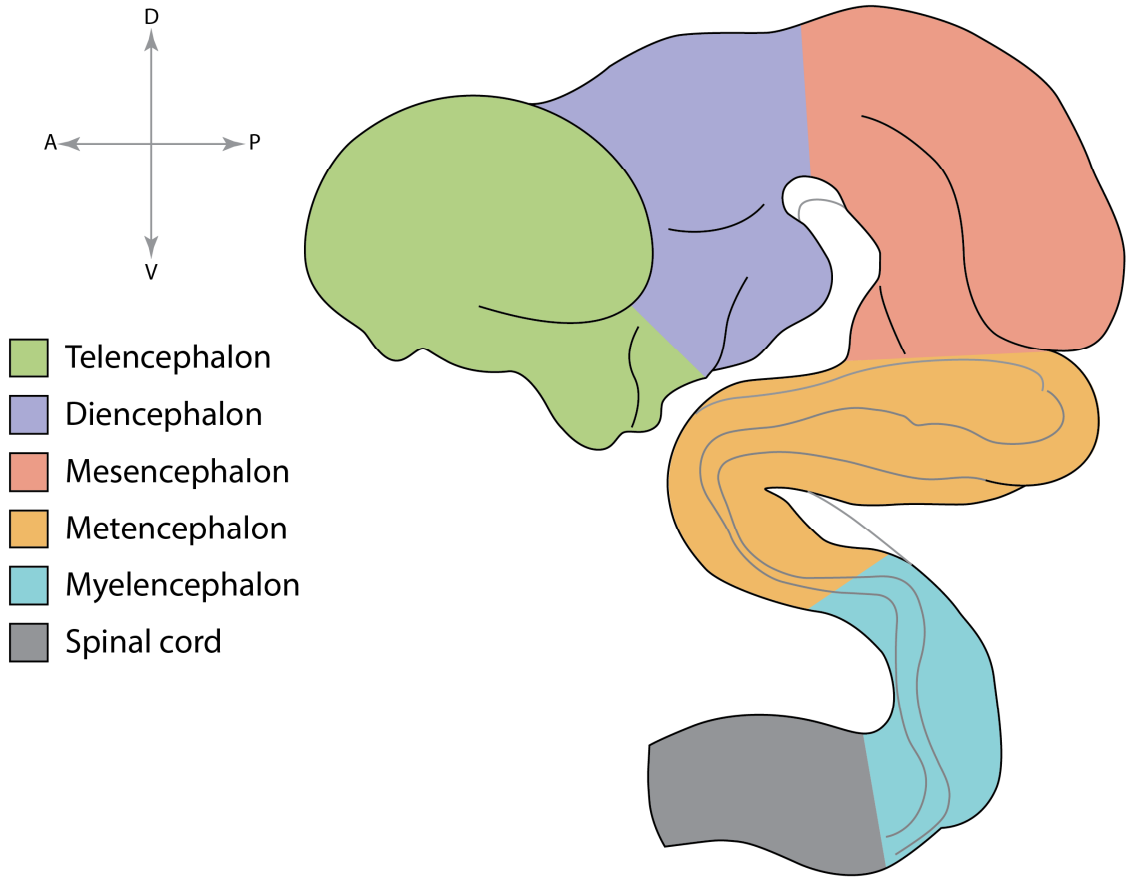

Figure 1.11: Schematic of a PCW5 human fetal brain in sagittal section showing the major CNS segments. The telencephalon and diencephalon together comprise the prosencephalon, while the metencephalon and myelencephalon together comprise the rhombencephalon.

As the neural plate undergoes folding to generate the neural tube, the mediolateral axis of the neural plate axis is converted into the dorsal-ventral (D-V) axis (Figure 1.12). The leading edges of the neuroectoderm-epithelial boundary from either end will fuse together in the midline to form the roof plate dorsally. The roof plate becomes a source of BMP signals to pattern the dorsal neural tube (Murielle et al., 2002). The floor plate will form ventrally under the influence of Sonic Hedgehog (SHH) signaling from the notochord (located below the neural plate) by homeotic induction; SHH secreted from the floor plate will in turn pattern the ventral neural tube (Murielle et al., 2002). In the

midbrain, hindbrain, and spinal cord, BMP signals will specify populations of ascending interneurons dorsally; SHH will specify motor neurons ventrally. A population of interneurons will also arise close to center, where both BMP and SHH gradients are low. Hence, following DV specification the embryo will have strips of motor, intermediate, and sensory neuron progenitors running parallel to the midline posteriorly from the midbrain. In the forebrain however, BMP and SHH specify different populations. Dorsally, BMP signaling in the midline (called cortical hem) will specify the choroid plexus (Hébert et al., 2002; Fernandes et al., 2007). On the ventral side, gradients of SHH from the notochord will establish a ventral territory and specify various classes of neurons depending on the concentrations of SHH the progenitors are exposed to (Murielle et al., 2002). The entire cortex is derived from the dorsal telencephalon, while the ventral telencephalon will give rise to the striatum, the septal area and hypothalamus, as well as nearly all interneurons in the cortex.

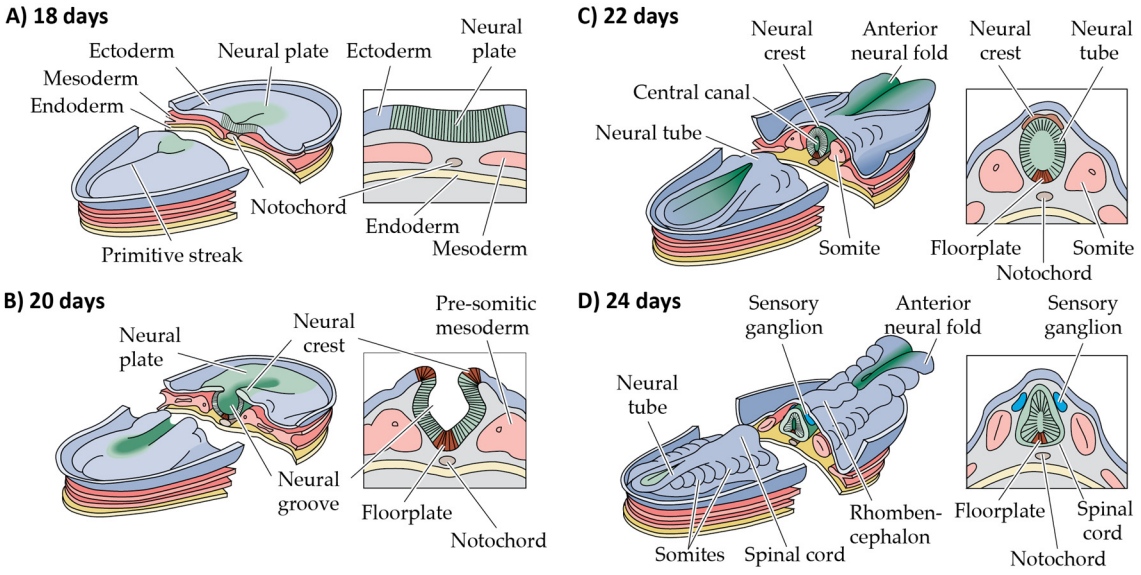

Figure 1.12: Schematic of neural tube formation in a human embryo at A) 18 days, B) 20 days, C) 22 days, and D) 24 days post conception showing folding of the neural plate and neural tube closure. Modified from Purves et al. (Purves, 2012).

Organization of the cerebral cortex

There are three different modules that comprise the cerebral cortex, named based on their phylogenetic origins: the archicortex, paleocortex, and neocortex (Figure 1.13). The archicortex is evolutionarily the most ancient structure of the cerebral cortex, while the neocortex is the most recent and the largest contributor in the mammalian brain. Histologically, both the archi- and paleo-cortices are comprised of three to four discrete layers of neurons, while the neocortex is comprised of six layers and is exclusively present in mammals (Cheung et al., 2010). Two major neuronal types are found in these layers: about 80% of the cells are pyramidal neurons, which are the primary processing unit of the cortex, while the rest are interneurons. While there is an enormous diversity in the types of pyramidal cells, they are all excitatory in nature, share glutamate as their primary

neurotransmitter, and project over long distances either to other parts of the cortex or to subcortical structures (Kumamoto and Hanashima, 2014).

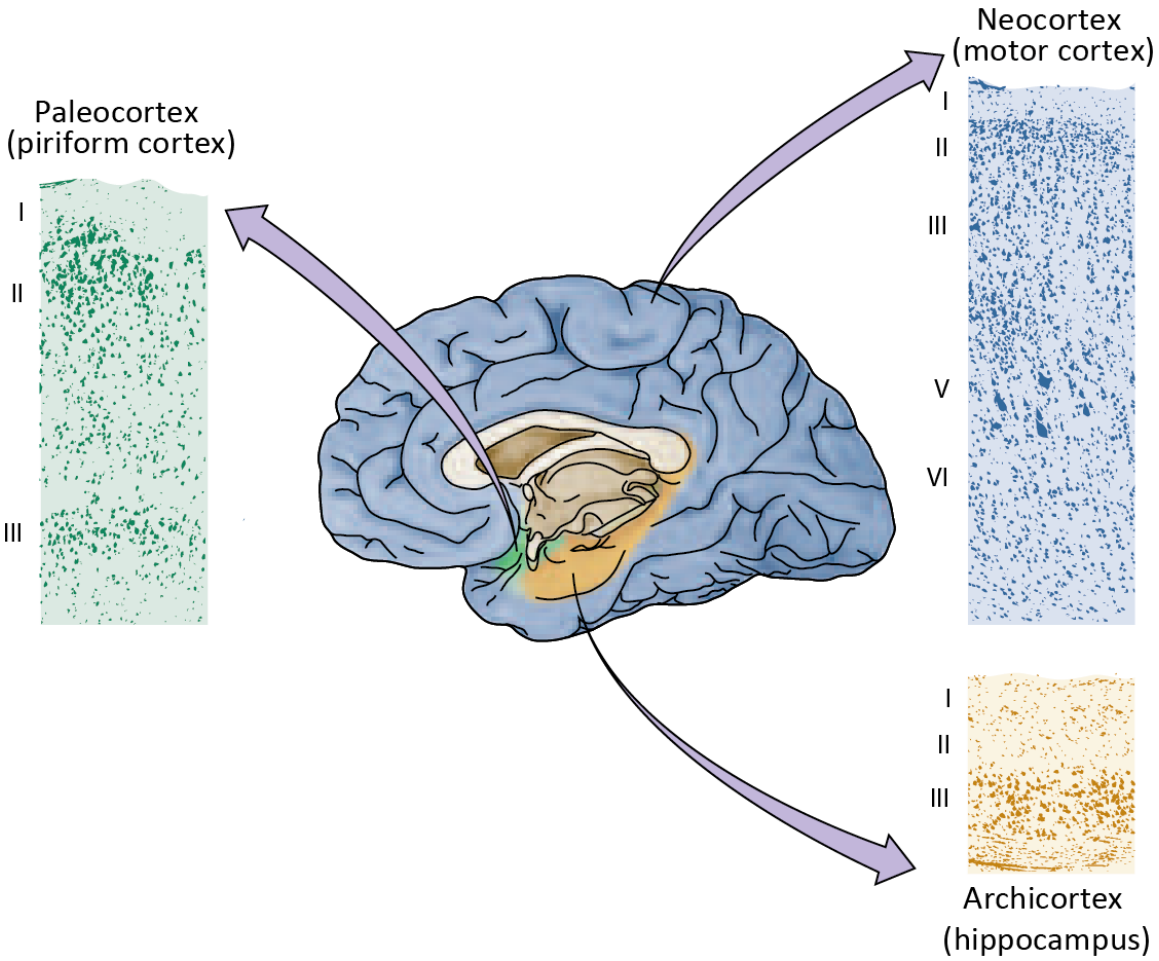

Figure 1.13: The three modules of the cortex – the archicortex, paleocortex, and neocortex. Modified from Purves et al. (Purves, 2012).

Unlike pyramidal cells, which arise locally in the dorsal telencephalon, interneurons are generated in the ventral telencephalon and migrate tangentially into the dorsal telencephalon. They are inhibitory in nature, secrete GABA (γ -aminobutyric acid) as their primary neurotransmitter, and are intimately associated with pyramidal neurons to regulate their activity and influence local circuitry (Hansen et al., 2013; Ma et al., 2013). Most interneurons in the cortex are generated in three areas of the fetal telencephalon,

all located ventrally: the medial, lateral, caudal ganglionic eminences (Kepecs and Fishell, 2014). It has been proposed that interneurons may be formed dorsally specifically in the NHP and human neocortex; however this remains the subject of debate as human cases of ventral forebrain hypoplasia lack most major classes of interneurons in the cortex (Fertuzinhos et al., 2009; Molnar and Butt, 2013; Whalley, 2013; Radonjic et al., 2014). A specific type of interneuron, called Cajal-Retzius (CR) cells are found exclusively during development and are glutamatergic in nature, unlike other interneurons (Soriano and Del Rio, 2005). CR cells are generated in three locations in the cortex: the cortical hem, the septal area, and the pallial-subpallial boundary, from which they migrate to Layer I of the cortex. During corticogenesis, CR cells are essential for secretion of the extracellular glycoprotein reelin, which enables migration of pyramidal neurons destined for the superficial layers (Soriano and Del Rio, 2005).

The six layers of the neocortex are morphologically, molecularly, functionally, and electrophysiologically distinguishable (Figure 1.14). It is believed that the hodological properties of the laminae-specific neurons are encoded in the progenitors that generate them (Dehay et al., 2015). The subplate and cortical layer VI neurons connect the cortex to the thalamus, hence their designation as corticothalamic projection neurons (CThPN). Layer V consists of large pyramidal cells that connect the cortex to various subcortical structures such as the spinal cord, brainstem, and striatum. They are henceforth referred to as subcortical projection neurons (SCPNs). Layer IV contains stellate shaped neurons and send projections within cortical structures and across the corpus callosum; it is the largest recipient of thalamocortical afferents. Layers II-III are comprised of small

pyramidal neurons that mainly send projections intra-cortically. Together, I will refer to layers II-IV henceforth as callosal projection neurons (CPN). Some neurons in layers II-IV do not send axonal tracts cross the corpus callosum but rather project into other areas of the cortex - hence they are also referred to as intracortical projection neurons.

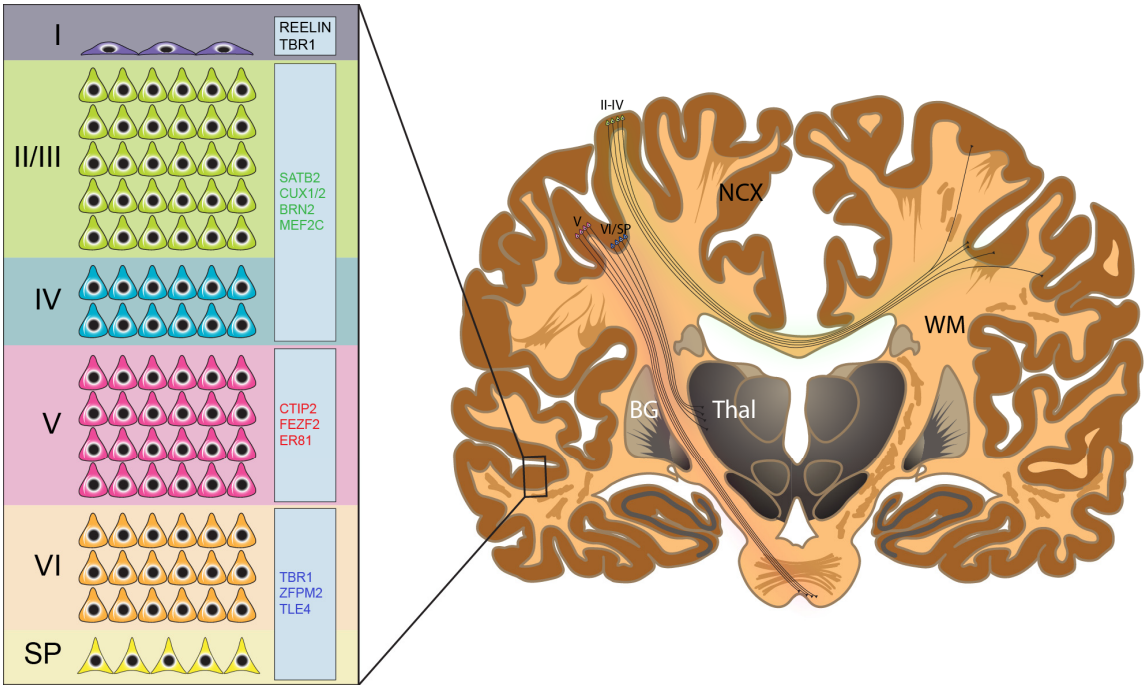

Figure 1.14: Coronal section through an adult human brain showing the neocortex in dark brown. The six layers of neocortex are shown on the left, together with relevant molecular markers expressed in these layers. Markers shaded green (SATB2, CUX1/2, BRN2, MEF2C) are specific for CPNs, red (CTIP2, FEZF2, ER81) for SCPNs, while blue (TBR1, ZFPM2, TLE4) are for CThPNs. The typical projections of each of these classes of neurons is shown on the right. The markers labeled in red, green, and blue are enriched in their respective layers. NCX: neocortex, WM: white matter, BG: basal ganglia, SP: subplate, Thal: thalamus.

The progenitors underlying corticogenesis

Neuroepithelial cells generated during gastrulation initially form a pseudostratified columnar epithelium. Following neural tube closure, they progressively become

elongated and acquire bipolar projections, which are classical features of radial glial cells (RGs; Figure 1.15) (Kriegstein and Alvarez-Buylla, 2009). RGs have their cell bodies located close to the ventricular cavity in an area called the ventricular zone (VZ). As the master progenitors of the entire CNS (Anthony et al., 2004), they can divide both symmetrically to generate two daughter RGs as well as asymmetrically to generate a daughter RG and a migratory neuron (Noctor et al., 2004). The former mode of cell division predominates immediately after neural tube closure, while the latter mode predominates during the neurogenic phase of corticogenesis. Asymmetric cell division of RGs – and hence neurogenesis - occurs around E12.5 in mouse embryos (PCW6 in humans). RGs express molecular markers of: 1) neural identity (such as PAX6, SOX2, PLZF, BLBP), 2) apico-basal polarity (e.g. ZO1, aPKC, PAR3/6, N-CAD, prominin, β-catenin), 3) Notch signaling (e.g. CBF1, Notch1, Hes1/3/5), and 4) cortical and areal identity (e.g. FOXG1, LHX2, EMX1/2, OTX2, NR2F1) (Figure 1.15). In addition to generating all the neurons in the nervous system, they also give rise to all macroglia, such as astrocytes and oligodendrocytes at later stages of corticogenesis (Kriegstein and Alvarez-Buylla, 2009).

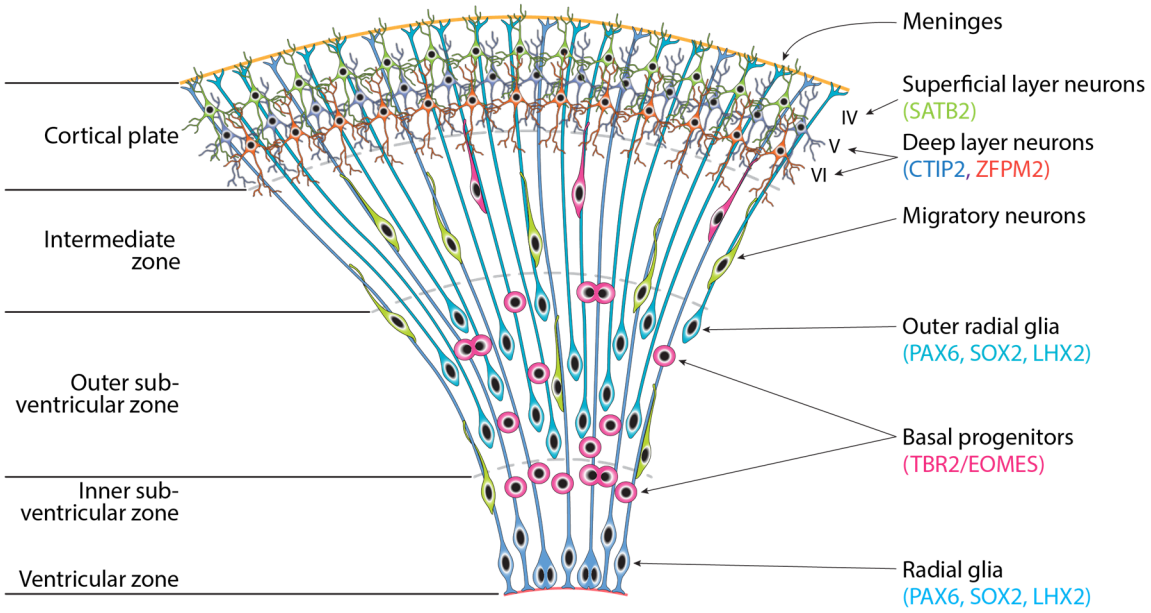

Figure 1.15: Schematic of the progenitor compartments in the human fetal cortex at PCW14 showing the ventricular zone, inner and outer subventricular zone, and the cortical plate. The superficial layer neurons have to migrate past the deep layer neurons in the cortical plate.

The Notch signaling pathway is essential for the maintenance of RG fate both at early later stages of corticogenesis by inhibition of pro-neural bHLH factors (Figure 1.16) (Lui et al., 2011; Taverna et al., 2014). Indeed, all components of the Notch pathway are enriched in RGs except for notch ligands, which are provided by their differentiating progeny. Deletion of CBF1 (also known as RBPJ), a DNA binding cofactor of the Notch Intracellular Domain (NICD) results in premature neurogenesis, exhaustion of the RG pool, and severe thinning of the cortical wall (Imayoshi et al., 2010). Similar phenotypes are observed with deletion of MIB1 (Mindbomb 1), an E3 ubiquitin ligase required for endocytosis of Notch ligands in signal-sending cells to promote NICD generation in signal receiving cells (Yoon et al., 2008), or with triple knockout of the bHLH factors Hes1/3/5, all Notch effector genes (Hatakeyama et al., 2004). Conversely, mouse mutants of Numb and Numblike – which are asymmetrically inherited by RGC daughter cells and inhibit Notch signaling in

one of the daughter cells – display striking defects in neuronal differentiation and laminar formation (Li et al., 2003). This is accompanied by a sharp increase in RG proliferation and a delayed cell cycle exit. Together, these studies firmly establish a requirement for Notch in the maintenance of the early neuroepithelium and RGs (Lui et al., 2011), a role that is conserved from Drosophila neuroblasts (Gaiano and Fishell, 2002). How Notch maintains the cells in an RG state is less well understood. It is known that Notch represses proneural bHLH genes such as Ascl1 and Neurog1/2 in RGs in an oscillatory manner (Imayoshi and Kageyama, 2014). Current models propose that upon asymmetric division of RGs, Notch signaling remains active in only of the daughter cells because of two factors. First, there is an asymmetric inheritance of the basal process by one of the daughters, and with it, the ability to respond to Notch ligands presented by differentiated cells in the SVZ. Second, the unbound Numb is inherited by the non-basal process bearing daughter cell. Numb can functionally inhibit Notch and permit expression of the proneural bHLH factors, thus allowing neuronal differentiation to proceed (Lui et al., 2011). However, in the daughter cell that inherits the basal process, Numb is sequestered by the apical junctional complexes and rendered inactive. This permits active Notch signaling and maintenance of RG fate.

In addition to RGs, which lie in the VZ, there are two other proliferative cell types that have been described in mammals: intermediate progenitor cells (IPs), and basal radial glia (bRG). Both these progenitor types arise by asymmetric division of RGs and occupy a compartment called the subventricular zone (SVZ) which lies above the VZ in the radial plane (Figure 1.15). The SVZ is itself divided into inner and outer compartments, with IPs

being the main cellular composition of the inner SVZ. The outer SVZ (OSVZ) has a much more diverse composition of progenitors which include IPs, bRGs, and other transit amplifying progenitors (Lui et al., 2011). The OSVZ is a prominent zone in carnivores and has undergone massive expansion in NHPs relative to both the VZ and inner SVZ (Figure 1.17) (Reillo et al., 2011). There is a strong correlation between the size of the OSVZ and the extent of gyrencephaly in the various mammalian species, suggesting that progenitor expansion has a direct consequence on the cortical surface area and hence, cognitive function.

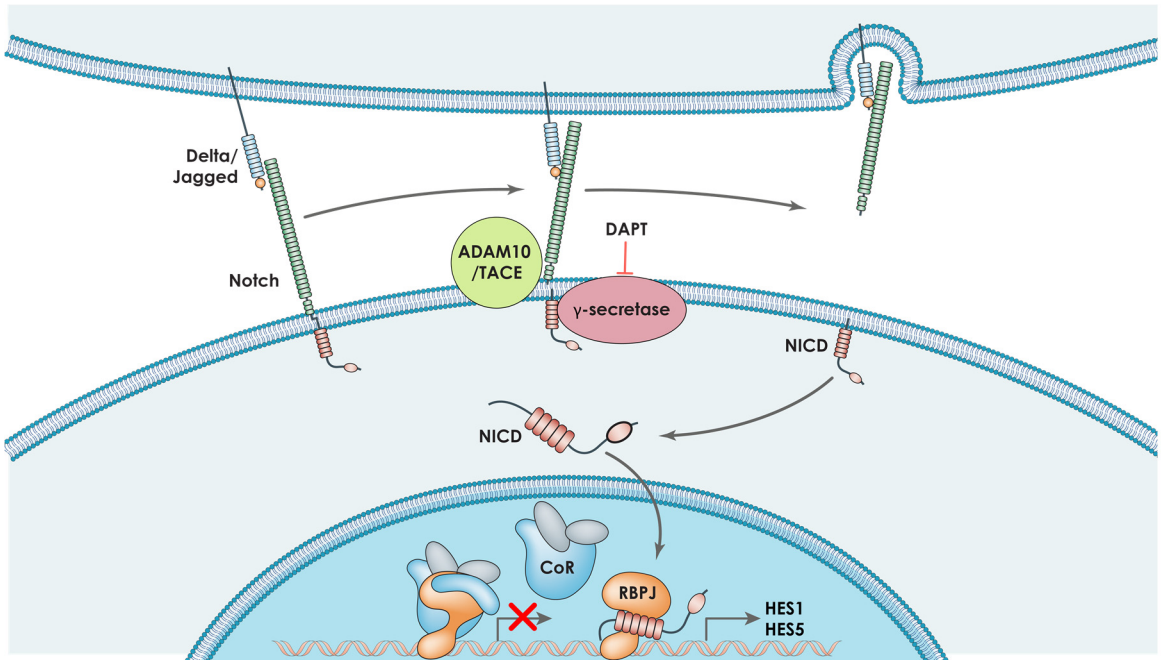

Figure 1.16: The Notch signaling pathway.

Asymmetric division of RGs can generate neurons directly, but a large number of RGs also generate neurons indirectly through IPs. IPs are found in all eutherians and are characteristic feature of a six layered cortex. They are multipolar cells that lack both apical and basal processes and are identified by their expression of TBR2 (also called EOMES)

(Figure 1.15). This TxF is both necessary and sufficient to give rise to this cell type (Sebastian et al., 2008; Sessa et al., 2008). IPs are thought to be transit amplifying progenitors that contribute cells to all layers of the cortex (Vasistha et al., 2014), even though originally they were believed to largely contribute to the superficial cortical layers (Arnold et al., 2008). It is thought that up to two-thirds of all pyramidal cells in the mouse cortex arise indirectly from RGs via IPs (Vasistha et al., 2014). Consistent with this observation, an artificial increase in the proliferative rate of the IPs in mice via overexpression of cyclin D/CDK4 results in an increased thickness of a normal six layered cortex (Nonaka-Kinoshita et al., 2013). The importance of IP's to human corticogenesis is provided by the observation that TBR2 silencing on both alleles due to a balanced translocation is associated with severe brain defects in children including microcephaly, polymicrogyria, agenesis of the corpus callosum, mental disability, motor delay, and early lethality (Baala et al., 2007). Recent studies also suggest that IPs also have an areal identity, and that they relay the positional information of the VZ RGs to the cortical plate. In Tbr2 knockout mice, the areal map of the SVZ is altered, and this is reflected in cortical plate arealization (Elsen et al., 2013).

Unlike RGs, IPs are exclusively neurogenic (Ken-ichi et al., 2007) and also provide Notch ligands (such as Dll) for the maintenance of RGs and presumably bRGs (Campos et al., 2001; Ken-ichi et al., 2007; Yoon et al., 2008). The behavior of IPs differs between mice and NHPs, as mouse IPs mostly undergo terminal symmetric differentiation into neurons, while NHP IPs have the potential to asymmetrically self-renew for a few divisions prior to terminal neuronal differentiation (Kriegstein et al., 2006; Lui et al., 2011; Betizeau et al.,

2013). This property contributes to the overall theme of progenitor amplification in the NHP cortex and allows for the increase in the size, number, and diversity of neurons in the neocortex. IPs have been shown to require thyroid hormone for self-renewal that act via αvβ3 integrin receptors (Denise et al., 2014).

The third progenitor type, bRG cells, have been described only recently (Figure 1.15) (Fietz et al., 2010; Hansen et al., 2010). bRGs are found in most mammalian species studied, though they are present in significant numbers only in species with a prominent OSVZ (Reillo et al., 2011). bRGs are the predominant progenitor during mid- to late-corticogenesis in NHPs and humans (Hansen et al., 2011; Marion et al., 2013). They share most characteristics of RGs, including marker expression, reliance on notch signaling for self-renewal, ability to divide both symmetrically and asymmetrically, as well as the ability to give rise to IPs neurons (Lui et al., 2011; Elena et al., 2013; Borrell and Gotz, 2014; Sun and Hevner, 2014). bRGs differ from RGs in three ways: first, they do not contact the ventricular surface and only possess a basal process; second, they are located in the OSVZ rather than the VZ; and third, they appear much later in development compared to RGs, about PCW12 in humans. Since bRG cells do not contact the ventricles, they do not express markers of apico-basal polarity (Fietz et al., 2010). Though initially thought to be specific to gyrencephalic species due to the enormous expansion of the OSVZ in this group, it is now known that lissencephalic NHPs such as marmosets and rodents also possess bRGs that divide infrequently (Garcia-Moreno et al., 2012; Hevner and Haydar, 2012; Kelava et al., 2012). Intriguingly, an artificial localized increase in the number of bRGs in mice – which normally only have rare bRG cells – by gene knockdown of a DNA

binding protein TRNP1 results in localized gyrification of a normally smooth cortex (Stahl et al., 2013). Furthermore, overexpression of cyclin D/CDK4 in the OSVZ of ferrets – which are gyrencephalic species – results in an increased surface area of the cortex accompanied by additional cortical folds (Nonaka-Kinoshita et al., 2013). However, this treatment does not induce folding in mice despite increasing the cortical thickness and marginally increasing the cortical surface area. Hence, it is the frequency of bRG cells (and other basal progenitors) as well as their cell cycle characteristics (such as a shortened G1-phase as discussed below) rather than their presence *per se* that contributes to gyrencephaly. Regardless, bRGs are well positioned to contribute to the increasing diversity and number of CPNs over evolution due to their appearance during the developmental timeframe of this neuronal class. Together with their suspected role in gyrencephaly, it is likely that their presence has contributed to improved cognitive abilities in humans, itself thought to be due to expansion of the superficial cortical layers (Figure 1.16) (Hill and Walsh, 2005; Lui et al., 2011; Reillo et al., 2011; Dehay et al., 2015).

Other progenitors have also been reported in the VZ and SVZ of mammals (such as subapical progenitors and short neural precursors) (Pilz et al., 2013) but it is unclear if they are bonafide class of progenitors or an intermediate state of transition between RGs to IPs or between various bRGs (Betizeau et al., 2013; Greig et al., 2013). With this introduction of the various progenitors populating the developing brain, I will now turn to our current understanding of the establishment of cortical layers during corticogenesis.

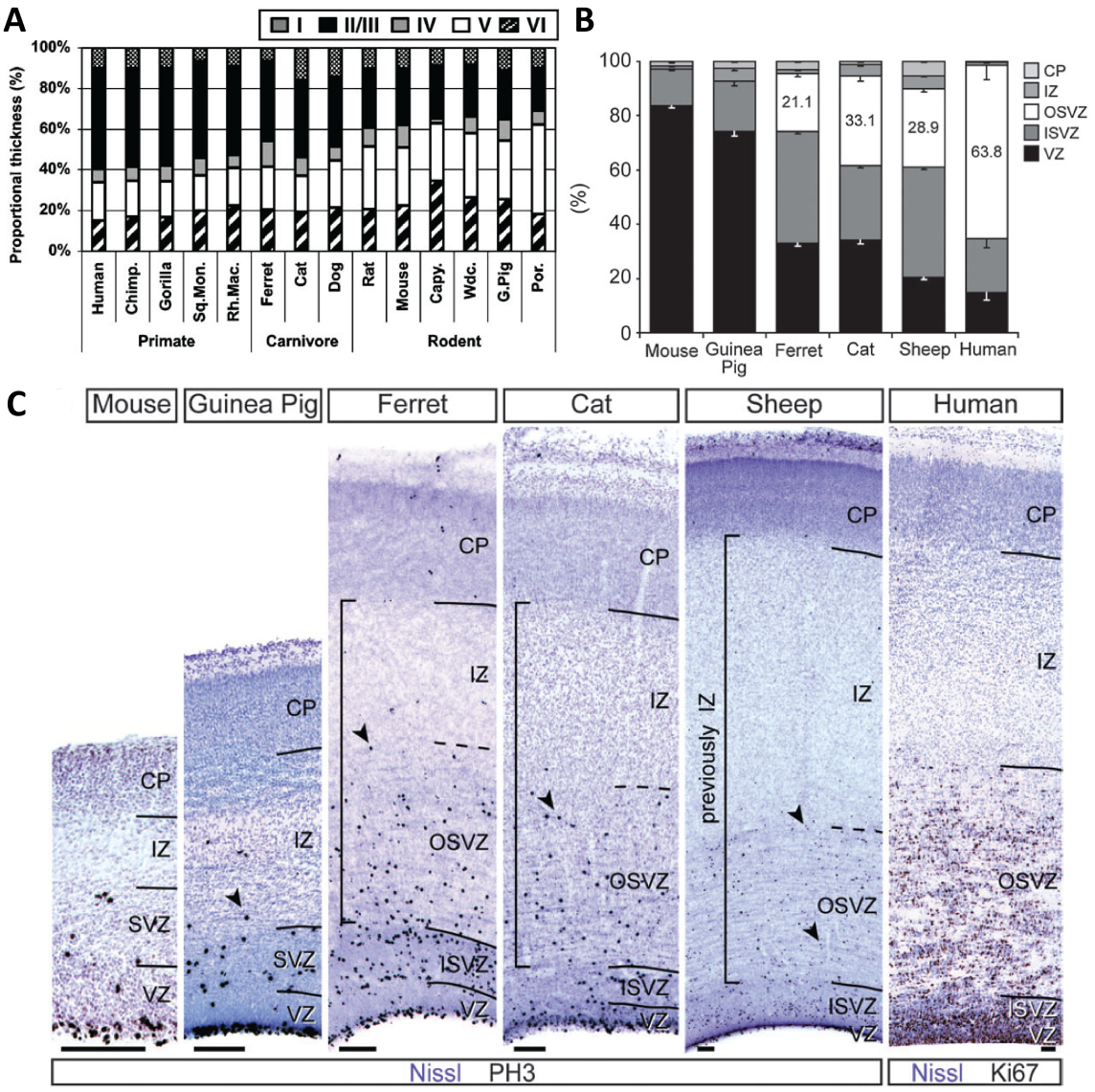

Figure 1.17: Primate specific aspects of corticogenesis. A) There is a progressive increase in the relative thickness of the superficial cortical layers (that contain CPNs) during mammalian evolution. B) This increase is manifested during development as an increase in size of OSVZ, the major site of neurogenesis of superficial layers. C) Nissl stained cross-sections of the cerebral cortex from different species at identical developmental stages showing an increase in OSVZ thickness from mouse to humans. Panel A adapted from (Hutsler et al., 2005), panels B and C adapted from (Reillo et al., 2011). Scale bars: 100µm.

Establishment of the six-layers during corticogenesis

From classic birth-dating studies in NHPs, it is known that the neocortex is generated in an inside-out manner, with waves of neuronal migration from the proliferative zone into the cortical plate to form layers VI, V, IV, and II-III, in that order (Figure 1.18) (Pasko, 1974). This mass migration splits the early cortical plate (called preplate) into subplate and Layer I neurons, which will have an important role later in migration, axonal pathfinding, and synaptogenesis of neurons in the other layers (Kwan et al., 2012). The inside-out manner of neuronal generation has been shown to be conserved in all mammalian species studied including mice, ferrets, and NHPs (Angevine and Sidman, 1961; Pasko, 1974; Jackson et al., 1989), though the timing varies considerably between species (Figure 1.19). Hence, CThPN are formed first (along with Layer I CR cells), followed by SCPNs, while CPNs are formed last. In *reeler* mutant mice, there is a severe disorganization of the normally continuous laminae and a complete inversion of the layers in some areas (Boyle et al., 2011). The *reeler* phenotype is due to a mutation in reelin, a large glycoprotein involved in migration of superficial neurons (mostly CPNs) through its interaction with three receptors: ApoER2, VLDLR and EphrinB (Bouche et al., 2013). This mouse mutant highlights the importance of Layer I CR cells in establishing the laminar pattern observed in the neocortex and provides strong evidence that the connectivity of all classes of cortical projection neurons is dependent on their birth date rather than their final position in the cortical plate. Thus, the molecular identity of projection neurons and their neuronal connectivity is determined by the intrinsic properties of the neurons and their progenitors rather than their position in the cortical plate (Rakic, 1988; Han and Sestan, 2013).

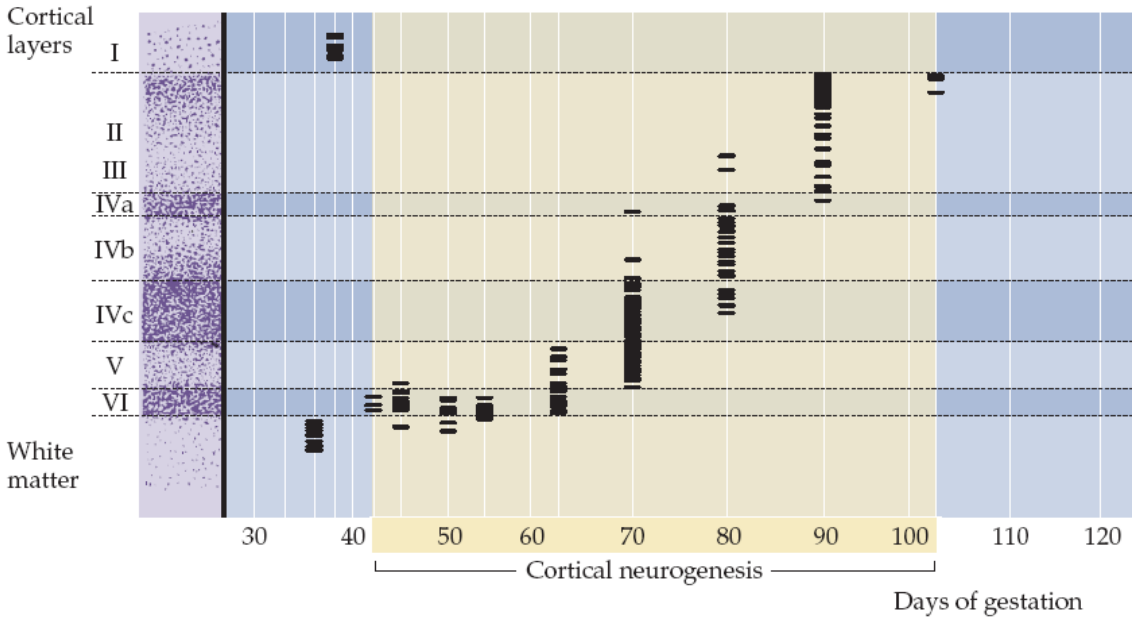

Figure 1.18: Inside-out pattern of neuronal migration in a developing NHP cortex. The proliferating cells were labeled with tritiated [^{3}H] thymidine and the label retaining cells followed in the postnatal cortex (3 months). Image adapted from Purves et al. (Purves, 2012); original experiment detailed in (Pasko, 1974).

During the course of development, the symmetric and asymmetric cell divisions of a given RG form a clonal proliferative unit. The daughter neurons resulting from the asymmetric divisions migrate towards the cortical plate using the parental RG as scaffolding, and maintain a spatial register with it throughout (Torii et al., 2009). Collectively, the clonal proliferative unit and the daughter neurons stacked above them form an ontogenetic column. This is principle idea behind the Radial Unit hypothesis originally proposed by Rakic (Rakic, 1988). Daughter neurons from the same parental RGs are more likely to form functional electrical connections with each other, and are functionally similar (Li et al., 2012; Yu et al., 2012). Thus the neocortex can be viewed as a parallel array of overlapping ontogenetic columns, with the number of *symmetric* proliferative divisions of parental RGs in these columns determining the size of a cytoarchitectonic area. On the other hand,

the number of *asymmetric* divisions underwent by RGs (and their daughter progenitors) determines the thickness of the cortex in a given area. These columns are then refined on the basis of incoming cortical inputs from subcortical structures such as the thalamus as discussed below. In the adult cortex, the ontogenetic columns of development are represented as cortical columns, which are the basic computational unit of the cerebral cortex.

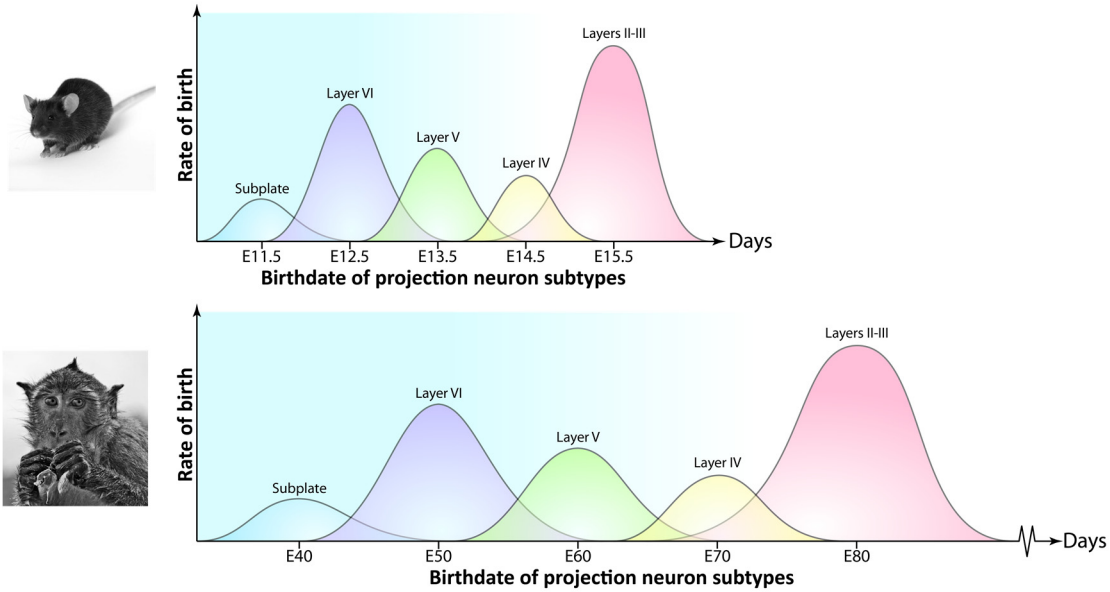

Figure 1.19: The timing of corticogenesis in mice and NHPs. In mice, corticogenesis takes place over a 5 day period, while in NHPs, it takes about 50 days. The peaks of corticogenesis are an approximate and the rate of birth is not shown to scale. Modified from Rakic and Greig et al. (Rakic, 1974; Greig et al., 2013).

While there is strong experimental support of the Radial Unit model, recent findings have mandated several revisions to it. First, most interneurons – which are also essential contributors to the cortical columns, arise in the ventral telencephalon and migrate tangentially to populate the various layers in these columns. Second, in NHPs there is an expanded proliferative compartment of progenitors derived from RGs, which are the

predominant contributors to the superficial cortical layers. Due to the presence of this compartment, there is a logarithmic amplification of neurons in an ontogenetic column, resulting in a lateral expansion of the area occupied by RG clones from the ventricular to the pial surface. Hence, in NHPs the ontogenetic column is shaped like an inverted cone, with the apex at the ventricular surface and the cortical layers forming the base. In mice, the columns are more cylindrical due to the absence of this secondary proliferative zone (Lui et al., 2011; Taverna et al., 2014).

It has been shown that formation of a six-layered cortex in mice requires the presence of two TxFs in particular: FOXG1 and LHX2. In the absence of either factor, the neocortex fails to be specified and is replaced either by archicortex (FOXG1) or by paleocortex (LHX2) (Molyneaux et al., 2007; Kumamoto and Hanashima, 2014). While LHX2 is only required in the early stages of neocortical specification, the requirement for FOXG1 continues even during corticogenesis, where it represses CR cell fate, sets the schedule of corticogenesis, and coordinates neuronal migration (Hanashima et al., 2004; Chou et al., 2009; Miyoshi and Fishell, 2012; Toma et al., 2014). BMPs and FGF8 are known to modulate FOXG1 levels after neural tube closure and formation of the telencephalon. However, the signaling pathway(s) that modulate FOXG1 and LHX2 at earlier stages of development are currently unknown. Since the requirement for TGFβ inhibition in cortical development is conserved in vertebrates, and among this group, only mammals have a six-layered cortex, such a pathway would be a candidate selector pathway for archicortical versus neocortical fate specification downstream of TGFβ inhibition. It should be noted that both LHX2 and FOXG1 are involved in telencephalic development in vertebrates that lack a six-layered

cortex, so it is likely that they have evolved a new function in the mammalian dorsal telencephalon (Hardcastle and Papalopulu, 2000; Hideki et al., 2005).

Areal specification of the neocortex

In addition to the laminar patterning in the radial axis described above, the neocortex also undergoes areal patterning in the rostro-caudal and M-L axis, which will enable subdivisions of the cortex into functional regions such as motor, sensory, auditory, etc. Each area in turn displays differences in gene expression patterns, connectivity, and functionality (O'Leary et al., 2007; Sansom and Livesey, 2009). Whether a neuron ends up in the frontal or the occipital cortex is predetermined by the location of its VZ precursor in the telencephalic neural tube (Figure 1.19). This is the basis for the "Protomap Hypothesis" (Rakic, 1988). The implication this model is that the areal blueprint of the cortex is established before the commencement of corticogenesis in response to signaling centers that pattern the progenitors rather than the post-mitotic neurons. Several studies have subsequently lent support to this model (O'Leary et al., 2007; Sansom and Livesey, 2009). The positional protomap contained within RGs is transmitted to the daughter neurons through IPs (Elsen et al., 2013). Later during corticogenesis, once the various layers have been populated with neurons, extrinsic influences such as those from the thalamus refine the molecular regionalization. This forms the foundation of the "Protocortex theory" (O'Leary, 1989). It is now appreciated that the two theories operate in developmental continuum, with signaling centers establishing the protomap and thalamocortical afferents refining this map and enabling molecular and functional sub-

regionalization (Lopez-Bendito and Molnar, 2003; Dehay and Kennedy, 2007; O'Leary et al., 2007).

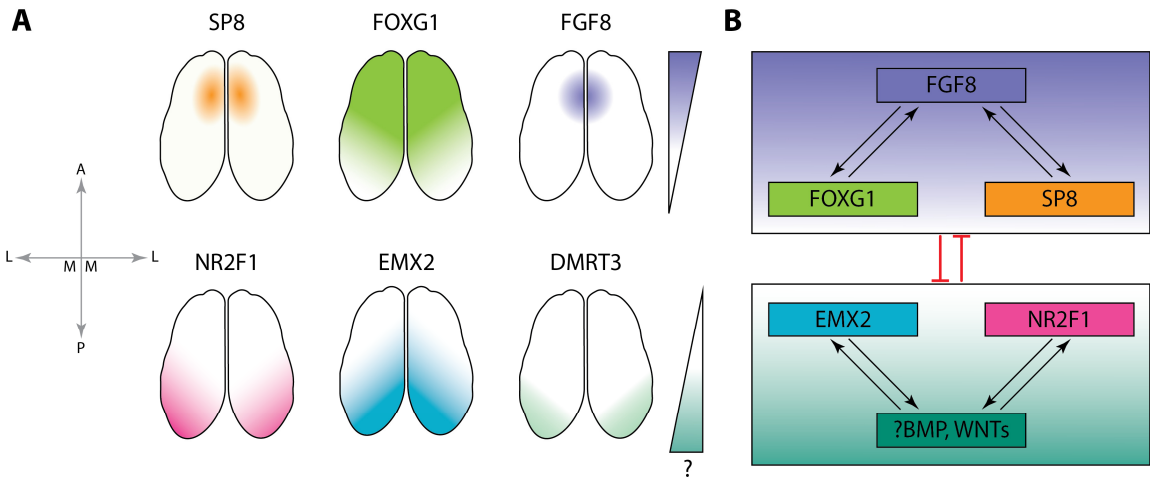

Figure 1.20: Schematic of TxF gradients thought to underlie rostrocaudal areal patterning in the cortex. A) SP, FOXG1, and FGF8 are enriched rostrally, while NR2F1 (COUP-TF1), EMX2 and DMRT3 are enriched caudally. Gradients of signaling establish TxF gradients with FGF8 acting as a rostralizing morphogen. The identity of the caudalizing morphogen has not been established, although BMPs and WNTs are candidates expressed in this region, B) The rostral and caudal TxFs and their morphogens form a cross-repressive regulatory network to maintain areal identity.

The expression gradients of various TxFs demarcate the embryonic areal 'protomaps'. These TxFs include PAX6, EMX2, FOXG1, NR2F1, and SP8 (Figure 1.20). The former three are enriched rostrally, while EMX2 and NR2F1 are enriched caudally. Conditional loss- and gain- of function studies have demonstrated that EMX2 specifies caudal areal identity in a concentration dependent manner while NR2F1 predominantly represses rostral fate (Sansom and Livesey, 2009). Conversely, SP8 specifies identities associated with rostral areas. Together, these TxFs impose an areal blueprint by cross-regulation of each other and of signaling molecules (Figure 1.20). Therefore, a given neocortical region is not defined by the expression of a single gene but rather by a set of genes operating at

different levels of activity (O'Leary et al., 2007). It is worth noting that our knowledge of areal patterning is based on studies in mice and there are some notable differences that have been observed in human fetuses. So while gradient patterns of NR2F1 and EMX2 can be demonstrated, PAX6 does not appear to have a gradient (Bayatti et al., 2008; Ip et al., 2010). Recent studies have shown enrichment of FGFR3 in the caudal cortex of the human fetal brain; this appears to be conserved from mice (Miller et al., 2014).

The signaling factors proposed to be involved in areal patterning include a) FGF8/15 from the anterior neural ridge, b) BMPs and WNTs from the cortical hem and lateral ridges, and c) SFRP2 (a Wnt antagonist) and neuroregulins from the antihem. Of these, only FGF8 has been shown to be a true determinant of areal patterning; evidence for other pathways is currently lacking. In utero electroporation of FGF8 greatly expands the rostral cortical boundary (Fukuchi-Shimogori and Grove, 2001). Strikingly, an ectopic source of FGF8 in the caudal cortex results in partial duplication of the somatosensory cortex, which normally lies in the frontal lobe. This supports an instructive role for FGF8 in rostral fate. Conversely, mice which are hypomorphic for FGF8 (i.e. express FGF8 at low levels) have an enlarged caudal cortex at the expense of the rostral cortex (Garel et al., 2003); overexpression of soluble dominant negative FGFR3C (which inhibits FGF8 signaling) has a similar effect (Thomson et al., 2009). FGF8 promotes the expression of rostral TxF (SP8 and FOXG1) while simultaneously repressing EMX2 and NR2F1 (Figure 1.20) (O'Leary et al., 2007; Hebert and Fishell, 2008; Sansom and Livesey, 2009).

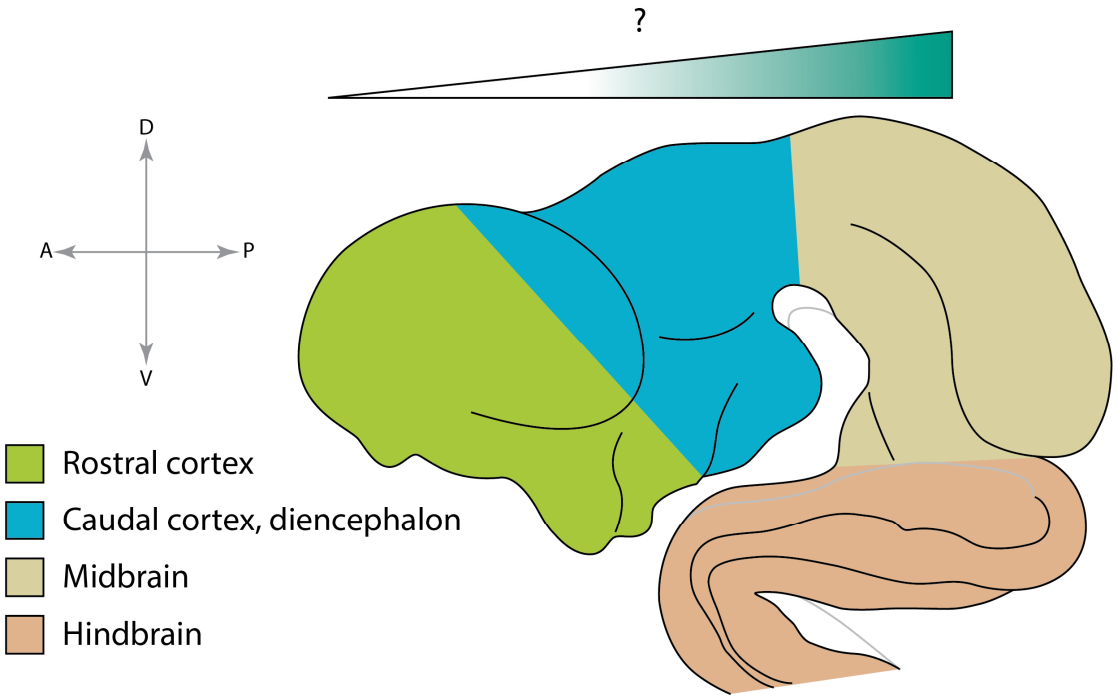

Figure 1.21: Schematic of a PCW5 human fetal brain in the sagittal section. The rostral and caudal cortex represent two different domains, and the signaling responsible to establishing caudal cortical identity has not been identified yet.

Apart from FGF signaling, it is not known if any other signaling pathways can affect TxF gradients to a similar extent or if there are any pathways acting upstream of FGF. While both BMPs and WNTs can regulate EMX2 expression, whether they affect areal patterning more globally remains to be determined (Theil et al., 2002). Importantly, genetic and lineage-tracing analyses suggest that the rostral and caudal cortical domains established by the signaling pathways have distinct fates (Kimura et al., 2005). While the rostral cortex is confined to a neocortical fate, the caudal cortex can contribute to the caudal neocortex, hippocampus (archicortex) as well as cortical hem, choroid plexus and thalamic structures (Figure 1.21) (Kimura et al., 2005; Kumamoto and Hanashima, 2014). The implication here is that a signaling pathway that modulates areal patterning of the cortex – specifically of

the caudal cortex – can also modulate selector activity between archicortex and neocortex as discussed in the previous section.

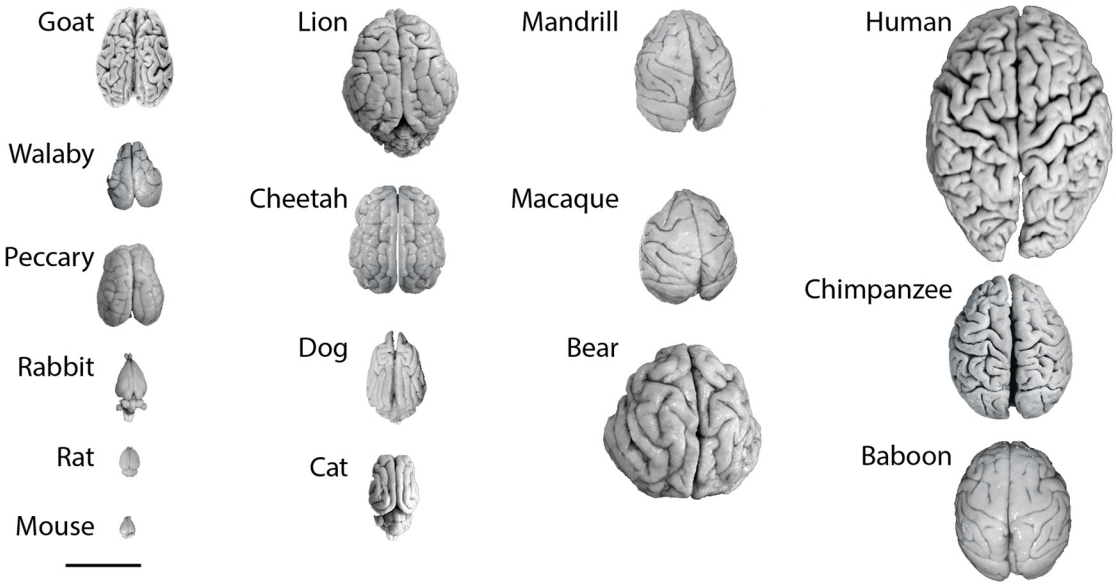

Figure 1.22: The relative sizes and extent of gyrencephaly observed in various eutherian mammals. Modified from Javier, 2011 (Defelipe, 2011). Scale bar: 5cm.

Primate specific aspects of neocortical development

Concurrent with the massive enlargement of the neocortex in NHPs (Figure 1.22), several NHP-specific adaptions can be observed during development (Geschwind and Rakic, 2013). These include an expansion of the OSVZ progenitor compartment to enable increased production of the superficial layer neurons, as mentioned in the previous section (Lui et al., 2011). Quantitatively, humans have a 1000-fold increase in the number of neurons compared to mice, however it takes only 20-fold the amount of time to generate these neurons (Geschwind and Rakic, 2013). This is achieved by multiple developmental adaptations: 1) an increase in the fraction of symmetric cell divisions in

the various progenitor compartments described above, 2) an increase in the total number of asymmetric cell divisions individual progenitors can undergo, and 3) a prolonged (3-4X) cell cycle followed by acceleration during genesis of the superficial layers (Figure 1.23) (Kornack and Rakic, 1998; Hill and Walsh, 2005; Lui et al., 2011). It is estimated that while mouse cortical progenitors undergo about 11 cell divisions, NHP cortical progenitors undergo about 28 - in humans this number is probably still higher (Hill and Walsh, 2005). Moreover, within a NHP brain, relative differences in progenitor proliferation underlie parcellation of specific brain areas as postulated by the protomap hypothesis (Lukaszewicz et al., 2005; Geschwind and Rakic, 2013).

Given the essential role of the cell cycle during evolutionary expansion and corticogenesis, not surprisingly, many NHP specific adaptations target the cell cycle related organelles or genes (Bae et al., 2015). For instance, several human-specific amino acid substitutions are found in genes that are targeted to the mitotic spindle or the kinetochore and present in the human mid-fetal germinal zones (e.g. CASC5, KIF18A, SPAG5). Additionally, the evolution of two centromere-specific genes, ASPM and CDK5RAP2, is strongly correlated with brain size. More recently, it was shown that a hominid-specific gene ARHGAP11B is enriched in human RGs and bRGs compared to mice (Florio et al., 2015). This gene arose after divergence from chimpanzees by gene duplication of a conserved gene (ARHGAP11A), and when overexpressed in mice, it increases the size of the SVZ by promoting symmetric differentiation of RGs into basal progenitors such as IPs and bRGs. Remarkably, overexpression of ARHGAP11B can induce gyrification of the normally lissencephalic mouse cortex in a fraction of injected mice.

Mutations in many genes that result in severe brain disorders in humans do not have a severe phenotype when introduced in mice, suggesting human-specific requirements of such genes (Geschwind and Rakic, 2013; Bae et al., 2015). The NHP genome also has about 100 novel microRNAs, many of which are enriched in the OSVZ and target several cell cycle and differentiation genes (Dehay et al., 2015). These genes – while more ancient than the microRNAs– have also co-evolved with their target miRNAs allowing them to exert a regulatory influence over proliferation (Arcila et al., 2014).

In addition to changes to the coding region of the genome, recent studies also emphasize the role of noncoding regions during evolutionary expansion and corticogenesis (Bae et al., 2015). In many cases, these changes lie in enhancer regions that influence the expression of genes directly or indirectly involved in progenitor cell cycle. Indeed, the human genome has a large number of enhancers that serve as developmental enhancers during corticogenesis, and which have no known homologues in mice (Capra et al., 2013). For instance, an enhancer of FZD8 – a WNT receptor – lies in a human accelerated region (HAR) of the genome and targets expression of FZD8 to the neocortex. Compared to the corresponding chimpanzee enhancer, the human FZD8-HAR enhancer can drive robust expression of reporters and FZD8 in the mouse neocortex. Intriguingly, expression of FZD8 in the mouse neocortex driven by the human, but not chimp HAR enhancer can accelerate RG cell cycle reentry and increase neocortical size (Boyd et al., 2015). Other studies have shown expression of a long non-coding RNA from a HAR specifically in CR cells specifically during development (Pollard et al., 2006). Since CR cells play important roles in migration and placement of neurons as discussed above, it is possible that noncoding HARs exert

influence on laminae and circuit formation. Human-specific noncoding promoter regions have also been shown to play a role in corticogenesis. For instance, several human genes display multiple promoters (Bae et al., 2015). One such gene, GPR56, encodes a receptor that binds to extracellular matrix proteins and regulates progenitor proliferation. There are 17 alternative promoters for GPR56 in humans compared to 5 in mice. A human-specific promoter enables GPR56 expression specifically in the perisylvian sulcus, the area of the brain involved in language and vocalization. Patients with mutations in this promoter region develop perisylvian polymicrogyria associated with language difficulties and intellectual disability, presumably due to impaired progenitor proliferation in this area (Bae et al., 2014).

Strong transcriptional differences are also observed across cortical areas between mice, NHPs, and humans at equivalent stages of development (Geschwind and Rakic, 2013; Miller et al., 2014; Bae et al., 2015). These differences are enriched in the progenitor and laminar compartments and are attributable to gene expression patterns and/or multiple splice variants. For instance, human RGs – but not mouse RGs – express the ligand PDGFD and its cognate receptor PDGFRβ; together they promote proliferation and cell cycle progression of human RGs in slice cultures (Lui et al., 2014). Another example of species-specific expression are certain TxFs (TFAP2C, FOS and EGR1) which are expressed in human, but not mouse RGs during superficial layer corticogenesis (Pollen et al., 2014). While the functions of these TxFs in human RGs are unknown, they are candidate Notch targets and hence may also be involved in maintenance of progenitor fate and/or regulate cell cycle. Another example is Trnp1, a DNA binding protein of unknown function that

promotes symmetric RG self-renewal in mice. Intriguingly, the human fetal cortex shows regional differences in TRNP1 expression in the VZ, with low expression in areas anticipating high gyrification such as the occipital cortex. Indeed, knockdown of Trnp1 in mice promotes gyrification of the cortex by promoting the transition of RGs to bRGs (Stahl et al., 2013). Thus in this instance, the dynamic changes in TRNP1 expression in human fetal brains result in a predetermined pattern of cortical folding compared to mice, which show high levels of expression during corticogenesis. Lastly, human SVZ (inner and outer) displays high level of extracellular matrix components and cell adhesion molecules; this is thought to contribute to the higher self-renewal ability of human IPs compared to mouse IPs as well as the self-renewal of bRGs, which lack an apical process (Simone et al., 2012).

Together, these various genetic and cellular changes contribute to the increased number of cytoarchitectonic areas, more types and numbers of neurons, increased diversity and size of the subplate, as well as increased complexity of the frontal cortex, all of which define human corticogenesis (Geschwind and Rakic, 2013). Importantly, this highlights the differences between mouse and human corticogenesis and emphasizes the need to study human corticogenesis in a relevant cellular and developmental context (Bae et al., 2015). Due to the ethical considerations involving primate fetal research and the limitations in availability of fetal tissue, embryonic stem cells can provide a useful platform for modeling corticogenesis and serve as a hypothesis-generating tool.

Figure 1.23: Differences between rodent and primate corticogenesis at equivalent stages of development. In mice, corticogenesis takes place over 6 days, while in monkeys it take places over 60 days. The OSVZ becomes the major site of neurogenesis in the monkey cortex after E65, while the VZ declines over time. This is in contrast to mice, where VZ is the predominant site of neurogenesis throughout. Multiple genetic and cell cycle differences between the two species are thought to underlie this pattern of development as described in the text. CP: cortical plate, ISVZ: inner subventricular zone, IZ: intermediate zone, MZ: marginal zone, OSVZ: outer subventricular zone, SP: subplate, VZ: ventricular zone. Adapted from Dehay and Kennedy, 2007 (Dehay and Kennedy, 2007). Scale bar: 100µm.

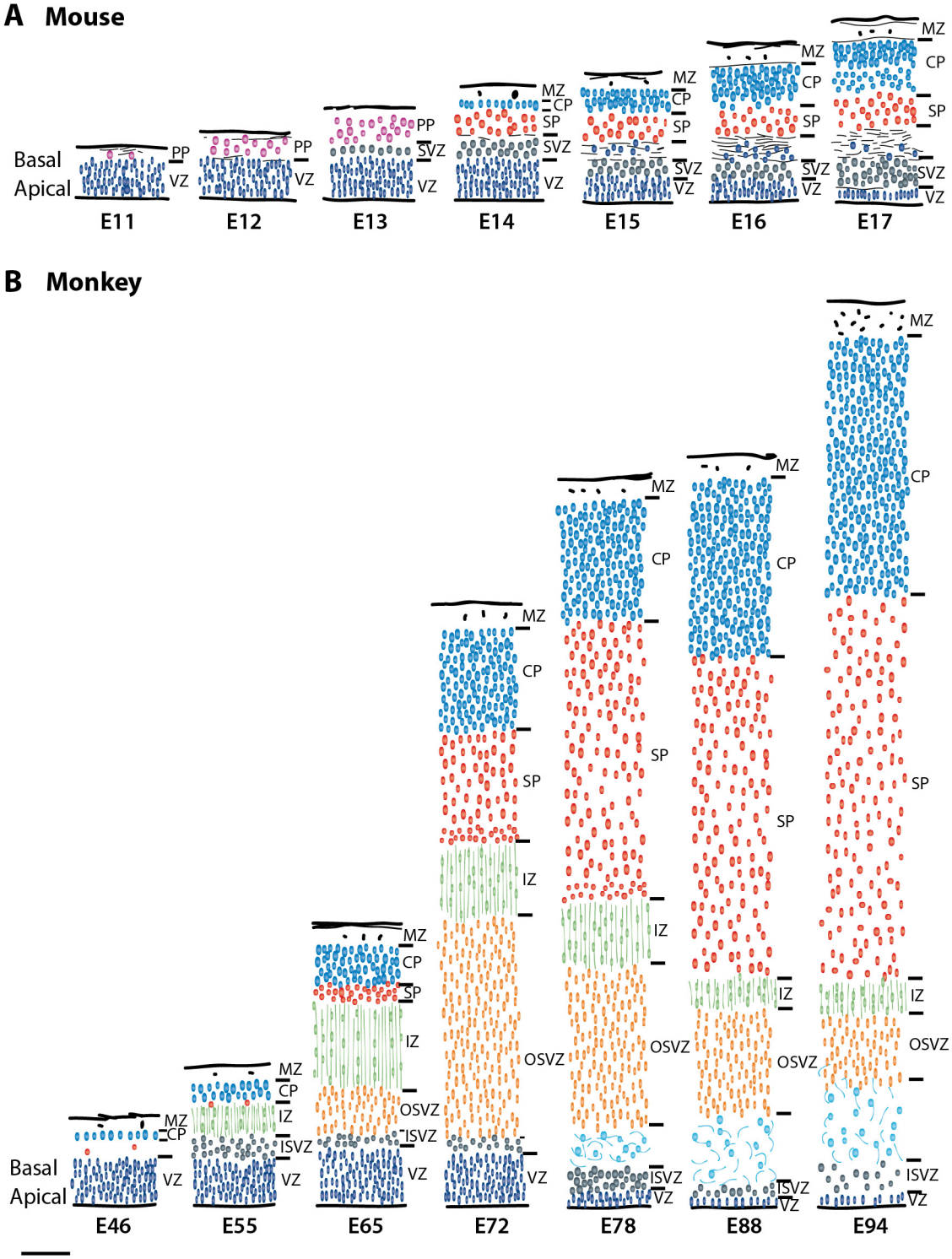
A Mouse
Basal
Apical
PP
VZ
SVZ
MZ
CP
SP
E11
E12
E13
E14
E15
E16
E17
B Monkey
IZ
OSVZ
ISVZ
E46
E55
E65
E72
E78
E88
E94

THE CELLULAR BASIS OF CORTICAL LAYER FORMATION

The classical 'Progressive Restriction' model of corticogenesis

The earliest studies to determine the cellular basis of cortical layer formation were carried out in mice using tritiated (^{3}H) thymidine injections into pregnant mice followed by autoradiography of the embryonic brain (Angevine and Sidman, 1961). The labeled thymidine is incorporated into actively dividing cells, and retained in the daughter cells upon asymmetric division that can be detected in the cortical plate. This established that corticogenesis occurs in an inside-out fashion as mentioned above. More detailed experiments involving ^{3}H-thymidine injections into pregnant macaques at multiple gestational time points followed by immunohistochemical detection in the postnatal visual cortex have confirmed this principle in NHPs (Rakic, 1974).

More sophisticated lineage-tracing analyses were subsequently carried out using replication defective retroviruses expressing β-galactosidase (a lineage tracer), which labels only actively proliferating cells, in this case RGs (Luskin et al., 1988; Walsh and Cepko, 1988; Reid et al., 1995). This work has demonstrated that the progeny of RGs during early – but not late corticogenesis – are able to contribute to all layers of the cortex; the later born neurons are restricted to a superficial laminar fate. This is referred to as the "Progressive Restriction Model" (Figure 1.24A). Progressive restriction is also supported by studies in transgenic and chimeric mice in which in only a fraction of RGs express β-gal (Tan and Breen, 1993; Soriano et al., 1995; Kuan et al., 1997; Tan et al., 1998). In these mice, local dispersion of labeled neurons spanning the CP is observed, in

addition to a separate origin and migratory route for interneurons. There are also other lines of experimental evidence. For instance, transplantation of ^{3}H-thymidine labeled early stage VZ progenitors from ferrets into early stage ferret VZ can form both superficial and deep layer neurons, whereas transplantation into late stage VZ predominantly gives rise to superficial layer neurons (McConnell, 1988; McConnell and Kaznowski, 1991). Late stage progenitors however, are only able to contribute to superficial layer neurons, both in the early or late transplants (McConnell and Kaznowski, 1991; Frantz and McConnell, 1996).

Other groups have followed the fate of clonal lineages generated by individual progenitors *in vitro* (Shen et al., 2006). Using molecular markers to stain for cortical layers, the timing of deep versus superficial layer neurogenesis was determined to be an intrinsically determined property i.e. the progenitors become more restricted in their ability to generate various layers over time. Thus while early stage progenitors could give rise to neurons expressing markers of various layers, late stage progenitors were more restricted in their potential. It is worth noting that there are major caveats to interpreting this study. First, the authors consistently saw a large number of Layer I CR cells from the individual progenitors. Since CR cells are formed from a different source as described above, this suggests a contamination in their cultures from extra-dorsal cortical sources. Second, the neurons derived from these progenitors showed minimal differentiation into superficial cortical neurons in their culture conditions, suggesting that the protocols utilized were suboptimal. Third, the presence of both superficial and deep layer markers in the same clonally derived lineage was not actually demonstrated.

Further support for the progressive restriction model comes from Cre recombinase based lineage-tracing studies, which allow for fate mapping of progenitors without experimental manipulation of the embryo. The method involves expression of the bacterial enzyme Cre recombinase expressed from a tissue-specific gene locus, which itself is either endogenous or part of a bacterial artificial chromosome. When crossed to reporter mice, Cre can recognize loxP sites that are positioned around a fluorescent protein reporter to make it conditionally dependent on Cre for its expression. By adding an estrogen receptor domain (ER^{T2}) to Cre, the activity of Cre can be controlled with a small molecule agonist or ER^{T2}, tamoxifen. Hence fate mapping during embryogenesis can be controlled both spatially (via a tissue-specific promoter) as well as temporally (via ER and tamoxifen administration).

Using this strategy, Chao et al. labeled the progeny of cells expressing the TxF Fezf2 at various time points during development (Guo et al., 2013). Fezf2 is expressed in the VZ starting at E8.5 and is maintained only during corticogenesis of deep layers, after which it cannot be detected (Hirata et al., 2004). Congruently, its expression is maintained in post-mitotic neurons of the deep layers, but not in superficial layer neurons. It has been proposed that Fezf2 may mark deep layer restricted progenitors during corticogenesis (Greig et al., 2013). When crossed to reporter mice, early induction of Fezf2-$CreER^{T2}$ (E12.5) resulted in reporter expression in neurons in multiple layers as well as glial cells, suggesting that Fezf2 is not predominantly expressed in lineage-restricted cells. Moreover, later induction of Fezf2 (E14.5) could also label neurons in the superficial layers (together with glia), even though Fezf2 is below the detection threshold at the mRNA level

at later stages. Clonal analysis of the fate-mapped cells by low dose tamoxifen induction strongly suggested progressive restriction of progenitors. Lastly, the authors fate-mapped RGs expressing the TxF Cux2 (see below) and showed that the majority of lineage traced neurons contributed to both superficial and deep layers and expressed markers representative of both at P0.

More recently, Gao et al. utilized MADM (Mosaic Analysis of Double Markers) to fate map rare individual progenitors in the Emx1 lineage and carried out clonal analysis of the progeny (Gao et al., 2014). Emx1 is a TxF that is specifically expressed in the dorsal neocortical progenitors that will give rise to glutamatergic neurons starting at E8.5. The study of Gao et al. shows that the vast majority of single progenitors labeled in the G2 phase of the cell cycle from E11.5-E13.5 give rise to progeny that contribute to all layers of the cortex at P21 and express markers appropriate for CPNs and SCPNs. Progenitors labeled at later stages (E15.5) are restricted in their potential and can only contribute to the superficial layers, consistent with progenitor restriction. Moreover, a significant fraction of individual RGs (1 in 6) also give rise to astrocytes, establishing them as truly multipotent. Importantly, the authors did not observe any clones containing only glial cells, suggesting that in the Emx1+ lineage, glial cells and neurons share parental progenitors. Finally, through a series of elegant modeling experiments, they have also demonstrated that the neuronal output of RGs is very deterministic, with each RG contributing to about 8 neurons prior to terminal cell division.

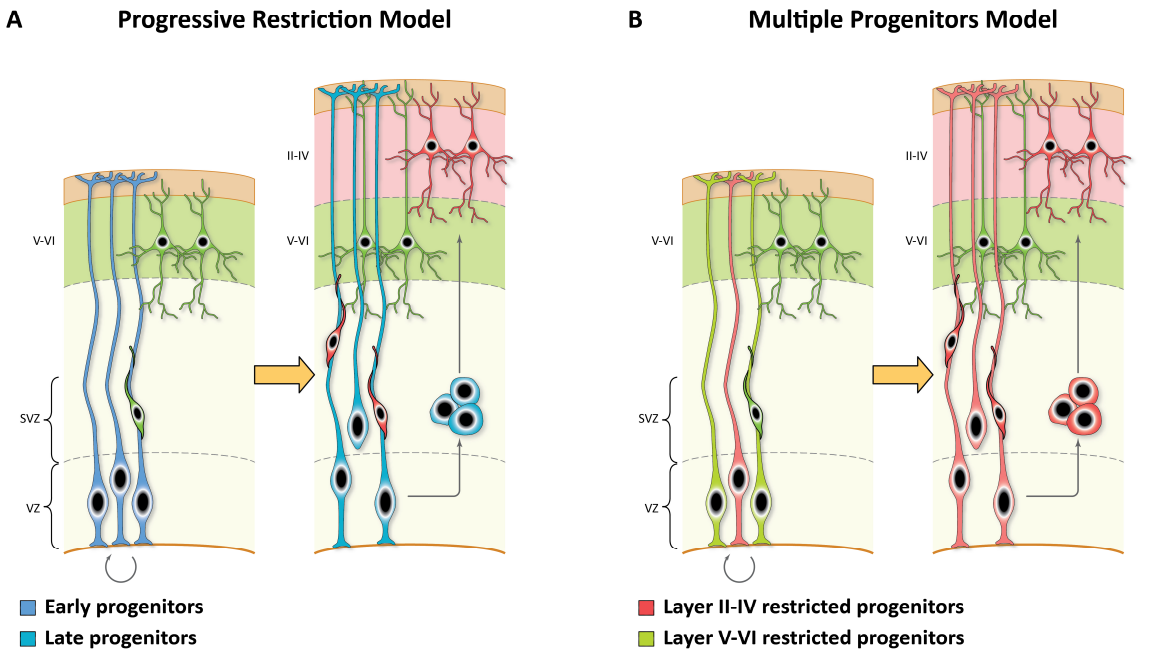

Figure 1.24: The two models of cortical layer formation in mammals: A) Progressive Restriction Model. B) Multiple Progenitors Model. The color code of the progenitors is meant to highlight the differences in the two models.

The Multiple Progenitor model of corticogenesis

More recently, an alternative model of cortical layer generation has been proposed. Known as the "Multiple Progenitor" model, it postulates the existence of lineage restricted progenitors that are predestined to give rise to only one lineage or a set of related lineages (Figure 1.24B) (Franco et al., 2012; Franco and Müller, 2013). Hence according to this model, an early multipotent progenitor diverges into separate progenitors for CPNs, SCPNs, CThPNs, and possibly glial cells at an early stage of corticogenesis. The model also allows for nested lineages so that multipotent and fate restricted can coexist in the same compartment, but are lineally related (Greig et al., 2013; Costa and Muller, 2014). Direct experimental evidence for this model relies largely

on fate mapping based on one TxF – Cux2 (also known as Cutl2) – in RGs. Cux2 is known to be the most specifically expressed gene in superficial layer neurons (CPNs) in mice, monkeys, and humans (Céline et al., 2004; Nieto et al., 2004; Arion et al., 2007; Bernard et al., 2012; Zeng et al., 2012). Studies in mice have shown that Cux2 is also enriched in the SVZ, where it is co-expressed in IPs thought to give rise to the superficial layer neurons (Céline et al., 2004; Nieto et al., 2004). However, migrating interneurons also express Cux2 and make up a large contingent of Cux2+ cells in the mouse SVZ (Guo et al., 2013). Notwithstanding the non-pyramidal expression of Cux2, Franco et al. demonstrated using an array of genetic tools that Cux2 can be used to lineage trace a fraction of RGs at E10.5 in the mouse, before corticogenesis has commenced (Franco et al., 2012). Remarkably, these RGs give rise to daughter neurons that are restricted in their potential to CPNs expressing Satb2, which is a necessary and sufficient TxF to generate this population of neurons. Intriguingly, the minority of Cux2-lineage traced pyramidal cells that settled in the deeper layers also express Satb2, suggesting that the Cux2+ RG lineage is already committed to a CPN fate as early at E10.5. Enforced cell cycle exit of the Cux2+ RGs does not change their fate and they still take on a CPN fate, albeit prematurely. Moreover, Cux2+ RGs mostly divide symmetrically during formation of the deep layer neurons (SCPN and CThPNs), and only during later stages coinciding with superficial layer corticogenesis do they divide asymmetrically. Hence, according to the Multiple Progenitor model, the progenitors destined to give rise to superficial and deep layers are already fundamentally different at the earliest stages of corticogenesis in terms of their relative frequency, mode of cell division, and neuronal fate. The Cux2+ RGs do however seem to share the

requirement for Notch and WNT/β-catenin signaling for self-renewal with non-lineage traced RGs.

Previous studies that support progenitor restriction model can also be reinterpreted to support the multiple progenitor model (Franco and Muller, 2013; Greig et al., 2013; Han and Sestan, 2013). For instance, in addition to showing neuronal progeny populating multiple layers, retroviral lineage tracing also reveals a large number of clones that exist in a restricted laminar distribution. This suggests the presence of lineage restriction in some fraction of labeled progenitors. Furthermore, the transplantation of early stage progenitors could potentially contain a mixture of lineage-restricted cells that respond to temporally restricted cues for differentiation. Hence the deep layer specified progenitors only differentiate into deep layer neurons when transplanted at an early stage; at this time the transplanted superficial layer progenitors are largely proliferative. The latter can only respond to the differentiation signals at an advanced stage of corticogenesis. Transplantation of late stage progenitors into the cortex only gives rise to superficial layer neurons only in a stage appropriate manner, because the deep layer progenitors have been depleted by then.

The strongest support of the Progressive Restriction model to date comes from the studies of Gao et al. (Gao et al., 2014) using the MADM strategy. MADM preferentially labels dividing cells due to its dependence on recombination during the G2 phase, where 4n chromosomes are present. The authors used the $CreER^{T2}$ system under the control of the Emx1 promoter to induce recombination; thus, their fate mapping is dependent on

the fidelity of the MADM strategy. It is conceivable that recombination of the MADM alleles is biased towards a progenitor class that is slowly dividing i.e. spends more time in the G2-phase and has not yet transitioned to the fast dividing Cux2+ lineage restricted radial glia. This might explain why the majority of the MADM labeled clones were found in both the superficial and deep layers of the cortex. Support for this comes from the observation that most RGs labeled with MADM give rise to 8-9 neurons. This is in contrast with lineage tracing studies of IPs (which are derived from RGs) using Tbr2-Cre, which show that the majority of IPs labeled at early stages give rise to 16 and above neurons (Vasistha et al., 2014). Since a single RG can give rise to one or two IPs by asymmetric or symmetric division respectively, the number of neurons generated by RGs comes out to be higher when estimated with this strategy. Hence MADM might be labeling progenitors in an unbiased manner and hence not detecting lineage-restricted progenitors (Gil-Sanz et al., 2015).

The experiments of Guo et al. with Fezf2-CreER^{T2} lineage tracing conclusively establish that Fezf2 is not a good marker of the various lineage-restricted progenitors, if they exist (Guo et al., 2013). However, their assertion that the progeny of Cux2+ RGs contribute to pyramidal neurons to all layers of the cortex has been called into question recently (Gil-Sanz et al., 2015) for two reasons. First, the Cux2-Cre and Cux2-CreER^{T2} mouse line used by Guo et al. did not recapitulate the endogenous Cux2 mRNA expression faithfully because of their breeding strategy, since the Cux2 locus seems to be strongly dependent on the genetic background. Indeed, crossing these mice to outbred mice could recover the original pattern of Cux2 expression seen by Franco et al. (Gil-Sanz et al., 2015).

Second, it is unclear if Guo et al. were analyzing the progeny of single clones (Gil-Sanz et al., 2015).

Due to the increased complexity of the NHP proliferative zone – from an increase in the types and numbers of progenitors, to their distinctive behaviors, and the larger number of CPN required – it remains an open possibility that the Multiple Progenitor model may apply to NHP corticogenesis. Moreover, the inherent limitations of the techniques applied so far in mouse models preclude a definitive conclusion on the validity of this model even in mice. It is a common consensus that single cell studies of progenitors and their lineages is required at the level of lineage-tracing and RNA-seq in order to definitively resolve these issues (Costa and Muller, 2014; Bae et al., 2015).

The molecular basis of laminar patterning

An understanding of the molecular mechanism of how RGs switch from generation of deep layers to superficial layers is lacking at present. Inhibition of β–catenin/WNT signaling, RA signaling from the meninges and CSF to the RG end feet, and feedback signaling of post-mitotic neurons to the RGs via neurotrophins (NT3) have all been suggested as possible mechanisms for progenitor restriction and the laminar switch (Mutch et al., 2009; Siegenthaler et al., 2009; Lehtinen et al., 2011; Parthasarathy et al., 2014). The extent to which these pathways play a role in promoting the restriction, the nature of the underlying restriction itself, and whether these pathways are acting downstream of a primary event remain unclear and are a subject of debate (Zhou et al.,

2006; Chatzi et al., 2011; Munji et al., 2011). Regardless of the model of corticogenesis considered, there is considerable evidence for feedback signaling from the post-mitotic neurons to the RGs both in generation of subsequent cortical layers, as well as gliogenesis from RGs (Barnabe-Heider et al., 2005; Namihira et al., 2009; Seuntjens et al., 2009; Toma et al., 2014).

Altering the G1-length of the cell cycle of progenitors can also change the laminar fate of neurons (Pilaz et al., 2009). An enforced reduction of the G1-phase in mice by overexpression of cyclins promotes cell-cycle reentry of progenitors at the cost of neuronal differentiation. This applies both VZ RGs and SVZ TBR2+ progenitors and results in an overall increase in the size of the progenitor pool as well as an increase in the surface area of the cortex, as is the case in primates. Interestingly, the delayed exit of progenitors eventually leads to an increase in the number of neurons being generated at the new birthdate, in this case superficial layer neurons. This would suggest that the laminar fate of neurons is intrinsically encoded in RGs, as reducing the G1-phase decreases the timespan (and likelihood) of RGs and IPs to respond to external signals, if such signals exist. Alternatively, external signals may be responsible for setting this intrinsic program of laminar formation in the first place, but at a much earlier time during development.

The expansion of both progenitor pools upon Cyclin D/CDK4 overexpression and surface area of the cortex has been reported by other groups as well (Lange et al., 2009). Additionally, modulating the G1-phase by overexpression of cyclin E or the cell cycle inhibitor $p27^{Kip1}$ can also alter the increase or decrease the rate of progenitor cell-cycle

reentry in primates, respectively (Lukaszewicz et al., 2005). Mathematical modeling indicate that regional differences in the expression of such cell cycle modulators may contribute to regulation of the size of the superficial layers between the different cortical areas. Together, current studies suggest that a decrease in G1-phase of progenitors, as is observed at later stages in primates (Kornack and Rakic, 1998), promotes an expansion of the superficial cortical layers and CPNs. The signal(s) that orchestrate a decrease in the G1-phase of primate progenitors are not known at present, although the ligand PDGFD and its cognate receptor PDGFRβ, expressed specifically in human RGs, may contribute (Lui et al., 2014).

PSCs AS MODELS FOR NEOCORTICAL INDUCTION AND PATTERNING

Most of our understanding of the molecular basis of corticogenesis comes from studies in mice. However, many differences between human, NHP, and mouse corticogenesis are already appreciated at the cellular, genetic, and clinical level, as described above. Due to the genetic intractability of NHPs, ethical issues surrounding experimentation, as well as limited availability of fetal tissue, there is a paucity of molecular studies in this system. To study unique traits of the primate cortex, specifically *homo sapiens* cortex in terms of its progenitors, developmental trajectory, diversity of neurons, and function requires a detailed study in a relevant developmental and cellular context. As neural plate formation starts at PCW3 and corticogenesis at PCW5-6 in humans, direct studies in embryos are prohibitive. However, as I will discuss in this section hPSCs have been used to model early

human development and provide a viable alternative to study human-specific features of corticogenesis.

To what extent does the artificial nature of *in vitro* corticogenesis correspond to *in vivo* development? A number of studies have established that PSCs respond to appropriate signaling cues, follow the same developmental trajectories, and even faithfully recapitulate organogenesis in three-dimensions when provided with appropriate culture conditions. As discussed above, the requirement for BMP inhibition for neuroepithelial induction is conserved *in vitro* in mESCs from *in vivo* forebrain development (Bachiller et al., 2000; Di-Gregorio et al., 2007; Kamiya et al., 2011). Moreover, the temporal hierarchy of development from PSC derived neural progenitors follows the *in vivo* tempo closely. For instance, neuronal fate precedes astroglial fate specification *in vivo* (Kriegstein and Alvarez-Buylla, 2009). Similarly, neurons are generated before glial cells over the same time period as embryonic development *in vitro* in both human and mouse PSCs (Gaspard et al., 2008; Naka et al., 2008; Okada et al., 2008; Yichen et al., 2012). Similarly, in neural progenitors derived from both mouse and human PSCs, the temporal emergence of laminar neurons *in vitro* corresponds to their *in vivo* timing (Eiraku et al., 2008; Gaspard et al., 2008; Shi et al., 2012; Taisuke et al., 2013). This also true for mouse and human PSCs that have been caudalized to generate spinal cord progenitors (Wichterle et al., 2002; Li et al., 2005) or ventralized to generate interneurons (Maroof et al., 2010; Maroof et al., 2013; Nicholas et al., 2013). Cortical-specified PSCs also mimic the molecular progression of markers from progenitors to neurons. When grafted into the cerebral cortex of newborn mice, they possess an area-specific identity and can develop patterns

of axonal projections and contribute to the local circuitry (Eiraku et al., 2008; Gaspard et al., 2008). Furthermore, hESC-derived cortical neurons and interneurons maintain their intrinsic developmental and maturation programs, even when transplanted into mouse brains (Espuny-Camacho et al., 2013; Maroof et al., 2013; Nicholas et al., 2013).

Recently, human and mouse PSCs have also been shown to mimic *in vivo* nervous system development in three dimensions. Provided the right environmental signals (such as TGFβ inhibition) and extracellular matrix components, PSCs can self-organize *in vitro* into telencephalic, cerebellar, retinal, pituitary or otic placodes (Eiraku et al., 2011; Suga et al., 2011; Nakano et al., 2012; Kadoshima et al., 2013; Koehler et al., 2013; Muguruma et al., 2015). Strikingly, the hPSC-derived cortical 'embryoid bodies' or 'organoids' also demonstrate human-specific characteristics of corticogenesis, such as the longer timescale of development, the presence of bRGs at later stages, as well as features of microcephaly when derived from patient IPSCs (Kadoshima et al., 2013; Lancaster et al., 2013). The three-dimensional cortex can also be patterned appropriately into different cortical areas using known developmental cues (Eiraku et al., 2008; Kadoshima et al., 2013). These observations suggest that the program for corticogenesis is intrinsically encoded in the neural progenitors, from tissue-level morphogenesis to patterning and laminar formation. Indeed, these human-specific features of corticogenesis are also observed in two dimensional, monolayer cultures (Shi et al., 2012).

Together, these studies establish that hPSCs faithfully recapitulate *in vivo* development spatially, temporally, and by extension, mechanistically. Hence, hPSCs can be used to

generate specific predictions on the molecular aspects of laminar and areal specification during corticogenesis. These predictions can be very meaningful if combined with endpoint readouts in human fetal material.

CHAPTER 2: MATERIALS AND METHODS

CELL CULTURE OF HUMAN EMBRYONIC STEM CELLS

The RUES1 and RUES2 hESCs lines were derived in our lab and have been described previously (James et al., 2006; Lacoste et al., 2009). Both lines were maintained in feeder-free conditions on Matrigel-coated dishes and cultured in conditioned medium (CM) or mTESR (Stem Cell Technologies) with daily media changes. Whenever mTESR was used, hESC cultures were adapted to the medium for at least 2-3 passages prior to experiments. For the preparation of CM, mitotically inactivated MEFs were seeded at a density of 1.0×10^7 cells per 150 mm dish and incubated in HUESM for 24hrs. CM was collected and supplemented with 20ng/mL bFGF prior to feeding the hESCs. For expansion, hESCs were grown as colonies and enzymatically passaged with 1 mg/mL dispase by incubating at 37 for 7min. followed by three washes with DMEM/F12. In some instances, ReLeSR (Stem Cell Technologies) was used for dissociation and passaging per manufacturer's instructions. The composition of HUESM and other media is given in Table 6.1.

NEURAL INDUCTION OF EGFP-T2A-SMAD7 CELLS

Clonal RUES1 TRE::EGFP-T2A-SMAD7 cells were generated as described in the section below and maintained in CM like regular hESCs. Two to three days before the start of the experiments, the cells were pre-treated for 1hr with 10µM ROCK-inhibitor (Y-27632) and

passaged as single cells with Accutase (Stem Cell Technologies). ROCK-inhibitor strongly diminishes dissociation-induced apoptosis and increases cloning efficiency (Watanabe et al., 2007). The cells were subsequently plated onto Matrigel-coated wells at a density of 15,000-30,000cells/cm^2 in CM supplemented with ROCK-inhibitor and hygromycin for three days. At this point, the wells were >95% confluent and DOX (2μg/mL) was added to the medium. This was considered Day 0 of induction. Media was replaced every day with DOX for the duration of the experiment; DOX was excluded for the control wells. For the MEK-inhibitor experiments, the cells were seeded onto Matrigel-coated wells as before, and MEK-inhibitor was added at various time points depending on the experiment. For BMP4/TGFβ1-challenge experiments, the cells were passaged in dispase and seeded as colonies. Where applicable, the TGFβ inhibitor SB431542, the BMP inhibitor LDN193189, and MEK-inhibitor PD0325901 (Tocris) were used at concentrations of 10μM, 100nM and 1μM, respectively. BMP4 and TGFβ1 were used at concentrations of 50ng/ml and 25ng/ml, respectively. Media was replenished daily in all conditions.

NEURAL INDUCTION AND CORTICAL DIFFERENTIATION OF hESCs WITH SMALL MOLECULE INHIBITORS

Before the start of the experiment, Matrigel was plated onto 12-well plates or 10cm dishes at a dilution of 1:35 in DMEM/F12 overnight. Human ESC lines were grown on Matrigel with CM containing 20ng/mL bFGF. Once the colonies were to be passaged, they were pre-incubated in 10μM ROCK-I for 1hr and incubated with Accutase (Stem Cell

Technologies) at 37°C for 20min. Cells were triturated with a pipet to ensure single cells. Accutase was diluted with 4X media and the cells were counted. About 50,000cells/cm^2 were spun down and plated onto the Matrigel plates. Media was replaced every day with CM/bFGF/ROCK-I until the cells were confluent. At this point cells were washed with PBS once and then 3N media with 10µM SB431542 and 100nM LDN193189 (SB/LDN henceforth) was added per well/dish. This was considered Day 0 of differentiation. SB/LDN media was changed every day for 12 days. The composition of 3N is provided in Table 6.2.

On days 9-10, cells with primitive neuroepithelial morphology (small nuclei, tightly packed) become apparent. At this point, the neuroepithelium was passage onto laminin (LAM) coated plates to form rosettes. On day 11, dispase was added directly to the medium at 1:10 v/v, and cultures incubated for 3min. at 37°C. After three washes with DMEM/F12 to get rid of excess dispase, media was replaced with SB/LDN and the neuroepithelial sheets were gently broken into clumps by scraping with a 2mL pipette. The clumps were seed onto LAM-coated dishes at high density. The procedure for making LAM-coated plates is described below. Beyond day 15, media was replaced with 3N every other day. Rosettes started appearing around day 16-20. At this point, 20ng/mL FGF2 was added for 4 days. Between days 24-26, the rosette structures were dissociated with Accutase at 37°C for 10min. Accutase was neutralized with 4X media and the cells suspension spun down for 5min at 300g. Single cell suspension of neural progenitor cells was ensured by incubating the pellet with DNAse I (200U/mL) for 15 min. at room temperature and passing the cells through a cell strainer. Neural progenitors were then

plated at a density of 200,000cells/cm^2 onto polyornithine/laminin/collagen /fibronectin (PLCF) dishes in 3N medium. From this point on, LAM was added to 3N media at a 1:500 dilution (final conc. 2µg/mL) at every other media change to prevent clumping and detachment of neurons. Appearance of anterior neural markers was confirmed by antibodies to PAX6, OTX2, SOX2, PLZF, TBR2, and FOXG1. The progenitors typically differentiated into various cortical layers over several weeks and cultures became predominantly neuronal around Day 35. Cultures were maintained for 90-100 days. An identical protocol was followed for monkey ESCs, except that the cells were passaged at day 7 to form rosettes, and then at day 20 to form neurons.

For Bromodeoxyuridine (BrdU) incorporation studies, 10µg/mL of BrDU stock (BD Biosciences; 1:1,000 dilution) was added to the culture medium for *one* day at days 45, 70, and 95.

PCLF coated plates were prepared as follows: poly-ornithine (Sigma) was diluted in water to 100µg/mL, added to the wells/dishes and incubated at 37°C for 4hrs. Following the incubation, the solution was aspirated and the wells rinsed with distilled water twice. For collagen coating, collagen I solution (advanced Biomatrix) was diluted 1:100 in PBS, added to wells and incubated at 37°C for 2 hours. For LAM coating, laminin (Life Technologies) was diluted in PBS to 20µg/mL (1:50) together with 2µg/mL Fibronectin, mixed thoroughly and added to the wells/dish. The plates were incubated at 37°C overnight. The next day, the solution was aspirated, and the plates washed with PBS once before use.

Where required, the following small molecules and growth factors were used: IWP2 (2.5μM), Ascorbic acid (200μM), BDNF (10ng/mL), NT3 (10ng/mL), 4-hydroxy tamoxifen (2μM), CHIR99021 (0.5-3μM), DAPT (20μM).

CELL CULTURE OF MOUSE AND MONKEY EMBRYONIC STEM CELLS

Two monkey ESC lines were used in this study: Macaca Nemestrina, and Macaca Mulatta. They ESCs were cultured and passaged in CM + bFGF and maintained on Matrigel similar to as described above for hESCs. For the mouse studies, two mouse ESC lines were used: 46C SOX1-EGFP reporter (made by Austin Smith, kindly provided by Laura Grabel), and SOX2-EGFP V6 (kindly provided by Konrad Hochedlinger). Mouse ESCs were maintained in defined medium in LIF + 2i conditions; the composition of the base medium is given in Table 6.3. The two inhibitors in this cocktail ("2i") are CHIR99021 (GSK3β inhibitor) and PD0325901 (MEK inhibitor). LIF + 2i was used at the following concentrations: LIF, 1000U/mL, CHIR99021, 3μM and PD0325901, 10μM. The mESCs were plated on gelatin coated plates made as follows: 0.1% gelatin solution (Millipore) was added to tissue culture dishes for 20min. at room temperature, after which the gelatin was aspirated and the plates allowed to dry for another 20min. Mouse ESCs were typically split every 5 days with 0.25% trypsin (Life Technologies) added for 10min. and incubated at 37°C. After this incubation, 10% fetal bovine serum (FBS) containing DMEM was added at 4X amount to neutralize the trypsin. Typically, the cells were split at a ratio of 1:1,000 added directly to LIF+2i medium without centrifugation.

NEURAL INDUCTION OF MOUSE PSCs

For mouse ESCs, we modified existing protocols to convert them first into EpiSCs. Mouse ESCs were seeded at high density (100,000 cells/cm^2) on LAM- and fibronectin- coated plates, made as described above. The next day, medium was switched to CM + 10ng/mL bFGF + 2.5µM IWP2 for three days. At this point, the mESCs took on the flat, circular morphology of hESC colonies. Like hESCs, EpiSCs rely on Activin and FGF (present in CM) to self-renew. EpiSC colonies were confirmed to express pluripotency markers such as OCT4, SOX2, and NANOG. Neural differentiation was initiated with base medium + SB/LDN at similar concentrations to that used for hESCs. This was considered day 0 of induction. SB/LDN was maintained for three days, with media change only the first day. Neural differentiation was monitored with the SOX1-EGFP reporter line. EGFP was seen within 4 days of induction and coincided with rosette formation. Subsequent differentiation was carried out on PCLF plates by dissociating the rosettes with trypsin for 10min. at 37°C followed by neutralization with FBS containing medium. The cells were plated in 3N medium at a density of 150,000cells/cm^2. Media was changed every other day henceforth. IWP2 was added for some experiments at a concentration of 0.5µM between days 0-5.

CLONING AND MOLECULAR BIOLOGY

Plasmids for cloning as well as Gibson assembly were designed and archived in Lasergene Seqbuilder (DNAStar). In all instances, PCR of inserts or backbone was carried out with Q5 polymerase (New England Biolabs) or GC-rich PCR system (Roche). Typical parameters for Q5 polymerase were: denaturation at 98°C for 1min., followed by 25-35 cycles of denaturation 98°C for 10s, annealing at 50-72°C for 30s, and extension at 72°C for 30s/kb; the final extension was at 72°C for 2min. For the GC-rich PCR system, amplification was carried out in two steps: in the first step, denaturation was carried out at 95°C for 3min., followed by 10 cycles of denaturation 95°C for 30s, annealing at 45-65°C for 30s, and extension at 72°C for 45s/kb. The second step comprised of 25 cycles of denaturation 95°C for 30s, annealing at 45-65°C for 30s, and extension at 72°C for 45s/kb; the final extension was at 72°C for 7min. The annealing temperature used for the GC-rich PCR kit was 3°C less than the lower melting temperature of the two primers, while for Q5 polymerase the annealing temperature was calculated using an online tool (http://www.neb.com/). Betaine (1M) was added to Q5 polymerase kit in cases of GC-rich templates, while 0.5M resolution solution was used with the GC-rich PCR system. Primers were synthesized by Integrated DNA Technologies and are listed in Table 6.8. Ultramers were used where the primer size exceeded 50bp. For regular cloning, plasmids, PCR products, or synthesize fragments were digested with restriction enzymes in the appropriate 1X buffer in a 40µL reaction at 37 or 55°C for 4-8hrs. When required, blunting and phosphorylation of the digested ends was carried out with the Quick Blunting kit or if blunting was not desired, with T4 polynucleotide kinase by incubation at 37°C for 30min.

in T4 ligase buffer. Removal of nucleotides and buffers was achieved with the PCR purification kit or the MinElute PCR purification kit (Qiagen). DNA digests were typically run on a 0.7% agarose gel at 125V for 45min. and purified with Qiaquick gel extraction kit (Qiagen). Plasmid backbones were dephosphorylated in all instances with Antarctic Phosphatase in a 50µL reaction at 37°C for 20min. and inactivated at 65°C for 10min. In some cases, fragments of double stranded DNA (~500bp) were synthesized commercially (Integrated DNA Technologies) and digested for assembly. Up to three-fragment ligation was carried out with the Quick ligation kit for 10min. at room temperature using a vector to insert ratio of 1:3. Stbl3 bacteria (Life Technologies) were used for routine cloning of inserts and were left to grow overnight at 37°C. Bacterial cultures were inoculated for mini or midi preps and incubated at 37°C with shaking at 260rpm for 16-20hrs. Mini or midi preps were carried out with QIAprep spin miniprep or Plasmid plus midi kits (Qiagen), respectively. Bacterial colonies were screened with Clonechecker (Life Technologies) followed by sequencing (Genewiz). Sequences were assembled in Lasergene Seqman (DNAStar). Restriction enzymes, Antarctic phosphatase, Quick ligation kit, T4 polynucleotide kinase, T4 ligase, and Quick blunting kit were all purchased from New England Biolabs.

When constructing ePiggybac vectors, BamHI/NotI sites were used for cloning coding sequences downstream of the promoter and were introduced by PCR. BglII, BclI, or BBsI sites were utilized when BamHI sites were unavailable in the coding sequence, while PspOMI or BBsI sites were utilized when NotI was unavailable. Six base pairs of random non-palindromic sequences were introduced at the 5’ end of each primer to distance the

restriction enzyme sites from the end of the DNA fragment. The following Kozak consensus sequence was added right before the initiation codon of all open reading frames (initiation codon underlined): CGCCACCATG. Where required, XhoI/BamHI sites were used to replace the upstream promoter in ePiggybac backbone. Lastly, AscI sites were utilized for cloning the ePiggyBac cassettes (with inverted terminal repeats) into the AAVS1 homology donor.

For creation of the FUCCI triple reporter lines, three constructs were generated: ePB-CAG::Venus-Gem(1-110)/PURO, ePB-CAG::mCherry-CDT1/BSD and ePB-CAG::mCerulean-H2B/NEO. ePB-CAG::Venus-Gem(1-110)/PURO was made by PCR cloning of Venus, followed by digestion with BamHI/BsrGI. Human geminin (Gem) fragment (1-110AA) was synthesized and digested with BsrGI/NotI. Three way ligation of Venus and Gem was then carried out into the BamHI/NotI site of ePB-CAG::MCS/PURO. An identical procedure was followed for ePB-CAG::mCherry-CDT1(30-120)/BSD, except that the synthesized fragment was CDT1 (30-120AA), and an ePB-CAG::mCherry/BSD vector was digested with BsrGI and NotI and used for ligation. mCerulean-H2B was PCR cloned, digested with BamHI/NotI, and ligated into the BamHI/NotI site of ePB-CAG::MCS/NEO to create ePB-CAG::mCerulean-H2B/NEO.

Oligomer annealing was carried out to introduce new restriction sites into vector backbones or to introduce FEZF2 CRISPR guides into the Cas9 X335 vector backbone. The following components were mixed together in a 10µL reaction: 1µL of forward and reverse oligos (100µM each), 1µL 10X T4 ligation buffer, 6.5µL of nuclease-free water, and

0.5µL of T4 polynucleotide kinase. The mixture was annealed in a thermocycler using the following parameters: 37°C for 30min., 95°C for 5min., 90°C for 1min., followed by a ramp down of -5°C/min for 13 cycles. The resulting annealed double-stranded DNA with overhangs was stored at -20°C and diluted 1:200 before being used for ligation.

CONSTRUCTION OF TALENS, CRISPRS AND HOMOLOGY DONORS

Gene specific TALEN plasmids were constructed for the SOX2 and CUX2 loci using published protocols utilizing the Golden Gate strategy (Sanjana et al., 2012). The TALEN targeter tool (https://tale-nt.cac.cornell.edu/) was used to design locus specific TALENs with a high percentage (>50%) of CG binding TALEs, 19 repeat variable dinucleotides (RVDs) for both left and right TALENs, and spacers of 15-19 nucleotides. For the FEZF2 CRISPR, a nickase mutant (D10A) of the Streptococcus pyogenes Cas9 that cleaves only one strand of DNA was utilized because of its higher specificity (Cong et al., 2013). The appropriate CRISPR site was selected using an online resource (http://crispr.mit.edu/) and cloned into the pX335 Cas9-nickase backbone (Ran et al., 2013) by digesting with BBsI restriction sites and oligomer annealing. The final sequences of TALENs and CRISPRs used for subsequent experiments are provided in Chapter 6: Appendix. The homology donor typically had five components: the 5' homology arm, a reporter or Cre recombinase, a selection cassette flanked by Frt or VloxP sites, a 3' homology arm, and a vector backbone. About 1kb of each homology arm was amplified by PCR from genomic DNA of hESCs. pBlueScript was used as the vector backbone. In all cases, PCR was carried out with Q5

For targeting the AAVS1 (also known as PPP1R2C) locus, a previously published TALEN pair and homology donor was used (Hockemeyer et al., 2011). The AAVS1 SA-2A-puro-pA homology donor (Addgene) was modified as follows: the SA-2A-puro-pA cassette was release by digestion with HindIII and replaced with annealed oligos with complementary overhangs containing an internal AscI site. This modification permitted direct cloning of all ePiggyBac based vectors, as both the 5' and 3' inverted terminal repeats of ePiggyBac are flanked by AscI sites.

For creation of an knock-in reporter line, an inverted tdTomato flanked by dual loxP sites was PCR cloned from the pAAV-FLEX-tdTomato construct (Addgene) and introduced into the BamHI/NotI site in the ePB-CAG::MCS/BSD. The FLEX-tdTomato/BSD cassette with ITRs was released from the vector backbone by digestion with AscI. This cassette was then introduced into the AAVS1 homology donor to generate AAVS1-HD CAG::FLEX-tdTomato/BSD.

CONSTRUCTION OF THE DRAGONBOW VECTORS

The DRAGONBOW (Doxycycline Regulated Auto-excisable Genetic Labeling of Neurons Based On brainboW) system is comprised of two constructs, one that stochastically labels the nuclei, while the other stochastically labels the cell membranes. For construction of the DRAGONbow constructs, we obtained the Nucbow and Palmbow constructs from Jean Livet (Loulier et al., 2014). Palmbow was digested with NdeI/NotI and the resulting

cassette ligated into ePB-CAG::MCS/NEO digested with the same enzymes. This plasmid was in turn digested with XmaI/EcoRV to remove the H2B-EBFP2 and replaced with cytoplasmic TagBFP2. TagBFP2 was designed have an AgeI restriction site (compatible with XmaI) and a blunt end (compatible with EcoRV) and were introduced by PCR. The final construct was named ePB-CAG::Membow/NEO. Two modifications were introduced into the Nucbow construct: it was first digested with XmaI/EcoRV to remove the H2B-EBFP2 and replaced with TetOn-T2A-PURO using AgeI/EcoRV. T2A is a post-translational self-cleaving peptide that allows for 1:1 stoichiometric expression of proteins on either side of it. This modified construct was subsequently digested with NsiI/AscI to release the vector backbone from the modified Nucbow cassette. An ePiggyBac backbone containing the 5' and 3' piggybac inverted terminal repeats was PCR cloned and ligated to the NsiI/AscI fragment using Gibson assembly. The final construct in ePiggyBac was named ePB-CAG::DRAGONbow/PURO. To induce recombination of the DRAGONbow constructs, a DOX inducible Cre construct was made for targeting to the endogenous AAVS1 locus. Two Lox5171 sites were introduced at either end of Cre recombinase by PCR to make it auto-excisable. This PCR product was digested with BBsI/NotI – sites also introduced by PCR – and cloned into the ePB-TRE::MCS/BSD vector digested with BamHI/NotI. The resulting construct was digested with ClaI/MfeI to introduce a synthesized SV40 intron into the Cre coding sequence; this was found to be critical to prevent auto-excision of Cre in bacteria after transformation. The final construct, ePB-TRE::CRE(lox5171ae)/BSD was then digested with AscI and cloned into the AAVS1 homology donor to generate AAVS1-HD TRE::CRE(lox5171ae)/BSD.

GENERATION OF TRANSGENIC CELL LINES

Nucleofection was used to introduce the plasmids into hESCs to generate ePiggyBac, CRISPR, or TALEN modified cell lines (Lacoste et al., 2009). Cultures were pretreated for 1hr with 10µM ROCK-inhibitor and dissociated with Accutase (Stem Cell Technologies) for 20min. Cells were then triturated with a pipet to ensure single cell suspension and the Accutase diluted out with 4X medium. Cells were counted and desired amount resuspended in nucleofection solution L (Amaxa) and the needed cocktail of constructs. For ePiggyBac insertions, typically 200,000 cells were used, while for TALEN and CRISPR modifications, about 2,000,000 cells. Nucleofection was performed with program setting B-016 on an Amaxa Nucleofector II (Lonza). The transfected cells were then plated drop-wise onto Matrigel plates containing CM supplemented with 10µM ROCK-inhibitor. The inhibitor was removed after 48hrs and colonies allowed to form over the next several days. Antibiotic selection was typically started at day 4 after nucleofection. When needed, the following concentrations of antibiotics were used: 2µg/mL of puromycin, 10µg/mL blasticidin, 200µg/mL hygromycin, or 500µg/mL G418. Selected colonies could be seen within 2-5 days after antibiotic initiation. Media was changed for 8-10 days in the presence of selection to allow the colonies to grow. Individual colonies were then picked under an IVF hood with a 10µL pipette tip and dropped into 10µM ROCK-I containing medium with a P20 pipette. Colonies were broken down by vigorous pipetting and plated on Matrigel or feeder cells. Once the various clones had been successfully established,

they were assayed by either PCR of the locus for TALEN or CRISPR clones using primers listed in Table, and/or subjected to functional analysis based on the nature of the plasmid inserted (e.g. expression of fluorescent protein, live imaging, or differentiation). All clones were karyotyped after expansion to ensure chromosomal stability after genetic modification(s).

For generation of the RUES1 TRE::EGFP-T2A-SMAD7 line, 1µg of transposase, 2µg of ePB-CAG::rTA-M2/HYGRO, and 2µg of ePB-TRE::SMAD7-T2A-EGFP plasmids were nucleofected into the cells. After 3 days of recovery, hygromycin selection was started and maintained for about 10 days when large resistant colonies became visible. For selection of a clonal RUES1 TRE::EGFP-T2A-SMAD7 line, 10 hygromycin resistant colonies were picked manually and grown on feeder layers in CM. Each clone was subsequently split into two 24-well plates. One plate was induced with 2µg/ml doxycyline (DOX) while the other was maintained without DOX. The line displaying homogenous and brightest EGFP expression in the induced plates was chosen for subsequent experiments. This clone was expanded from the uninduced plate and frozen down. Similar protocols were followed for derivation of the RUES2 TRE::EGFP-T2A-SMAD7 line, except that clonal selection was not carried out.

FUCCI triple transgenic lines were made in the RUES2 background following the above protocol with 1µg of transposase, 1µg of ePB-CAG::Venus-hGeminin/PURO, and 1µg ePB-CAG::mCherry-CDT1/BSD and 1µg of ePB-CAG::mCerulean-H2B/NEO plasmids. Following expansion and triple antibiotic selection with puromycin, blasticidin, and neomycin, 16

clones were expanded and assayed for triple expression of fluorescent proteins by confocal analysis of live cultures. The clone with brightest and most homogenous expression of all three fluorescent proteins was selected and grown for further experiments.

The CAG::Citrine and CAG::H2B-Citrine lines were made on an RUES2 background by nucleofection of 0.5µg of transposase together with 1µg of either ePB-CAG::Citrine/NEO or ePB-CAG::H2B-Citrine/NEO plasmids. The cells were then cultured and selected with either neomycin or puromycin for 10 days. After this period, expression of fluorescent proteins in the cytoplasmic or nuclear compartments was visualized in live cultures. One clone displaying the most homogenous signal was selected for each line, expanded for use, and karyotyped.

The triple transgenic CUX2::CreERT2 || FEZF2::NeonGreenV5 || AAVS1-CAG::FLEX tdTomato line was also created in the RUES2 background by three sequential nucleofection and selection cycles. In the first round, 2µg of CUX2::CreERT2/PURO(flox)-TK homology donor was nucleofected into 2,000,000 early passage hESCs together with 0.5µg each of CUX2 right and left TALENs. The cells were grown and selected with puromycin as described above, except that 2µM ganciclovir was also added for negative selection of random integrations. After 2.5 weeks of growth, 22 clones were selected for further characterization by PCR genotyping, sequencing and karyotyping. One clone, which satisfied all criteria, was expanded and subjected a second round of nucleofection with 2µg of AAVS1-HD CAG::FLEX tdTomato/BSD homology donor and 0.5µg each of

AAVS1 right and left TALENs. These cells were selected with blasticidin and expanded for 10 days. Finally, the resulting non-clonal cells were nucleofected a third time with 5µg of the FEZF2::NeonGreenV5/NEO(vflox) homology donor and 10µg of the nickase FEZF2 CRISPR vector (X335). The nucleofected cells were grown and selected in neomycin for 14 days and 12 clones were expanded for PCR genotyping. Out of the clones that were found to be suitable, one clone was chosen for further experiments, expanded, and frozen down. A list of primers used for genotyping is provided in Table 6.10.

The DRAGONbow lines were also created sequentially in the RUES1 hESC background. Two million cells were nucleofected with of 0.5µg of transposase together with 2.5µg each of ePB-CAG::DRAGONbow/PURO and ePB-CAG::Membow/NEO. After four days, the transgenic cells were dual-selected with neomycin and puromycin for 10 days. Since ePB-CAG::Membow/NEO has TagBFP2 in the first position, these colonies could be visualized under epifluorescence with the cyan filter. A second round of nucleofection was carried out on this clone to introduce DOX-inducible CRE into the endogenous AAVS1 locus. In order to do this, 2µg of the AAVS1-HD TRE::CRE(lox5171ae)/BSD homology donor and 0.5µg each of AAVS1 right and left TALENs were introduced into the cells as before. The resulting cells were allowed to grow for 4 days and selected with blasticidin for 10 days. Twelve clones were then picked based on high TagBFP2 brightness and expanded. Each clone was assayed for expression of various combinations of fluorescent proteins by addition of 0.5µg/mL of DOX for 8hrs and subsequent analysis after 48hrs. The clone displaying the broadest color palette of lineages at this time was expanded, frozen down, and used for subsequent experiments.

LIVE IMAGING

For live imaging of fluorescent proteins, ESCs or neural rosettes were seeded onto 35mm μ-dishes (ibidi) and cultured in the appropriate growth medium. At the start of the experiment, the dish lids were replaced with the transparent adapter lid and the dishes loaded into the 37°C incubation chamber of LCV110 VivaView Microscope (Olympus) or CV1000 Spinning disc confocal (Olympus). Images were typically acquired every 15-20min. for varying periods depending on the experiment. Where triple fluorescence was required, the preferred fluorescent proteins were mCerulean (cyan), mCitrine (yellow), and mCherry (red). The exposure settings were usually between 200-400ms. Acquisition parameters were set on a custom interface on Metamorph software (Molecular Devices) for the LCV110. Data analysis was carried out on Fiji (Schindelin et al., 2012) and using custom scripts made in MatLab (MathWorks). The graphs resulting from the analysis were plotted in Mathematica (Wolfram).

EMBRYONIC BRAIN CRYOSECTIONING AND PROCESSING

Fetal brains were obtained from either mouse embryos (E12.5-E18.5) or human aborted fetuses (5-20 PCW). For extraction of brain tissue from mouse embryos, timed pregnant female mice were euthanized at the required stage following institutional guidelines. Surgery was then performed to remove the uterus and extract the embryos into PBS. The

amniotic sac and placenta were then separated and the embryonic head dissected out with a scalpel. For E18.5 and P0-10 pups, the brains were removed from the skull. The tissues were then fixed overnight in 4% PFA and washed in PBS three times. Subsequently, they were cryoprotected with 30% sucrose solution overnight, equilibrated in OCT for 2hrs, and mounted onto a mold. The mold was snap frozen in a mixture of dry ice and isopropanol for 5min. and stored at -80°C. For sectioning, the samples were brought down to -20°C for two to three hours. The cryostat (Leica CM3050 S) was set to a chamber temperature of -18°C and an object temperature of -16°C during this incubation phase. The brains were sectioned at a thickness of 12µm and mounted onto superfrost slides, which were stored at -80°C.

Human fetal brain tissue was obtained from the Human Developmental Biology Resource (http://www.hdbr.org/). The brains were fixed in 4% PFA and washed multiple times in PBS. The fetal brains were then serially cryoprotected in 5%, 15%, and 30% sucrose (in PBS-/-) at 4°C for overnight at each concentration. For more advanced fetal stages (15-20 PCW), the brains were left in 30% for two days to allow them to sink completely. The meninges were subsequently dissected, and the larger brains were dissected further into three parts (Appendix) to allow OCT to permeate into the ventricles. The brains were then allowed to equilibrate in OCT as follows: tissues were swirled in a weighing boat to ensure OCT entry into the ventricles, the air bubbles were removed, and the weighing boat left at 4°C overnight in OCT. Custom molds were made for each brain tissue using 123Design (Autodesk) and 3D printed using the high quality setting in Replicator 2 (Makerbot). The next day, tissues were mounted into the molds (Appendix) and overlaid with OCT. The

mold was snap frozen as above and stored at -80°C until sectioning. For sectioning, the same protocol was followed as for mouse brain sections, except that the tissues were sectioned at 12-20µm thickness. Thinner sections were cut for 10PCW brains while thicker settings were used for the 15PCW brains.

IMMUNOFLUORESCENCE STAINING

Monolayer cultures of hESCs or neural progenitors were fixed in 4% paraformaldehyde (PFA) for 20min. To avoid detachment of neurons, a stock solution of PFA was diluted in culture medium and pre-warmed to 37°C. After two washes in PBS, the plates were blocked and permeabilized in blocking buffer (3% normal donkey serum in 0.2% Triton-X100) for 1hr. Primary antibodies were diluted in block buffer and the cultures incubated in them at 4°C overnight. The list of primary and secondary antibodies used in the study and their respective dilutions are given in Tables 6.4 to 6.6. The plates were subsequently washed in wash buffer (0.1% Tween20 in PBS) three times for 30min. each and incubated in appropriate Alexafluor-conjugated secondary antibodies (Life Technologies) for 1hr at room temperature. The secondary antibodies were also diluted to 1:1,000 in block buffer. After three further washes for 15min. each in wash buffer, DAPI (dilution 1:5,000) was added to the plates in PBS for 15min. Imaging was performed on a LSM 550 Pascal confocal microscope (Zeiss). Immunofluorescent (IF) staining for SMAD C-terminal phosphorylation and BMP4/TGFβ-challenge experiments were carried out using the same

protocol except that the epitopes were demasked and permeabilized with 1% SDS in PBS at 37°C for 30min. prior to blocking.

For fixation of neurons in monolayer cultures, several modifications were made to the protocol. The fixative comprised of PFA resuspended to 4% in 3N medium with 10% (w/v) sucrose to allow the PFA to sink rapidly. The fixative was warmed to 37°C before being applied to the cultured cells. After three washes in PBS for 10min. each, the cultures were blocked and permeabilized in 3% normal donkey serum and 0.2% Triton-X100/PBS for 30min. at room temperature. Primary antibodies (Chapter 6: Appendix) were diluted in block buffer and added to the cultures for 1.5 hours at room temperature. This was followed by three washes with PBS for 5min. each. The appropriate Alexafluor conjugated secondary antibodies (all from Life Technologies; Chapter 6: Appendix) were diluted 1:1,000 in block buffer along with Hoescht33342 nuclear counterstain (1:10,000 dilution) and added to the cultures for 30min. at room temperature. The cultures were subsequently washed twice with PBS for 10min. each. Where required, cover slips were mounted onto the slides with 65µL of Fluoromount G or ProLong Diamond Antifade reagent (Life Technologies) if the cells were expressing fluorescent proteins. If using ibidi µ-plates, aqueous ibidi mounting medium was added to the wells. For larger wells, use PVA mounting medium with DABCO (Sigma) was used for mounting. Four to six color imaging was performed on either LSM 710 confocal microscope (Zeiss) or ImageXpress Micro (Molecular Devices). The channels utilized have been indicated in Chapter 6: Appendix. Data analysis was carried out on Fiji (Schindelin et al., 2012) and using custom scripts made in MatLab (MathWorks).

For staining of human and mouse brain sections, the protocol was modified to include a 4 hour incubation at 60°C in HIER buffer. HIER is comprised of 10mM Tris Base and 1mM EDTA solution adjusted to pH 9. Following incubation, the glass slides were placed in a humidifying chamber and blocked, permeabilized and stained essentially as described for monolayer cultures, using identical dilutions of primary and secondary antibodies. The sections were mounted in ProLong Diamond Antifade reagent and allowed to air dry overnight. The sections were imaged on a confocal at an optical section of 10µm using 405, 488, 568, 594 and 647nm lasers at 12-bit resolution.

For BrdU staining, 2N HCl (diluted in water) was added to the fixed neuronal cultures and incubated at 37°C for 20min. to break open the DNA. HCl was aspirated and the cultures washed with PBS three times before proceeding with primary antibody incubation as described above.

IMAGE QUANTIFICATION

Quantification of cells was carried out on immunofluorescent images or movies using custom code written by Christoph Kirst or Aryeh Warmflash. Images were acquired at 12-bit resolution for quantification purposes and stitched in Zen software 2012 or ImageJ. Nuclear proteins were used as far as possible for quantification. In cases where cytoplasmic markers were used, either flow cytometry or automated counting of images was carried out. The intensity of staining was normalized to DAPI stains for

immunofluorescent images. For analysis of the DRAGONbow lineage tracing, a custom pipeline was designed by Christoph Kirst for analysis. This involved collaborative filtering of the raw images, followed by SLIC for background removal, and lastly superpixel detection and segmentation. The software was programmed to generate color clusters, which were quantified.

MICROARRAY ANALYSIS

Samples were lysed on ice with the mirVana miRNA isolation kit (Ambion) at the following timepoints: 6, 12, and 24hrs and days 2, 3, 5 and 7 post-DOX induction. Each time-point was represented by 2-4 replicates. The extracted RNA was treated with Turbo DNA-free kit (Ambion) and 5µg of RNA was used for microarray analysis. Microarray hybridization was carried out by Rockefeller University Genomics Resource Center on the Illumina platform and data normalization and analysis was carried out with GeneSpring v11.5 software (Agilent Technologies) and Matlab (MathWorks Inc). For microarray analysis, we first obtained lists of genes associated with fates and signaling pathways. Those associated with pathways were from the KEGG pathway database and were downloaded from the Molecular Signatures Database (Subramanian et al., 2005). For neural fate, we used all genes associated with gene ontology keywords: "Nervous System Development", "Generation of neurons", "Brain Development", and "Regulation of nervous system development." Gene lists were downloaded from http://amigo.geneontology.org/. For pluripotency genes, we used the list published by (Suarez-Farinas et al., 2005)

supplemented with the following genes: TDGF1, NANOG, DNMT3B, FOXD3, OTX2, MYOSINX, HEY2, FGF4, REX, and NODAL. These genes are known to be upregulated in hESCs but were excluded from that study for technical reasons. For each list of genes, custom software written in MATLAB was used to find all genes on the list that were up or down regulated by at least 1.5 folds at any time point during SMAD7 mediated neural induction, perform hierarchal clustering of the resulting genes, and generate heatmaps for visualization. Gene ontology analysis was carried out with the DAVID bioinformatics tool using the biological processes option (Huang da et al., 2009b, a).

RT-PCR AND QUANTITATIVE PCR

A hybrid protocol was utilized for RNA extraction in which samples were lyzed with Trizol and RNA was extracted with RNeasy Mini kit (Qiagen). Briefly, cell were lysed at room temperature, homogenized thoroughly, and incubated at room temperature for 5 min. Chloroform was added to the homogenate (0.2 ml chloroform per mL Trizol used) and the mixture vortexed vigorously. After 3min., the sample was spun at 12,000xg for 15min. at 4°C. The aqueous phase was then extracted and an equal volume of 100% RNA-free ethanol was added. After mixing, the sample was passed through an RNeasy column (Qiagen) seated on a vacuum manifold. Between washes, an on-column DNase digestion was carried out Dnase I (Qiagen) at room temperature for 15min. After further washes to remove salt, the column was spun in a centrifuge for 2min. at max speed to remove the remaining buffer in the column. Next, the RNA was eluted from the column membrane in

RNase-free water by incubating at room temperature for 1-2min., and then spun down at max speed. About 1µg of total RNA was reverse transcribed with Transcriptor First strand synthesis kit (Roche) and quantitative real-time PCR reactions were performed with a LightCycler 480 SYBR Green I Master Kit (Roche), both following manufacturer's instructions. Typical reactions for reverse transcription were carried out in a 20µL volume using these parameters: denaturation of RNA with anchored-oligodT(18) primer at 65°C for 10min., followed by incubation with a mixture of dNTPs, RNase inhibitor, reverse transcriptase, and enzyme buffer at 50°C for 1hr. cDNA was subsequently diluted 10-folds and stored at -80°C before being used for used for qPCR or RT-PCR. qPCR was carried out in a LightCycler480 (Roche) with 384-well blocks in a 10µL reaction per well with SYBR green I. The following parameters were used: pre-incubation at 95°C for 5min. (ramp rate 4.8°C/s), followed by 45 cycles of denaturation 95°C for 10s (ramp rate 4.8°C/s), annealing at 55°C for 10s (ramp rate 2°C/s), and extension at 72°C for 12s (acquisition mode: single, ramp rate 4.8°C/s). The melting curve was plotted using standard parameters. For RT-PCR, GoTaq polymerase (Promega) was used; the parameters were: denaturation at 95°C for 2min., followed by 35 cycles of denaturation 95°C for 30s, annealing at 55°C for 30s, and extension at 72°C for 20s; the final extension was at 72°C for 5min. Primers used for the qPCR experiments are listed in Table 6.7. Results for RT-PCR and qPCR were normalized to the house keeping gene ATP5O and from 3-4 technical replicates for each time point. Statistical significance and RNA quantitation relative to un-induced hESCs was determined with REST using the Pair-Wise Fixed Reallocation Randomization Test (Pfaffl et al., 2002) and data was plotted in Office Excel (Microsoft).

FLOW CYTOMETRY

Human ESCs or neural progenitors at time points indicated in the text were detached with Accutase (Stemgent) at 37°C for 15min. They were then washed in PBS and fixed in 2% paraformaldehyde (PFA) for 10min. at 37°C. For staining of intracellular antigens, samples were permeabilized in 90% methanol in PBS for 30min. on ice. Samples were blocked in incubation buffer (0.5% BSA in PBS) at room temperature for 10min. and subsequently incubated in primary antibodies in incubation buffer at room temperature for 1hr (Chapter 6: Appendix). For conjugated antibodies, the samples were washed three times in incubation buffer and analyzed directly. For unconjugated antibodies, samples were washed three times again as before and incubated in Alexafluor-conjugated secondary antibodies in incubation buffer for 30min. at room temperature. Samples were washed again as before and then analyzed. Controls included untreated cells, isotype-only and secondary antibody-only samples. Analysis was carried out in BD-LSRII and FCS data was imported into DiVa (v5; Becton Dickinson) or FlowJo Software (v9; Treestar Inc.) for statistical analysis and visualization. In instances where RNA needed to be extracted from reporter lines, the cells were detached as described and sorted as live cells directly into Trizol (Life Technologies) for cell lysis and RNA extraction. The sorting in this case was carried out by the flow cytometry core facility using BD FACSAriaII (BD Biosciences).

WESTERN BLOT

To detect C-terminal phosphorylation of SMAD1 and SMAD2 after SMAD7-induction, cells were grown in CM for 3 or 7 days, after which they were trypsinized, washed twice in PBS and transferred to SDS-sample buffer for lysis. Protein lysate (40µg) was boiled for 5min. in SDS-sample buffer then subjected to SDS-PAGE and subsequently transferred into nitrocellulose membrane. The membranes were blocked in 5% milk in TBS-T at room temperature for 1hr, incubated with primary antibodies overnight at 4°C, and washed with TBS-T four times (for 10min. each). The samples were subsequently incubated with HRP-conjugated secondary antibodies at room temperature for 1hr and washed in TBS-T again four times (for 10min. each). Detection was performed using the enhanced chemiluminescence reagent (Amersham Pharmacia Biotech). Western blot was performed with the following primary antibodies: total- and phospho-SMAD1 and SMAD2, α-tubulin, and SMAD7. The details of these antibodies are provided in Chapter 6: Appendix.

CHAPTER 3: HUMAN EMBRYONIC STEM CELLS CAN ACQUIRE AN ANTERIOR NEURAL FATE BY A DEFAULT MECHANISM

As described in Chapter 1, inhibition of ongoing TGFβ signaling is sufficient to establish neural fate in amphibian embryos as posited by the "default model" of neural induction (Hemmati-Brivanlou and Melton, 1992, 1994). However, the Activin/Nodal branch can signal through both canonical and non-canonical pathways, and it is unclear if inhibition of both these pathways is required for neural induction, and if the default model applies to hESCs if only the canonical branch of TGFβ signaling is inhibited. In this chapter, I will establish the sufficiency canonical Activin/Nodal and BMP pathway inhibition in anterior neural fate specification of hESCs.

Threshold-specific activation of R-SMADs has been shown to regulate cell fate decisions in all embryonic cells. For example, intermediate R-SMAD2/3 and low R-SMAD1/5/8 signaling are necessary for the maintenance of the hESC pluripotency. Higher input of SMAD2/3 signaling results in induction of mesoderm and endoderm, while higher threshold of SMAD1/5/8 signaling results in trophectodermal differentiation (Xu et al., 2005; Yu et al., 2011). The default state of neural fate represents maximal inhibition of TGFβ activity. This inhibition can occur by secreted inhibitors, such as noggin, chordin, follistatin, and cerberus, as well as intracellular inhibitors of signal transduction such as SMAD6 and SMAD7. Both secreted and the known small molecule inhibitors of TGFβ inhibit both canonical and non-canonical branches of the pathway, as can SMAD6. While there is ample evidence demonstrating that early frog and mammalian embryonic cells default directly to neural fate of telencephalic character in the absence of TGFβ signaling

(Ozair et al., 2013), it is unknown if inhibition of non-canonical components of the TGFβ signaling pathway are also involved. Also, as discussed in the introduction, there is also controversy about the involvement of the FGF-MEK signaling in neural induction.

Several protocols have been developed for neural induction in mammalian ESCs, with most utilizing small molecule inhibitors of the TGFβ pathway (Watanabe et al., 2005; Smith et al., 2008; Chambers et al., 2009; Li et al., 2011) or simply FGF (Ying et al., 2003; Pankratz et al., 2007). However the interpretation of the early events leading to neural induction in these studies has been complicated by several factors: a) usage of small molecule inhibitors that block both canonical and non-canonical branches, b) neuralization has not been shown unequivocally to be a result of direct conversion, c) the character of generated neural tissue is heterogeneous, and d) in some studies, anterior neural fates are not generated. These limitations have precluded a definitive conclusion on the requirement for canonical TGFβ inhibition in mammalian neural induction.

Among the many inhibitors of TGFβ signaling, SMAD7 is known to be a potent, cell autonomous inhibitory SMAD that functions downstream of receptor activation, and is a specific inhibitor of both R-SMADs, but not the non-canonical branch of signaling (Su Myung et al., 2013). During development, activation of either Activin/Nodal or BMP pathways can induce SMAD7 transcription in most cells, where it acts as a negative feedback regulator of both these branches (Yan et al., 2009).

To test rigorously whether the default model of neural induction applies in humans, and to establish if inhibition of the canonical TGFβ pathway is sufficient for this activity, we

over-expressed SMAD7 in an inducible manner in hESCs. In this chapter, I demonstrate that SMAD7 overexpression is sufficient to directly convert hESCs from pluripotency to telencephalic fate, just as in frog embryonic cells (Casellas and Brivanlou, 1998). Global and time-course transcriptome analysis allowed evaluation of transcriptional response elicited by other signaling pathways in response to SMAD7 expression and TGFβ inhibition, specifically indicating down-regulation of FGF-MAPK signaling components in human neural induction. MEK inhibition significantly accelerated telencephalic neural conversion under pluripotency conditions, suggesting that FGF-MAPK has no role in neural induction in the presence of TGFβ inhibition.

SMAD7 INHIBITS TGFβ SIGNALING AND INDUCES NEURAL FATE IN hESCs

SMAD7 mRNA injections are sufficient to directly induce telencephalic fate in *Xenopus* pluripotent embryonic cells (Casellas and Brivanlou, 1998). In order to address whether increasing SMAD7 levels could also completely inhibit TGFβ signaling and convert hESCs to neuroepithelia, we used the ePiggyBac transposon system (Lacoste et al., 2009) to generate a Tet-inducible bicistronic expression cassette encoding EGFP (used as lineage tracer), attached to human SMAD7 via self-cleaving peptide sequence (Figure 3.1A). A second construct constitutively expressing Hygromycin (Hyg) resistance and reverse transactivator (rTA-M2) was also generated. These constructs, along with a plasmid encoding the transposase, were transfected into an hESC line, RUES1 (James et al., 2006), and grown in Hyg selection. A Hyg-resistant clonal line called RUES1 TRE::EGFP-T2A-

SMAD7 was isolated and further expanded (Figure 3.1B). Addition of Doxycycline (DOX) led to the EGFP expression (Figures 3.1C and 3.2A) as well as strong induction of SMAD7 compared to endogenous SMAD7 as determined by Western blot (Figure 3.2B).

After 48 hours of induction, the cells displayed marker changes consistent with exit from pluripotency as observed by the decreases in OCT4 (see below) and undetectable NANOG expression (Figure 3.2C). Since the SMAD2 branch of the TGFβ pathway has been shown to be necessary for the maintenance of hESC pluripotency (James et al., 2005; Vallier et al., 2005), exit from pluripotency was consistent with SMAD7-inhibition of Activin/Nodal signaling. Activation of R-SMADs occurs by C-terminal phosphorylation of serine residues and nuclear translocation. Functional analysis confirmed that SMAD7 was indeed inhibiting R-SMADs by preventing C-terminal phosphorylation as determined by Western blot (Figure 3.1B). IF confirmed that SMAD7-induced hESCs were resistant to R-SMAD C-terminal phosphorylation in the presence of TGFβ1 and BMP4 ligands (Figure 3.2A). In addition, SMAD7-induced cells failed to upregulate the trophectodermal marker CDX2 in response to BMP4 after 48 hours of DOX induction and did not show morphological changes of trophectodermal differentiation, whereas it could be readily detected in un-induced BMP4 treated cells (Figure 3.2C). These results establish that in hESCs SMAD7 expression inhibits TGFβ signaling biochemically and functionally.

Examination of the induced cells by cell type-specific markers demonstrated induction of neural markers at day 11 such as PAX6, OTX2, SOX1, and NFH (Figure 3.1C). A marker of migratory neuronal progenitors, DCX was also demonstrable at this time point. Flow

cytometric quantification of PAX6 demonstrated that at day 11 about 97% of the EGFP positive RUES1 TRE::EGFP-T2A-SMAD7 cells had adopted a neural fate (Figure 3.5A). We were able to confirm expression of these markers and efficient induction of PAX6 in an independent RUES1 TRE::EGFP-T2A-SMAD7 clone, as well as another SMAD7 expressing hESC line, RUES2 TRE::EGFP-T2A-SMAD7 (data not shown). As induction of neural fate occurred by simple addition of DOX to the pluripotency culture medium, without the requirement of any other changes in extrinsic factors, this initial experiment establishes that SMAD7-induction was sufficient for neural conversion under these conditions.

Figure 3.1: SMAD7-induction promotes homogeneous neural conversion of hESCs.

A. Schematic of the ePiggyBac constructs used to create the SMAD7 cell line from RUES1 hESCs. The ePB-HYGRO-CAG-rTA/M2 codes for a tetracycline transactivator that binds to the TRE promoter sequence in ePB-TRE::EGFP-T2A-SMAD7 only in the presence of DOX and permits inducible SMAD7 expression. The T2A peptide enables post-translational cleavage of SMAD7 from EGFP.

B. Experimental setup for time-course immunocytochemical and qPCR/microarray analysis.

C. IF microscopy reveals extensive expression of the neural determinant PAX6 on day 11 under pluripotency conditions. Strong co-localization of PAX6 with another neural-specific gene SOX1 is also observed, while near-complete overlap is seen with the forebrain-midbrain marker OTX2. Clusters of PAX6+ cells are surrounded by migratory DCX+ neurons. NFH+ cells with features of mature neurons are also seen in areas of DCX+ cells.

Scale bars: 200µm.

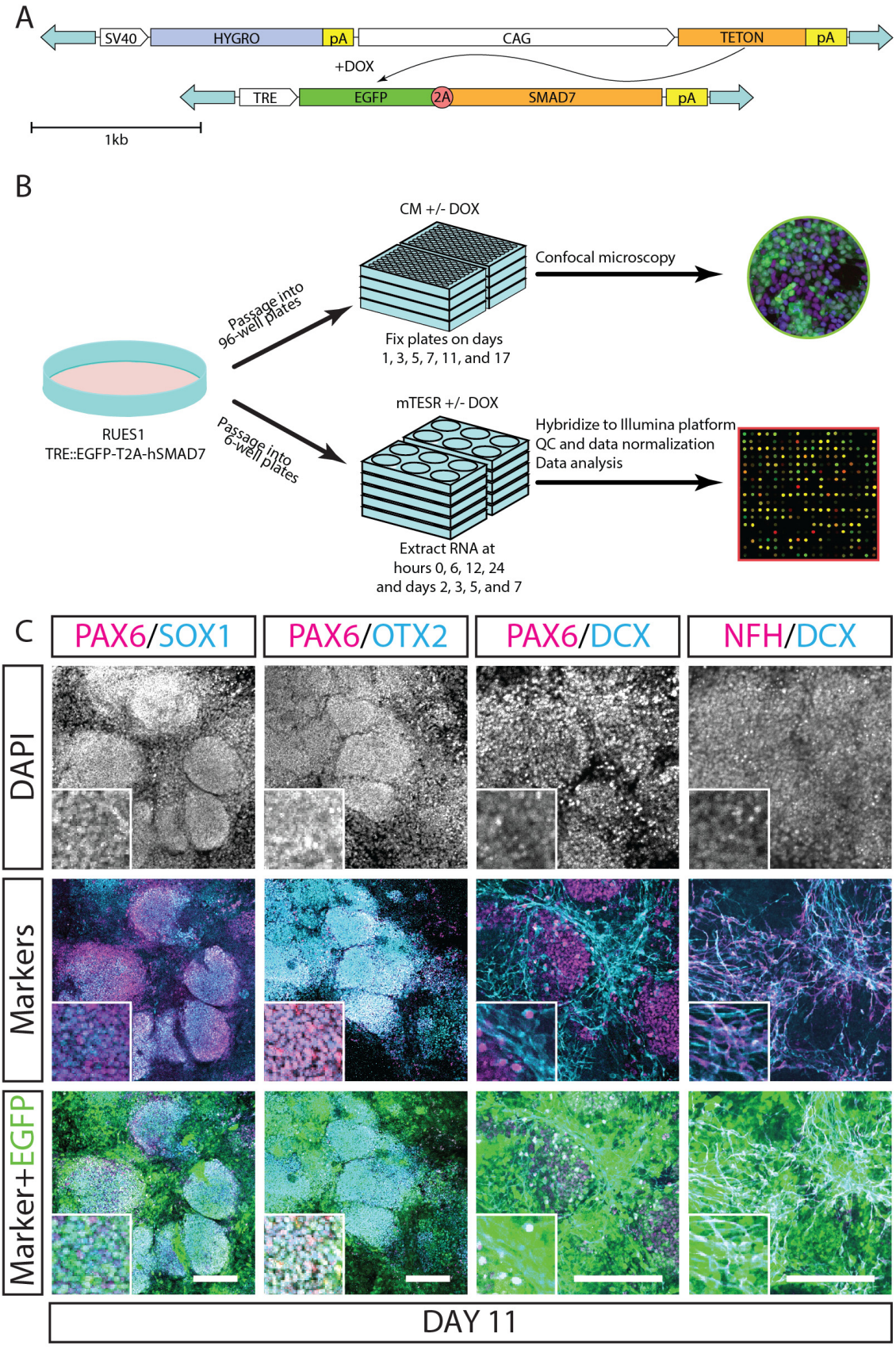
A
SV40
HYGRO
pA
CAG
TETON
pA
+DOX
TRE
EGFP
2A
SMAD7
pA
1kb
B
CM +/- DOX
Confocal microscopy
Passage into 96-well plates
Fix plates on days 1, 3, 5, 7, 11, and 17
RUES1
TRE::EGFP-T2A-hSMAD7
Passage into 6-well plates
mTESR +/- DOX
Hybridize to Illumina platform
QC and data normalization
Data analysis
Extract RNA at hours 0, 6, 12, 24 and days 2, 3, 5, and 7
C
PAX6/SOX1
PAX6/OTX2
PAX6/DCX
NFH/DCX
DAPI
Markers
Marker+EGFP
DAY 11

Figure 3.2: SMAD7 inhibits canonical Activin/Nodal and BMP signaling in hESCs and prevents alternative fates.

A. Immunocytochemistry confirms attenuation of SMAD2/3 and SMAD1 C-terminal phosphorylation in SMAD7-induced cultures on exposure to high doses of BMP4 and TGFβ1. RUES1 TRE::EGFP-T2A-SMAD7 cultures were induced with DOX for 24hrs, challenged with 25ng/ml TGFβ1 and 50ng/ml BMP4 for 1.5hrs and subsequently fixed. Sytox is used here as a nuclear counterstain.

B. Western blot demonstrating loss of C-terminal phosphorylation (and hence activity) of SMAD1 and SMAD2 in RUES1 TRE::EGFP-T2A-SMAD7 cultures on DOX induction on Days 3 and 7.

C. Uninduced TRE::EGFP-T2A-SMAD7 cells respond to BMP4 by upregulating the trophectodermal marker CDX2, whereas DOX-induced cells are resistant to trophectodermal differentiation. In addition, induced cells downregulate NANOG as it is a direct downstream target of Activin/Nodal signaling. Induction of CDX2 coincided with nuclear localization of P-SMAD1/5. Cultures were induced with DOX for 24hrs, challenged with 50ng/ml BMP4 for 48hrs and subsequently fixed. Sytox is used here as a nuclear counterstain.

Scale bars: 200μm.

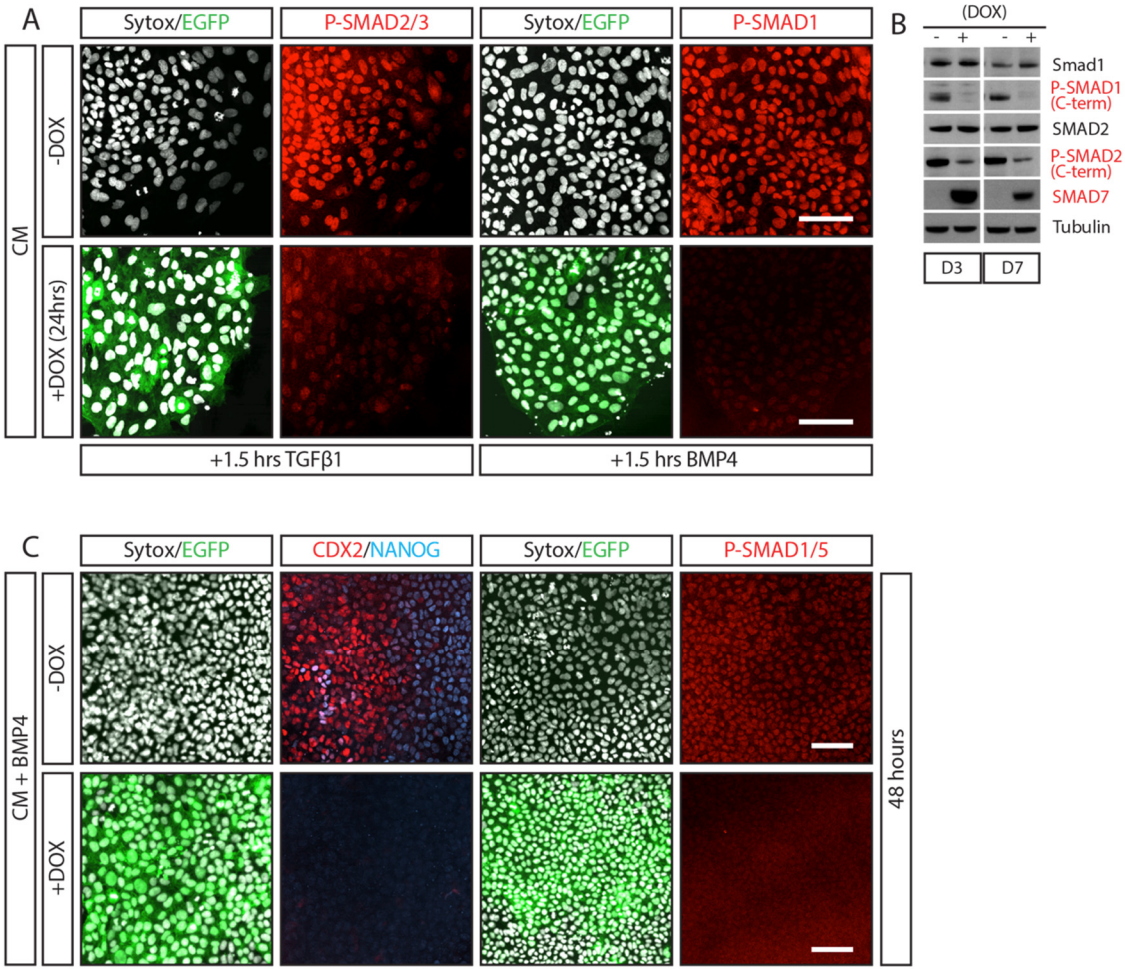
A
Sytox/EGFP
P-SMAD2/3
Sytox/EGFP
P-SMAD1
CM
-DOX
+DOX (24hrs)
+1.5 hrs TGFβ1
+1.5 hrs BMP4
B
(DOX)
- + - +
Smad1
P-SMAD1 (C-term)
SMAD2
P-SMAD2 (C-term)
SMAD7
Tubulin
D3
D7
C
Sytox/EGFP
CDX2/NANOG
Sytox/EGFP
P-SMAD1/5
CM + BMP4
-DOX
+DOX
48 hours

TIMING OF SMAD7-MEDIATED NEURAL INDUCTION

To determine the exact timing of conversion from pluripotency to neural fate, time-course microarray studies at discrete time points following SMAD7-induction were performed in parallel with IF of cell type-specific molecular markers (Figure 3.1B). Transcriptome analysis of induced RUES1 TRE::EGFP-T2A-SMAD7 transgenic cells was done every day for 7 days, and at 3 time points during the first day (6, 12, and 24 hours), and analyzed relative to un-induced controls. Parallel confocal IF was extended to day 11.

Time-course heatmaps showed that at the transcriptional level the expression of a panel of molecular markers of pluripotency (Suarez-Farinas et al., 2005) including NANOG, OCT4, DMNT3B, ETS1, BAMBI, GDF3, ZFP42, and LEFTY2, were down-regulated by day 1-2, and were lost after one week of Dox induction (Figure 3.3A; see also Table 6.11). This was independently confirmed by qPCR for OCT4 and NANOG (Figure 3.3C), and by IF for OCT4 (Figure 3.3D). Interestingly, we also observed transient up-regulation of the epiblast marker ZIC2 (day 3), and a sustained up-regulation of the epiblast and anterior neural fold marker POU3F1 (data not shown), as has been reported for mouse embryos *in vivo*, and mESCs *in vitro* (Kamiya et al., 2011; Zhu et al., 2014). This suggests that even though hESCs share defining characteristics with mouse epiblast stem cells (mEpiSCs) (Hanna et al., 2010), they still pass through an epiblast-like phase during neural conversion. The decline of pluripotency gene expression coincided with the gradual expression of early neural markers, including OTX2, PAX6, NR2F2, POU3F1, HES5, HESX1, SIX3, DACH1, ZNF521, and SIP1, which were induced at days 2-5 (Broad Molecular Signature Database; Figure 3.3B

and Table 6.11). Induction of more mature neuronal markers was also observed in this time window. Expression of PAX6 and SOX1 was confirmed independently by qPCR and IF (Figure 3.3C-D). No expression of the neural crest determinant TxF SOX10 was observed by IF or qPCR (Figures 3.3C and 3.4). It has been shown that neural crest induction require high levels of WNT signaling (Menendez et al., 2011); this finding points to low to moderate levels of WNT in our culture system. Flow cytometry for PAX6 and the pan-neural marker NCAM supported the gradual acquisition of neural fate by the SMAD7 expressing cells (Figure 3.5A-C). NCAM is known to be expressed by both *Xenopus* neuroepithelial cells as well as hPSC-derived PAX6+ neuroepithelial cells (Kintner, 1988; Lee et al., 2015). Flow cytometric quantification of PAX6 demonstrated that at day 11 the majority (97%) of the EGFP positive cells had adopted a neural fate (Figure 3.5A). In addition, expression of markers of more differentiated neuronal cells was readily detectable by IF at day 5 for NCAM and days 7 for DCX and NFH (Figure 3.5C-E). Taken together, the results from time-course microarray, qPCR, and IF demonstrate that SMAD7-mediated neural induction in TRE::EGFP-T2A-SMAD7 cells starts after 3 days post-DOX induction in feeder-free pluripotency conditions.

FIigure 3.3: SMAD7 is sufficient for neural conversion of hESCs under conditions favoring pluripotency without contamination by non-neural lineages.

A. *Heatmap of pluripotency genes changing by more than or equal to 2-fold on SMAD7-induction under pluripotency conditions. The complete list of genes is provided in Table 6.11.*
B. *Time-course heatmap from global transcriptome analysis of SMAD7-induced cultures showing gradual acquisition of a neural fate. Genes up- or down- regulated by more than or equal to 2-fold are shown. The complete list of genes is provided in Table 6.11.*
C. *qPCR of lineage-specific genes between Days 1-13 of DOX induction. A decrease in transcripts of pluripotency genes (OCT4, NANOG) and absence of ectodermal (KRT14), neural crest (SOX10), endodermal (SOX17), or mesodermal (BRA, MIXL1) lineage transcripts is observed. The small upregulation of BRA between days 2-5 was not accompanied by nuclear localization of the protein on IF (see also Figure 3.6A-B). Upregulation of PAX6 is also seen.*

Time-course expression of neural and pluripotency markers between days 1-17 in SMAD7-induced cultures are shown in D-F.

D. *The pluripotency marker OCT4 is strongly down-regulated Day 3 onwards.*
E. *Upregulation of PAX6 is first seen at Day 5 and stays up till Day 17.*
F. *PAX6 expression is paralleled by expression of another early neuroepithelial gene SOX1, which disappears entirely by Day 17. Between days 3-11, there is a strong overlap between domains of PAX6 and SOX1 expression.*

qPCR data is presented as LOG_2-fold change over uninduced hESCs. ATP5O was used for internal normalization at each time point. Bars represent n = 3-4 ± SEM. Scale bars: 200µm.

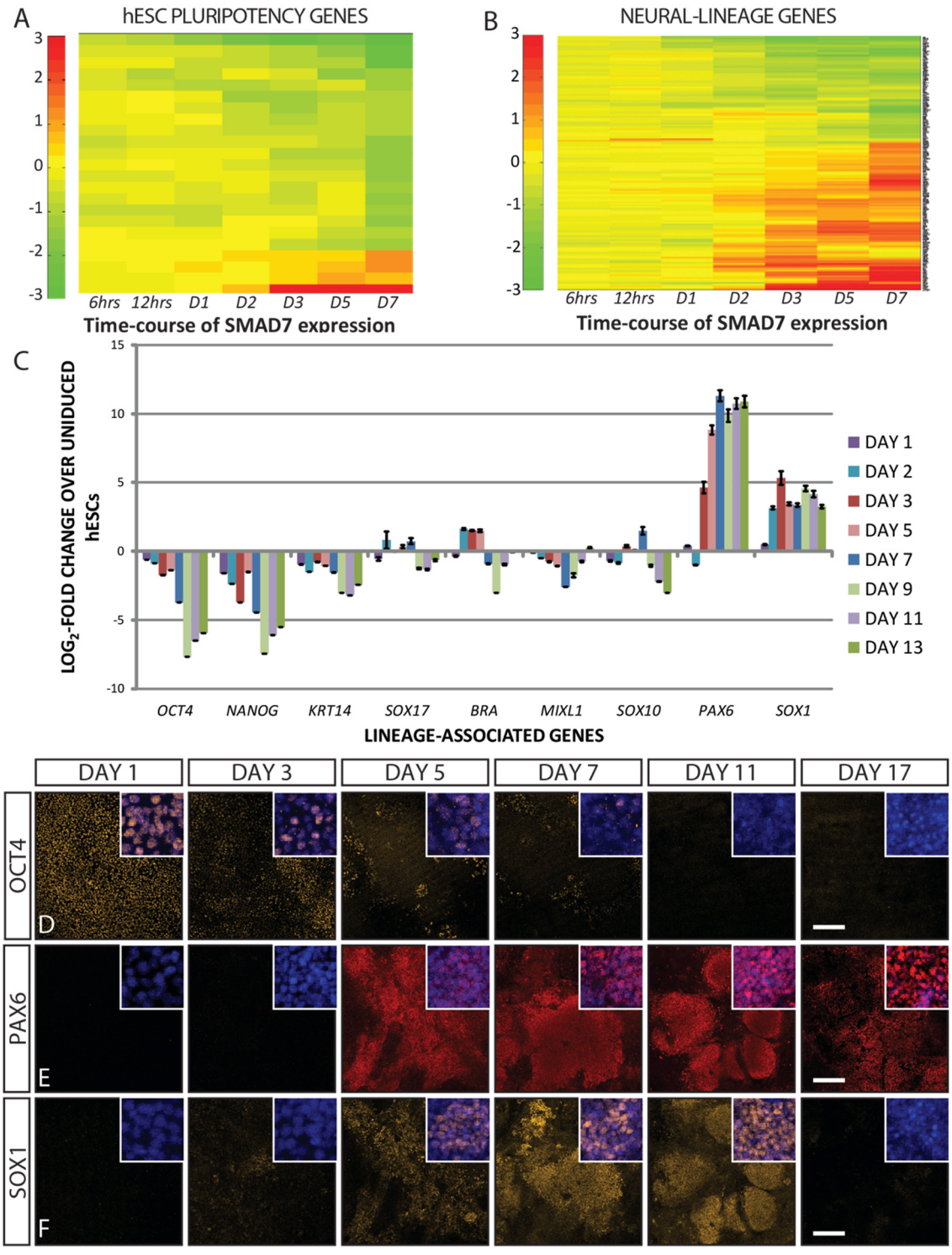
A
hESC PLURIPOTENCY GENES
3
2
1
0
-1
-2
-3
6hrs 12hrs D1 D2 D3 D5 D7
Time-course of SMAD7 expression
B
NEURAL-LINEAGE GENES
3
2
1
0
-1
-2
-3
6hrs 12hrs D1 D2 D3 D5 D7
Time-course of SMAD7 expression
C
LOG2-FOLD CHANGE OVER UNIDUCED hESCs
15
10
5
0
-5
-10
OCT4 NANOG KRT14 SOX17 BRA MIXL1 SOX10 PAX6 SOX1
LINEAGE-ASSOCIATED GENES
DAY 1
DAY 2
DAY 3
DAY 5
DAY 7
DAY 9
DAY 11
DAY 13
DAY 1
DAY 3
DAY 5
DAY 7
DAY 11
DAY 17
OCT4
D
PAX6
E
SOX1
F

The dynamics of expression of neural TxFs support the neural inducing activity of SMAD7 via inhibition of the Activin/Nodal-SMAD2/3 and BMP-SMAD1/5/8 branches. For example, it is known that Activin/Nodal-SMAD2/3 signaling maintains pluripotency in hESCs by directly maintaining expression of NANOG, a core pluripotency gene (Vallier et al., 2009a). Together, NANOG SOX2 and OCT4 act in a feed-forward loop to promote expression of each other and repress many differentiation specific genes in ESCs (Boyer et al., 2005). Inhibition of Activin/Nodal-SMAD2/3 by SMAD7 down-regulates NANOG and promotes expression of the zinc finger homeodomain TxF ZEB2, as shown here by qPCR and microarray data (Figure 3.7A and E). ZEB2 has previously been shown to promote neuroectodermal differentiation and prevent mesendodermal of hESCs (Chng et al., 2010). In addition, SMAD7 induction promoted induction of OTX2 and NR2F2 (Figure 3.7B and E), which are among the earliest TxFs expressed during neural differentiation of hESCs (Greber et al., 2011; Rosa and Brivanlou, 2011). OTX2 in turn can directly activate transcription of the neural determinant PAX6 in hESCs (Greber et al., 2011). NR2F2 on the other hand represses OCT4 expression directly and promotes expression of other neural-specific markers, as shown previously (Rosa and Brivanlou, 2011).

Inhibition of BMP-SMAD1/5/8 branch during neural induction is also known to trigger characteristic patterns of gene expression that our recapitulated in our SMAD7 induction dataset. For instance, Inhibition of BMP signaling is known to stabilize the neural program by maintaining expression of SOX2 (Greber et al., 2011). Maintenance of SOX2 is observed in our microarray (data not shown). Absence of BMP signaling is also known to promote expression of cell-intrinsic neural determinants, such as the zinc finger TxF ZNF521, which

is necessary and sufficient for neural induction in hESCs (Kamiya et al., 2011). ZNF521 was also strongly induced under SMAD7 induction at Day 11 (data not shown). Lastly, BMP inhibition prevents induction of non-neural germ layers (trophectoderm and mesendoderm) as shown below (Figure 3.3C and 3.6). Indeed, previous studies have shown that low BMP signaling together with down-regulation of OCT4 is a prerequisite for neuroectodermal specification in hESCs (Wang et al., 2012b).

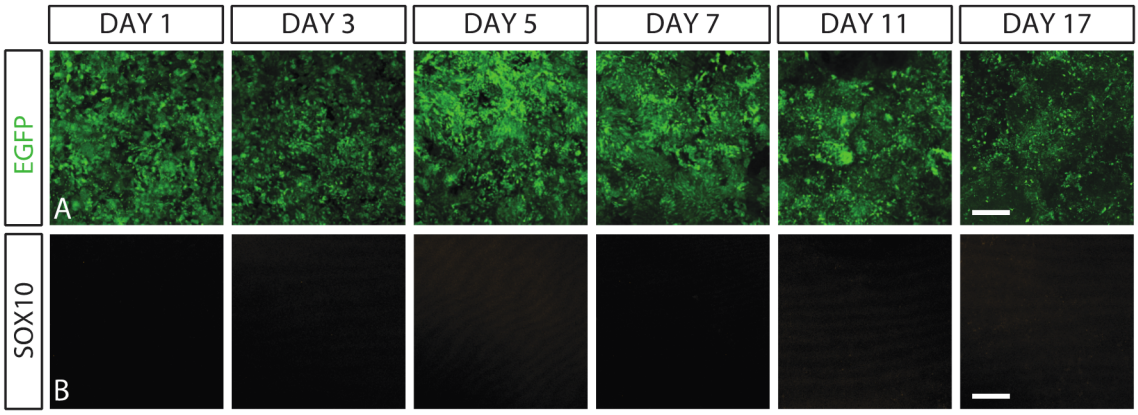

Figure 3.4: SMAD7-induced cells do not express the neural crest marker SOX10. A) EGFP expression in induced cultures. B) Absence of the neural crest lineage TxF SOX10 by IF analysis. Scale bars: 200µm.

Figure 3.5: Efficient neuralization in SMAD7-induced hESCs under conditions favoring pluripotency.

A. *Flow cytometry of EGFP+ cells showing that majority of SMAD7-induced cells become PAX6+ by Day 12 of induction under pluripotency conditions.*
B. *Dynamics of NCAM expression on DOX induction as determined by flow cytometry. About 85% of EGFP+ cells are also NCAM+ by Day 7, and this correlates with PAX6 expression observed by IF (See Figure 3F). NCAM+ cells comprise about 90% of EGFP+ cells on Day 11.*
C. *IF of SMAD7-induced cultures selectively expressing the surface marker neural cell adhesion molecule (NCAM; CD56) on Day 11 of DOX (lower panels). Almost complete co-localization with EGFP+ cells is seen. A few NCAM+ cells are also seen in uninduced cultures (upper panels).*
D. *Time-course analysis of differentiating SMAD7-induced cells shows that the migrating neuronal marker doublecortin (DCX), a marker of early neuronal differentiation, is observed at later time points (Days 11-17) in cells with clear neuronal morphology.*
E. *The post-mitotic neuronal marker NFH is also observed in these cultures at these time points. While co-localization of DCX and NFH as well as PAX6 and DCX was seen in some areas, they are largely mutually exclusive. EGFP fluorescence is not displayed here for clarity.*

Scale bars: 200μm.

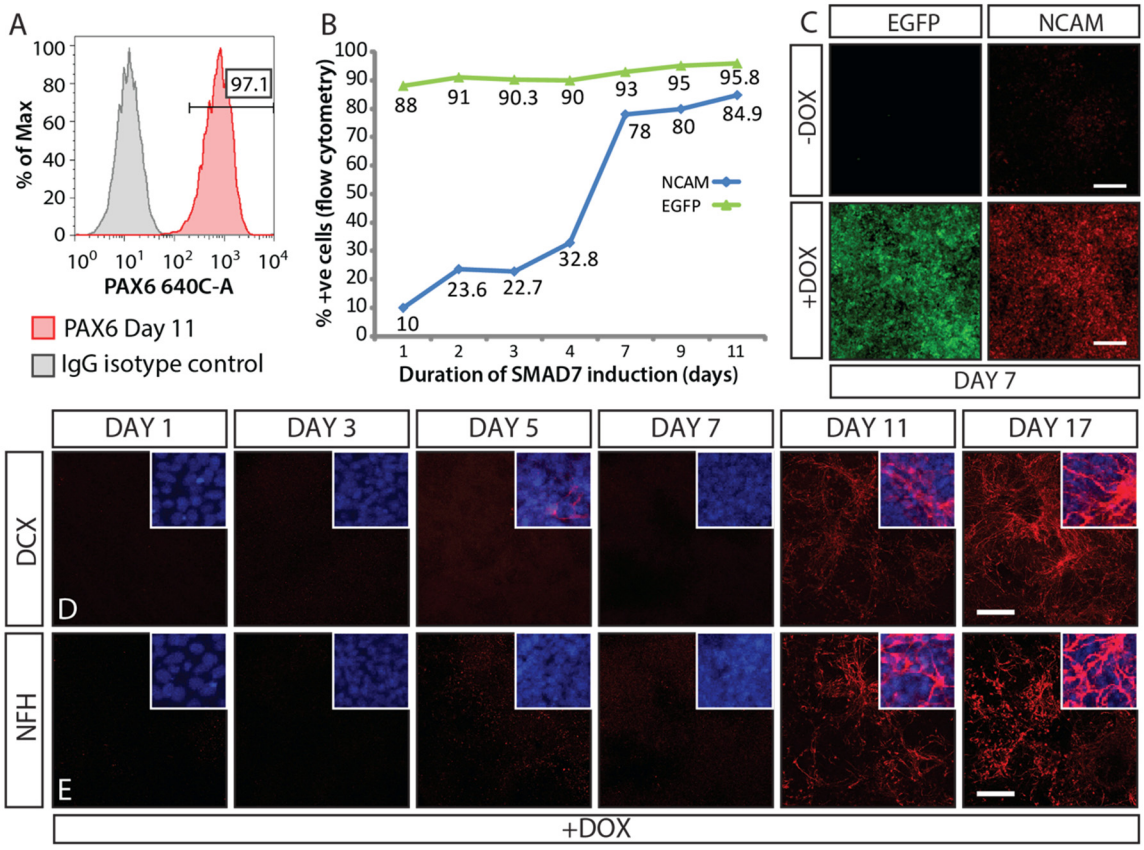
A
% of Max
97.1
PAX6 640C-A
PAX6 Day 11
IgG isotype control
B
% +ve cells (flow cytometry)
88
91
90.3
90
93
95
95.8
10
23.6
22.7
32.8
78
80
84.9
NCAM
EGFP
Duration of SMAD7 induction (days)
C
EGFP
NCAM
-DOX
+DOX
DAY 7
DAY 1
DAY 3
DAY 5
DAY 7
DAY 11
DAY 17
DCX
NFH
D
E
+DOX

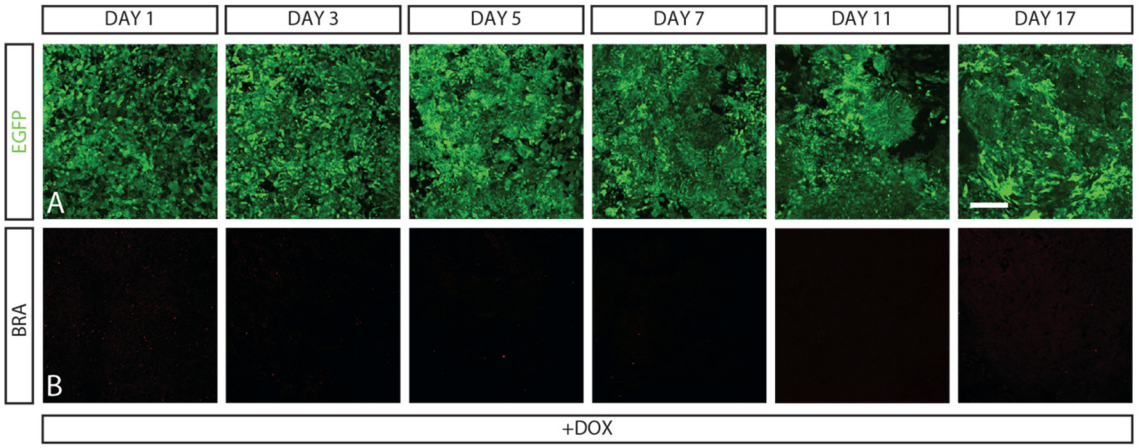

Figure 3.6: SMAD7-mediated neural induction is direct and does not take place through mesodermal intermediates. A) EGFP expression in induced cultures. B) Absence of the mesodermal lineage TxF BRA (brachyury) by IF. Scale bars: 200µm.

SMAD7-MEDIATED NEURAL INDUCTION IS DIRECT

Pluripotent cells can adopt a neural fate by either direct or secondary/concomitant induction of other embryonic germ layers such as mesoderm, organizer/node, endoderm, or extra-embryonic tissue. To address whether SMAD7 mediated neural conversion was direct, we analyzed the microarray data set, which indicated that DOX-induced RUES1 TRE::EGFP-T2A-SMAD7 cells did not express markers of other embryonic germ layers. These included Brachyury (BRA), MIXL1, HAND1, for mesoderm; SOX17, GATA4 or GATA6, for endoderm; CDX2, EOMES, β-HCG, KLF5, for trophectoderm; and KRT14 for non-neural ectoderm, at any time point (data not shown). This conclusion was independently confirmed by qPCR for BRA and MIXL1 for mesoderm and SOX17 for endoderm (Figure 3.3C) and by IF for BRA and SOX17 (Figure 3.6 and data not shown). This was also true for the non-neural ectoderm marker KRT14 and the neural crest progenitor marker SOX10

(Figures 3.3C and 3.4). Importantly, SMAD7 did not induce expression of organizer/node specific markers such as GSC, MIXL1, FOXD3, or FOXA2 (also demarcating the floor plate at later time points) (Tamplin et al., 2008), demonstrating that neural fate induction was not following or concomitant with the formation of the organizer/node. These results provide evidence for direct induction of neural fate from pluripotent RUES1 cells and support the validity of the second attribute of the default model: direct conversion from pluripotency to neural fate.

Figure 3.7: SMAD7 imposes an anterior identity in neuralized hESCs.

A. qPCR of neural lineage genes between Days 1-13 of DOX induction. A robust increase in neural lineage transcripts such as SIP1, SOX1, and BRN2 as well as anterior neural transcripts such as OTX2, SIX3, LHX2, and FOXG1 is seen. Primers specific to the anterior neural specific isoform of OTX2 were used. No change in the hindbrain marker HOXB4 is observed.

Time-course expression of dorsal and ventral forebrain markers between Days 1-17 in SMAD7-induced cultures are shown in 4B-4D. Human ESCs were induced in conditions favoring pluripotency as before.

B. The first marker up-regulated is the anterior marker OTX2. Near complete co-localization of OTX2 is seen with PAX6 D5 onwards, suggesting a neural, rather than anterior visceral endodermal source of expression of OTX2.

C. The dorsal neural tube marker PAX3 is also seen in the cultures between D5-17. Patchy expression of PAX3 was noticeable at these time-points. During mouse development, PAX3 is expressed in some parts of the dorsal forebrain early on.

D. Clusters of cells expressing the ventral telencephalic (medial ganglionic eminence) marker NKX2.1 are also observed in the cultures in a mutually exclusive manner to PAX6.

E. Time-course heatmap from global transcriptome analysis showing expression of genes associated with forebrain signature. Genes up- or down- regulated by more than or equal to 2-fold are shown. The list of genes is also provided in Table 6.12.

qPCR data is presented as LOG_2-fold change over uninduced hESCs. ATP5O was used for internal normalization at each time point. Bars represent n = 3-4 ± SEM. Scale bars: 200µm.

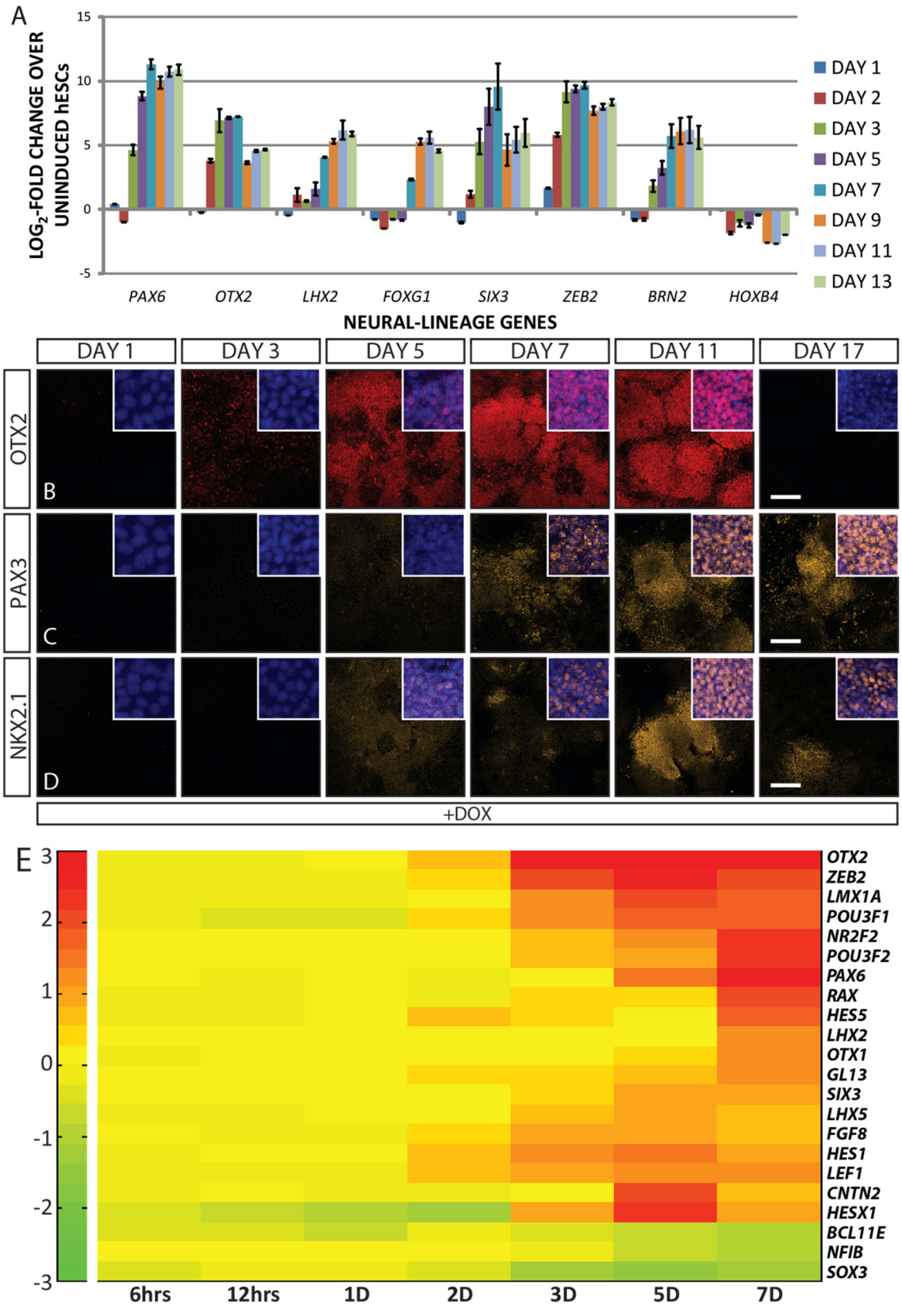
A
LOG2-FOLD CHANGE OVER UNINDUCED hESCs
15
10
5
0
-5
PAX6
OTX2
LHX2
FOXG1
SIX3
ZEB2
BRN2
HOXB4
NEURAL-LINEAGE GENES
DAY 1
DAY 2
DAY 3
DAY 5
DAY 7
DAY 9
DAY 11
DAY 13
DAY 1
DAY 3
DAY 5
DAY 7
DAY 11
DAY 17
OTX2
B
PAX3
C
NKX2.1
D
+DOX
E
3
2
1
0
-1
-2
-3
OTX2
ZEB2
LMX1A
POU3F1
NR2F2
POU3F2
PAX6
RAX
HES5
LHX2
OTX1
GL13
SIX3
LHX5
FGF8
HES1
LEF1
CNTN2
HESX1
BCL11E
NFIB
SOX3
6hrs
12hrs
1D
2D
3D
5D
7D

NEURAL TISSUE INDUCED BY SMAD7 IS TELENCEPHALIC IN IDENTITY

Finally, we addressed the character of SMAD7-induced neural fate globally in function of time followed by independent confirmation with qPCR and IFs. We first looked at the antero-posterior identity. Microarray data indicated the presence of the most anterior neuronal fate in SMAD7-induced cells, as evidenced by expression of the anterior-specific neural genes such as OTX1/2, SIX3, LHX2, ZNF521, LHX5, SP8, LIX1, LMO4, RAX, SIX6, and GLI3 (Figure 3.7A and E; see also Table 6.12). This was also confirmed by Gene Ontology analysis of enriched genes on Day 7 (Figure 3.8). Induction followed a temporal hierarchy. For example, genes induced by at least five-fold by DOX included OTX2 and ZEB2, first induced at Day 2, PAX6 and SIX3 at Day 3, LHX2 and FOXG1 at day 7, and BRN2 (POU3F2) at later time points. Early expression of OTX2 was confirmed by IF (Figure 3.7B). However, markers of midbrain (EN2), hindbrain, or spinal cord (HOXB4) were not detected at any time point, suggesting specific induction of human telencephalic fate. Examination of dorsal-ventral markers established the presence of dorsal and ventral cell types within the forebrain territory, as demonstrated by the expression of NKX2-1 and PAX3 (Figure 3.7C). NKX2-1 is a marker of ventro-lateral fate (medial ganglionic eminence), and was detected in rare clusters, but the most ventral fate (floor plate) did not seem to be induced, as FOXA2 expression was not detected (data not shown). This suggests the absence of the most ventral fate. Together, these results establish that the third attribute of the default model – i.e., anterior neural conversion – is also valid in hESCs, as in frogs, and supports the notion that the molecular circuitry underlying early neural induction is evolutionarily conserved in humans.

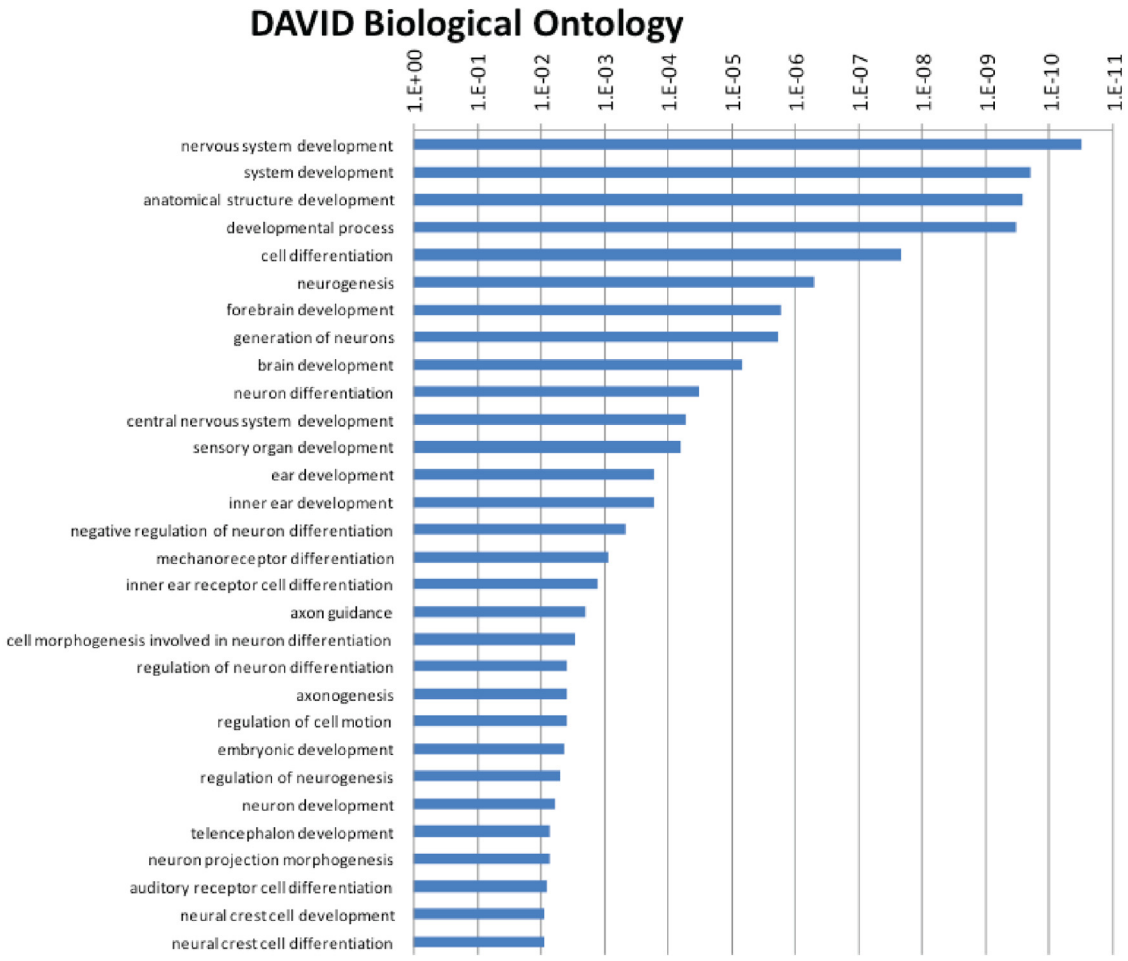

Figure 3.8: DAVID gene ontology of D7 SMAD7-induced cultures. GO shows enrichment for genes involved in forebrain fate and neuroepithelial identity.

INHIBITION OF FGF-MEK SIGNALING PROMOTES SMAD7-MEDIATED NEURAL FATE

FGF-MEK signaling is required for the maintenance of pluripotency through NANOG expression in hESCs (Chen et al., 2011), but not mESCs. Additionally, the FGF-MEK signaling pathway has been proposed to be required for mammalian neural induction (Stavridis et al., 2007; LaVaute et al., 2009). Due to the requirement of FGF and Activin/Nodal signaling for maintenance of the pluripotent state of hESCs, it has been

suggested that hESCs represent an epiblast-like state rather than the ICM state of mESCs. A brief exposure of FGF-MEK signaling is required for mESCs to become epiblast cells, which can then be grown in the presence of Activin, like their hESC counterparts (Hanna et al., 2010). For mESCs neural induction, FGF might be required initially simply to allow the transition of mESCs to an epiblast fate, but not later for neural induction (Kunath et al., 2007; Sterneckert et al., 2010).

In order to obtain high-resolution views of the secondary signaling events operating downstream of SMAD7-mediated neuralization, we analyzed genes pertaining to the developmentally relevant signaling pathways in our time-course microarray. Interestingly, we found an overall down-regulation in many components of FGF/MAPK signaling and upregulation of several cell-intrinsic inhibitors of MAPK signaling in our analysis (Figure 3.9A and Table 6.13). These inhibitors included the dual-specificity phosphatase inhibitor (DUSP4), the cell intrinsic FGF and WNT inhibitors of the SHISA family (SHISA2 and SHISA3), as well as a FGF/EGF cell intrinsic inhibitor of the SPROUTY family (SPRY1). We followed up on these observations to address the relevance of FGF-MEK signaling in hESC neural induction. FGF-MEK signaling was inhibited using the specific MEK1/2-inhibitor PD0325891 to block the pathway downstream of the receptor under pluripotency conditions. MEK-inhibitor was added to RUES1 TRE::EGFP-T2A-SMAD7 cultures at 0, 12, 24 and 48hrs after DOX-induction, and cells were cultured in the presence of the inhibitor until day 7 of DOX-induction. No discernible differences in neural conversion were detected between these conditions as determined by PAX6 and OCT4 IF

on day 7 (Figure 3.9C), excluding the possibility of MEK1/2 signaling involvement in the epiblast-like transition or neural conversion during this period of hESC differentiation.

The dynamics of neural induction were then determined by combined MEK-inhibition and SMAD7-induction in hESCs. We used the highly specific MEK-inhibitor PD326901 at a concentration that can eliminate MEK/ERK phosphorylation in hESCs as determined by Western blot and protein arrays (data not shown). RUES1 TRE::EGFP-T2A-SMAD7 cells were cultured in pluripotency conditions and subsequently treated with MEK-inhibitor, DOX, and MEK-inhibitor/DOX combinations. cDNA was generated from cells after 0, 1, 3, 5, and 7 days of treatment. qPCR demonstrated that PAX6, ZNF521, SIP1, and POU3F2 expression increased to significantly higher levels in the MEK-inhibitor/SMAD7 condition compared to SMAD7 only and MEK-inhibitor only conditions (Figure 3.9B and 3.9E). While low levels of PAX6 transcripts were induced by MEK-inhibitor alone (data not shown), the other neural determinants SIP1, ZNF521 and POU3F2 were not induced in this condition (Figure 3.9E). Furthermore, while down-regulation of the pluripotency transcripts OCT4 and NANOG was also seen in MEK-inhibitor alone, SMAD7 and MEK-inhibitor/SMAD7 conditions demonstrated a more robust down-regulation of these transcripts (Figure 3.9E). Compared to SMAD7 only, MEK-inhibitor/SMAD7 condition showed higher levels of PAX6 (3-fold), the intrinsic neural determinant ZNF521 (25-fold), and the neural POU-domain TxF POU3F2 (6-fold) on Day 5, comparable levels of the neural fate determinant SIP1, and an almost complete loss of NANOG and OCT4 expression during this time. Intracellular flow cytometry on Day 7 of the MEK-inhibitor/SMAD7 combination for the neural genes PAX6 and SOX2 confirmed expression of these factors in >90% of EGFP+ cells

compared to 67% of PAX6 cells in the SMAD7-only condition (Figure 3.9D). Together, these results demonstrate that FGF-MEK-ERK signaling has an inhibitory, rather than an instructive, role in hESC neural induction, and points to TGFβ inhibition as sufficient for neural conversion. Since inhibition of MEK alone can directly up-regulate some neural genes and down regulate pluripotency genes, this suggests that FGF-MEK signaling may be directly repressing neural genes in hESCs, as has be shown in mEpiSCs (Greber et al., 2010). The combination of SMAD7-induction and early MEK inhibition strongly promotes expression of neural genes, coupled with down-regulation of pluripotency genes and results in robust neural conversion of hESCs.

Figure 3.9: MEK-inhibition promotes SMAD7-mediated neural conversion under conditions favoring pluripotency.

A. *Time-course heatmap of the MAPK pathway in induced hESCs showing down-regulation of several MAPK related genes and upregulation of cell-intrinsic MAPK inhibitors. Genes changing by more than or equal to 1.5-fold are shown on this heatmap. The complete list of genes is provided in Table 6.13.*
B. *Quantitative RT-PCR for PAX6 transcripts in MEK-inhibitor (blue), SMAD7 (green), and MEK-inhibitor/SMAD7 (red) combinations in pluripotency conditions. MEK-inhibitor/SMAD7 and SMAD7 result in significantly higher increase in PAX6 expression relative to MEK-inhibitor alone, with the MEK-inhibitor/SMAD7 combination leading to a >3-fold increase in PAX6 on D5 compared to SMAD7. qPCR data is presented as relative fold-change over MEK-inhibitor treated hESCs.*
C. *MEK-inhibition before epiblast-like transition does not prevent neural conversion in SMAD7-induced cultures. Addition of MEK-inhibitor at 0, 12, 24 and 48hrs after SMAD7-induction did not result in observable differences in PAX6 expression or down-regulation of OCT4 on D7 of induction. The time labels above the figures represent the time of addition of MEK-inhibitor after DOX-induction.*
D. *Flow cytometry for EGFP, PAX6, and SOX2 in the MEK-inhibitor/SMAD7 combination shows that >90% of the cells are positive for these markers by D7 of induction in conditions favoring pluripotency. SOX2 is expressed in both pluripotent cells as well as neuroepithelial cells.*
E. *qPCR of anterior neural genes between Days 1-7 of MEK-inhibitor (blue), SMAD7 (red), and MEK-inhibitor/SMAD7 (green) combinations. Transcripts for anterior neural genes FOXG1, LHX2, OTX2, and ZNF521 BRN2 (POU3F2) and SIP1 are all significantly higher in the MEK-inhibitor/SMAD7 combination compared to SMAD7 alone. Down-regulation of the pluripotency genes OCT4 and NANOG is also more robust in this combination than MEK-inhibitor alone.*

qPCR data is presented as LOG_2-fold change over uninduced hESCs. ATP5O was used for internal normalization at each time point. Bars represent n = 3-4 ± SEM. Scale bars: 200µm.

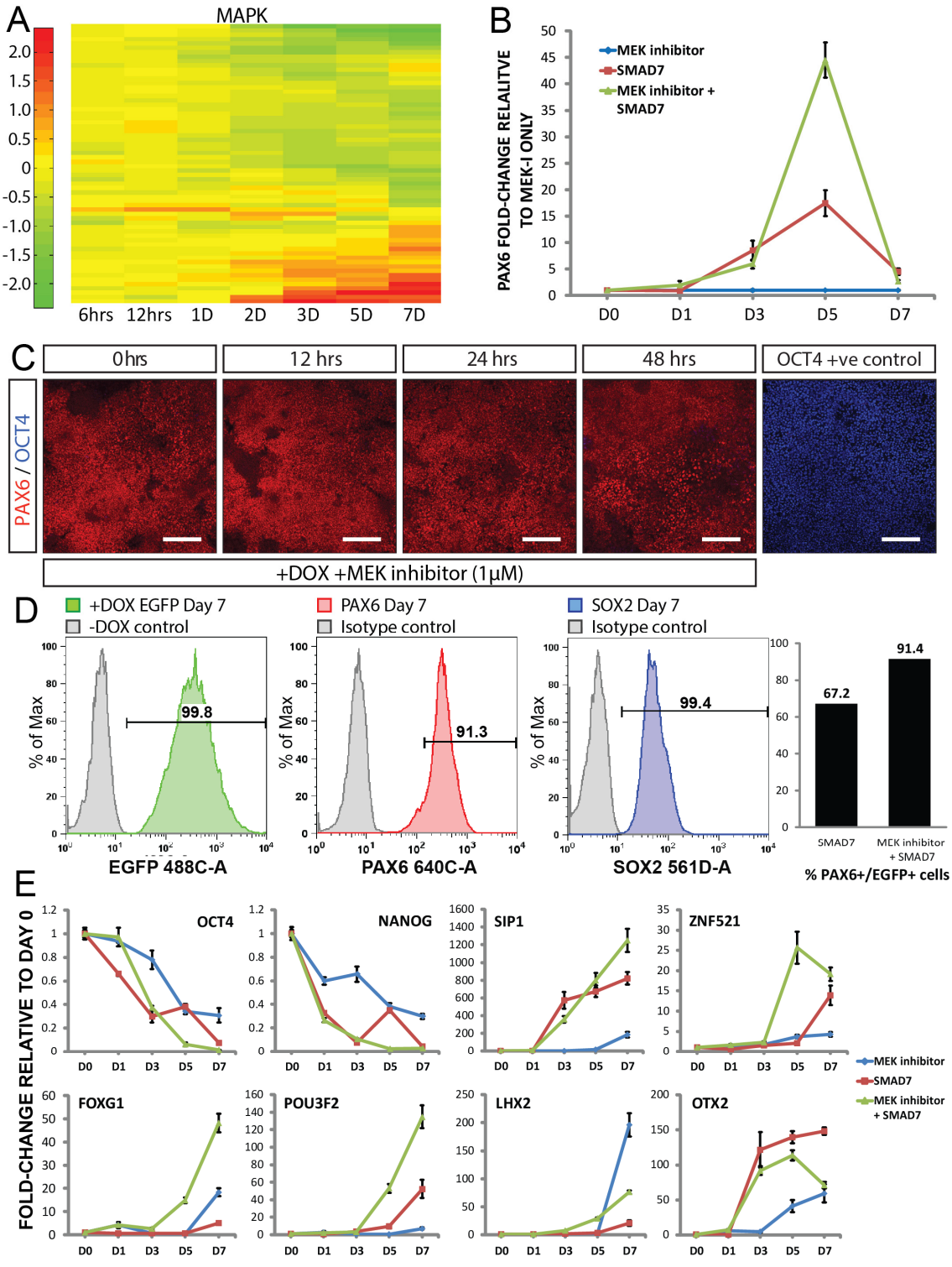
A
MAPK
2.0
1.5
1.0
0.5
0
-0.5
-1.0
-1.5
-2.0
6hrs 12hrs 1D 2D 3D 5D 7D
B
PAX6 FOLD-CHANGE RELALITVE TO MEK-I ONLY
MEK inhibitor
SMAD7
MEK inhibitor + SMAD7
D0 D1 D3 D5 D7
C
0hrs
12 hrs
24 hrs
48 hrs
OCT4 +ve control
PAX6 / OCT4
+DOX +MEK inhibitor (1μM)
D
+DOX EGFP Day 7
-DOX control
PAX6 Day 7
Isotype control
SOX2 Day 7
Isotype control
% of Max
99.8
91.3
99.4
EGFP 488C-A
PAX6 640C-A
SOX2 561D-A
67.2
91.4
SMAD7
MEK inhibitor + SMAD7
% PAX6+/EGFP+ cells
E
FOLD-CHANGE RELATIVE TO DAY 0
OCT4
NANOG
SIP1
ZNF521
FOXG1
POU3F2
LHX2
OTX2
MEK inhibitor
SMAD7
MEK inhibitor + SMAD7

Figure 3.10: Time-course comparison of lineage-specific genes expressed in MEK-inhibitor+SMAD7 induced cultures versus SMAD7-only controls. A) Addition of MEK-inhibition accelerates an anterior neural fate without changing expression of other germ layer lineage genes as compared to B) SMAD7 induction alone.

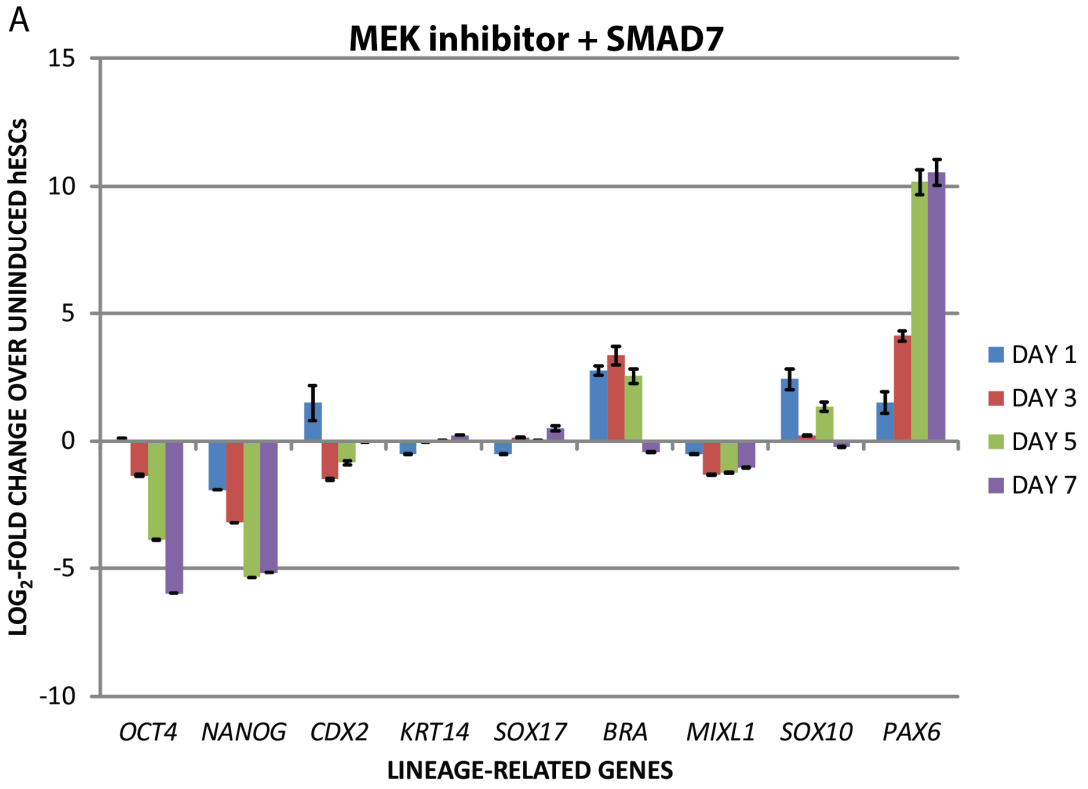
A
MEK inhibitor + SMAD7
15
10
5
0
-5
-10
LOG2-FOLD CHANGE OVER UNINDUCED hESCs
OCT4
NANOG
CDX2
KRT14
SOX17
BRA
MIXL1
SOX10
PAX6
LINEAGE-RELATED GENES
DAY 1
DAY 3
DAY 5
DAY 7

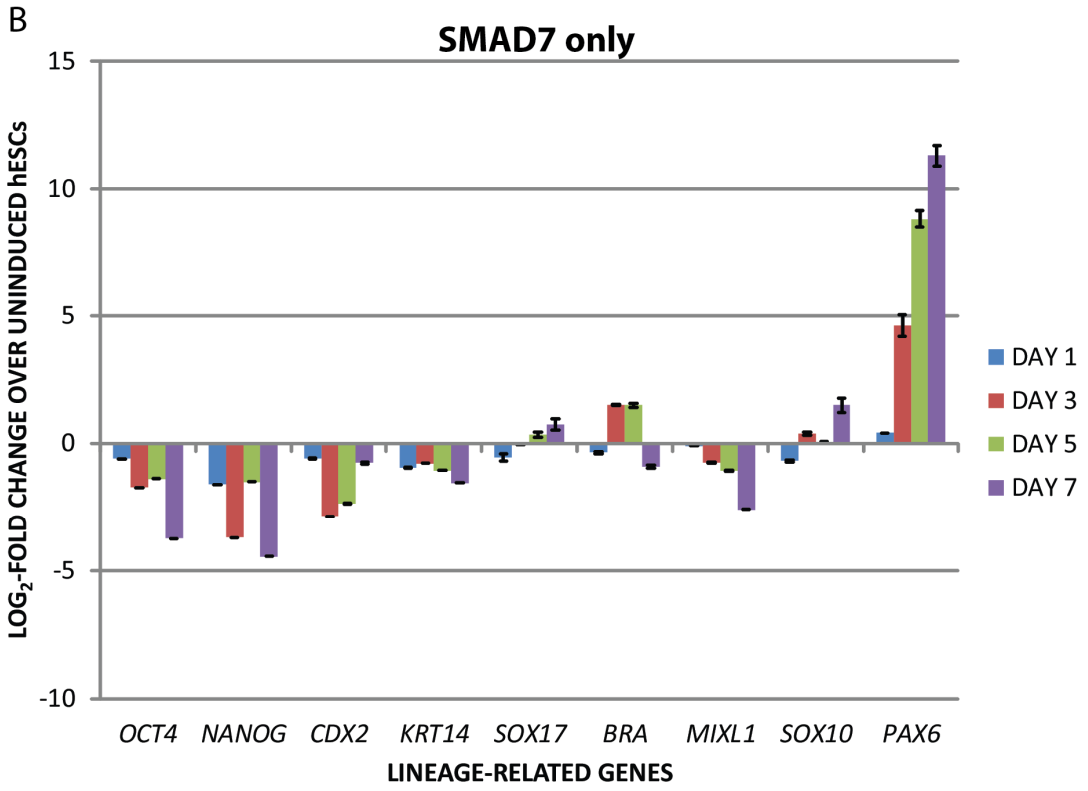
B
SMAD7 only
15
10
5
0
-5
-10
LOG2-FOLD CHANGE OVER UNINDUCED hESCs
OCT4
NANOG
CDX2
KRT14
SOX17
BRA
MIXL1
SOX10
PAX6
LINEAGE-RELATED GENES
DAY 1
DAY 3
DAY 5
DAY 7

COMBINED SMAD7 INDUCTION AND MEK INHIBITION PROMOTES ANTERIOR NEURAL FATE

MEK-inhibition was then tested to ascertain whether it alters the anterior neural profile imposed by SMAD7 induction alone. In addition to promoting neural fate, qPCR confirmed that combined MEK and TGFβ inhibition also enhanced acquisition of an anterior fate. The MEK-inhibitor/SMAD7 combination accelerated the expression of the forebrain TxF FOXG1, as compared to SMAD7-induction alone (Figure 3.9E) and resulted in ~10 fold greater expression of FOXG1 transcripts at Day 7, the last time point tested. Like SMAD7 alone, these changes were also direct and did not significantly induce non-neural lineage genes, as evidenced by absence of expression of mesoderm, endoderm, non-neural ectoderm, and trophectoderm lineage markers (see Figure 3.10A-B). Importantly, the neural crest marker SOX10 was also not induced in the MEK-inhibitor/SMAD7 combination. Interestingly, MEK-inhibitor alone could also up-regulate FOXG1 to a greater extent than the SMAD7-only condition, although to a considerably lesser extent than that of the MEK-inhibitor/SMAD7 combination, suggesting that MEK1/2-ERK and TGFβ-SMAD signaling might be regulating FOXG1 expression. In addition, higher expression levels were seen for the forebrain determinant LHX2 at Day 7 (3-fold), as well as the rostral neural gene ZNF521 (25-fold) between Days 5-7 in the MEK-inhibitor/SMAD7 combination compared to SMAD7-only conditions. Comparable expression of OTX2 was observed until Day 3, after which slightly lower levels were observed (Figure 3.9E). Based on these results, we can conclude that combined inhibition

of FGF-MEK and TGFβ-SMAD signaling significantly accelerates the acquisition of neural fate in hESCs without changing the anterior character of the cells.

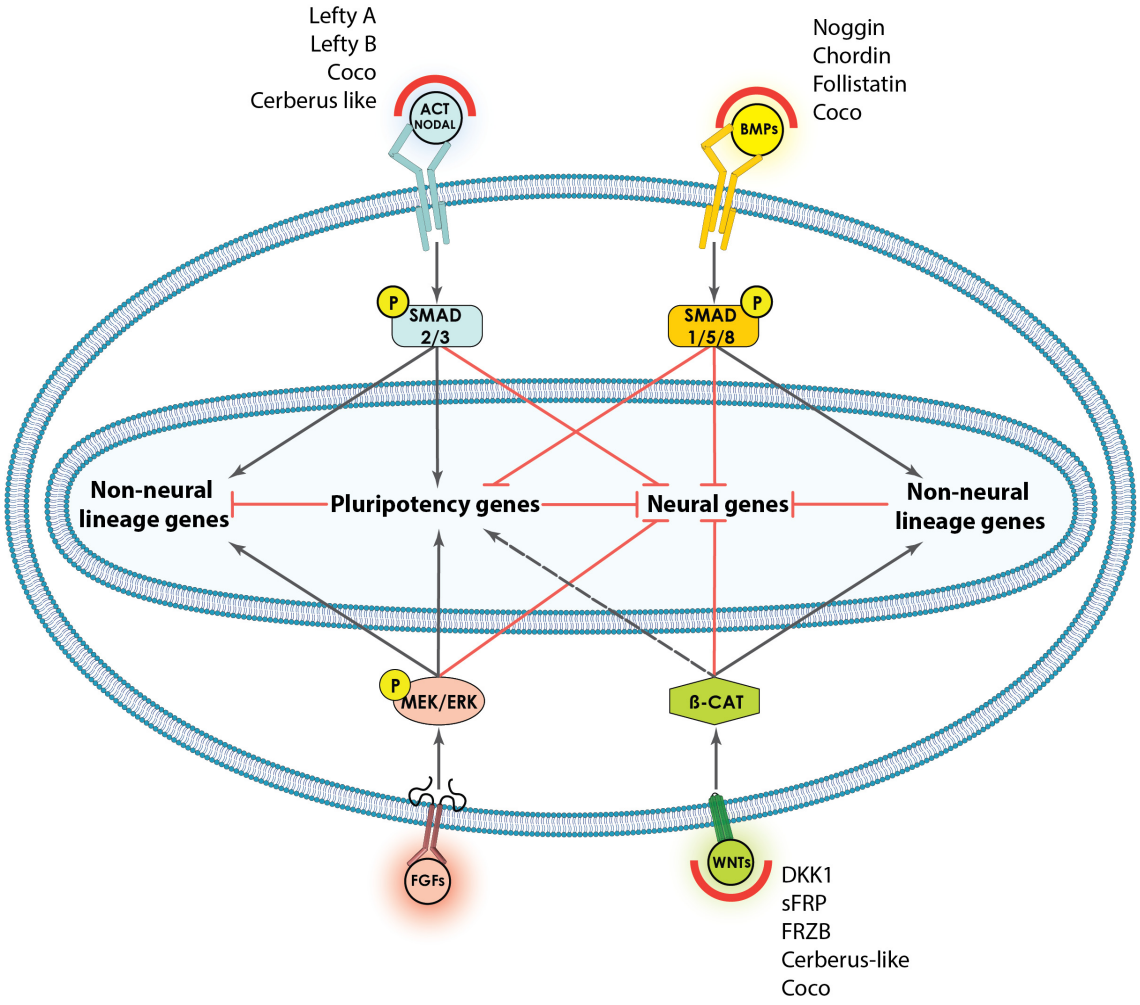

Figure 3.11: Proposed model of the 'default' neural differentiation of hPSCs. The pathways mediating pluripotency such as FGF-MEK and ACTIVIN/NODAL-SMAD2/3 repress neural fate directly and indirectly through pluripotency TxFs. Our data suggests that maintenance of pluripotency requires inhibition of the default state of differentiation, i.e. the neural fate. Arrows represent activation while hatches represent inhibition. The dashed line represents aDirect evidence for

SUMMARY

We demonstrate here that SMAD7, a cell-intrinsic inhibitor of canonical TGFβ signaling, is sufficient to directly convert pluripotent hESCs to an anterior telencephalic fate while preventing induction of non-neural and posterior neural fates. Time-course gene expression revealed down-regulation of MAPK components, and combining MEK1/2 inhibition with SMAD7-mediated TGFβ inhibition promoted telencephalic conversion. FGF-MEK and TGFβ-SMAD signaling maintain hESCs by promoting pluripotency genes and repressing neural genes. Our findings suggest that in the absence of these cues, pluripotent cells revert to an intrinsic program of neural fate. Hence the “primed” state of hESCs requires inhibition of the “default” state of neural fate acquisition (Figure 3.11). This suggests an evolutionarily conserved mechanism of forebrain specification from amphibians.

CHAPTER 4: *IN VITRO* CORTICOGENESIS REVEALS EXISTENCE OF MULTIPOTENT PROGENITORS AND NEURONAL RESTRICTION *IN VIVO*

Human embryonic stem cells can recapitulate many early developmental events faithfully, including germ layer differentiation, developmental timing, and even organogenesis (Kadoshima et al., 2013; Nicholas et al., 2013; Warmflash et al., 2014). There is a strong interest in utilizing hPSC-derived tissues for disease modeling and cell replacement therapies. However, in many instances the cell types being generated in the various differentiation protocols are poorly defined and not relevant to the disease context. This is partly due to our incomplete understanding of the events underlying corticogenesis and neuronal diversity, especially in humans. While mouse models have been greatly informative with respect to human development and diseases, many diseases of the human cortex cannot be adequately modeled in mice, such as microcephaly, autism, many psychiatric illnesses, and neurodegenerative diseases (Geschwind and Rakic, 2013; Bae et al., 2015). Hence the ability to make defined neuronal types for any application requires a better understanding of human neural development.

In this chapter, I will discuss my efforts in this direction to establish hPSCs as a model for studying early corticogenesis using TGFβ inhibition as a starting point. By harnessing the strength of *in vitro* manipulations and combining them with single cell and population level quantitative analysis, we show that *in vitro* corticogenesis recapitulates many aspects of human corticogenesis. We also provide evidence for “progressive restriction” of human neural progenitors at the level of individual progenitors as has been suggested in mice. Intriguingly, our parallel analysis of human fetal brains shows a heretofore-

unappreciated pattern of laminar marker restriction over the course of development. Based on our findings, we propose a neuronal restriction model of cortical lamination where restriction at the level of progenitors manifests in patterns of expression of fate determinant in neurons. This has implications for understanding diseases where abnormalities in laminar cytoarchitecture and neuronal differentiation are observed, such as autism (Stoner et al., 2014). Lastly, the transgenic approaches, reporters, lineage-tracing tools, and the novel analytical approaches we use here are broadly applicable for studies of various aspects of hPSC differentiation and organogenesis.

SMALL MOLECULE INHIBITION OF TGFβ SIGNALING IS SUFFICIENT TO INITIATE A PROGRAM OF CORTICAL DIFFERENTIATION FROM MAMMALIAN PSCs

We first sought to optimize our protocol of cortical differentiation using recently available and specific small molecule inhibitors of Activin/Nodal and BMP signaling (referred to as SB/LDN). We also switched to serum free conditions as albumin in serum has intrinsic signaling activity as was observed by others and us (Blauwkamp et al., 2012; Nakano et al., 2012) (data not shown). Under these conditions, hESCs could be readily differentiated into primitive neuroepithelium at near purity. Upon replating the neuroepithelium on laminin, the cultures developed into a rosette-like morphology as has been described before (Figure 4.1D). The neuroepithelium and rosettes were found to homogeneously co-express markers of dorsal telencephalic and neocortical identity including OTX2 (97.5%), FOXG1 (93.5%), and LHX2 (93.9%) (Figure 4.1A-C). Moreover, the rosette

structures recapitulated the radial organization of the early ventricular zone, with a central cavity with N-CAD+ margins (comparable to ventricles) and PAX6+ neural progenitors lining the central cavity. Subventricular zone IPs, which express the TxF TBR2 were found outside the PAX6+ domain (Figure 4.1D). This organization was observed in the majority (91.7%) of rosettes on day 25. At this point the cells were dissociated into single cells and allowed to differentiate into neurons for a prolonged period of time. At late stages of cultures (>day 70), we observed the emergence of PAX6+ progenitors with only one long process. The timing of emergence, morphology, and marker expression of these progenitors is consistent with bRG cells, which have also been observed by other groups (Shi et al., 2012; Kadoshima et al., 2013; Lancaster et al., 2013). Importantly, no markers of interneurons or their progenitors (NKX2-1, DLX2) were observed at any point during the differentiation process, suggesting that our cultures were uniformly of dorsal telencephalic identity (data not shown).

We also tested for expression of cortical markers at different time points. On day 55, we were able to observe expression of deep layer markers such as TBR1 and CTIP2, which are initially uniformly expressed in the cortical plate (Figure 4.1F) (Onorati et al., 2014). Using a CRISPR transgenic knock-in reporter line (see Figure 6.3 for details), we were also able to demonstrate expression of FEZF2 at this time point, and its co-expression with CTIP2. FEZF2 is known to be expressed in SCPNs as well as the progenitors. At late time points in culture, we were able to observe expression of several known CPN markers such as SATB2, BRN2, and MEF2C (Figure 4.1F). Together, this suggests that in our *in vitro* culture conditions Activin/Nodal and BMP inhibition drives acquisition of neocortical fate by

hESCs, and that the neural progenitors derived from this transition are competent to generate SCPNs and CPNs.

Additionally, we also wanted to test if TGFβ inhibition was sufficient for conversion of other hPSCs and PSCs derived from other mammalian species into a neural fate. We used two mouse ESC lines (46C SOX1-EGFP and V6 SOX2-EGFP), two monkey ESC lines (M. Mulatta and M. Nemestrina) and two human ESC lines (RUES1 and RUES2) for our experiments. The mouse ESCs were first differentiated into EpiSCs as it has been shown that EpiSCs are competent for germ differentiation and resemble hESCs more closely. To this end, mouse ESCs were cultured in hESC medium (CM + FGF) for three days with a WNT inhibitor IWP2. EpiSC conversion was manifested by appearance of flat colonies similar to hESCs rather than dome-shaped colonies typical of mESCs. Presence of pluripotent markers such as OCT4, SOX2, and NANOG were demonstrated by IF (Figure 4.2A).

The two mouse EpiSCs, together with monkey and human ESCs were subjected to SB/LDN conditions for varying periods of time. The cultures were fixed at the following days after induction: 6 days for mouse EpiSCs, 11 days for monkey ESCs, and 17 days for human ESCs. The number of cells that have underwent neural conversion was assessed by SOX1+ cells for mouse PSCs and PAX6 for monkey and human PSCs. This was because SOX1 is the first marker of neural fate in mouse, compared to primates, where PAX6 is the earliest marker (Zhang et al., 2010). Quantification of these results showed that all six PSCs were able to undergo neuralization in the presence of SB/LDN, with human cells showing the

highest efficiencies (>90%) and monkey and mouse PSCs showing efficiencies of 75-85% (Figure 4.2B).

We conclude that TGFβ inhibition is sufficient for neural induction and an evolutionarily conserved property of mammalian PSCs.

Figure 4.1: hPSCs can recapitulate early corticogenesis in vitro downstream of TGFβ inhibition. A) Schematic overview of the protocol used for cortical differentiation. B) Neuroepithelium generated using this protocol uniformly express markers of telecephalic and neocortical fate such as PAX6, LHX2, FOXG1, OTX2, PLZF and EMX1 C) Quantification of co-expression of LHX2, FOXG1, and OTX2 with PAX6. The schematic shows a sagittal section of the PCW5 fetal brain while the colored areas are expected domains of expression of LHX2, FOXG1, and OTX2. Dorsal forebrain progenitors should express all three together with PAX6. D) Upon passaging, the neuroepithelium self-organizes into rosettes expressing characteristic markers of embryonic germinal layers including a central cavity lined by PAX6+, NCAD+ cells and another layer of TBR2+ IPs. E) At late stages in culture, monopolar progenitors expressing PAX6 and p-Vimentin appear which are properties of OSVZ bRG cells. F) The neural progenitors can also be differentiated into SCPNs expressing deep layer markers such as BRN2, CTIP2, and FEZF2, as well as CPNs expressing superficial layer markers such as SATB2, BRN2, and MEF2C. Scale bars: 100µm.

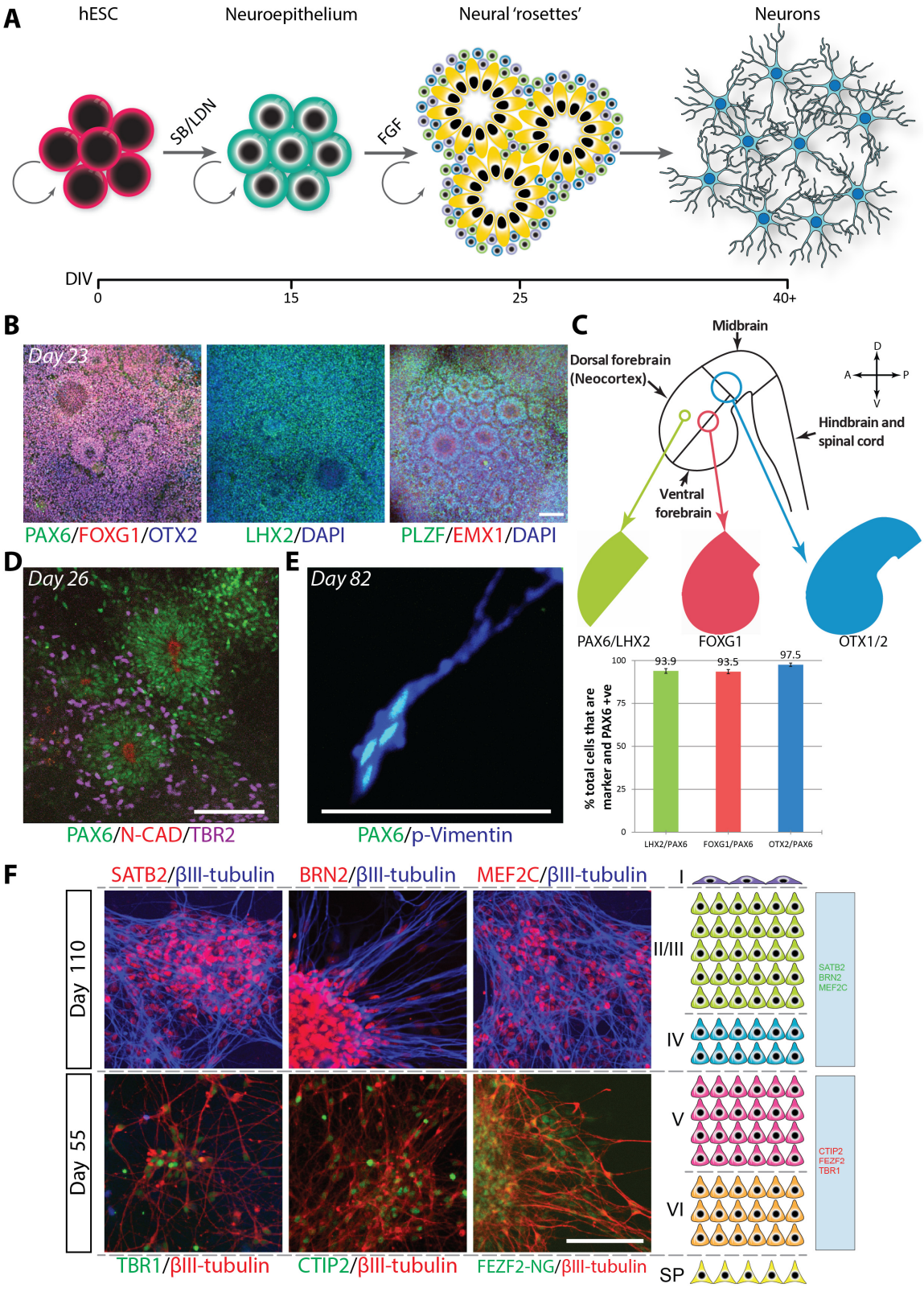
A
hESC
Neuroepithelium
Neural 'rosettes'
Neurons
SB/LDN
FGF
DIV
0
15
25
40+
B
Day 23
PAX6/FOXG1/OTX2
LHX2/DAPI
PLZF/EMX1/DAPI
C
Midbrain
Dorsal forebrain
(Neocortex)
Hindbrain and
spinal cord
Ventral
forebrain
D
A
P
V
PAX6/LHX2
FOXG1
OTX1/2
% total cells that are
marker and PAX6 +ve
93.9
93.5
97.5
LHX2/PAX6
FOXG1/PAX6
OTX2/PAX6
D
Day 26
PAX6/N-CAD/TBR2
E
Day 82
PAX6/p-Vimentin
F
SATB2/βIII-tubulin
BRN2/βIII-tubulin
MEF2C/βIII-tubulin
Day 110
Day 55
I
II/III
IV
V
VI
SP
SATB2
BRN2
MEF2C
CTIP2
FEZF2
TBR1
TBR1/βIII-tubulin
CTIP2/βIII-tubulin
FEZF2-NG/βIII-tubulin

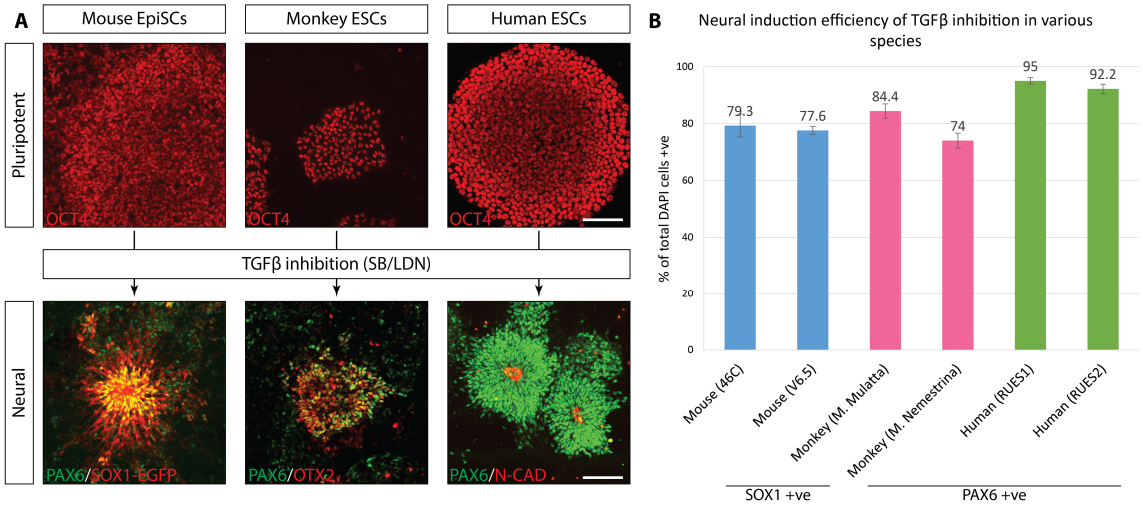

Figure 4.2: Pluripotent cells from various species can be converted into neural fate on TGFβ inhibition with small molecules. A) Top panels: Mouse EpiSCs, monkey and human ESCs all expressing the pluripotency marker OCT4. On application of SB/LDN, all three PSCs differentiate into neural fate as indicated by SOX1 reporter expression in mouse EpiSCs and PAX6, OTX2, and N-cadherin expression in NHP and human ESCs. The bottom panels show neural rosettes from each species. PAX6 is a neocortical marker in mouse. The timescale of differentiation varied between the three species. B) Quantification of neural markers in two different lines of each species. Sox1 is the first neural marker expressed in differentiation of mESCs while PAX6 is the first neural marker expressed in hPSC differentiation (Zhang et al., 2010). n=3 experiments per PSC line. Scale bars: 100µm.

hPSC-DERIVED NEURAL PROGENITORS DISPLAY DYNAMIC RADIAL GLIAL PROPERTIES

In the next set of experiments, we wanted to test if neural progenitors derived *in vitro* display the dynamic cell cycle behavior that has been shown in mouse and human RG cells in *ex vivo* cultures (Noctor et al., 2001; LaMonica et al., 2013). These behaviors include interkinetic nuclear migration (INM) and positioning of the nuclei at the ventricular surface during M-phase of the cell cycle (Figure 4.3E). In order to monitor the cell cycle

behavior and movements of *in vitro* derived neural progenitors, we derived a transgenic hESC line expressing FUCCI markers and a Histone-H2B tagged cerulean fluorescent protein using the ePiggyBac system (Figure 4.3A-C) (Lacoste et al., 2009). FUCCI markers are comprised of Venus and mCherry fluorescent proteins fused to the ubiquitinated domains of GEMININ (amino acids 1-110) and CDT1 (amino acids 30-120), respectively. GEMININ normally accumulates during the S→M-phase of the cell cycle, after which it is degraded; conversely, CDT1 accumulates in the G0/G1-phase and is actively degraded in the S→M phases (Figure 4.3B). Hence in FUCCI cells, Venus expression is seen in the nucleus in the S to M-phase of the cell cycle, while mCherry is observed in the nucleus either in the G1-phase or upon cell cycle exit (i.e. G0 phase). We added an H2B-tagged cerulean fluorescent protein (CFP) to enable visualization of the cells in the M-phase, wherein there is a brief period when cells are no longer expressing Venus-GEM(1-110), and have not yet accumulated mCherry-CDT1(30-120) (Figure 4.3B). H2B-CFP shows a spike in intensity during the M-phase due to chromatin condensation and accumulation of the chromosomes on the spindle axis (Figure 4.3C and D).

Upon selection with Puromycin, Blasticidin, and Neomycin, we generated clonal hESC triple reporter lines stably expressing high levels of the FUCCI markers and H2B-CFP (Figure 4.3C). Live imaging and single cell analysis of FUCCI/H2B-CFP line confirmed the accumulation of Venus in the S→M phase, of mCherry in the G1-phase, as well as the M-phase spike of H2B-CFP (Figure 4.3D). We next differentiated the FUCCI/H2B-CFP hESCs into neuroepithelium with SB/LDN, and subsequently replated them to allow rosette formation. Based on RG movement in the ventricular zone, it would be expected that

green cells (i.e. progenitors in S→M phase) move inwards and accumulate close to the VZ while red cells (i.e. progenitors in G1 and post-mitotic G0 neurons) move away from it and accumulate away from the ventricles. Indeed, this was observed in cortical slices derived from brains of E13 transgenic FUCCI mice (Figure 4.3E) (Sakaue-Sawano et al., 2008; Abe et al., 2013). Remarkably, we observed identical cell cycle dynamics upon live imaging of D25 rosettes, including INM over a three day period (Figure 4.3H). This was confirmed upon population level analysis, where green cells accumulated close to the center of the rosette structure, while green cells on the periphery were gradually replaced by bright red G0/G1 cells (Figure 4.3G-H). Interestingly, there was a decrease in the fraction as well as the intensity of green cells over the 72-hour period at a single cell level; this is attributable to the lack of media change during the live-imaging period. Self-renewal signals (such as insulin) are present in the culture medium and would be depleted over time if not replaced. The decrease in green cells was accompanied by a corresponding increase in the number and intensity of red cells at a signaling (Figure 4.3G-H), suggesting post-mitotic neuronal fate due to accumulation of CDT1. These patterns of FUCCI marker segregation was observed for 12/12 rosettes that were imaged (data not shown). Hence we conclude from FUCCI/H2B-CFP experiments that neural rosettes demonstrate self-organization similar to what is seen *in vivo*, and that *in vitro* derived neural progenitors demonstrate INM.

Figure 4.3: hPSC-derived neural progenitors display dynamic radial glial properties. A) Schematic of the three ePiggyBac cassettes and their respective antibiotic selection markers used to generate the transgenic FUCCI/H2B-CFP line. B) Schematic of FUCCI marker dynamics during cell-cycle. Green is indicates actively dividing ("GO"), while red indicates cell cycle pause or exit ("STOP"). C) Image of a FUCCI/H2B-CFP clone used for further experiments. Expression of all three transgenes can be observed. D) Single cell dynamics of FUCCI/H2B-CFP over a 36 hour period. The expected behaviors of all three markers are observed. The arrowheads indicate M-phase of the cell cycle, that corresponds to a spike in H2B-CFP fluorescence. E) Schematic of RG cell cycle dynamics and overlay of triple marker expression corresponding to phase of RG cell cycle. F) Single cell analysis of FUCCI dynamics over a 72-hour period. Each dot represents a single cell, while the intensity of the dot represent the intensity of flourescent protein expression. The y-axis represent distance from the center of the rosette structure (highlighted in H). The number and intensity of green can be seen to be decreasing over time, while for red cells they are increasing. G) The density of cells as a function of distance from the center at three time points: t=0, t=36hrs and t=72hrs. The restriction of green cells to the center of the rosette and accumulation of red cells away from the rosette over time can be seen. H) Montage of a single rosette from the above experiment at 6:20hr intervals showing the pattern of FUCCI emerging over the 72 hr period. The images are timestamped on the bottom left. The small circle indicates the center of the rosette, while the larger circle dermarcates the rosette boundary. Scale bars: 100µm.

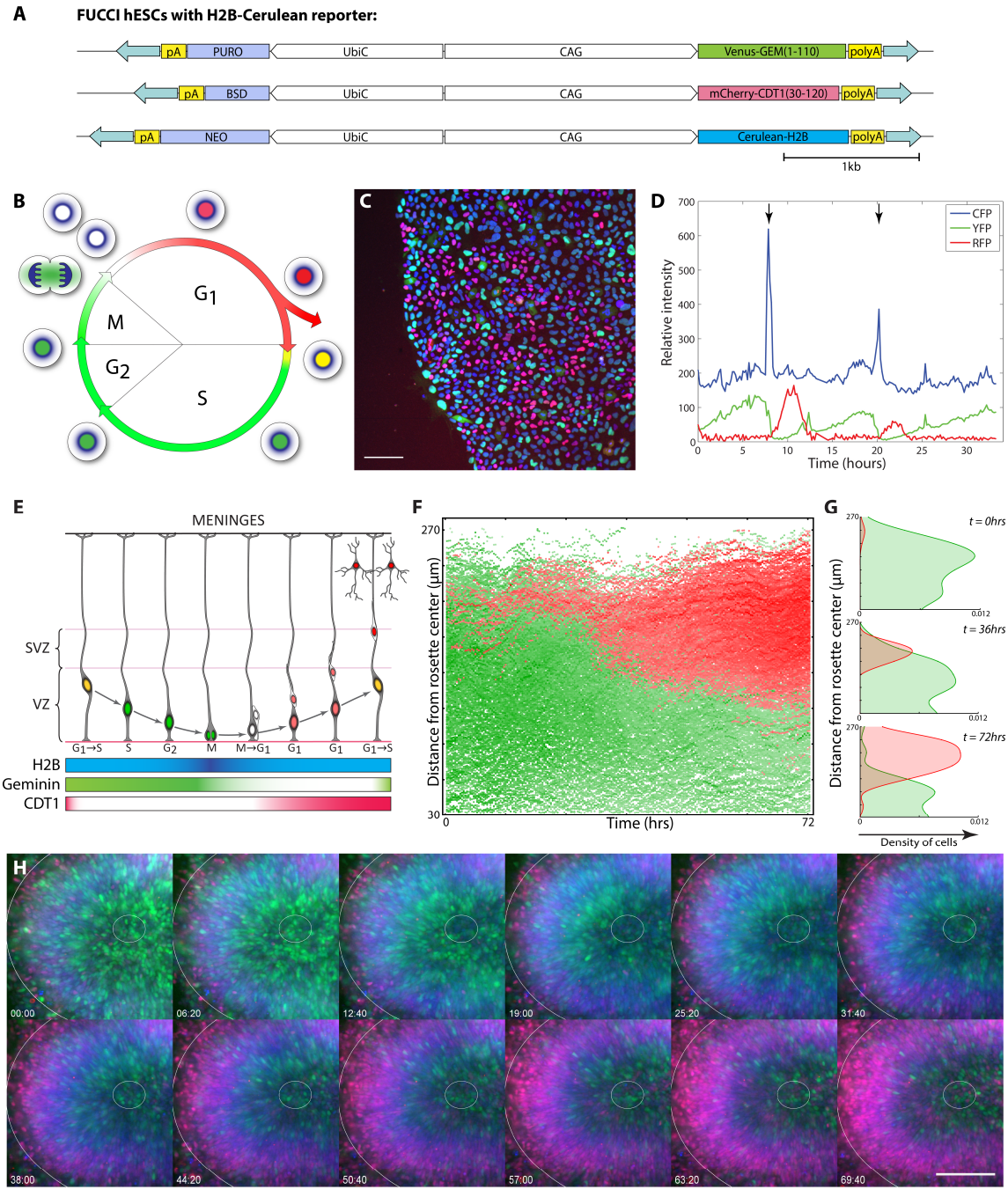
A
FUCCI hESCs with H2B-Cerulean reporter:
pA
PURO
UbiC
CAG
Venus-GEM(1-110)
polyA
pA
BSD
UbiC
CAG
mCherry-CDT1(30-120)
polyA
pA
NEO
UbiC
CAG
Cerulean-H2B
polyA
1kb
B
G1
M
G2
S
C
D
CFP
YFP
RFP
Relative intensity
Time (hours)
E
MENINGES
SVZ
VZ
G1→S
S
G2
M
M→G1
G1
G1
G1→S
H2B
Geminin
CDT1
F
Distance from rosette center (μm)
Time (hrs)
G
t = 0hrs
t = 36hrs
t = 72hrs
Distance from rosette center (μm)
Density of cells
H
00:00
06:20
12:40
19:00
25:20
31:40
38:00
44:20
50:40
57:00
63:20
69:40

hPSC-DERIVED NEURAL PROGENITORS ALSO DISPLAY MITOTIC BEHAVIORS AND SIGNALING PROPERTIES OF RADIAL GLIA

We next looked for periventricular mitotic events, as is also characteristic of RG cells. Live imaging of FUCCI/H2B-CFP rosettes demonstrated mitotic chromosomes close to the center of the rosette (Figure 4.4A). Additionally, we tracked single progenitors as they approached the center of the rosettes and divided next to the central cavity, with daughter cells moving away from it. Two examples are shown in Figure 4.4A. Next, we fixed and stained rosettes on day 24 with N-cadherin, which is an apical polarity marker, and phospho-histone H3, which marks chromosomes in the M-phase of the cell cycle (Figure 4.4B). Upon quantification, we observed that a large majority of mitotic nuclei (83.9%) were present next to N-cadherin+ rosette centers (Figure 4.4C). Some mitotic events were also observed away from the rosette center in both live imaging and pH3 staining; these were presumably dividing IP cells.

In the next set of experiments, we wanted to determine if *in vitro* derived progenitors generated in our protocol also require Notch signaling for maintenance, as has been shown for RG cells *in vivo* and *ex vivo*. Rosettes were derived from the FUCCI/H2B-CFP line and live imaging carried out in the presence or absence of the small molecule γ-secretase inhibitor, DAPT. Notch signaling requires γ-secretase for cleavage of the intracellular domain upon activation. DAPT strongly suppresses Notch signaling, as determined by qRT-PCR for the Notch target gene, HES5 (Figure 4.4D). Media was

changed every day for both control and DAPT-treated rosettes in this experiment to ensure that self-renewal signals were not depleted. Remarkably, within 14 hours of DAPT application, we observed a dramatic increase in the number of red FUCCI cells, suggesting that Notch inhibition was forcing cell cycle exit of the progenitors (Figure 4.4E). By the end of the 72 hour period, virtually all green cells had disappeared, were replaced by bright red cells, and the rosette structure had complete collapsed in 24/24 rosettes observed. This was not simply due to migration of green cells away from the field of view, as we were unable to find any green cells in the entire well upon fixation of cultures (data not shown). Quantification of the fraction of cells expressing green or red FUCCI markers confirmed the dramatic phenotype on DAPT application (Figure 4.4F). Both phase contrast microscopy and immunostaining confirmed that the progenitors were losing contact with the rosette and subsequently differentiating into post-mitotic neurons expressing the early cortical plate marker TBR1 (Figure 4.4G-H).

We conclude from these experiments that *in vitro* derived neural progenitors undergo M-phase events next to the apical boundary they form in rosettes, and that Notch signaling is essential for self-renewal of TGFβ inhibition derived neural progenitors.

Figure 4.4: hPSC-derived neural progenitors display mitotic behaviors and signaling properties of RGs. A) Schematic showing increase in M-phase signal intensity of H2B-CFP. The montage on the right was made at intervals of 20min. and tracks two individual progenitors (red and white arrow) as they move towards the center of the rosette, divide close to the apical surface and the daughter cells moving away to the basal side. B) Day 24 rosettes stained with N-CAD and phospho-histone H3 show clustering of pH3+ cells close to the NCAD+ apical surface. C) Quantification of the position of pH3+ cells in rosettes. D) qRT-PCR of Notch target gene HES5, and the progenitor markers PAX6, SOX1, and SOX2 in the presence of DAPT and WNT signaling modulators. indicating the specific effect of DAPT on HES5, n=4 technical replicates. E) Montage of typical control and DAPT treated rosettes demonstrate collapse of rosette structure and disappearance of green cells. The montage is at 7 hr intervals. F) Quantification of the fraction of red and green cells in three control and DAPT treated cultures. G) On phase-contrast, maintenance of rosette morphology is seen in control cultures while conversion to a bipolar, neuronal morphology is seen in DAPT treated cells. H) The neuronal cells in G) stain with the early cortical marker TBR1 and the neuronal marker βIII-tubulin. Scale bars: 100μm.

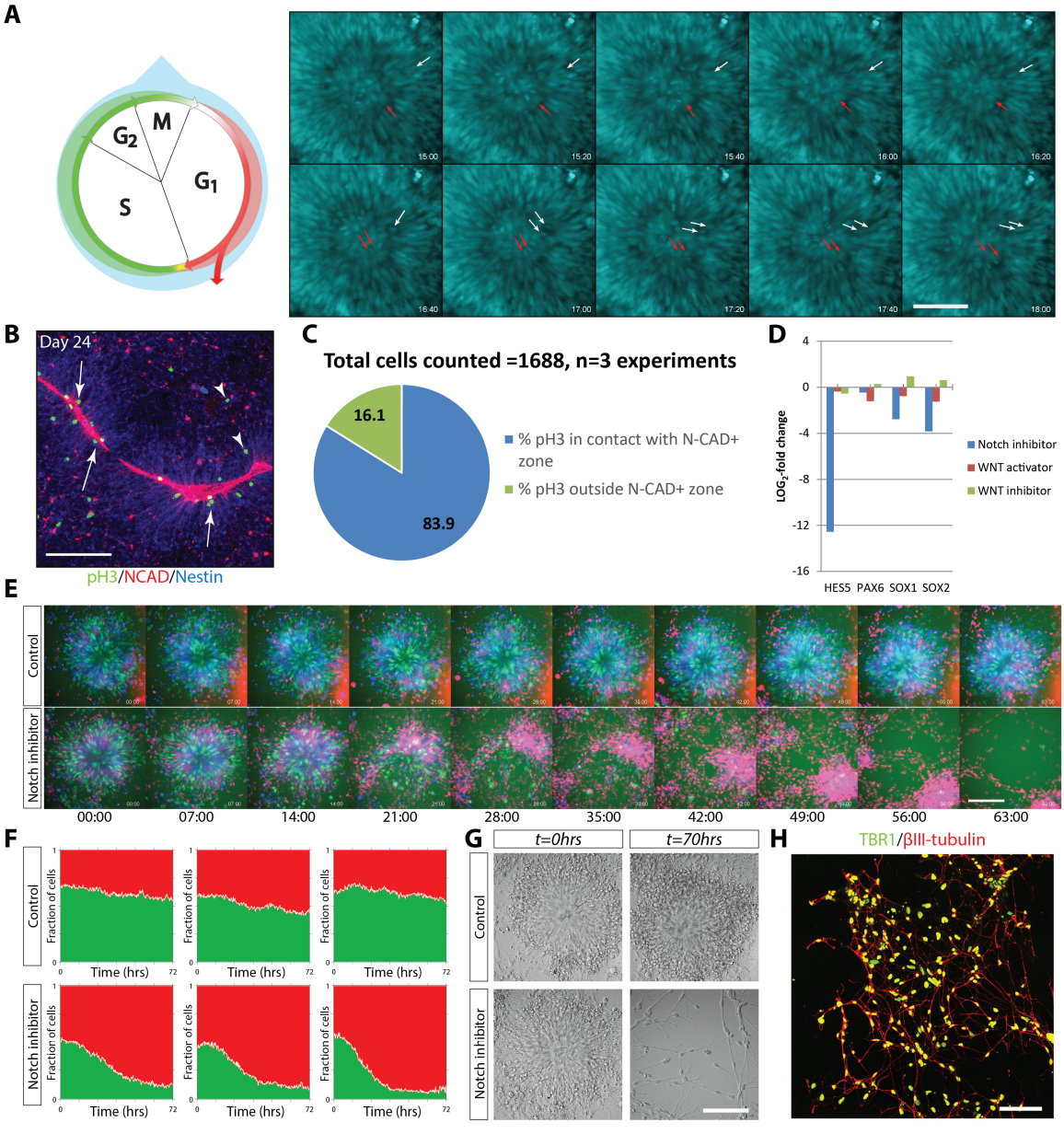
A
M
G2
G1
S
15:00
15:20
15:40
16:00
16:20
16:40
17:00
17:20
17:40
18:00
B
Day 24
pH3/NCAD/Nestin
C
Total cells counted =1688, n=3 experiments
16.1
83.9
% pH3 in contact with N-CAD+ zone
% pH3 outside N-CAD+ zone
D
LOG2-fold change
4
0
-4
-8
-12
-16
HES5 PAX6 SOX1 SOX2
Notch inhibitor
WNT activator
WNT inhibitor
E
Control
Notch inhibitor
00:00
07:00
14:00
21:00
28:00
35:00
42:00
49:00
56:00
63:00
F
Control
Notch inhibitor
Fraction of cells
Time (hrs)
G
t=0hrs
t=70hrs
Control
Notch inhibitor
H
TBR1/βIII-tubulin

EARLY NEUROEPITHELIUM CAN BE PATTERNED ON THE ROSTROCAUDAL AXIS WITH WNT MODULATION

We hypothesized that WNT signaling can alter the areal pattern of the cortex based on its expression in the zona limitans intrathalamica (ZLI) at the junction of the telencephalon and diencephalon (Braun et al., 2003). FGF8 has a well-established role in rostral areal specification, but a corresponding factor for caudalization of the cortex has not been described. We hypothesized that moderate activation of β-catenin could generate caudal cortical neuroepithelium. ESCs were subjected to neural induction via TGFβ inhibition, and a small molecule WNT activator (CHIR99021; 0.5μM) or inhibitor (IWP2; 0.5μM) were added between days 2-10 and replenished every day. RNA was harvested at 0, 5, and 10 days of induction (Figure 4.5A).

Strikingly, inhibition of WNT signaling with IWP2 resulted in an upregulation in rostral markers such as FOXG1 and FGF8 while decreasing posterior markers such as EMX2 and COUP-TF1 (Figure 4.5B). Conversely, moderate activation of WNT pathway with a GSK3β inhibitor resulted in an increase in caudal markers (EMX2, NR2F1) and a concurrent decrease in rostral markers (FOXG1, FGF8). Importantly, this change in rostral-caudal axis specification required moderate levels of WNT activation. At higher levels of WNT activity, the neuroepithelium is switched from telencephalic to midbrain identity (data not shown). Furthermore, changes in expression patterns of areal genes occurred in the absence of changes to markers of general neural fate such as PAX6 and SOX2 (Figure 4.5C). It is worth noting that while PAX6 is expressed in a high rostral-low caudal gradient

in mouse telencephalon, it does not demonstrate this pattern in human embryos (Bayatti et al., 2008; Ip et al., 2010).

Of interest, WNT signaling regulated the expression of LHX2 together with FOXG1 (Figure 4.5B-C). Since LHX2 and FOXG1 are determinants of neocortical fate, intermediate levels of WNT signaling may act as a selector pathway at the neocortex-archicortex bifurcation, just as FGF8 does at the paleocortex-neocortex boundary anteriorly. In mice, LHX2 is required to suppress hippocampal organizer fate, which is dependent on WNT signaling (Hebert and Fishell, 2008), while loss of FOXG1 results in conversion of the neocortex into archicortex (Muzio and Mallamaci, 2005). Hence while TGFβ inhibition by itself is sufficient to promote cortical fate, FGF8 and WNT signaling determine the areal fate as well as the type of cortex generated. Intriguingly, we also saw upregulation of thalamic markers (FOXB1 and IRX3; data not shown). Since the caudal cortex is thought to be part of the domain that also gives rise to the diencephalon (Kimura et al., 2005), our data supports a role of intermediate WNT signaling in generation of the caudal cortex-diencephalic territory.

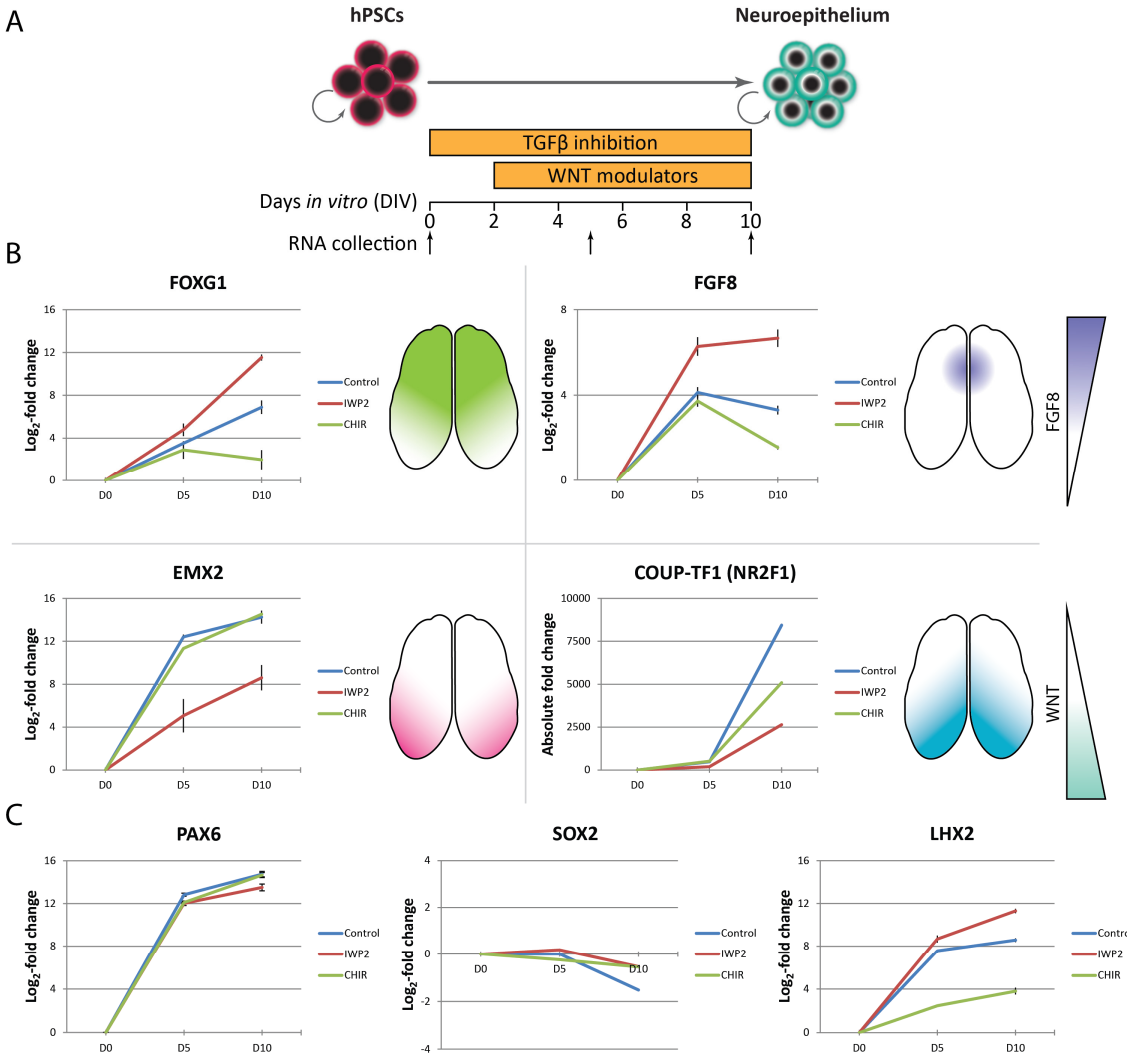

Figure 4.5: WNT signaling modulates the cortical areal identity in hPSC-derived neuroepithelium. A) Timetable of differentiation and RNA collection. B) Time course RT-PCR of FOXG1, FGF8, EMX2, and COUP-TF1 in control, WNT inhibited and WNT activated conditions. The schematics outline the expected patterns of expression. C) Changes in gene expression patterns of areal genes occurred in the absence of changes to markers of general neural fate such as PAX6 and SOX2. LHX2 was found to be regulated by WNT signaling. Hence inhibition of WNT anteriorizes cortical neuroepithelium.

LINEAGE-TRACING OF SINGLE NEURAL PROGENITORS REVEALS PRESENCE OF MULTIPOTENTIAL PROGENITORS THAT GIVE RISE TO BOTH SCPNs AND CPNs

We next wanted to establish the clonal neuronal output of individual progenitors generated in our differentiation paradigm. To this end, two transgenic lines were established, one expressing Citrine fluorescent protein, and other Citrine fused to H2B (Figure 4.6A-B). These lines were differentiated into neural rosettes using TGFβ inhibition, and on day 30 were subjected to flow cytometry to obtain single progenitors (Figure 4.6C-D). The individual progenitors were then mixed and seeded at a dilution of 1:1000 each onto isochronic unlabeled cultures that were differentiated in parallel using the same protocol (Figure 4.6C-D). This was done because single progenitors do not survive well as single cells, and also to provide a more physiological environment for differentiation, since newborn neurons interact extensively with progenitors as well as other newborn neurons *in vivo*. The mixing strategy enabled us to determine whether clonal output of a progenitor was indeed derived from a single labeled progenitor or a random probability of two progenitors attaching to the culture plate next to each other despite the very low density of seeding.

The cultures were maintained for a period of 110 days, which corresponds to 16 weeks of human post-conception development. After this period, the neuronal cultures were fixed and stained for cortical layer makers. We chose CTIP2, which is expressed by SCPNs of layer V, and BRN2, which is expressed by CPNs of layers II-IV (Figure 4.6F). Only the H2B-citrine clones were quantified by automated imaging and analyses. We observed a small

number of clones (<5) that cells expressing both nuclear and cytoplasmic fluorescent proteins, and these were excluded from the analysis. We only considered clones that were 10 cells in size and above, reflecting at least four cell divisions. Analysis of the clones revealed that the majority of the clones ranged from 10-30 cells in size (Figure 4.6G). The vast majority of these clones (78%) stained for both CTIP2 and BRN2. Interestingly, a fraction of these clones (4.6%) stained for only one marker, while significant number of clones (11.5%) displayed a mixed pattern of staining (Figure 4.6H). Within these mixed clones, BRN2+ cells coexisted with cells co-expressing CTIP2/BRN2. This might reflect the transient requirement for superficial layer transcription factors in deep layer corticogenesis, as has been shown to be the case in the mouse (Dino et al., 2014). Alternatively, this might reflect post-mitotic refinement of deep layer cortical neurons, which is also known to take place during corticogenesis (Fishell and Hanashima, 2008).

We also looked at the distribution of BRN2 and CTIP2 positive cells in the clones. On average, nearly two-thirds (67.5%) of all cells across all clone sizes were BRN2 positive; the rest were either CTIP2 positive or unlabeled (Figure 4.6I). This large fraction of CPNs likely represents the enhanced requirement of superficial layer neurons that is characteristic of primate corticogenesis. A consistent fraction of unlabeled cells was also seen in all clone sizes that represented 5.4% of the total number of cells counted. We speculate these cells are either subplate neurons or progenitor cells.

Hence, based on these results, we conclude that majority of human neural progenitors derived from hESCs can give rise to both deep and superficial layer neurons at a single cell

level. This has been shown to be the case for mouse radial glia by independent groups (Guo et al., 2013; Gao et al., 2014); however it has remained the subject of debate due to recent data postulating the existence of progenitors predestined to give rise to superficial layers (Franco et al., 2012). Our analysis also suggests considerable heterogeneity of the progenitor populations in terms of their self-renewal ability.

Figure 4.6: Lineage-tracing of individual neural progenitors in vitro. A) Clone RUES2 lines expressing Citrine or H2B-Citrine. B) Schematic of ePiggybac constructs used to generate hESC lines. C) Schematic of the experiment used to identify the clonal output of single progenitors. D) FACs plot showing isolation of single neural progenitor cells on day 30 of neural differentiation, from left to right: control RUES2, RUES2 Citrine, and RUES2 H2B-Citrine. The plots show that >95% of cells were still expressing the fluorescent proteins on differentiation. E) Neural rosettes generated by RUES2 Citrine and RUES2 H2B-Citrine lines, close to the stage at which they were sorted. F) Examples of individual Citrine+ progenitors giving rise to CTIP2+ and BRN2+ neurons on day 110. G) The clonal size distribution of clones analyzed on Day 110. H) The fraction of analyzed clones expressing various cortical layer markers. I) The ratio of laminar marker expression in various clone sizes is constant and biased towards BRN2+ cells. Scale bars in A), E) and F) represent 100µm.

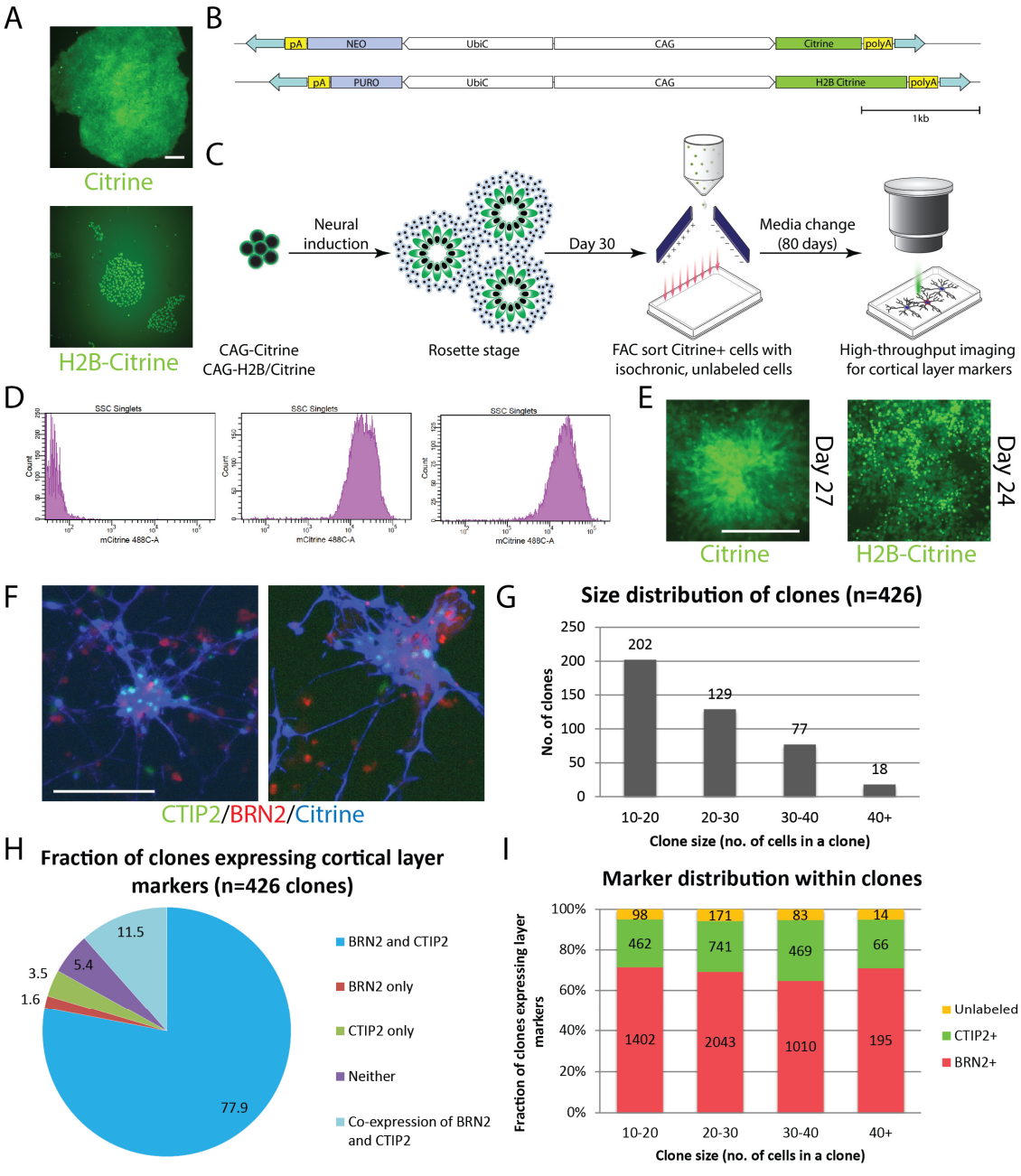
A
Citrine
H2B-Citrine
B
pA
NEO
UbiC
CAG
Citrine
polyA
pA
PURO
UbiC
CAG
H2B Citrine
polyA
1kb
C
Neural induction
Day 30
Media change (80 days)
CAG-Citrine
CAG-H2B/Citrine
Rosette stage
FAC sort Citrine+ cells with isochronic, unlabeled cells
High-throughput imaging for cortical layer markers
D
SSC Singlets
mCitrine 488C-A
E
Day 27
Day 24
Citrine
H2B-Citrine
F
CTIP2/BRN2/Citrine
G
Size distribution of clones (n=426)
No. of clones
202
129
77
18
10-20
20-30
30-40
40+
Clone size (no. of cells in a clone)
H
Fraction of clones expressing cortical layer markers (n=426 clones)
11.5
5.4
3.5
1.6
77.9
BRN2 and CTIP2
BRN2 only
CTIP2 only
Neither
Co-expression of BRN2 and CTIP2
I
Marker distribution within clones
Fraction of clones expressing layer markers
98
462
1402
171
741
2043
83
469
1010
14
66
195
10-20
20-30
30-40
40+
Clone size (no. of cells in a clone)
Unlabeled
CTIP2+
BRN2+

CUX2 LINEAGE TRACED PROGENITORS REPRESENT A SMALL POPULATION OF hPSC-DERIVED NEURAL PROGENITORS AND ARE FATE RESTRICTED

Based on the results in the previous section, we surmised that the majority of CPNs in our system were generated from multipotent progenitors. However, a small fraction of the clones contained CPN layers markers only, or cells co-expressing CPN and SCPN markers (Figure 4.6H). Hence, there exists a possibility that either a subclass of CPNs is generated by lineage-restricted progenitors or that multipotent progenitors were contributing to lineage restricted progenitors (Greig et al., 2013). It has been shown that CUX2 expression can mark the lineage-restricted progenitors that are destined to give rise to rise to CPNs in mice (Franco et al., 2012). In order to establish if CUX2 was marking lineage-restricted progenitors in our culture system, conditional reporter hESC lines were generated using genome-editing tools. CreER^{T2} was knocked into the CUX2 locus using TALENs designed to target the first coding exon (Figure 4.7A; see also Figure 6.1). After selection and confirmation of clones, a FLEX-tdTomato reporter cassette (Fenno et al., 2014) was knocked into the AAVS1 'safe harbor' locus, again using TALENs. Recombination was confirmed by PCR of the regions on either side of the homologous arms (Figure 4.7B). In this CUX2- CreER^{T2} reporter lines, tdTomato reporter expression is dependent on a) expression of CUX2, and b) presence of Tamoxifen (TAM) in the culture medium allowing for spatial and temporal control of lineage-tracing (Figure 4.7C).

Days 15-30 were chosen for addition of TAM, as large numbers of deep layer cortical neurons start emerging after day 30 in our differentiation protocol. TAM induction resulted in detectable tdTomato expression as early as 20 days of neural induction in a small fraction of the cells. TdTomato expression was observed in neural rosettes (Figure 4.7D) and there was a progressive increase in the size of the clones over a period of 70 days. This suggests that the reporter recombination had taken place in a progenitor population. At day 80, the cultures were fixed and stained for BRN2 and CTIP2 as before (Figure 4.7E). Upon quantification of marker co-expression, we found that tdTomato+ cells induced at Days 15-30 were more likely to express BRN2+ than unlabeled cells (74.8% vs. 47.6%) (Figure 4.7G). A fraction of BRN2+ cells also co-labeled with CTIP2 cells, however it is unclear if these CTIP2+ cells were of superficial or deep layer identity (see next section). Importantly, we were only able to label a small fraction of the cells in the population when TAM was added between days 15-30 in repeated experiments (0.26-0.49%; between 9,000-11,000 cells counted) (Figure 4.7F), suggesting that lineage-restricted cells do not comprise a major population of cells in our differentiation protocol at the time points analyzed. Since our cortical cultures are predominantly comprised of CPNs at later stages, we conclude that CUX2 labels lineage-restricted progenitors but contributes only a small number of CPNs in *in vitro* neural differentiation. We cannot at present rule out the possibility that CUX2+ progenitors represent a transient state during the course of differentiation to CPNs or are specified later in these cultures.

The number of CUX2 positive cells increased considerably when TAM was added after Day 80, but these cells were not quantified because a large number of CPNs have already been

generated by this phase and TAM would induce recombination in post-mitotic neurons in addition to lineage pre-fated progenitors.

Figure 4.7: Lineage-tracing of CUX2 neural progenitors in hPSCs. A) Double transgenic conditional reporter RUES2 hESCs expressing Cre-ER^{T2} from the CUX2 locus and the FLEX-tdTomato conditional reporter under a constitutive active promoter at the AAVS1 safe harbor locus. Expression of CUX2 in the presence of TAM in culture medium induces recombination at the reporter locus and tdTomato expression. B) PCR confirmation of targeted transgenesis. Lanes 1-2 confirm 5' and 3' CUX2-CreER^{T2} insertions, respectively, while lanes 3-4 confirm 5' and 3' CAG-tdTomato/FLEX insertions, respectively. Expected band sizes for lanes 1-4: 1273, 1264, 934, and 1127 base pairs.C) Schematic timetable of TAM induction. The time of induction is from start of neural induction. TGFβ inhibition is maintained for the initial 12 days. D) Lineage traced tdTomato+ cells at rosette stage (left panel), early differentiation (middle panel) and mid differentiation (right panel) stages showing an increase in clone size. This suggests that CUX2 was labeling a progenitor population. E) TdTomato+ CUX2+ lineage derived cells preferentially express BRN2. Low magnification view (left panel), high magnification view (right panel). Arrows point to tdTomato positive cells expressing BRN2, arrowheads point to tdTomato positive cells expressing CTIP2. F) CUX2-lineage traced cells comprise a low fraction of the total cells. G) Quantification of BRN2 and CTIP+ cells in TdTomato+ and TdTomato– cell populations. CUX2 lineage traced cells are more likely to express BRN2 than non-CUX2 expressing cells . Scale bars in D) and E) represent 100µm.

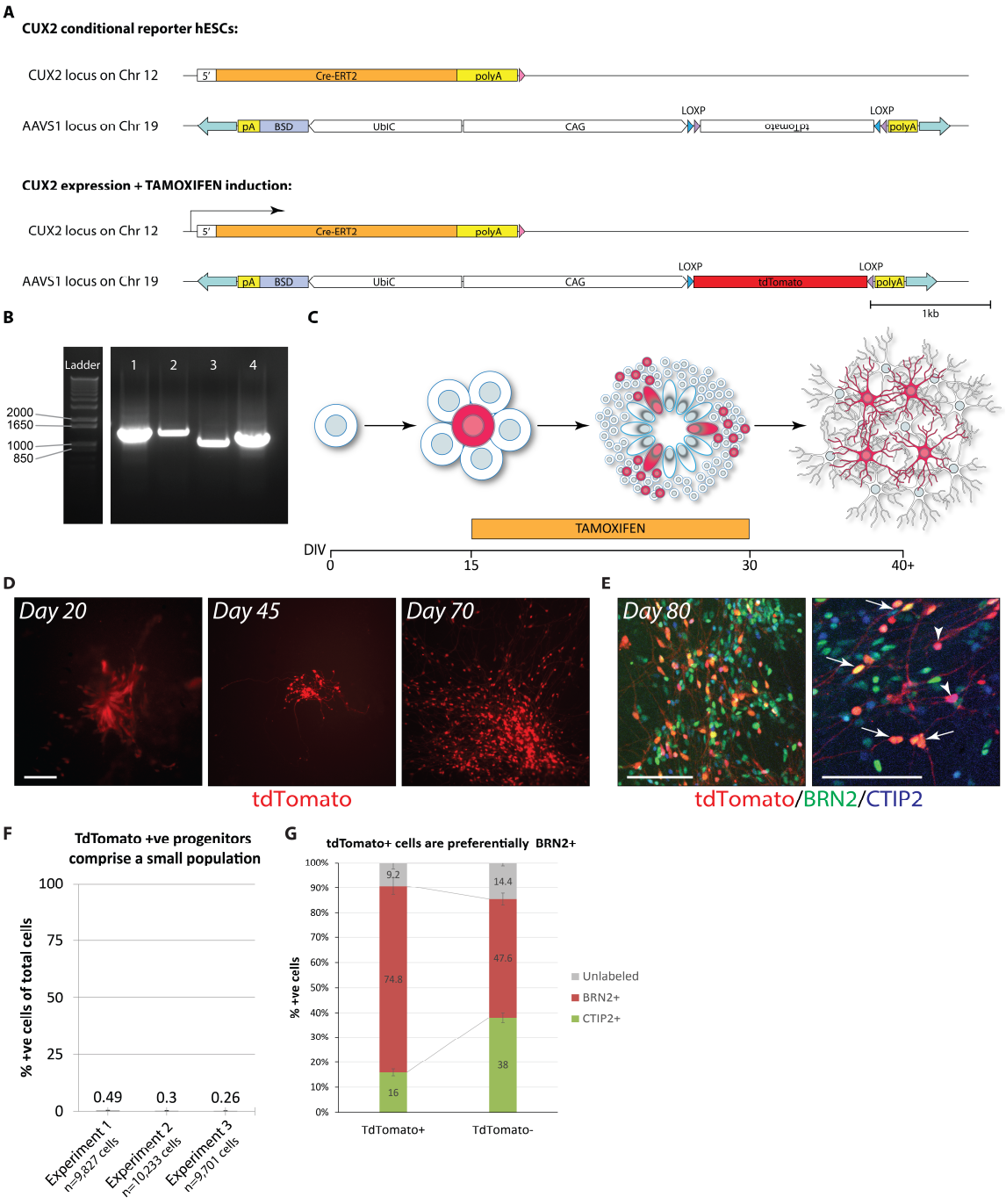
A
CUX2 conditional reporter hESCs:
CUX2 locus on Chr 12
5'
Cre-ERT2
polyA
AAVS1 locus on Chr 19
pA
BSD
UbiC
CAG
LOXP
tdTomato
LOXP
polyA
CUX2 expression + TAMOXIFEN induction:
CUX2 locus on Chr 12
5'
Cre-ERT2
polyA
AAVS1 locus on Chr 19
pA
BSD
UbiC
CAG
LOXP
tdTomato
LOXP
polyA
1kb
B
Ladder
1
2
3
4
2000
1650
1000
850
C
TAMOXIFEN
DIV
0
15
30
40+
D
Day 20
Day 45
Day 70
tdTomato
E
Day 80
tdTomato/BRN2/CTIP2
F
TdTomato +ve progenitors comprise a small population
% +ve cells of total cells
100
75
50
25
0
0.49
0.3
0.26
Experiment 1 n=9,827 cells
Experiment 2 n=10,233 cells
Experiment 3 n=9,701 cells
G
tdTomato+ cells are preferentially BRN2+
% +ve cells
100%
90%
80%
70%
60%
50%
40%
30%
20%
10%
0%
9.2
74.8
16
14.4
47.6
38
TdTomato+
TdTomato-
Unlabeled
BRN2+
CTIP2+

HUMAN FETAL BRAINS DEMONSTRATE CPN GENES IN SCPNs AT MID-CORTICOGENESIS, UNLIKE IN MICE

In order to validate marker expression for our hPSC studies, and to explore temporal progression of SCPN and CPN marker expression *in vivo*, human fetal brains were obtained at PCW10 and PCW15 (i.e. time points corresponding to our *in vitro* culture) (Figure 4.8A). The brains were dissected, embedded, and sectioned onto slides (Figure 6.4A-F). Many interesting differences were found in patterns of marker expression between mouse and human mid-corticogenesis brains in the VZ, SVZ as well as the cortical plate, some of which have been reported previously (Hansen et al., 2010). We focused on the expression of laminar markers in particular. In the mouse brain, SATB2 is expressed in callosal projection neurons and is required for their formation (Britanova et al., 2008). CTIP2 (or BCL11B) on the other hand, is expressed in SCPN's and is involved in their specification (Chen et al., 2008); while NURR1 is a marker of subplate neurons (Wang et al., 2010). These genes have also been shown to be expressed in the expected cell populations at later stages of human fetal development (Wang et al., 2010; Onorati et al., 2014).

Strikingly, we observed expression of SATB2 in the entire cortical plate at PCW15 of development (Figure 4.8B-G). Even more surprisingly, SATB2 in the deep layers completely co-localized with either CTIP2 only or with both CTIP2 and NURR1 (Figure 4.8C-G). This is unexpected when compared to mouse development, where SATB2 starts to be expressed at mid-corticogenesis (E13.5), and in only in a small subpopulation of

deep cortical plate neurons at E15.5 (Figure 6.5A) (Alcamo et al., 2008; Britanova et al., 2008). Additionally, SATB2 is known to post-mitotically repress CTIP2 and is only rarely expressed in the same neurons in the cortex (Baranek et al., 2012; Srinivasan et al., 2012; Srivatsa et al., 2014) (see also Figure 6.5A).

The observations of co-labeling held true in different areas as well as at different rostrocaudal levels of the human PCW15 cortex (Figure 4.8C-D and data not shown). Upon quantification, nearly all CTIP2+ and/or NURR1+ cells were found to co-express SATB2 (Figure 4.8H-I). Importantly, the number of cells in the cortical plate not labeled by any of the three markers was very low in all instances. Hence, the PCW15 cortex was divided into three zones: a deep layer expressing all three, a middle layer co-expressing SATB2 and CTIP2, and the most superficial layer expressing predominantly SATB2 only with a small population of SATB2/CTIP2+ cells (Figure 4.8J-K). There were quantitative differences in the fraction of cells expressing the various combinations in the different areas, even though the relative ratios were comparable (Figure 4.8L). Interestingly, a small fraction of cells (<1%) in the deep layers expressed SATB2 only (Figure 4.8E, box IV).These cells might be neurons in transit to the superficial cortical plate where the majority of the cells are SATB2 positive; alternatively, they might reflect a different class of projection neurons.

We saw similar patterns of expression when SATB2 was replaced with another superficial layer TxF MEF2C (Layers II-IV), or when CTIP2 was replaced with ER81 or SOX5 (Layer V markers), as well as when NURR1 was replaced with TLE4 or TBR1, both corticothalamic

neuronal markers (Figure 6.5B-C). This suggests that projection neuron class-determinants are not rigidly locked to a layer-specific expression initially; rather they are broadly expressed in the deeper layers of the cortical plate along with expression in the more superficial layers.

If neuronal restriction is taking place in the PCW15 brain, we reasoned that it should be possible to observe superficial layer markers at an earlier stage of human cortical development, when the superficial cortical layers have not been generated. Furthermore, given the fidelity of our hPSC-derived cortical cultures, co-expression of superficial and deep layer neurons should be observed at some stages of *in vitro* differentiation. We next turned our attention to these questions.

Figure 4.8: Human PCW15 brains demonstrate different patterns of laminar expression at mid-corticogenesis compared to mice. A) Gross anatomy of PCW15 brain. Sectioning and staining was carried out on the right hemisphere. B) Coronal section through the frontal cortex show staining for CTIP2, SATB2 and NURR1. C) Magnified view of box I in B) showing the demarcation between superficial cortical plate (sCP) and deep cortical plate (dCP). SATB2 is expressed throughout the cortical plate, while CTIP2 and NURR1 are restricted to the deep cortical plate. SATB2 positive, SATB2/CTIP2 positive and SATB2/CTIP2/NURR1 positive domains can be appreciated D) Higher magnification of box II in figure B) showing similar domains of expression as in C). E) The left panel is a magnified view of box III in D) located in the sCP. The arrows point to SATB2/CTIP2 positive cells in the sCP. The right panel is a magnification of box IV in D) which is located in the dCP. The arrowheads point to SATB2/CTIP2 positive cells in the dCP while the open arrows point to SATB2 positive only cells; the rest of the cells are SATB2/CTIP2/NURR1 positive. F) Color space representation of the image in D) after segmentation demonstrating the three domains of marker expression clearly. The segmentation was gated to remove low expressing and background cells. G) Segmentation results from the area under box I in B) for individual channels superimposed on the original image. Presence of SATB2 throughout the CP can be seen. H) Quantification of marker distribution in F). I) Quantification of marker distribution in G). J) Distribution of markers along the cortical plate in F). K) Distribution of markers along the cortical plate in G). The distance on y-axis in J) and K) is relative to the lowest part of the dCP. L) Relative fraction of cells expressing the various markers in boxes I and II. All cells are SATB2 positive. Scale bars: A) 1cm, B) 1mm, C-E) 100µm.

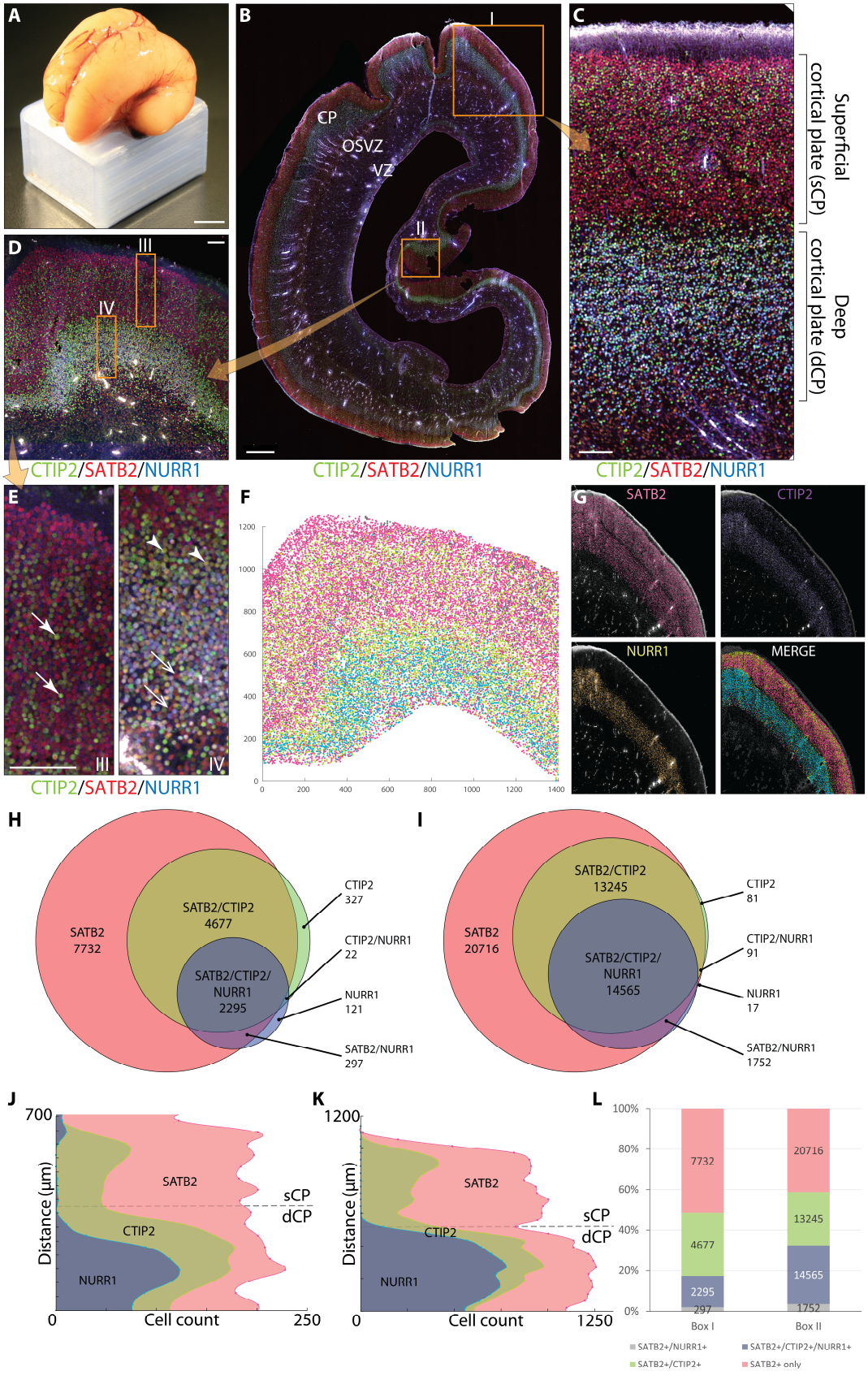
A
B
C
D
E
F
G
H
I
J
K
L
CP
OSVZ
VZ
I
II
III
IV
Superficial cortical plate (sCP)
Deep cortical plate (dCP)
CTIP2/SATB2/NURR1
CTIP2/SATB2/NURR1
CTIP2/SATB2/NURR1
CTIP2/SATB2/NURR1
SATB2
CTIP2
NURR1
MERGE
SATB2 7732
SATB2/CTIP2 4677
SATB2/CTIP2/ NURR1 2295
CTIP2 327
CTIP2/NURR1 22
NURR1 121
SATB2/NURR1 297
SATB2 20716
SATB2/CTIP2 13245
SATB2/CTIP2/ NURR1 14565
CTIP2 81
CTIP2/NURR1 91
NURR1 17
SATB2/NURR1 1752
Distance (µm)
Cell count
SATB2
CTIP2
NURR1
sCP
dCP
Box I
Box II
SATB2+/NURR1+
SATB2+/CTIP2+/NURR1+
SATB2+/CTIP2+
SATB2+ only

To establish if deep layer neurons in *in vitro* cultures expressed superficial layer markers at comparable stages of development, the cultures were subjected to a one day pulse of bromodeoxyuridine (BrdU) at various stages of differentiation corresponding to 45, 70 and 95 days after induction (Figure 4.9A). The cultures were maintained for a total of 100 days, which is equivalent to about 14.5 weeks of development. The neural cultures were then fixed and stained for BrdU, together with two markers: BRN2 (CPN marker) and CTIP2 (SCPN marker). Analysis of BrdU expressing cells showed that the majority of CTIP2 positive cells born on day 45 and 70 were also BRN2 positive (98.6% and 93.2% respectively); the majority of neurons born on day 95 however, were not (33.6%) (Figure 4.9B). This could be because the CTIP2+ neurons born on day 95 haven not had enough time to express BRN2 because the cultures were fixed 5 days later. Indeed, in the PCW15 fetal brain we observe CTIP2 expression earlier in the SVZ compared to BRN2 in the cortical plate (data not shown). In contrast to CTIP2, the majority of BRN2+ neurons did not co-express CTIP2 at any of the three stages (Figure 4.9C), in parallel with SATB2 expression in the superficial cortical plate of PCW15 brains.

Finally, we stained a PCW10 human fetal cortex with the range of markers we used for PCW15 brain. Gross anatomy of the PCW10 brain is shown in Figure 6.4A. As expected, we observed expression of CPN markers throughout the cortical plate, together with SCPN genes such CTIP2, TBR1, and NURR1. An example of SATB2 staining in the PCW10 cortical plate is shown in Figure 4.9D-F. The cortical plate in the PCW10 brain was thus divided into two domains, one co-expressing SATB2/CTIP2/NURR1 and the one above it

expressing SATB2/CTIP2 only. As expected, there was no domain of SATB2 only expressing cells since superficial layer neurons are not yet present at this stage of development.

Taken together, our data suggests that the neurons in human fetal corticogenesis become progressively limited in their ability to express various projection neuron determinants. We propose that this inside-out restriction in ability to express neuronal class-determinants is a reflection of the restriction occurring at the level of the progenitors that are giving rise to the different types of projection neurons. This restriction manifests during corticogenesis as limitations in what the neuronal progeny of these progenitors can express after formation of each layer i.e. “progressive neuronal restriction” follows “progressive progenitor restriction” (Figure 4.10). The expression of CPN genes in the deep layers may be essential for generation of certain classes of SCPN’s, such as corticostriatal neurons which project subcortically to the striatum but in the contralateral hemisphere, and hence have to cross the corpus callosum (Azim et al., 2009). The presence of small numbers of CTIP2 cells in the superficial cortical plate at this stage may indicate that the progenitor switch is asynchronous and gradual in terms of its output due to the shift from VZ to OSVZ neurogenesis. Alternatively, CTIP2 might be required for the differentiation of a subclass of CPNs in the superficial layers. This progressive restriction of post-mitotic neuronal determinants has been observed in mice as *within* CPN subtypes (Azim et al., 2009), suggesting that this might be a generalized property.

Over the course of development, post-mitotic refinement of these TxF determinants would ensure the laminar specific expression observed in adults (Johnson et al., 2009;

Greig et al., 2013). These post-mitotic refinements can occur by input from various subcortical structures, especially the thalamus, but also other projection neurons (Chou et al., 2013; Pouchelon et al., 2014). It is important to note that at PCW15 – the stage we have analyzed here – thalamocortical afferents have not yet invaded the cortical plate in human fetal development; these afferents only reach the cortical plate after PCW20 (Lee et al., 2005). Hence the pattern of TxF expression we observe here is likely representative of the raw, unrefined neuronal output of the progenitors present at this stage. This is discussed in further detail in Chapter 5.

Figure 4.9: hPSC-derived SCPNs and early human fetal brains both show co-expression of CPN and SCPN genes. A) Schematic of BrdU labeling of in vitro derived cortical progenitors. BrdU was added at days 45, 70, and 95 of differentiation for one day. All three groups were subsequently fixed and stained on D100. B) Fraction of BrdU/CTIP2+ cells either co-expressing BRN2 or CTIP2 only at days 45, 70, or 95. The majority of CTIP2+ populations born on days 45 and 70 co-express BRN2 by day 100, while the majority of CTIP2+ cells born on day 95 do not. C) Fraction of BrdU/BRN2+ cells co-expressing CTIP2 or BRN2 only at the same time points. The majority of BRN2+ cells do not co-express CTIP2, as is observed in the PCW15 fetal brain. D) Immunocytochemistry of the PCW10 human fetal brain, a time point at which there are no CPNs and the entire cortical plate is comprised of early born neurons destined for the deep layers. Two patterns of expression are observed: NURR1/CTIP2/SATB2 co-expressing cells, presumably destined to form layer VI/subplate cells, and CTIP2/SATB2+ co-expressing cells, likely destined to form layer V. E) Quantification of marker distribution in D). F) Distribution of markers along the cortical plate in D). Scale bars: 100µm.

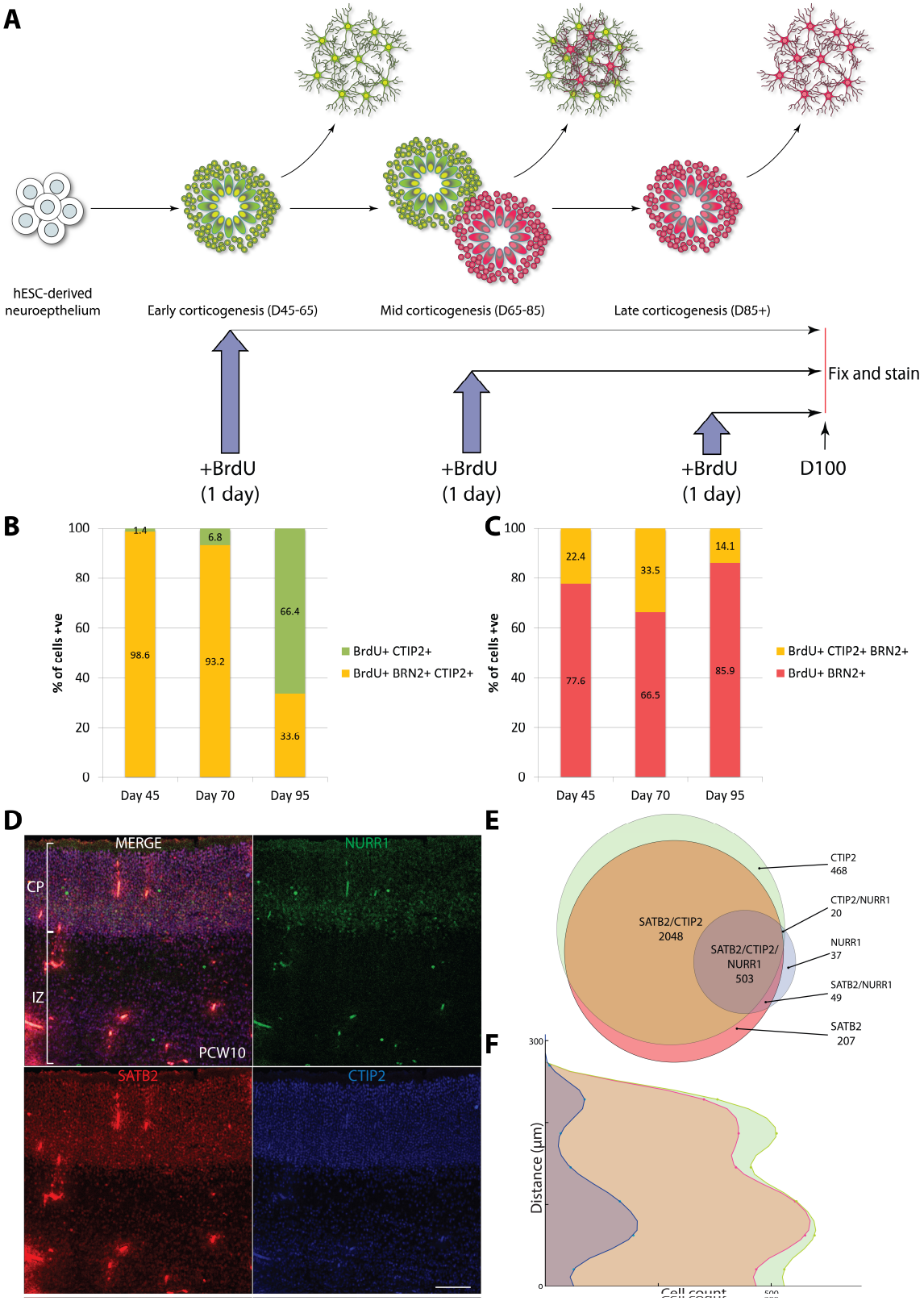
A
hESC-derived neuroepthelium
Early corticogenesis (D45-65)
Mid corticogenesis (D65-85)
Late corticogenesis (D85+)
Fix and stain
+BrdU (1 day)
+BrdU (1 day)
+BrdU (1 day)
D100
B
% of cells +ve
100
80
60
40
20
0
1.4
98.6
6.8
93.2
66.4
33.6
Day 45
Day 70
Day 95
BrdU+ CTIP2+
BrdU+ BRN2+ CTIP2+
C
% of cells +ve
22.4
77.6
33.5
66.5
14.1
85.9
Day 45
Day 70
Day 95
BrdU+ CTIP2+ BRN2+
BrdU+ BRN2+
D
MERGE
NURR1
CP
IZ
PCW10
SATB2
CTIP2
E
CTIP2
468
CTIP2/NURR1
20
SATB2/CTIP2
2048
SATB2/CTIP2/
NURR1
503
NURR1
37
SATB2/NURR1
49
SATB2
207
F
300
Distance (µm)
0
Cell count

This neuronal restriction model has important implications for not only understanding corticogenesis, but also human diseases that are thought to arise during development such as autism and neuropsychiatric diseases. Both these conditions demonstrate defects in laminar gene expression and circuit formation (Geschwind and Rakic, 2013; Stoner et al., 2014). Neuronal restriction provides a conceptual link between how defects in progenitors could affect laminar development and neuronal hodology, which in turn underlies cortical circuit formation. Additionally, understanding the biological basis of neuronal restriction in hPSC-derived cultures will facilitate an understanding of the developmental origins of neuronal diversity, including neurons that are specifically enriched in the primate brain (Geschwind and Rakic, 2013).

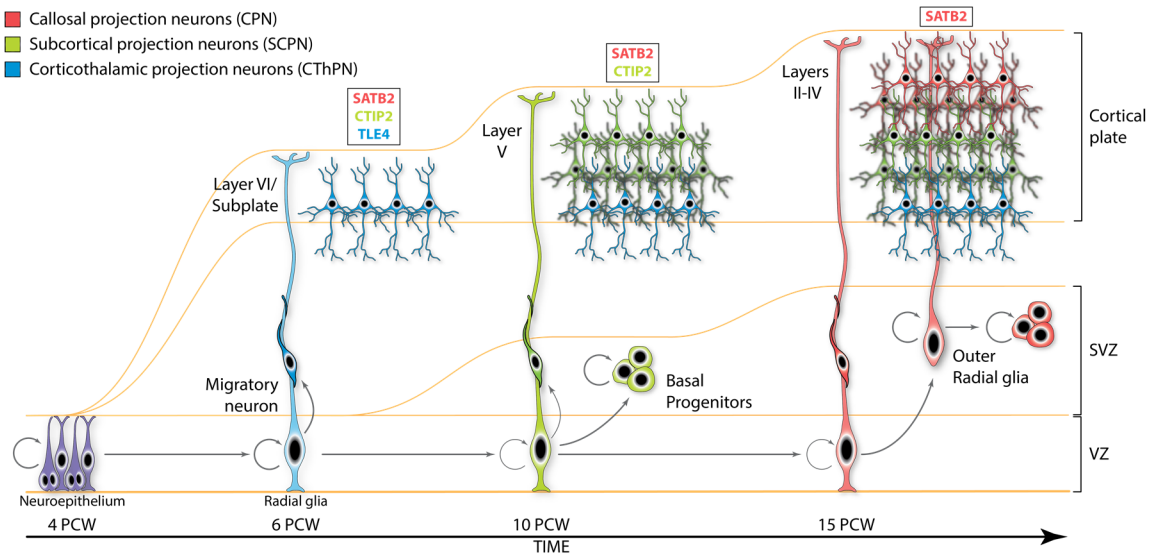

Figure 4.10: "Progressive neuronal restriction" model. Progressive limitation in the ability of the daughters neurons of VZ/OSVZ to express various projection neuron class-determinants over time might be a manisfestion of the progressive restriction happening within the progenitors themselves. Further refinement of these early patterns of expression to the adult patterns would require input from other projection neurons or subcortical sources (e.g. the thalamus).

SUMMARY

Here we use hESCs as a model to study human corticogenesis and show that neural progenitors derived from hESCs recapitulate forebrain marker expression and differentiation potential of all the major progenitor types involved in human corticogenesis. Using FUCCI transgenic hESCs, we observe dynamic cell-cycle properties of RGs at a single cell and population level. We use this *in vitro* model of differentiation to show that neuroepithelium derived from hESCs by TGFβ inhibition can be areal-patterned on the rostrocaudal axis by modulating WNT signaling. This positions WNTs as candidates to caudalize the cerebral cortex in vivo, which has not been shown to date. Using transgenic hPSCs, we demonstrate that individual hPSC-derived neural progenitors have the potential to differentiate into both SCPNs and CPNs, lending support to the "Progressive Restriction" model of corticogenesis. CUX2-lineage traced progenitors represent a small pool of precursors that appear to be destined to a CPN fate. However, given the low fraction of these cells, their contributions to CPNs in our system are likely to be minimal. We propose that CUX2 progenitors represent a transient state on the differentiation time-line rather than a separate class of progenitors, at least in human corticogenesis. Finally, we show differences in cortical marker expression in the human fetal cortex during mid-corticogenesis compared to mice and propose that these differences are due to "progressive neuronal restriction". This neuronal restriction is a manifestation of progressive progenitor restriction and is conserved in our *in vitro* differentiation model.

CHAPTER 5: DISCUSSION

THE REQUIREMENT FOR TGFβ INHIBITION TO INDUCE NEURAL FATE IS CONSERVED FROM XENOPUS AND WITHIN MAMMALS

It is rather remarkable that inhibiting TGFβ signaling has the same outcome over hundreds of millions of years of evolution. This is because while the body plan is conserved in chordates, the complexity of neural derivatives and the underlying transcriptional circuitry have changed drastically. For instance, in the Xenopus cortex, only two to three layers of organized cells can be appreciated, mammals can have up to six layers that are specialized into different areas. Moreover, even within mammals, the primate neuroepithelium generates a more complex organization of progenitors and neurons, yet the underlying pathway that enables this to happen has remained the same. Intriguingly, the requirement for BMP inhibition to establish a neural domain evolved early in bilaterians, as was discussed in Chapter 1.

We have shown that cell-intrinsic inhibition of *canonical* TGFβ signaling via the inhibitory SMAD7 is sufficient to impose a neural fate in hESCs. This neuroepithelium is of anterior character, as defined by several criteria. Significantly, this conversion can take place very efficiently and even under pluripotency conditions. Inhibition of TGFβ by SMAD7 occurs in both the cytoplasm and the nucleus, and SMAD7 acts at many nodes to achieve this inhibition, including promotion of receptor degradation, disruption of receptor SMAD

binding, inhibition of SMAD4-DNA complex formation in the nucleus, and recruitment of transcriptional repressors to SMAD binding sites (Yan et al., 2009).

Our results also demonstrate that FGF-MEK has an inhibitory, rather than an instructive role in neural induction in the presence of TGFβ inhibition. However, we cannot at this time rule out the possibility that other branches of FGF signaling, namely, PI3K-AKT, and PLCɣ-Ca^{2+} may have a role in neural induction. It is plausible that different branches of FGF signaling may have contradictory roles in neural induction, and this will need to be addressed in future studies. It is worth mentioning that other studies have reporter similar findings, and FGF receptor inhibition (rather than MEK inhibition as we did) also promoted neural induction in these studies (Greber et al., 2011).

As mentioned in the Chapter 1, human PSCs are thought to closely resemble the primed pluripotent of mEpiSCs. The fact that Activin/Nodal and FGF signaling are required to maintain the pluripotent mEpiSC and hESC state, inhibition of the "default" state of neural differentiation can been viewed as a prerequisite for maintenance of the "primed" pluripotent state *in vitro*.

SMAD7 IS A POTENT NEURAL INDUCER AND ITS LEVELS ARE TIGHTLY REGULATED DURING DEVELOPMENT

Overexpression of SMAD7 has a potent neuralizing effect in hPSCs, as it does in animal caps of the Xenopus embryo (Casellas and Brivanlou, 1998). Since our work on SMAD7,

other groups have shown that in a screen of neuralizing factors, SMAD7 had among the most potent neuralizing activity in mPSCs (Yamamizu et al., 2013). *In vivo*, SMAD7 is a TGFβ inducible gene, acting in a feedback loop to regulate TGFβ signaling (Nakao et al., 1997). Because of its strong neural inducing activity, it is essential to regulate the levels of SMAD7 very closely to prevent its unchecked activity. This is done through two known mechanisms. First, SMAD7 protein is targeted for degradation by the E3 ligase RNF12 in embryos (Zhang et al., 2012). Indeed, zebrafish embryos with RNF12 morpholinos have a larger head and anterior phenotypes, together with loss of mesoderm derivatives. Additionally RNF12 knockout mESCs had higher levels of SMAD7 and could undergo neural differentiation even in the presence of BMP. Second, the SMAD7 mRNA has sequences in the 5' and 3' untranslated regions (UTR) that act as mRNA destabilizers and target it for degradation via the nonsense-mediated decay (NMD) pathway in pluripotent cells (Lou et al., 2014). Knockdown of NMD components results in SMAD7 upregulation and increased neural differentiation in pluripotent teratocarcinoma cells by inhibition of TGFβ signaling.

Hence, it is unlikely that SMAD7 has a predominant role in neural induction *in vivo*, as the role of TGFβ inhibition is fulfilled by the extracellular inhibitors released by the node/organizer. It may however act redundantly with these inhibitors once the process has started to stabilize the neural fate.

HOW DOES TGFβ INHIBITION PROMOTE DEFAULT NEURAL INDUCTION IN hPSCs?

Gain- and loss- of function approaches have permitted scrutiny of the mechanisms operating downstream of TGFβ inhibition by which pluripotent cells undergo neural conversion. Inhibition of Activin/Nodal down-regulates NANOG and promotes expression of ZEB2 (also known as SIP1 and ZFHX1B), a SMAD binding protein (Chng et al., 2010). In pluripotent cells, ZEB2 limits the mesoderm inducing effects of Activin/Nodal signaling and is repressed directly by the pluripotency factors NANOG and OCT4. On Activin/Nodal inhibition, ZEB2 promotes neuroectodermal differentiation of EpiSCs and hESCs. Neural induction of hESCs also promotes expression of NR2F2 (also known as COUP-TFII), which is among the earliest TxFs expressed during neural differentiation of hESCs as shown by our group and others (Rosa and Brivanlou, 2009; Greber et al., 2011). In pluripotent hESCs, OCT4 and the OCT4-induced microRNA mir-302 regulate expression of NR2F2 by transcriptional and post-transcription mechanisms, respectively, whereas in the differentiating neuroectoderm, NR2F2 directly represses OCT4 expression and promotes expression of other neural specific markers such as PAX6.

BMP inhibition also contributes to neuroectodermal differentiation through various mechanisms. First, it promotes the specificity of neural induction by inhibiting induction of non-neural germ layers such as trophectoderm, mesoderm, and non-neural ectoderm (Greber et al., 2011). Indeed, inhibition of BMP signaling together with down-regulation of OCT4 is a prerequisite for neuroectodermal specification in hESCs (Wang et al., 2012a). Second, inhibition of BMP signaling may serve to stabilize the neural fate by maintaining

expression of neural genes such as SOX2 (Greber et al., 2011). Third, inhibition of BMP signaling permits expression of cell-intrinsic neural determinants, such as the zinc finger TxF, ZNF521, which is necessary and sufficient for neural induction in hESCs as well as EpiSCs (Kamiya et al., 2011). Znf521 acts by directly transactivating neural promoters such as such as Sox3, Sox1, N-cad, and Pax6 in concert with the co-activator p300. Importantly, Znf521 can only promote a neural fate in EpiSCs and hESCs, but not in mESCs, suggesting a conservation of downstream wiring between the primed state of EpiSCs and hESCs. Znf521 is potently inhibited by BMP signaling at this stage. Lastly, BMP inhibition also promotes acquisition of anterior neural fate, as neural induction in the absence of BMP inhibitors appears to generate neuroepithelium of posterior identity in both EpiSCs and hESCs (Patani et al., 2009; Chng et al., 2010; Lupo et al., 2013).

FGF signaling maintains pluripotency in EpiSCs and hESCs; in hESCs but not EpiSCs, the FGF-MEK-ERK cascade directly regulates NANOG expression (Greber et al., 2010; Chen et al., 2012). Hence one way removal of FGF supports neural induction is by promoting down-regulation of pluripotency TxFs and thereby permitting expression of the default neural program. In addition, FGF-MEK-ERK signaling directly represses expression of the neural determinant paired box TxF PAX6 in hESCs as well as EpiSCs. Indeed, small molecule inhibition of either the FGF receptor or deletion of MEK itself causes upregulation of PAX6 expression (Greber et al., 2010; Greber et al., 2011; Hamilton and Brickman, 2014). Additionally, inhibition of FGF signaling also promotes induction of the forebrain and midbrain enriched homeobox TxF OTX2 in hESCs. OTX2 in turn directly binds to the PAX6 promoter and enhances its expression in hESCs (Greber et al., 2011).

hPSCs CAN MODEL EARLY CORTICAL DEVELOPMENT AND CELL INTRINSIC BEHAVIORS

Based on our multiple assays, we observed striking similarities between hPSC-derived neural progenitors and the known behaviors of RGs *in vivo*. These included not only molecular markers, but also cell cycle dynamics, self-organization into complex multi-layered structures, as well as signaling requirements. Additionally, the hPSC-derived neurons also generated the two other progenitor types found during development, namely IPs and bRGs. This suggests that brain development is a largely self-contained process at the initial stages, with signaling centers in the neural ridge, meninges, and cortical hem contributing to patterning, progenitor maintenance, neuronal migration, and axon guidance at later stages. This is also supported by recent studies utilizing three-dimensional aggregates of hPSCs that recapitulate of many milestones of corticogenesis (Kadoshima et al., 2013; Lancaster et al., 2013). In my hands, three-dimensional organoids displayed significant inter- and intra-experiment variability and thus may need to be optimized further before they can be used reliably. Moreover, the single cell tracking and lineage tracing as we carry out here is either not possible or reliable in 3D space at present. Once some of these issues are resolved, 3D organoids could be a good model to study corticogenesis in a 3D environment closer to its natural environment, and also to study organization that cannot be studied in 2D, such as gyrus formation.

There are specific aspects of the 2D *in vitro* system that could also use further optimization. For instance, in our in vitro cultures, there was a gradual depletion in the number of progenitors in the cultures, and a failure to maintain a rosette state beyond 50

days. These may be linked to the lack of self-renewal cues in the culture conditions, or a bias towards neuronal differentiation in our cultures. Future studies will need to address the nature of these self-renewal cues. Some clues have come from recent studies in human fetal brains which showed that PDGFD and its cognate receptor PDGFRβ maintain self-renewal and basal dispersion of human RGs (Lui et al., 2014). The cerebrospinal fluid *in vivo* also provides a rich niche of signaling molecules such as IGF2, BMPs, and RA which may also contribute to self-renewal (Lehtinen et al., 2011). Moreover, even though the composition of the extracellular matrix (ECM) in the OSVZ of the developing brain is not understood, it is believed to play an important role in maintaining self-renewal of the basal progenitors (Fietz et al., 2010; Simone et al., 2012; Denise et al., 2014), as well as neuronal migration (Boyle et al., 2011). Since we maintain *in vitro* progenitors in laminin and fibronectin for the entire duration of differentiation, it is possible that absence of ECM laid down by non-neural cells also contributes to failure to maintain the rosette stage in our cultures. Lastly, the range of neurons produced by the hPSC-derived progenitors will need to be documented more thoroughly in terms of their subsequent molecular profile, and importantly, their hodology upon transplantation into mouse brains.

Overall, the recent proliferation of human genome modification technologies, combined with live imaging, and single cell resolution analyses provide distinct advantages to the *in vitro* system that can complement mouse *in vivo* work. As an added benefit, hPSCs also demonstrate human-specific aspects of corticogenesis. Thus, this system can be used to model early development as well as disease, and provides an unlimited supply of material to generate hypothesis that can be tested for in vivo relevance in human fetal samples.

WNT SIGNALING IS A PATTERNING FACTOR FOR THE CAUDAL TELENCEPHALON

There is considerable interest in using IPSC and hPSC derived neural progenitors to generate therapeutically relevant, defined populations of neurons that can used for drug screens, disease modeling, and perhaps cell replacement. However, our ability to generate defined populations is limited due to the heterogeneous nature of differentiation, even within forebrain progenitors. By changing the level of WNT signaling, we were able to pattern the progenitors on the rostrocaudal axis concurrently with their acquisition of neural fate based on expression of various molecular markers. This provides direct support for the protomap hypothesis, which postulates that the areal determination of the cortex is made at the level of early progenitors that map their areal fate onto the neurons.

Other groups have utilized WNT signaling to promote midbrain fates from hPSCs (Kriks et al., 2011; Kirkeby et al., 2012); we have also confirmed these findings. The key breakthrough in our experiments was the realization that moderate to low levels of WNT signaling could also maintain forebrain fate while promoting a caudal cortical identity. While a role for WNT signaling has been speculated in determination of caudal cortical identity in mice, it has never been shown to be a direct areal patterning agent in the cortex. We suggest that WNT achieves its effect at an early stage of forebrain specification, which is why mouse studies might have missed the effect since most areal patterning studies have looked at the cortex after E11, after the rostrocaudal identity has

already been established. Significantly, in addition to providing insights into arealization in the mammalian cortex, our results also suggest that by changing the areal pattern, early WNT signaling may also act as a selector for generation of a six-layered neocortex versus a three-layered archicortex. This is because WNT inhibition upregulates FOXG1 and LHX2, two TxFs that are known to be essential for neocortical fate, while WNT activation down-regulates them both while promoting caudal cortical marker expression. Lastly, we also observe upregulation of diencephalic markers upon moderate WNT activation. This supports the notion that the caudal cortex and diencephalon share embryologic origins (Kimura et al., 2005), and require a similar signaling pathway for their specification. This raises the intriguing possibility that thalamic tissue could be generated by further refinement of this protocol – a feat that has not been achieved so far using mouse or human PSCs.

Further experiments are needed to confirm the stable identity of the post-mitotic neurons derived from the areally specified progenitors. This work will be aided by recent transcriptomic analysis of the fetal human cortex, which found genes enriched in the rostral or caudal cortices in the different germinal zones as well as the cortical plate (Miller et al., 2014). Such analysis will be complemented by studies on human fetal material to confirm RNA expression at the protein level. In this regard, we note that cortical progenitors generated in the presence of TGFβ and WNT inhibition generate neurons that stain for AUTS2, which is known to be enriched in the frontal cortex (Bedogni et al., 2010). Conversely, neurons generated from progenitors subjected to TGFβ inhibition and moderate WNT activation do not.

PROGENITOR AND NEURONAL RESTRICTION AND ITS IMPLICATIONS

Based on our analysis of hPSC-derived single neural progenitors, we surmise that individual human neural progenitors have the *potential* to form projection neurons of different identities. This is in line with observations made in the mouse cortex (Guo et al., 2013; Gao et al., 2014). Our work does not rule out the possibility that there are lineage-restricted progenitors in the primate cortex, however if present, they likely comprise only small fraction of the progenitor population. This is supported by our studies of conditional CUX2 reporter hPSCs that can be lineage-traced based on CUX2 expression. Experiments in these transgenic lines support the notion that CUX2 expression labels progenitors that are predestined to form CPNs rather than SCPNs. However, CUX2 lineage traced cells comprise a very small percentage of progenitors, even at a stage when nearly the entire culture is comprised of progenitors. More likely, CUX2 marks a fraction of progenitors that are further down progenitor restriction and have switched to production of CPNs. In summary, our *in vitro* studies in human neural progenitors favors the Progenitor Restriction Model which was originally formulated from lineage-tracing and transplantation experiments, and recently established in mouse genetic experiments.

One advantage of the *in vitro* system we describe here is the complete lack of interneurons – which arise in the ventral telencephalon – and confound lineage-tracing analysis due to their expression of CUX2 (Guo et al., 2013). Induction of interneurons

requires sustained levels of SHH, which is not present in our cultures, and the generated neural progenitors uniformly express markers of dorsal telencephalic territory.

Recent microarray analysis of the early second trimester fetal cortex has revealed transcriptomic patterns of gene expression in the VZ to CP (Miller et al., 2014). Interestingly, very few genes are found to be differentially expressed between the superficial and deep layers of the cortical plate at this stage of development, even though at later stages the expression patterns are more distinct (Johnson et al., 2009). Since the earlier stage represents the direct output of the VZ and OSVZ progenitors, this suggests that the superficial and deep layers may share similar gene expression programs, and perhaps a similar cell-of-origin. In our studies of laminar expression in the human fetal PCW15 cortex, we observed robust expression of CPN-specific TxFs throughout the cortical plate, and broad co-expression of markers of subplate, CThPN, SCPN, and CPN identity in the earliest born neurons (i.e. deepest in the cortical plate). This is different from the situation in the mouse cortex, where co-expression of these determinants is infrequent and transient. Intriguingly, later born neurons expressed markers of SCPN and CPN identity, but not of subplate or CThPN identity. Finally, the latest born neurons expressed markers of CPNs, and a small fraction also expressed SCPN markers. This led us to propose that the neurons are being restricted in terms of their fate choices over time, and that this neuronal restriction might be a manifestation of restriction occurring at the level of progenitors giving rise to these neurons, as we demonstrated in hPSC-derived progenitors.

Several lines of evidence support the observation of neuronal restriction. First, CPN TxFs are expressed uniformly in the cortical plate in the PCW10 fetal brain; at this time the majority of the neurons being born are destined for the subplate and layer VI. Second, we were able to observe co-expression of CPNs and SCPN markers in neurons generated from hPSCs over a similar time-period. Third, even though CPN determinants such as SATB2 is rarely found to be co-expressed in SCPNs and CThPN in mice, it is clearly necessary for their development, as was shown recently (Dino et al., 2014). Moreover, this requirement is cell intrinsic, as only knockout of SATB2 at early stages of corticogenesis – but not at later stages – results in loss of SCPNs. Loss of SATB2 also result in altered patterns of CThPN markers (such as ZFPM2). Fourth, SCPN determinants such as FEZF2 are also required for proper CThPNs expression of ZFPM2 in in mice (Shim et al., 2012). Together, these studies support a biological role for co-expression of various projection neuron determinants in the early born CThPN/subplate neurons and progressive limitation in the repertoire of later born CPNs.

It remains possible that a signaling cue in the cortical plate upregulates SCPN TxFs independently of progenitor restriction. However, we believe that this is an unlikely for multiple reasons. First, a fraction of SATB2 only cells are seen the deep cortical plate in the PCW15 cortex. Presumably, these cells are migratory cells on their way to the superficial cortical plate, which would suggest that they are already specified to their fate. Second, our *in vitro* cultures, which lack an organized cortical plate, also show neuronal restriction. This would suggest that co-expression of CPN and SCPN determinants is an intrinsic property of deep layer neurons. Third, in *reelin* knockout mice, a complete

inversion of layers is seen, and SATB2 positive CPNs are specified correctly even though they reach the deepest part of the cortical plate at much later stages and hence are not dependent on the signaling cues that exist at earlier stages (Britanova et al., 2006).

Taken together, we argue that neuronal restriction might be a general phenomenon, and perhaps even evolutionarily conserved one in mammals. The observed differences in mouse and human embryonic brains might be explained by the fact that the mouse cortical plate receives thalamic input at a much earlier stage (~E13.5) than human (>20PCW) (Lopez-Bendito and Molnar, 2003; Lee et al., 2005). Thus, thalamocortical refinement of gene expression of post-mitotic neurons in mice (which is known to occur) may begin earlier and concurrently with generation of the deep layers, leading to domains of TxF expression that resemble the adult state more closely (Chou et al., 2013; Pouchelon et al., 2014). In the human fetal cortex, these thalamocortical afferent reach the plate much later, hence we are able to observe the unrefined expression patterns of neurons at PCW15 and earlier.

The hierarchical nature of fate determinant expression in the human fetal cortex during development may reflect a rewiring of the transcriptional machinery for production of projection neuron class unique to the human brain. Additionally, this also may be a conserved principle of mammalian development that is exaggerated in human corticogenesis due to the longer timescale of development. Neuronal restriction also has important implications when it comes to understanding neuro-developmental and psychiatric diseases. Mutations in patients with schizophrenia are commonly in genes

implicated in autism, and many of these shared genes are transcriptional or chromatin modifiers (Ronan et al., 2013; McCarthy et al., 2014). The cortex of patients with autism show characteristic 'patch' defects in laminar gene expression and increased numbers of neurons in the frontal cortex (Stoner et al., 2014). It is conceivable that defects in fate restriction, either at the level of progenitors or neurons could change the relative ratios of various neuronal classes, thereby contributing to defects in cortical wiring. It is tempting to speculate that transcriptional repressors or chromatin modifiers might be essential for this restriction to take place for appropriate specification of the various projection neuron types. For example, mutations in a transcriptional repressor – MECP2 – underlie Rett Syndrome. In this disease, patients demonstrate clinical symptoms resembling autism. MECP2 is expressed in both progenitors as well as neurons (Muotri et al., 2010) and could potentially fulfil the roles of progenitor and neuronal restriction. This speculation awaits detailed analysis of laminar marker expression in Rett syndrome mouse embryonic brains or patient-derived IPSCs. Neuronal restriction provides a conceptual link as to how defects in genes that affect progenitors could affect laminar development and neuronal hodology.

Lastly, our combined studies of hPSC-derived neurons and comparative analysis of the human fetal cortex sets the baseline for further studies on refinement of our differentiation protocol. This will enable us to manipulate the cultures conditions so that neural progenitors – and their daughter neurons – mimic the *in vivo* milestones of corticogenesis more closely, allowing for a more stringent readout of *in vivo* development.

CONCLUSIONS AND FUTURE PERSPECTIVE

This body of work highlights the evolutionary conservation of pathways that operate during induction and patterning of the neural lineage in the embryo, and at the same time also demonstrates the evolutionary divergence of primate-specific features during corticogenesis. By combining *in vitro* human genome modification technologies with the default model of neural induction, we are now able to probe fundamental questions of human corticogenesis that could previously only be studied in model organisms. This *in vitro* system will complement studies in model organisms, and will be particularly useful to uncover mechanistic principles involved in generation of the various cortical neuronal projection classes as well as the diversity of neurons *within* each class. The novel genetic and analytical tools we describe here can be broadly used for *in vitro* studies of cell cycle dynamics, self-organization, lineage tracing, and live imaging of many PSC-derived tissue types.

We have demonstrated that TGFβ signaling inhibition can drive human PSCs to an anterior neural fate at near complete efficiencies and that this mechanism is conserved between mouse, primate, and human PSCs. Using FUCCI markers, we observe self-organization in radial progenitors, interkinetic nuclear migration, as well as a requirement for Notch signaling in progenitor maintenance, all of which are hallmarks of human neural progenitors *in vivo*. Together with region-specific marker analysis, we conclude that *in vitro* hPSC-derived neural progenitors are similar to their *in vivo* counterparts. We further demonstrate that the *in vitro* derived neuroepithelium can be patterned on the

rostrocaudal axis by manipulating WNT signaling. This finding provides insights into arealization in the mammalian cortex and suggests that early WNT signaling – or lack thereof – may act as a selector for generation of a six-layered neocortex versus a three-layered archicortex or diencephalic derivatives. We further utilize our *in vitro* system to establish that individual neural progenitors can be differentiated into cortical neurons representative of various projection neuron classes. This supports the "Progressive Restriction" model of corticogenesis. Combined with CUX2 lineage-tracing experiments, we believe that lineage-restricted progenitors are not a major source of CPNs. Lastly, based on *in vitro* experimentation and analysis of human fetal tissue, we propose that progressive progenitor restriction is manifested in progressive neuronal restriction.

My findings suggest the need to study human brain development directly in parallel with model organisms and raise several new questions. These include, but are not limited to: what is the relationship of the various progenitor types to the projection neuron classes at different stages of corticogenesis? How close are the *in vitro* generated neurons to their *in vivo* counterparts? What are the mechanisms underlying progenitor and neuronal restriction, and what happens when this restriction is manipulated? How do non-cell autonomous factors interact with cell-intrinsic programs to affect progenitor and neuronal restriction? Which of these programs plays a larger role in post-mitotic refinement of projection neuron classes? In my opinion, answering these questions will be key to understanding corticogenesis at an evolutionary and developmental level. They will also provide clues to the underlying pathology in neurodevelopmental disorders and, down the line, human cognitive ability.

Chapter 6: APPENDIX

TABLE 6.1: COMPOSITION OF HARVARD UNIVERSITY EMBRYONIC STEM CELL MEDIUM (HUESM)

HUESM media (500mL)
240mL DMEM w/ L-glutamine
100mL Knockout serum replacement
10mL B27 supplement w/o Vit A
5mL GlutaMAX
5mL Non-essential amino acids
5mL Penicillin/Streptomycin
900µL β-mercaptoethanol

TABLE 6.2: COMPOSITION OF 3N NEURAL INDUCTION MEDIUM

3N media (500mL)
240mL DMEM/F12 w/ L-glutamine
240mL Neurobasal
5mL B27 with Vitamin A
2.5mL N2 supplement
1.25 mL L-glutamine
2.5mL GlutaMAX
2.5mL Non-essential amino acids
2.5mL Sodium pyruvate
5mL Penicillin/Streptomycin
125µL 10mg/mL Insulin
Add fresh during neural induction: *10µM SB431542* *100nM LDN193189*
Add 1:500 Laminin D25+

All from Life Technologies

TABLE 6.3: COMPOSITION OF MOUSE ESC BASE MEDIUM

Base medium (500mL)
242mL DMEM/F12 with GlutaMAX
242mL Neurobasal
5mL Chemically defined lipids
5mL B27 supplement w/ RA
5mL Penicillin/Streptomycin
5mL Sodium pyruvate
2.5mL N2 supplement
2.5mL Glutamine
900µL β-mercaptoethanol
170µL 7.5% BSA fraction V (final: 25µg/mL of BSA)
0.5mL 10mg/mL Insulin
For mouse maintenance medium, add fresh to 50mL base medium:
1000U/mL LIF
1µM PD0325901 (MEK inhibitor)
3µM CHIR (GSK3β inhibitor)

TABLE 6.4: PRIMARY ANTIBODIES USED IN CHAPTER 3

Antibody	Manufacturer	Cat No.	Dilution	Application (s)
PAX6	DHSB		200	IF
PAX6	BD Biosciences	561552	100	FC
SOX2	Cell Signaling Technology	3579	200	FC
OCT3/4	BD Biosciences	611203	500	IF
OCT3/4	Santa Cruz Biotechnology	sc-9081	200	IF
NANOG	Abcam	AB21624	200	IF
CDX2	Abcam	AB15258	100	IF
BRACHYURY	R&D Systems	AF2085	500	IF
SOX17	R&D Systems	MAB1924	200	IF
OTX2	Abcam	ab21990	200	IF
NFH	Abcam	ab28029	1000	IF
PAX3	DHSB		100	IF
EN1	DHSB	4G11	100	IF
EN2	R&D Systems	MAB2600	100	IF
DCX	Cell Signaling Technology	4604	200	IF
NKX2.1	Epitomics	2044-1	100	IF
HOXB4	DHSB	I12	100	IF
SOX10	Santa Cruz Biotech	sc-17342	200	IF
SOX1	R&D Systems	AF3369	500	IF
GFP-FITC	Abcam	ab6662	400	IF
FOXG1	Neuracell	NCFAB	500	IF
GFP	Invitrogen	A-11122	500	IF
GFP	Santa Cruz Biotechnology	sc-9996	200	IF
NCAM1	BD Biosciences	557699		IF; FC

SMAD7	Santa Cruz Biotechnology	sc11392	1000	WB
Phospho-SMAD2/3	Cell Signaling Technology	9510	100	IF; WB
Total SMAD2				WB
Phospho-SMAD1/5/8		9511	100	IF; WB
Total SMAD1				WB

Abbreviations - IF: IF; FC: flow cytometry; WB: western blot

TABLE 6.5: PRIMARY ANTIBODIES USED IN CHAPTER 4

Antibody	Supplier	Cat No.	Type	Dilution
PAX6	BD Biosciences	561462	Ms	200
		561664	Ms-AF488	100
SOX2	Cell Signaling Technology	3579S	Rb	400
	R&D Systems	AF2018	Gt	500
FOXG1	StemCulture		Rb	500
OTX2	Abcam	ab21990	Rb	500
	SCBT	sc-30659	Gt	200
LHX2	Abcam	ab130256	Ms	200
	SCBT	sc-19344	Gt	50
PLZF	Calbiochem	OP128L-100UG	Ms	100
SOX1	R&D Systems	AF3369	Gt	500
TBR2	Abcam	ab23345	Rb	400
P-Vimentin	MBL	D076-3S	Ms	500
N-CAD	BD Biosciences	561554	PE	50
Nestin	Neuromics	CH23001	Ch	100
Beta-tubulin III	Covance	PRB-435P	Rb	1000
	R&D Systems	MAB1195	Ms	1000
MAP2	Abcam	ab28029	Ms	1000
Synapsin	Cell Signaling Technology	#4329	Rb	200
ER81	Abcam	ab81086	Rb	500
CTIP2	Abcam	ab18465	Rt	200
TBR1	Abcam	ab31940	Rb	200
		sc-15607	Gt	50
FEZF2	Bioss	bs-12148R	Rb	200

MEF2C	Cell Signaling Technology	5030	Rb	400
BRN2	SCBT	sc6029	Gt	200
CUX1	EMD Millipore	ABE218	Rb	200
CUX2	From David Waxman		Rb	200
SATB2	Abcam	ab51502	Ms	200
NURR1	R&D Systems	AF2156	Gt	100
SOX5	Abcam	ab94396	Rb	500
TLE4	From Stefano Stefani		Rb	1000
ZFPM2	SCBT	sc-10755	Rb	100
GFAP	Aves Lab		Ch	2000
P-Histone H3	Abcam	ab4178	Rb	500
BrdU-A488 conjugate	Life Technologies	B35131	Ms-AF488	100
V5	Abcam	Ab9116	Rb	500
RFP	Chromotek	5F8	Rt	1000

KEY: Ms, mouse; Rb, rabbit; Ch, chicken; Gt, goat; PE, phycoerythrin

TABLE 6.6: SECONDARY ANTIBODIES USED

Donkey secondary	Raised against	Manufacturer	Cat No.	Dilution
Alexa Fluor 488	Mouse	Life Technologies	A-21202	1000
Alexa Fluor 488	Rabbit	Life Technologies	A-21206	1000
Alexa Fluor 488	Goat	Life Technologies	A-11055	1000
Alexa Fluor 488	Rat	Life Technologies	A-21208	1000
Alexa Fluor 555	Mouse	Life Technologies	A-31570	1000
Alexa Fluor 555	Rabbit	Life Technologies	A-31572	1000
Alexa Fluor 555	Goat	Life Technologies	A-21432	1000
Alexa Fluor 568	Mouse	Life Technologies	A-10037	1000
Alexa Fluor 568	Rabbit	Life Technologies	A-10042	1000
Alexa Fluor 568	Goat	Life Technologies	A-11057	1000
Alexa Fluor 594	Mouse	Life Technologies	A-21203	1000
Alexa Fluor 594	Rabbit	Life Technologies	A-21207	1000
Alexa Fluor 594	Goat	Life Technologies	A-11058	1000
Alexa Fluor 647	Mouse	Life Technologies	A-31571	1000
Alexa Fluor 647	Rabbit	Life Technologies	A-31573	1000
Alexa Fluor 647	Goat	Life Technologies	A-21447	1000
Alexa Fluor 647	Chicken	Jackson ImmunoResearch	703-605-155	500
Alexa Fluor 680	Rabbit	Life Technologies	A-10043	1000
Alexa Fluor 680	Goat	Life Technologies	A-21084	1000
Alexa Fluor 680	Rat	Jackson ImmunoResearch	712-625-150	500

All secondary antibodies were IgGs

TALENS / CRISPR AND THEIR TARGETS IN hPSCs:

Below is a list of the sequences of the endogenous loci targeted in hESCs for creating transgenic lines and the sequences of the respective TALEN pairs or CRISPRs. TALENs were used for targeting the CUX2, and AAVS1 loci, while CRISPR-Cas9 system was used for targeting the FEZF2 locus. The design principles used for generating the TALENs and CRISPR constructs are detailed in Chapter 2: Materials and Methods.

In the case of the CUX2 locus, the underlined sequence marks the initiation codon and it lies in the spacer sequence where the FokI endonuclease will cleave and initiate homologous recombination with the donor construct. In the case of AAVS1 (also known as PPP1R12C) locus, the target site of the TALEN pairs lies in the 1st intron. The DNA sequence targeted by right and left TALENs on either side of the spacer is highlighted in caps. The specificity of TALENs for target DNA is determined by the amino acid sequence of their arrayed repeats, specifically their “Repeat Variable Dinucleotides” (RVDs). RVDs comprise two critical amino acids that determine the specificity of a given TALE repeat for the corresponding DNA base in the target sequence. These are provided for each targeted locus.

For the FEZF2 locus, the CRISPR target site includes the FEZF2 initiation codon and is highlighted in yellow; the initiation codon is underlined. The CRISPR-Cas9 target site is on the antisense strand and protospacer adjacent motif for Cas9 (NGG) on the antisense strand has been italicized.

CUX2 targeted sequence (plus strand):

T GCGCGTCTCGATAGCCCCC aagatggccgccaat GTGGGATCGATGTTTCAAT A

Left RVD:

NH HD NH HD NH NG HD NG HD NH NI NG NI NH HD HD HD HD HD

Right RVD:

NG NG NG HD NG NN NG HD NI HD HD NI NI NG HD HD NG

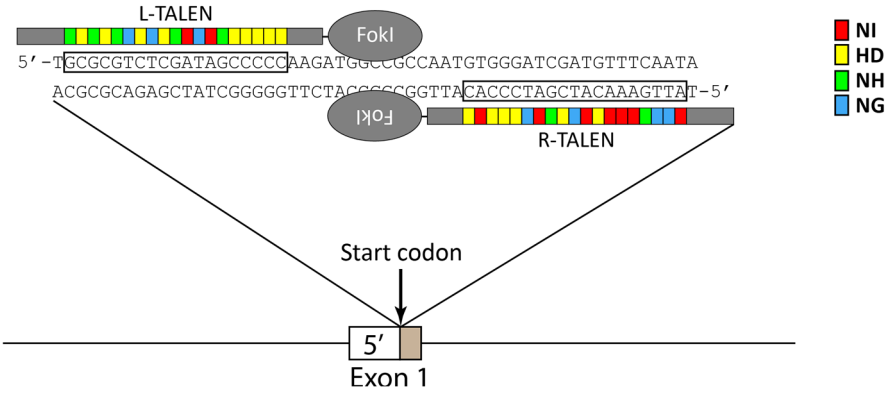

Figure 6.1: Schematic of the CUX2 genomic locus targeted by the TALEN pair (initiation codon) and the RVD arrays for left and right TALENs. RVD key: NI→A, HD→C, NH→G, NG→T.

AAVS1 targeted sequence (plus strand):

T CCCCTCCACCCCACAGT ggggccactagggac AGGATTGGTGACAGAAA A

Left RVD:

HD HD HD HD NG HD HD NI HD HD HD HD NI HD NI NN NG

Right RVD:

NG NG NG HD NG NN NG HD NI HD HD NI NI NG HD HD NG

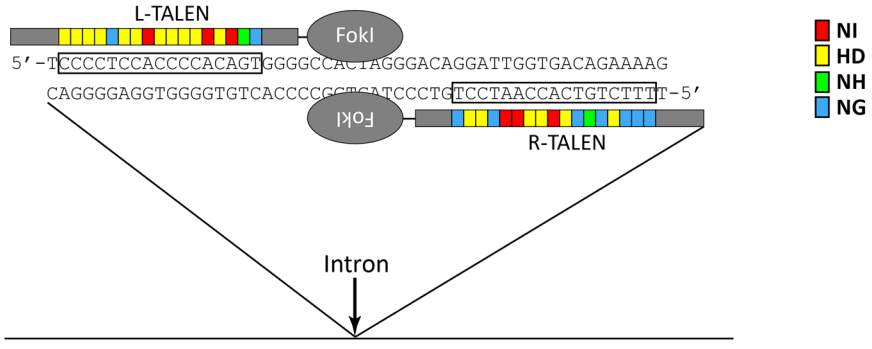

Figure 6.2: Schematic of the AAVS1 (PPP1R12C) genomic locus targeted by the TALEN pair (first intron) and the RVD arrays for left and right TALENs. RVD key: NI→A, HD→C, NH→G, NG→T.

FEZF2 targeted sequence (plus strand):

cggctcagctccgcgcgccatggcaagctcggcttccctg

CRISPR sequence:

GCCGAGCTTGCCATGGCGCG*CGG*

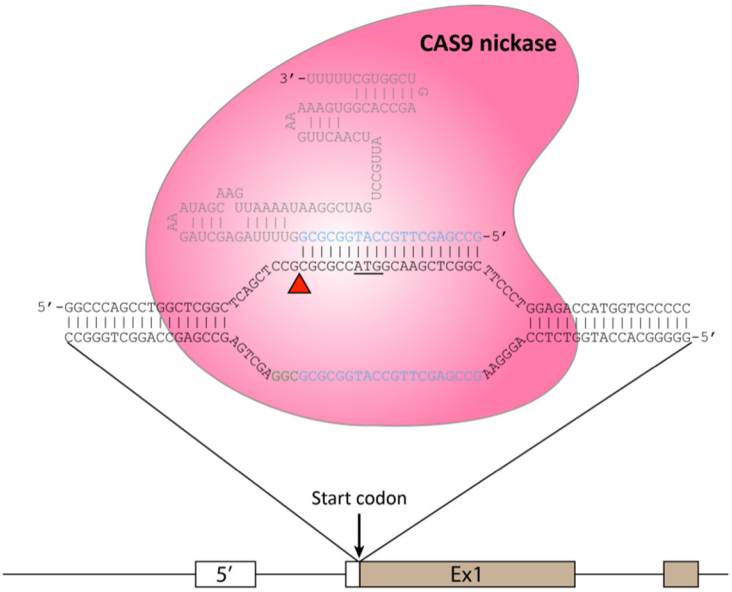

Fig 6.3: Schematic of the FEZF2 genomic locus and CRISPR guide RNA sequence. The tracrRNA sequence following the gRNA sequence is also shown. The CRISPR target site overlaps with the FEZF2 initiation codon. A nickase version of Cas9 – which only nicks a single DNA strand - was utilized to ensure specificity for the target site.

TABLE 6.7: PRIMERS USED FOR RT-PCR AND QUANTITATIVE PCR

Gene name	Forward	Reverse
SOX2	AACCCCAAGATGCACAACTC	GCTTAGCCTCGTCGATGAAC
SOX1	TCTGTTAACTCACCGGGACC	ACTCCAGGGTACACACAGGG
FOXG1	AGAAGAACGGCAAGTACGAGA	TGTTGAGGGACAGATTGTGGC
LHX2	TTACGGCAGGAAAACACGG	TGCCAGGCACAGAAGTTAAG
ZEB2	CCAATCCCAGGAGGAAAAAC	CAATACCGTCATCCTCAGCA
OTX2	GCTGGCTATTTGGAATTTAAAGG	GGGTTTGGAGCAGTGGAAC
SOX17	GGCGCAGCAGAATCCAGA	CCACGACTTGCCCAGCAT
BRA	ATGACAATTGGTCCAGCCTT	CGTTGCTCACAGACCACAG
SIX3	GCAAGAAACGCGAACTGG	GGTCCAATGGCCTGGTG
ZNF521	TGGGATATTCAGGTTCATGTTG	TTGGCAGGAGAGTCAAAGGT
SOX10	AGCTCAGCAAGACGCTGG	CTTTCTTGTGCTGCATACGG
NKX2.1	AGCACACGACTCCGTTCTCA	CCCTCCATGCCCACTTTCTT
EN2	GTGGGTCTACTGTACGCGCT	CTTGTCCTCTTTGTTCGGGT
HOXB4	CTGGATGCGCAAAGTTCAC	CTTCTCCAGCTCCAAGACCT
TBR2	CGCCACCAAACTGAGATGAT	CACATTGTAGTGGGCAGTGG
EMX2	CTCAGCCTCACGGAAACTCA	TTGCGAATCTGAGCCTTCTT
PAX6	TCACCATGGCAAATAACCTG	CAGCATGCAGGAGTATGAGG
BRN2	CCGCAGCGTCTAACCACTAC	GTGGGACAGCGCGGTGATCC
HES5	TCAGCCCCAAAGAGAAAAAC	GCTTCAGCTGCTCGATGCT
NR2F1	CGAGTACAGCTGCCTCAAAG	GGGTACTGGCTCCTCACGTA
FGF8	TACCAACTCTACAGCCGCAC	CTCTGCTTCCAAAGGTGTCC
FOXB1	CCGCCCTACTCGTACATCTC	CCTGTAGTAGGGGAAGCGGT
DMRT3	CTCTGCAGGCGCAGCTC	AGCCCTTACTCTTTGCCACA
ER81	GGCTTGCAGAAGCTCAGGTA	CTTGATTTTCAGTGGCAGGC
ATP5O	ACTCGGGTTTGACCTACAGC	GGTACTGAAGCATCGCACCT

*ATP5O was used as the housekeeping gene in all experiments

TABLE 6.8: PRIMERS USED FOR CLONING

Primer name	Sequence
Citrine (XFP) BamHI F	ATAATT*GGATCC*GCCACCATGGTGAGCAAGGGCGAGGAGC
Citrine (XFP) NotI R	GATATT*GCGGCCGC*TCACTTGTACAGCTCGTCCATGC
PGK-TK KpnI F	ATAATT*GGTACC*AGATTTAAATGCGGAATTCTACC
PGK-TK KpnI R	GATATT*GGTACC*TTCTGATGGAATTAGAACTTGG
H2B BamHI F	ATAATT*GGATCC*GCCACCATGCCAGAGCCAGCGAAGTCTGC
XFP NotI R	GATATT*GCGGCCGC*TCACTTGTACAGCTCGTCCATGC
NeonGreeenV5 BsrGI F	GTACAAGGGTAAGCCTATCCCTAACCCTCTCCTCGGTCTCGATTCTACG TAAGC
NeonGreeenV5 NotI R	GGCCGCTTACGTAGAATCGAGACCGAGGAGAGGGTTAGGGATAGGCT TACCCTT
BbsI Lox5171 Cre F	ATAATT*GAAGACATGATC*ATAACTTCGTATAATGTGTACTATACGAAGT TATACGCCACCATGGCCAATTTACTGACCGTAC
NotI Lox5171 Cre R	GATATT*GCGGCCGC*ATAACTTCGTATAGTACACATTATACGAAGTTATA TCACAGATCTTCTTCAGAAATAAGTTTTTGTTCCACCGGTCCATCGCCAT CTTCCAGCAGGCGCAC
Lox2272 TdTomato BclI F	GCGCCT*TGATCA*TTATTGTGCTGTCTCATCATTTTGG
LoxP Tdtomato NotI R	AATATT*GCGGCCGC*ACCTCTTCGAGGGACATAACTTCG
Dragonbow pBS F	CGACCTGCAGCCCAAGCTTGGATCCGATAAAAGTTTTGTTAC
Dragonbow pBS R	TGAACTACCTGCAGGATGCATCATCAATGTATCTTATCATGTCTG
TagBFP2 XmaI F	ATAATTCCCGGGCCACCATGGTGTCTAAGGGCGAAGAGC
TagBFP2 blunt R	/5PHOS/AGAGTTTAATTAAGCTTGTGCCCCAG
PacI Lox2272 TagBFP2 F	GATACATTAATTAAATAACTTCGTATAGGATACTTTATACGAAGTTATC CGCCACCATGCCAGAGCCAGC
EBFP2 BbvCI R	TCTTGACCTCAGCTTACTTGTACAGCTCGTCCATACCCAG
rtTA-PURO AgeI F	GATATTACCGGTGCCACCATGTCTAGACTGGACAAGAGCAAAGTC
rtTA-PURO EcoRV R	AGTCGAGATATCTCAGGCACCGGGCTTGCGGGTCATGC

TABLE 6.9: PRIMERS USED IN GIBSON ASSEMBLY OF HOMOLOGY DONORS

Primer name	Sequence
pBS F	CCCCGCGGTGGAGCTCCAGC
pBS R	CCGGTACCCAATTCGCCCTATAGTGAGTCG
5' CUX2 F	GCTGGAGCTCCACCGCGGGGACAACAGCAGAAACCTCCGAGG
5' CUX2 R	AATTGGACATCTTGGGGGCTATCGAGACGC
Cre-ERT2 F	AGCCCCCAAGATGTCCAATTTACTGACCGTAC
Cre-ERT2 R	TAGGAACTTCGAGAAGAGGGACAGCTATGAC
PGK-PURO F	CCCTCTTCTCGAAGTTCCTATACTTTCTAGAGAATAGGAACTTCAGTCT GAAGAGGAGTTTACGTCC
PGK-PURO R	CCGCACTAACGAAGTTCCTATTCTCTAGAAAGTATAGGAACTTCGCAGC TTCTGATGGAATTAGAACTTG
3' CUX2 F	TAGGAACTTCGTTAGTGCGGGCAGCGCCGG
3' CUX2 R	TAGGGCGAATTGGGTACCGGAAAGAGCAGGGAAGAGAGGAAAGAAA CAGAAGAAAAGC
5' FEZF2 F	GCTGGAGCTCCACCGCGGGGTGTTCGGGGCTGGCGCCGGTTC
5' FEZF2 R	ATTGGCTCATGGCGCGCGGAGCTGAGCCGA
Vflox-PURO F	TTGGCGTAATTCAATTTCTGAGAACTGTCATTCTCGGAAATTGAAGTCT GAAGAGGAGTTTACGTC
Vflox-PURO R	CAGAAATTGAGCAGCTTCTGATGGAATTAGAAC
3' FEZF2 F	TCAGAAGCTGCTCAATTTCTGAGAACTGTCATTCTCGGAAATTGAGCAA GCTCGGCTTCCCTGGA
3' FEZF2 R	TAGGGCGAATTGGGTACCGGTAGGAAACTGAGGCCCAACGAG

TABLE 6.10: PRIMERS USED FOR GENOTYPING TRANSGENIC LINES

Primer pairs	Sequence
PURO F	TCACCGAGCTGCAAGAACTCTTCC
PURO R	CCAGGAGGCCTTCCATCTGTTG
TK F	GATACCGCACCGTATTGGCAAG
TK R	CTTCCGAGACAATCGCGAACATC
CUX2 5' MA F	TGTCATGTTGCAAAGAACGGAGCC
CUX2 5' MA R	AATGCAGGCAAATTTTGGTGTACGG
CUX2 MA F	CCATGCATCGATGATATCAGATCC
CUX2 MA R	CAGAGAACACCTCCAAATCTAGG
CUX2 NA F	AAGATGGCCGCCAATGTGGGATCG
CUX2 GDNA 1R	ACTAGCGCTTCTCCATGGTCGC
CUX2 GDNA 1F	GATATTGAGTGCAGCCATTGAG
Cre-ERT2 R	TAGGAACTTCGAGAAGAGGGACAGCTATGAC
CreERT2-3 (F)	GCAGGGAGAGGAGTTTGTGTGC
CUX2 GDNA 1R	ACTAGCGCTTCTCCATGGTCGC
FEZF2 5' MA F	GTCCATGCGCCACATCCTAATGAGG
FEZF2 5' MA R	GATATTGCGGCCGCTCACTTGTACAGCTCGTCCATGC
FEZF2 3' MA F	CCATGCATCGATGATATCAGATCC
FEZF2 3' MA R	AGAAACCAGAGCCTTTTTCAG
FEZF2 NA F	CGACTAGGTGCTTATTAAATTGC
FEZF2 NA R	TTTCCAGAGCTCCGAGTAACTG
AAVS1 5' MA F	CACTTTGAGCTCTACTGGCTTCTGC
AAVS1 5' MA R	CAAGAATGCATGCGTCAATTTTACG
AAVS1 3' MA F	CAGACCGATAAAACACATGCGTC
AAVS1 3' MA R	GAGTGAGTTTGCCAAGCAGTCACC

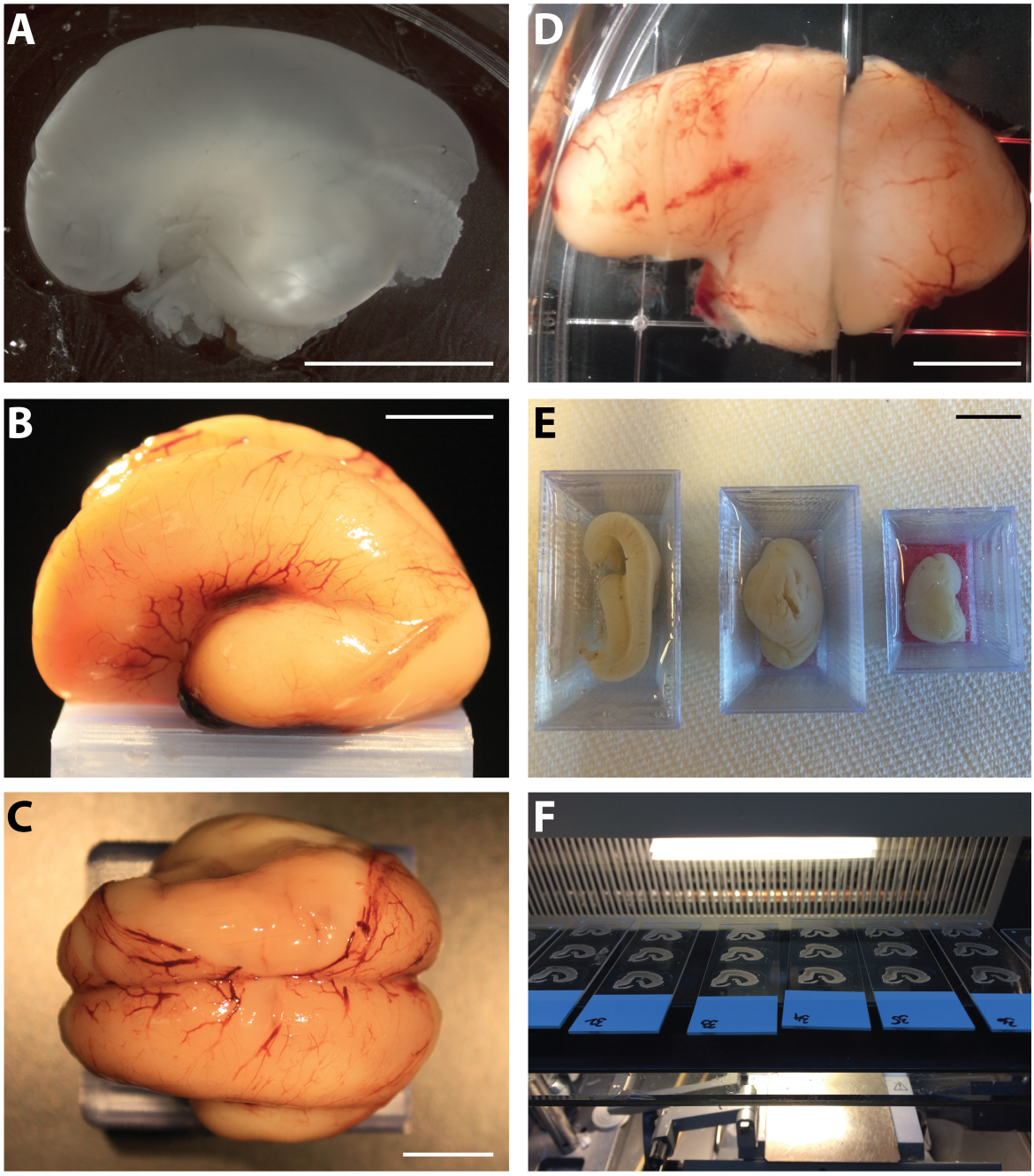

Figure 6.4: Human fetal brain gross anatomy. A) PCW10 brain, sagittal view. B) PCW15 brain, sagittal view. C) PCW15 brain, transverse view. D) PCW15 brain dissected into three parts for mounting and cryosectioning. Sagittal view is shown. E) Embedding the dissected brain areas in D) using custom 3D printed molds. F) Sectioned brain slices on slides. Scale bars: 1cm.

SUPPLEMENTARY FIGURE(S)

Figure 6.5: The mouse cortex displays distinct segregation of projection neuron classes while the human cortex does not at comparable stages of development. A) Mouse brain section from mid-corticogenesis (E15.5), a stage when CPNs are actively generated. The panel shows that CPNs (marked by SATB2), SCPNs (marked by CTIP2) and CThPN/subplate neurons (marked by NURR1) are largely found in distinct layers at this stage and the markers rarely overlap. Arrowheads indicate examples of cells co-expressing CTIP2 and SATB2 while arrows point to cells co-expressing SATB2, CTIP2 and NURR1. B) Low magnification view of human PCW15 frontal brain sections showing uniform staining across various cortical areas. The three panels emphasize that extensive co-expression of CPN determinants in the deep layers with SCPN and CThPN determinants is also seen when using different TxFs to identify projection neuron classes, i.e. the phenomenon of progressive neuronal restriction is not specific to an antibody or marker. C) Higher magnification view of the areas highlighted in B) demonstrating expression of various CPN TxFs (SATB2, MEF2C) in the deep cortical plate (CP). SCPN determinants (CTIP2, ER81) and CThPN genes (TBR1, TLE4, NURR1) are also co-expressed deep cortical plate. Scale bars: A) 100µm, B) 1cm, and C) 100µm.

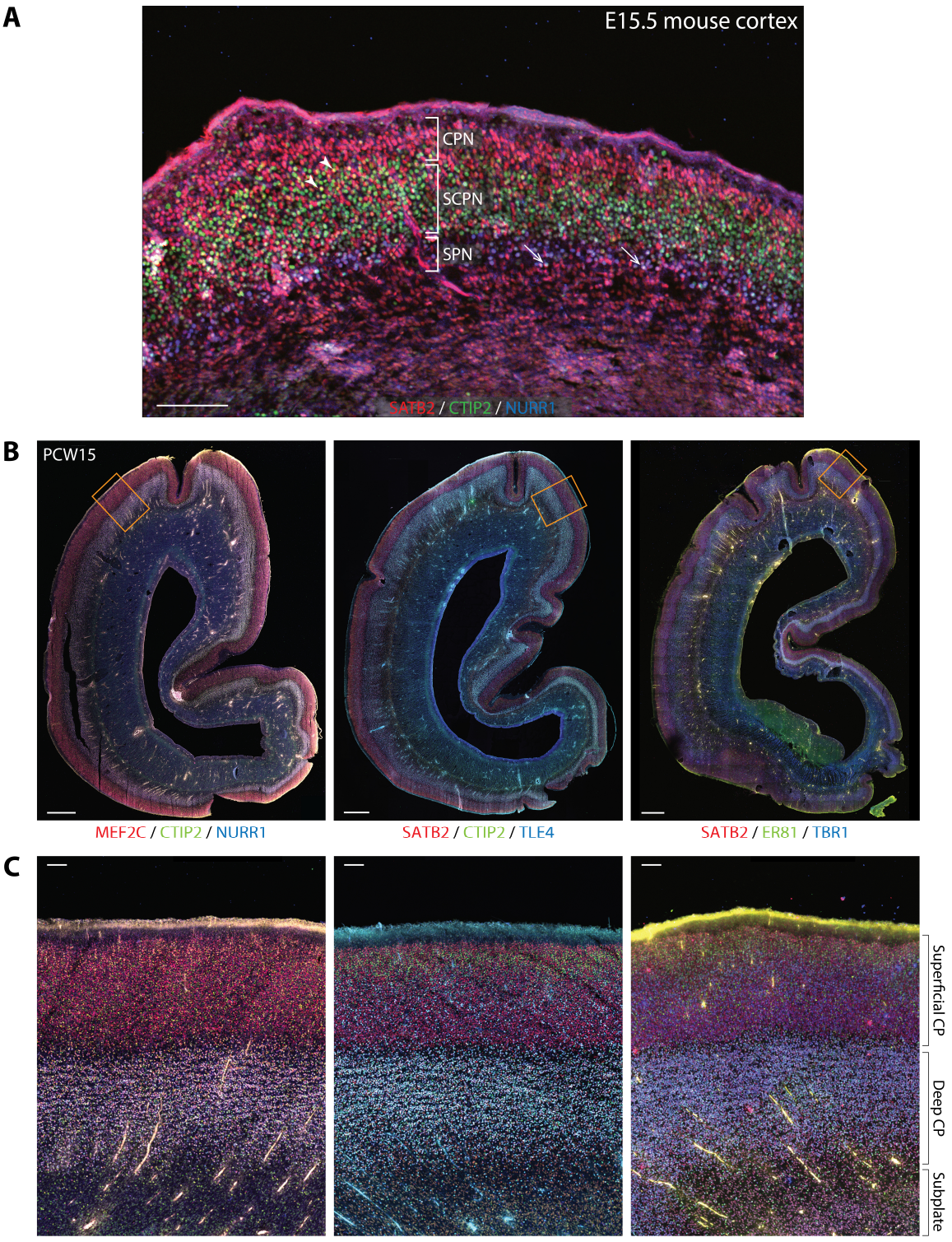
A
E15.5 mouse cortex
CPN
SCPN
SPN
SATB2 / CTIP2 / NURR1
B
PCW15
MEF2C / CTIP2 / NURR1
SATB2 / CTIP2 / TLE4
SATB2 / ER81 / TBR1
C
Superficial CP
Deep CP
Subplate

TABLE 6.11: LIST OF GENES CHANGING BY MORE THAN 2-FOLD IN FIGURE 3.3A-B IN THE ORDER DISPLAYED ON THE HEATMAP

A) Pluripotency	HMGCS1	OVOL2	MDK	LPAR1
NANOG	VCAN	COBL	TTC3	LMX1A
PIM2	SLC7A5	CDH1	HES5	IL1RAPL1
POU5F1	ADM	CDK6	RAX	RGMA
STC1	SOX3	ZIC3	NBL1	SOX11
SEMA6A	LPPR4	FGF2	LGALS1	CACNB3
DNAJB6	PAK1	NPTX1	BTG2	CDH2
FABP5	VLDLR	RCAN2	GPR56	CNTNAP2
NOLC1	RORB	BCL11B	POU3F2	SFRP1
ATP5H	SOD2	ADCY1	NR2F2	PCDH18
CD24	TUBB3	PLA2G10	RTN1	EFNB2
GULP1	NME1	BCAN	CAP2	COL1A1
HMGB3	JARID2	NEFM	ITGA5	UNC5A
GFPT2	MYLIP	SH3GL2	BBS2	HMX2
NASP	CNTN1	CBS	ACVR1B	FZD7
DNMT3B	SH3GL3	NFIB	CDKN1C	KNDC1
BCOR	PRNP	UGT8	SEMA6B	WNT4
PODXL	LAMC3	DCLK1	JAG1	WNT5A
UGP2	GPM6B	ATF5	AHNAK	SOX9
HEY2	CD9	CEBPB	SEMA5B	FGFR3
UBE2C	BCL11A	SPOCK1	COL4A5	CITED2
ASMTL	TNIK	TAGLN3	HES1	ZEB2
FZD5	ACSL3	COL2A1	LEF1	NTF3
OTX2	SHC1	FABP7	RGMB	HES4
	BEX1	OTX1	NRCAM	DLL1
	ID3	LHX2	FGF8	GAS1
	TIMP4	FOXA1	IRX5	FZD2
	COL5A2	PCDHB2	BMP7	FEZF1
B) Neural	PFN1	COL5A1	FZD8	NNAT
GAL	TUBB2A	FZD3	LHX5	MAP2
PCSK9	DYNLL2	CACNA1H	FZD5	CNTFR
THY1	DNMT3B	LRP2	ACCN1	PAX6
DNER	CD24	EFNB1	CNTN2	ENC1
CLDN11	SATB2	GLI3	LGI1	HESX1
FGF13	SEMA6A	SIX3	FEZ1	FRZB
NLGN4X	SLC1A3	MEG3	BMP2	EPHA4
LRP8	PDPN	EFHD1	ID2	OTX2
MBP	SMARCA2	CNTNAP1	POU3F1	CYP26A1

TABLE 6.12: LIST OF FOREBRAIN-ASSOCIATED GENES CHANGING BY MORE THAN 2-FOLD IN FIGURE 3.7E IN THE ORDER DISPLAYED ON THE HEATMAP

Forebrain associated genes
OTX2
ZEB2
LMX1A
POU3F1
NR2F2
POU3F2
PAX6
RAX
HES5
LHX2
OTX1
GLI3
SIX3
LHX5
FGF8
HES1
LEF1
CNTN2
HESX1
BCL11B
NFIB
SOX3

TABLE 6.13: LIST OF MAPK-PATHWAY GENES CHANGING BY MORE THAN 1.5-FOLD IN FIGURE 3.9A IN THE ORDER DISPLAYED ON THE HEATMAP

MAPKpathway	DUSP14	FGFR4	PRKCA	CACNA1H
DUSP5	DUSP1	ELK1	HSPA8	RASA1
PLA2G3	RRAS2	DAXX	RPS6KA2	CACNA1E
MAPK13	CACNG6	MAP2K1	ATF4	MAP4K4
GADD45G	MAP4K3	HSPA2	DDIT3	CACNA2D2
ARRB1	PRKX	RPS6KA1	JUND	FGF8
CASP3	CHUK	FGF13	JUN	FLNC
MYC	MAP2K3	PAK1	CRK	DUSP4
RAC3	MAPK9	PLA2G10	RRAS	GADD45A
TGFBR2	FGF19	NFKB1	PDGFRB	CACNB3
STMN1	RASGRP2	FLNB	EGFR	MAPK10
FOS	PPM1B	GNA12	FGF9	FGFR3
DUSP6	SRF	FGF2	HSPA1A	NTF3

CHAPTER 7: EPILOGUE

What kind of cortical neurons
Do human neural progenitors make?
That was the question,
I naïvely wanted to undertake.
Only later would I realize how often,
My decision would keep me awake!

You see, human pluripotent cells,
Take a long time to differentiate.
After all it is embryogenesis,
They are trying to recapitulate.
At least I had plenty of time to plan,
In the 15 weeks neurons took to generate!

"Please work the first time!"
That was my weekly prayer.
If all went well, the cultures would yield
Cortical neurons, layer by layer.
Right next to radial glia that serve as,
The source of neurons and the cellular conveyor.

So here is what I learned,
In order to reach radial glial fate:
Just inhibit Nodal and BMP signaling;
Neural tube organization the cells will recreate.
And if superficial layers are what you need,
Plan wisely, you might have to wait!

What are the mechanisms that underlie,
Formation of a layer-specific neuron?
I created transgenic lines to observe the changes,
Progenitors and their daughters had undergone.
Using a spectrum of fluorescent reporters,
Integrated randomly or knocked into an exon.

Via lineage-tracing I was able to see,
Clones expressing hues of red, green and blue.
And single progenitors giving rise to pyramidal cells,
Expressing markers from NURR1 to SATB2!
I also found clones containing neurons and glia,
Together these findings support an old model anew.

Does development *in vivo* follow predictions,
Made *in vitro* from a transgenic clone?
In the first trimester brain I searched,
From the cortical plate to the ventricular zone.
I found strong evidence for neuronal restriction,
Which till now had been unknown.

How these results make the human brain unique,
That is a problem I am still trying to navigate.
A few years and several failed experiments,
The answer will require to elucidate!
Within corticogenesis lay the key explanation,
That is the view towards which I gravitate.

Perhaps it is time to sign off now,
For a week or two at any rate.
I most look forward to not saying,
Each time I am on a lovely date:
"Can we please make this short?
I need to go check my culture plate!"

Support, resources, and great people,
Rockefeller provided all in profusion.
My gratitude to all involved,
They made it easier, the wee hours in seclusion.
With enough fond memories to last me a while,
What better way to reach my conclusion!

~The Rhyme of My Graduate Life, Zeeshan Ozair

CHAPTER 8: BIBLIOGRAPHY

Abe, T., Sakaue-Sawano, A., Kiyonari, H., Shioi, G., Inoue, K., Horiuchi, T., Nakao, K., Miyawaki, A., Aizawa, S., and Fujimori, T. (2013). Visualization of cell cycle in mouse embryos with Fucci2 reporter directed by Rosa26 promoter. Development *140*, 237-246.

Alcamo, E.A., Chirivella, L., Dautzenberg, M., Dobreva, G., Farinas, I., Grosschedl, R., and McConnell, S.K. (2008). Satb2 regulates callosal projection neuron identity in the developing cerebral cortex. Neuron *57*, 364-377.

Angevine, J.B., Jr., and Sidman, R.L. (1961). Autoradiographic study of cell migration during histogenesis of cerebral cortex in the mouse. Nature *192*, 766-768.

Anthony, T.E., Klein, C., Fishell, G., and Heintz, N. (2004). Radial glia serve as neuronal progenitors in all regions of the central nervous system. Neuron *41*, 881-890.

Arcila, M.L., Betizeau, M., Cambronne, X.A., Guzman, E., Doerflinger, N., Bouhallier, F., Zhou, H., Wu, B., Rani, N., Bassett, D.S.*, et al.* (2014). Novel primate miRNAs coevolved with ancient target genes in germinal zone-specific expression patterns. Neuron *81*, 1255-1262.

Arion, D., Unger, T., Lewis, D.A., and Mirnics, K. (2007). Molecular markers distinguishing supragranular and infragranular layers in the human prefrontal cortex. Eur J Neurosci *25*, 1843-1854.

Arnold, S.J., Huang, G.J., Cheung, A.F., Era, T., Nishikawa, S., Bikoff, E.K., Molnar, Z., Robertson, E.J., and Groszer, M. (2008). The T-box transcription factor Eomes/Tbr2 regulates neurogenesis in the cortical subventricular zone. Genes Dev *22*, 2479-2484.

Aubert, J., Dunstan, H., Chambers, I., and Smith, A. (2002). Functional gene screening in embryonic stem cells implicates Wnt antagonism in neural differentiation. Nature biotechnology *20*, 1240-1245.

Azim, E., Shnider, S.J., Cederquist, G.Y., Sohur, U.S., and Macklis, J.D. (2009). Lmo4 and Clim1 progressively delineate cortical projection neuron subtypes during development. Cereb Cortex *19 Suppl 1*, i62-69.

Baala, L., Briault, S., Etchevers, H.C., Laumonnier, F., Natiq, A., Amiel, J., Boddaert, N., Picard, C., Sbiti, A., Asermouh, A.*, et al.* (2007). Homozygous silencing of T-box

transcription factor EOMES leads to microcephaly with polymicrogyria and corpus callosum agenesis. Nat Genet *39*, 454-456.

Bachiller, D., Klingensmith, J., Kemp, C., Belo, J.A., Anderson, R.M., May, S.R., McMahon, J.A., McMahon, A.P., Harland, R.M., Rossant, J.*, et al.* (2000). The organizer factors Chordin and Noggin are required for mouse forebrain development. Nature *403*, 658-661.

Bae, B.I., Jayaraman, D., and Walsh, C.A. (2015). Genetic Changes Shaping the Human Brain. Dev Cell *32*, 423-434.

Bae, B.I., Tietjen, I., Atabay, K.D., Evrony, G.D., Johnson, M.B., Asare, E., Wang, P.P., Murayama, A.Y., Im, K., Lisgo, S.N.*, et al.* (2014). Evolutionarily dynamic alternative splicing of GPR56 regulates regional cerebral cortical patterning. Science *343*, 764-768.

Baranek, C., Dittrich, M., Parthasarathy, S., Bonnon, C.G., Britanova, O., Lanshakov, D., Boukhtouche, F., Sommer, J.E., Colmenares, C., Tarabykin, V.*, et al.* (2012). Protooncogene Ski cooperates with the chromatin-remodeling factor Satb2 in specifying callosal neurons. Proceedings of the National Academy of Sciences of the United States of America *109*, 3546-3551.

Barnabe-Heider, F., Wasylnka, J.A., Fernandes, K.J., Porsche, C., Sendtner, M., Kaplan, D.R., and Miller, F.D. (2005). Evidence that embryonic neurons regulate the onset of cortical gliogenesis via cardiotrophin-1. Neuron *48*, 253-265.

Bayatti, N., Sarma, S., Shaw, C., Eyre, J.A., Vouyiouklis, D.A., Lindsay, S., and Clowry, G.J. (2008). Progressive loss of PAX6, TBR2, NEUROD and TBR1 mRNA gradients correlates with translocation of EMX2 to the cortical plate during human cortical development. Eur J Neurosci *28*, 1449-1456.

Beddington, R.S. (1994). Induction of a second neural axis by the mouse node. Development *120*, 613-620.

Bedogni, F., Hodge, R.D., Elsen, G.E., Nelson, B.R., Daza, R.A., Beyer, R.P., Bammler, T.K., Rubenstein, J.L., and Hevner, R.F. (2010). Tbr1 regulates regional and laminar identity of postmitotic neurons in developing neocortex. Proceedings of the National Academy of Sciences of the United States of America *107*, 13129-13134.

Belo, J.A., Bachiller, D., Agius, E., Kemp, C., Borges, A.C., Marques, S., Piccolo, S., and De Robertis, E.M. (2000). Cerberus-like is a secreted BMP and nodal antagonist not essential for mouse development. Genesis *26*, 265-270.

Bendall, S.C., Stewart, M.H., Menendez, P., George, D., Vijayaragavan, K., Werbowetski-Ogilvie, T., Ramos-Mejia, V., Rouleau, A., Yang, J., Bosse, M.*, et al.* (2007). IGF and FGF cooperatively establish the regulatory stem cell niche of pluripotent human cells in vitro. Nature *448*, 1015-1021.

Bernard, A., Lubbers, L.S., Tanis, K.Q., Luo, R., Podtelezhnikov, A.A., Finney, E.M., McWhorter, M.M., Serikawa, K., Lemon, T., Morgan, R.*, et al.* (2012). Transcriptional architecture of the primate neocortex. Neuron *73*, 1083-1099.

Betizeau, M., Cortay, V., Patti, D., Pfister, S., Gautier, E., Bellemin-Menard, A., Afanassieff, M., Huissoud, C., Douglas, R.J., Kennedy, H.*, et al.* (2013). Precursor diversity and complexity of lineage relationships in the outer subventricular zone of the primate. Neuron *80*, 442-457.

Biehs, B., Francois, V., and Bier, E. (1996). The Drosophila short gastrulation gene prevents Dpp from autoactivating and suppressing neurogenesis in the neuroectoderm. Genes Dev *10*, 2922-2934.

Blauwkamp, T.A., Nigam, S., Ardehali, R., Weissman, I.L., and Nusse, R. (2012). Endogenous Wnt signalling in human embryonic stem cells generates an equilibrium of distinct lineage-specified progenitors. Nature communications *3*, 1070.

Borrell, V., and Gotz, M. (2014). Role of radial glial cells in cerebral cortex folding. Curr Opin Neurobiol *27*, 39-46.

Bouche, E., Romero-Ortega, M.I., Henkemeyer, M., Catchpole, T., Leemhuis, J., Frotscher, M., May, P., Herz, J., and Bock, H.H. (2013). Reelin induces EphB activation. Cell Res *23*, 473-490.

Bouwmeester, T., Kim, S., Sasai, Y., Lu, B., and De Robertis, E.M. (1996). Cerberus is a head-inducing secreted factor expressed in the anterior endoderm of Spemann's organizer. Nature *382*, 595-601.

Boyd, J.L., Skove, S.L., Rouanet, J.P., Pilaz, L.J., Bepler, T., Gordan, R., Wray, G.A., and Silver, D.L. (2015). Human-Chimpanzee Differences in a FZD8 Enhancer Alter Cell-Cycle Dynamics in the Developing Neocortex. Current biology : CB.

Boyer, L.A., Lee, T.I., Cole, M.F., Johnstone, S.E., Levine, S.S., Zucker, J.P., Guenther, M.G., Kumar, R.M., Murray, H.L., Jenner, R.G.*, et al.* (2005). Core transcriptional regulatory circuitry in human embryonic stem cells. Cell *122*, 947-956.

Boyle, M.P., Bernard, A., Thompson, C.L., Ng, L., Boe, A., Mortrud, M., Hawrylycz, M.J., Jones, A.R., Hevner, R.F., and Lein, E.S. (2011). Cell-type-specific consequences of Reelin deficiency in the mouse neocortex, hippocampus, and amygdala. J Comp Neurol *519*, 2061-2089.

Bradley, A., Evans, M., Kaufman, M.H., and Robertson, E. (1984). Formation of germ-line chimaeras from embryo-derived teratocarcinoma cell lines. Nature *309*, 255-256.

Braun, M.M., Etheridge, A., Bernard, A., Robertson, C.P., and Roelink, H. (2003). Wnt signaling is required at distinct stages of development for the induction of the posterior forebrain. Development *130*, 5579-5587.

Brennan, J., Lu, C.C., Norris, D.P., Rodriguez, T.A., Beddington, R.S., and Robertson, E.J. (2001). Nodal signalling in the epiblast patterns the early mouse embryo. Nature *411*, 965-969.

Britanova, O., Alifragis, P., Junek, S., Jones, K., Gruss, P., and Tarabykin, V. (2006). A novel mode of tangential migration of cortical projection neurons. Dev Biol *298*, 299-311.

Britanova, O., de Juan Romero, C., Cheung, A., Kwan, K.Y., Schwark, M., Gyorgy, A., Vogel, T., Akopov, S., Mitkovski, M., Agoston, D.*, et al.* (2008). Satb2 is a postmitotic determinant for upper-layer neuron specification in the neocortex. Neuron *57*, 378-392.

Brons, I.G., Smithers, L.E., Trotter, M.W., Rugg-Gunn, P., Sun, B., Chuva de Sousa Lopes, S.M., Howlett, S.K., Clarkson, A., Ahrlund-Richter, L., Pedersen, R.A.*, et al.* (2007). Derivation of pluripotent epiblast stem cells from mammalian embryos. Nature *448*, 191-195.

Campos, L.S., Duarte, A.J., Branco, T., and Henrique, D. (2001). mDll1 and mDll3 expression in the developing mouse brain: role in the establishment of the early cortex. J Neurosci Res *64*, 590-598.

Camus, A., Perea-Gomez, A., Moreau, A., and Collignon, J. (2006). Absence of Nodal signaling promotes precocious neural differentiation in the mouse embryo. Dev Biol *295*, 743-755.

Capra, J.A., Erwin, G.D., McKinsey, G., Rubenstein, J.L., and Pollard, K.S. (2013). Many human accelerated regions are developmental enhancers. Philos Trans R Soc Lond B Biol Sci *368*, 20130025.

Casellas, R., and Brivanlou, A.H. (1998). Xenopus Smad7 inhibits both the activin and BMP pathways and acts as a neural inducer. Dev Biol *198*, 1-12.

Céline, Z., Marie-Catherine, T., Rolf, B., and Harold, C. (2004). Dynamics of Cux2 Expression Suggests that an Early Pool of SVZ Precursors is Fated to Become Upper Cortical Layer Neurons. Cerebral Cortex.

Chambers, S.M., Fasano, C.A., Papapetrou, E.P., Tomishima, M., Sadelain, M., and Studer, L. (2009). Highly efficient neural conversion of human ES and iPS cells by dual inhibition of SMAD signaling. Nature biotechnology *27*, 275-280.

Chan, Y.S., Goke, J., Ng, J.H., Lu, X., Gonzales, K.A., Tan, C.P., Tng, W.Q., Hong, Z.Z., Lim, Y.S., and Ng, H.H. (2013). Induction of a human pluripotent state with distinct regulatory circuitry that resembles preimplantation epiblast. Cell stem cell *13*, 663-675.

Chang, C., and Harland, R.M. (2007). Neural induction requires continued suppression of both Smad1 and Smad2 signals during gastrulation. Development *134*, 3861-3872.

Chatzi, C., Brade, T., and Duester, G. (2011). Retinoic acid functions as a key GABAergic differentiation signal in the basal ganglia. PLoS Biol *9*, e1000609.

Chen, B., Wang, S.S., Hattox, A.M., Rayburn, H., Nelson, S.B., and McConnell, S.K. (2008). The Fezf2-Ctip2 genetic pathway regulates the fate choice of subcortical projection neurons in the developing cerebral cortex. Proceedings of the National Academy of Sciences of the United States of America *105*, 11382-11387.

Chen, G., Gulbranson, D.R., Yu, P., Hou, Z., and Thomson, J.A. (2011). Thermal Stability of FGF Protein is a Determinant Factor in Regulating Self-Renewal, Differentiation and Reprogramming in Human Pluripotent Stem Cells. Stem Cells.

Chen, G., Gulbranson, D.R., Yu, P., Hou, Z., and Thomson, J.A. (2012). Thermal stability of fibroblast growth factor protein is a determinant factor in regulating self-renewal, differentiation, and reprogramming in human pluripotent stem cells. Stem Cells *30*, 623-630.

Cheng, A.M., Thisse, B., Thisse, C., and Wright, C.V. (2000). The lefty-related factor Xatv acts as a feedback inhibitor of nodal signaling in mesoderm induction and L-R axis development in xenopus. Development *127*, 1049-1061.

Cheung, A.F., Kondo, S., Abdel-Mannan, O., Chodroff, R.A., Sirey, T.M., Bluy, L.E., Webber, N., DeProto, J., Karlen, S.J., Krubitzer, L.*, et al.* (2010). The subventricular zone is the

developmental milestone of a 6-layered neocortex: comparisons in metatherian and eutherian mammals. Cereb Cortex *20*, 1071-1081.

Chizhikov, V.V., and Millen, K.J. (2004). Mechanisms of roof plate formation in the vertebrate CNS. Nat Rev Neurosci *5*, 808-812.

Chng, Z., Teo, A., Pedersen, R.A., and Vallier, L. (2010). SIP1 mediates cell-fate decisions between neuroectoderm and mesendoderm in human pluripotent stem cells. Cell stem cell *6*, 59-70.

Chou, S.J., Babot, Z., Leingartner, A., Studer, M., Nakagawa, Y., and O'Leary, D.D. (2013). Geniculocortical input drives genetic distinctions between primary and higher-order visual areas. Science *340*, 1239-1242.

Chou, S.J., Perez-Garcia, C.G., Kroll, T.T., and O'Leary, D.D. (2009). Lhx2 specifies regional fate in Emx1 lineage of telencephalic progenitors generating cerebral cortex. Nature neuroscience *12*, 1381-1389.

Christopher, A.F., Stuart, M.C., Gabsang, L., Mark, J.T., and Lorenz, S. (2010). Efficient derivation of functional floor plate tissue from human embryonic stem cells. Cell stem cell *6*, 336-347.

Cong, L., Ran, F.A., Cox, D., Lin, S., Barretto, R., Habib, N., Hsu, P.D., Wu, X., Jiang, W., Marraffini, L.A*., et al.* (2013). Multiplex genome engineering using CRISPR/Cas systems. Science *339*, 819-823.

Coraux, C., Hilmi, C., Rouleau, M., Spadafora, A., Hinnrasky, J., Ortonne, J.P., Dani, C., and Aberdam, D. (2003). Reconstituted skin from murine embryonic stem cells. Current biology : CB *13*, 849-853.

Costa, M.R., and Muller, U. (2014). Specification of excitatory neurons in the developing cerebral cortex: progenitor diversity and environmental influences. Front Cell Neurosci *8*, 449.

Dal-Pra, S., Furthauer, M., Van-Celst, J., Thisse, B., and Thisse, C. (2006). Noggin1 and Follistatin-like2 function redundantly to Chordin to antagonize BMP activity. Dev Biol *298*, 514-526.

Davis, S., Miura, S., Hill, C., Mishina, Y., and Klingensmith, J. (2004). BMP receptor IA is required in the mammalian embryo for endodermal morphogenesis and ectodermal patterning. Dev Biol *270*, 47-63.

Defelipe, J. (2011). The evolution of the brain, the human nature of cortical circuits, and intellectual creativity. Front Neuroanat *5*, 29.

Dehay, C., and Kennedy, H. (2007). Cell-cycle control and cortical development. Nat Rev Neurosci *8*, 438-450.

Dehay, C., Kennedy, H., and Kosik, K.S. (2015). The Outer Subventricular Zone and Primate-Specific Cortical Complexification. Neuron *85*, 683-694.

Denise, S., Michaela, W.-B., Fong Kuan, W., Heike, H., and Wieland, B.H. (2014). Integrin αvβ3 and thyroid hormones promote expansion of progenitors in embryonic neocortex. Development (Cambridge, England) *141*, 795-806.

Di-Gregorio, A., Sancho, M., Stuckey, D.W., Crompton, L.A., Godwin, J., Mishina, Y., and Rodriguez, T.A. (2007). BMP signalling inhibits premature neural differentiation in the mouse embryo. Development *134*, 3359-3369.

Dincer, Z., Piao, J., Niu, L., Ganat, Y., Kriks, S., Zimmer, B., Shi, S.H., Tabar, V., and Studer, L. (2013). Specification of functional cranial placode derivatives from human pluripotent stem cells. Cell Rep *5*, 1387-1402.

Ding, J., Yang, L., Yan, Y.T., Chen, A., Desai, N., Wynshaw-Boris, A., and Shen, M.M. (1998). Cripto is required for correct orientation of the anterior-posterior axis in the mouse embryo. Nature *395*, 702-707.

Dino, P.L., Whitney, E.H., Emily, A.F., Gergana, D., John, R.H., Rudolf, G., and Susan, K.M. (2014). Satb2 Regulates the Differentiation of Both Callosal and Subcerebral Projection Neurons in the Developing Cerebral Cortex. Cerebral Cortex.

Dixon, J.E., Allegrucci, C., Redwood, C., Kump, K., Bian, Y., Chatfield, J., Chen, Y.H., Sottile, V., Voss, S.R., Alberio, R*., et al.* (2010). Axolotl Nanog activity in mouse embryonic stem cells demonstrates that ground state pluripotency is conserved from urodele amphibians to mammals. Development *137*, 2973-2980.

Eiraku, M., Takata, N., Ishibashi, H., Kawada, M., Sakakura, E., Okuda, S., Sekiguchi, K., Adachi, T., and Sasai, Y. (2011). Self-organizing optic-cup morphogenesis in three-dimensional culture. Nature *472*, 51-56.

Eiraku, M., Watanabe, K., Matsuo-Takasaki, M., Kawada, M., Yonemura, S., Matsumura, M., Wataya, T., Nishiyama, A., Muguruma, K., and Sasai, Y. (2008). Self-organized

formation of polarized cortical tissues from ESCs and its active manipulation by extrinsic signals. Cell stem cell *3*, 519-532.

Eldar, A., Dorfman, R., Weiss, D., Ashe, H., Shilo, B.Z., and Barkai, N. (2002). Robustness of the BMP morphogen gradient in Drosophila embryonic patterning. Nature *419*, 304-308.

Elena, T., Magdalena, G., and Wieland, B.H. (2013). The Cell Biology of Neurogenesis: Toward an Understanding of the Development and Evolution of the Neocortex. Annual Review of Cell and Developmental Biology.

Elsen, G.E., Hodge, R.D., Bedogni, F., Daza, R.A., Nelson, B.R., Shiba, N., Reiner, S.L., and Hevner, R.F. (2013). The protomap is propagated to cortical plate neurons through an Eomes-dependent intermediate map. Proceedings of the National Academy of Sciences of the United States of America *110*, 4081-4086.

Engberg, N., Kahn, M., Petersen, D.R., Hansson, M., and Serup, P. (2010). Retinoic acid synthesis promotes development of neural progenitors from mouse embryonic stem cells by suppressing endogenous, Wnt-dependent nodal signaling. Stem Cells *28*, 1498-1509.

Espuny-Camacho, I., Michelsen, K.A., Gall, D., Linaro, D., Hasche, A., Bonnefont, J., Bali, C., Orduz, D., Bilheu, A., Herpoel, A.*, et al.* (2013). Pyramidal neurons derived from human pluripotent stem cells integrate efficiently into mouse brain circuits in vivo. Neuron *77*, 440-456.

Evans, M.J., and Kaufman, M.H. (1981). Establishment in culture of pluripotential cells from mouse embryos. Nature *292*, 154-156.

Fainsod, A., Steinbeisser, H., and De Robertis, E.M. (1994). On the function of BMP-4 in patterning the marginal zone of the Xenopus embryo. EMBO J *13*, 5015-5025.

Fang, R., Liu, K., Zhao, Y., Li, H., Zhu, D., Du, Y., Xiang, C., Li, X., Liu, H., Miao, Z.*, et al.* (2014). Generation of naive induced pluripotent stem cells from rhesus monkey fibroblasts. Cell stem cell *15*, 488-496.

Fasano, C.A., Chambers, S.M., Lee, G., Tomishima, M.J., and Studer, L. (2010). Efficient derivation of functional floor plate tissue from human embryonic stem cells. Cell stem cell *6*, 336-347.

Fenno, L.E., Mattis, J., Ramakrishnan, C., Hyun, M., Lee, S.Y., He, M., Tucciarone, J., Selimbeyoglu, A., Berndt, A., Grosenick, L.*, et al.* (2014). Targeting cells with single vectors using multiple-feature Boolean logic. Nat Methods *11*, 763-772.

Fernandes, M., Gutin, G., Alcorn, H., McConnell, S.K., and Hebert, J.M. (2007). Mutations in the BMP pathway in mice support the existence of two molecular classes of holoprosencephaly. Development *134*, 3789-3794.

Fertuzinhos, S., Krsnik, Z., Kawasawa, Y.I., Rasin, M.R., Kwan, K.Y., Chen, J.G., Judas, M., Hayashi, M., and Sestan, N. (2009). Selective depletion of molecularly defined cortical interneurons in human holoprosencephaly with severe striatal hypoplasia. Cereb Cortex *19*, 2196-2207.

Fietz, S.A., Kelava, I., Vogt, J., Wilsch-Brauninger, M., Stenzel, D., Fish, J.L., Corbeil, D., Riehn, A., Distler, W., Nitsch, R.*, et al.* (2010). OSVZ progenitors of human and ferret neocortex are epithelial-like and expand by integrin signaling. Nature neuroscience *13*, 690-699.

Finley, M.F., Devata, S., and Huettner, J.E. (1999). BMP-4 inhibits neural differentiation of murine embryonic stem cells. J Neurobiol *40*, 271-287.

Florio, M., Albert, M., Taverna, E., Namba, T., Brandl, H., Lewitus, E., Haffner, C., Sykes, A., Wong, F.K., Peters, J.*, et al.* (2015). Human-specific gene ARHGAP11B promotes basal progenitor amplification and neocortex expansion. Science.

Franco, S.J., Gil-Sanz, C., Martinez-Garay, I., Espinosa, A., Harkins-Perry, S.R., Ramos, C., and Muller, U. (2012). Fate-restricted neural progenitors in the mammalian cerebral cortex. Science *337*, 746-749.

Franco, S.J., and Muller, U. (2013). Shaping our minds: stem and progenitor cell diversity in the mammalian neocortex. Neuron *77*, 19-34.

Franco, S.J., and Müller, U. (2013). Shaping our minds: stem and progenitor cell diversity in the mammalian neocortex. Neuron *77*, 19-34.

Frantz, G.D., and McConnell, S.K. (1996). Restriction of late cerebral cortical progenitors to an upper-layer fate. Neuron *17*, 55-61.

Fuccillo, M., Joyner, A.L., and Fishell, G. (2006). Morphogen to mitogen: the multiple roles of hedgehog signalling in vertebrate neural development. Nat Rev Neurosci *7*, 772-783.

Fukuchi-Shimogori, T., and Grove, E.A. (2001). Neocortex patterning by the secreted signaling molecule FGF8. Science *294*, 1071-1074.

Gafni, O., Weinberger, L., Mansour, A.A., Manor, Y.S., Chomsky, E., Ben-Yosef, D., Kalma, Y., Viukov, S., Maza, I., Zviran, A.*, et al.* (2013). Derivation of novel human ground state naive pluripotent stem cells. Nature *504*, 282-286.

Gaiano, N., and Fishell, G. (2002). The role of notch in promoting glial and neural stem cell fates. Annual review of neuroscience *25*, 471-490.

Gao, P., Postiglione, M.P., Krieger, T.G., Hernandez, L., Wang, C., Han, Z., Streicher, C., Papusheva, E., Insolera, R., Chugh, K.*, et al.* (2014). Deterministic progenitor behavior and unitary production of neurons in the neocortex. Cell *159*, 775-788.

Garcia-Moreno, F., Vasistha, N.A., Trevia, N., Bourne, J.A., and Molnar, Z. (2012). Compartmentalization of cerebral cortical germinal zones in a lissencephalic primate and gyrencephalic rodent. Cereb Cortex *22*, 482-492.

Garel, S., Huffman, K.J., and Rubenstein, J.L.R. (2003). Molecular regionalization of the neocortex is disrupted in Fgf8 hypomorphic mutants. Development *130*, 1903-1914.

Gaspard, N., Bouschet, T., Hourez, R., Dimidschstein, J., Naeije, G., van den Ameele, J., Espuny-Camacho, I., Herpoel, A., Passante, L., Schiffmann, S.N.*, et al.* (2008). An intrinsic mechanism of corticogenesis from embryonic stem cells. Nature *455*, 351-357.

Geschwind, D.H., and Rakic, P. (2013). Cortical evolution: judge the brain by its cover. Neuron *80*, 633-647.

Gil-Sanz, C., Espinosa, A., Fregoso, S.P., Bluske, K.K., Cunningham, C.L., Martinez-Garay, I., Zeng, H., Franco, S.J., and Muller, U. (2015). Lineage Tracing Using Cux2-Cre and Cux2-CreERT2 Mice. Neuron *86*, 1091-1099.

Gimlich, R.L., and Cooke, J. (1983). Cell lineage and the induction of second nervous systems in amphibian development. Nature *306*, 471-473.

Glaser, T., and Brustle, O. (2005). Retinoic acid induction of ES-cell-derived neurons: the radial glia connection. Trends Neurosci *28*, 397-400.

Godsave, S.F., and Slack, J.M. (1989). Clonal analysis of mesoderm induction in Xenopus laevis. Dev Biol *134*, 486-490.

Greber, B., Coulon, P., Zhang, M., Moritz, S., Frank, S., Muller-Molina, A.J., Arauzo-Bravo, M.J., Han, D.W., Pape, H.C., and Scholer, H.R. (2011). FGF signalling inhibits neural induction in human embryonic stem cells. EMBO J *30*, 4874-4884.

Greber, B., Wu, G., Bernemann, C., Joo, J.Y., Han, D.W., Ko, K., Tapia, N., Sabour, D., Sterneckert, J., Tesar, P.*, et al.* (2010). Conserved and divergent roles of FGF signaling in mouse epiblast stem cells and human embryonic stem cells. Cell stem cell *6*, 215-226.

Greig, L.C., Woodworth, M.B., Galazo, M.J., Padmanabhan, H., and Macklis, J.D. (2013). Molecular logic of neocortical projection neuron specification, development and diversity. Nat Rev Neurosci *14*, 755-769.

Guo, C., Eckler, M.J., McKenna, W.L., McKinsey, G.L., Rubenstein, J.L., and Chen, B. (2013). Fezf2 expression identifies a multipotent progenitor for neocortical projection neurons, astrocytes, and oligodendrocytes. Neuron *80*, 1167-1174.

Guo, G., Yang, J., Nichols, J., Hall, J.S., Eyres, I., Mansfield, W., and Smith, A. (2009). Klf4 reverts developmentally programmed restriction of ground state pluripotency. Development *136*, 1063-1069.

Hamada, H., Meno, C., Watanabe, D., and Saijoh, Y. (2002). Establishment of vertebrate left-right asymmetry. Nat Rev Genet *3*, 103-113.

Hamilton, W.B., and Brickman, J.M. (2014). Erk signaling suppresses embryonic stem cell self-renewal to specify endoderm. Cell Rep *9*, 2056-2070.

Han, W., and Sestan, N. (2013). Cortical projection neurons: sprung from the same root. Neuron *80*, 1103-1105.

Hanashima, C., Li, S.C., Shen, L., Lai, E., and Fishell, G. (2004). Foxg1 suppresses early cortical cell fate. Science *303*, 56-59.

Hanna, J.H., Saha, K., and Jaenisch, R. (2010). Pluripotency and cellular reprogramming: facts, hypotheses, unresolved issues. Cell *143*, 508-525.

Hansen, D.V., Lui, J.H., Flandin, P., Yoshikawa, K., Rubenstein, J.L., Alvarez-Buylla, A., and Kriegstein, A.R. (2013). Non-epithelial stem cells and cortical interneuron production in the human ganglionic eminences. Nature neuroscience *16*, 1576-1587.

Hansen, D.V., Lui, J.H., Parker, P.R., and Kriegstein, A.R. (2010). Neurogenic radial glia in the outer subventricular zone of human neocortex. Nature *464*, 554-561.

Hansen, D.V., Rubenstein, J.L., and Kriegstein, A.R. (2011). Deriving excitatory neurons of the neocortex from pluripotent stem cells. Neuron *70*, 645-660.

Hardcastle, Z., and Papalopulu, N. (2000). Distinct effects of XBF-1 in regulating the cell cycle inhibitor p27(XIC1) and imparting a neural fate. Development (Cambridge, England) *127*, 1303-1314.

Hartenstein, V., and Stollewerk, A. (2015). The Evolution of Early Neurogenesis. Dev Cell *32*, 390-407.

Hatakeyama, J., Bessho, Y., Katoh, K., Ookawara, S., Fujioka, M., Guillemot, F., and Kageyama, R. (2004). Hes genes regulate size, shape and histogenesis of the nervous system by control of the timing of neural stem cell differentiation. Development *131*, 5539-5550.

Hawley, S.H., Wunnenberg-Stapleton, K., Hashimoto, C., Laurent, M.N., Watabe, T., Blumberg, B.W., and Cho, K.W. (1995). Disruption of BMP signals in embryonic Xenopus ectoderm leads to direct neural induction. Genes Dev *9*, 2923-2935.

Hebert, J.M., and Fishell, G. (2008). The genetics of early telencephalon patterning: some assembly required. Nat Rev Neurosci *9*, 678-685.

Hébert, J.M., Mishina, Y., and McConnell, S.K. (2002). BMP Signaling Is Required Locally to Pattern the Dorsal Telencephalic Midline. Neuron *35*, 1029-1041.

Hedges, S.B., and Kumar, S. (2009). The timetree of life (Oxford ; New York: Oxford University Press).

Hemmati-Brivanlou, A., Kelly, O.G., and Melton, D.A. (1994). Follistatin, an Antagonist of Activin, Is Expressed in the Spemann Organizer and Displays Direct Neuralizing Activity. Cell *77*, 283-295.

Hemmati-Brivanlou, A., and Melton, D. (1997). Vertebrate embryonic cells will become nerve cells unless told otherwise. Cell *88*, 13-17.

Hemmati-Brivanlou, A., and Melton, D.A. (1992). A truncated activin receptor inhibits mesoderm induction and formation of axial structures in Xenopus embryos. Nature *359*, 609-614.

Hemmati-Brivanlou, A., and Melton, D.A. (1994). Inhibition of activin receptor signaling promotes neuralization in Xenopus. Cell *77*, 273-281.

Hemmati-Brivanlou, A., and Thomsen, G.H. (1995). Ventral mesodermal patterning in Xenopus embryos: expression patterns and activities of BMP-2 and BMP-4. Developmental genetics *17*, 78-89.

Hevner, R.F., and Haydar, T.F. (2012). The (not necessarily) convoluted role of basal radial glia in cortical neurogenesis. Cereb Cortex *22*, 465-468.

Hideki, A., Makoto, K., Tatsuya, T., Keiichi, U., Toshiaki, F., and Hitoshi, O. (2005). Lhx2 mediates the activity of Six3 in zebrafish forebrain growth. Developmental Biology.

Hill, R.S., and Walsh, C.A. (2005). Molecular insights into human brain evolution. Nature *437*, 64-67.

Hirata, T., Suda, Y., Nakao, K., Narimatsu, M., Hirano, T., and Hibi, M. (2004). Zinc finger gene fez-like functions in the formation of subplate neurons and thalamocortical axons. Dev Dyn *230*, 546-556.

Hockemeyer, D., Wang, H., Kiani, S., Lai, C.S., Gao, Q., Cassady, J.P., Cost, G.J., Zhang, L., Santiago, Y., Miller, J.C*., et al.* (2011). Genetic engineering of human pluripotent cells using TALE nucleases. Nature biotechnology *29*, 731-734.

Holley, S.A., Jackson, P.D., Sasai, Y., Lu, B., De Robertis, E.M., Hoffmann, F.M., and Ferguson, E.L. (1995). A conserved system for dorsal-ventral patterning in insects and vertebrates involving sog and chordin. Nature *376*, 249-253.

Holtfreter, J., and Hamburger, V. (1955). Amphibians. In analysis of Development, , B. H., Weiss, P. and Hamburger, V., eds. Philadelphia: W B Saunders Company, 230-296.

Huang da, W., Sherman, B.T., and Lempicki, R.A. (2009a). Bioinformatics enrichment tools: paths toward the comprehensive functional analysis of large gene lists. Nucleic Acids Res *37*, 1-13.

Huang da, W., Sherman, B.T., and Lempicki, R.A. (2009b). Systematic and integrative analysis of large gene lists using DAVID bioinformatics resources. Nat Protoc *4*, 44-57.

Hutsler, J.J., Lee, D.G., and Porter, K.K. (2005). Comparative analysis of cortical layering and supragranular layer enlargement in rodent carnivore and primate species. Brain Res *1052*, 71-81.

Imayoshi, I., and Kageyama, R. (2014). Oscillatory control of bHLH factors in neural progenitors. Trends Neurosci *37*, 531-538.

Imayoshi, I., Sakamoto, M., Yamaguchi, M., Mori, K., and Kageyama, R. (2010). Essential roles of Notch signaling in maintenance of neural stem cells in developing and adult brains. J Neurosci *30*, 3489-3498.

Ip, B.K., Wappler, I., Peters, H., Lindsay, S., Clowry, G.J., and Bayatti, N. (2010). Investigating gradients of gene expression involved in early human cortical development. J Anat *217*, 300-311.

Itsykson, P., Ilouz, N., Turetsky, T., Goldstein, R.S., Pera, M.F., Fishbein, I., Segal, M., and Reubinoff, B.E. (2005). Derivation of neural precursors from human embryonic stem cells in the presence of noggin. Molecular and cellular neurosciences *30*, 24-36.

Jackson, C.A., Peduzzi, J.D., and Hickey, T.L. (1989). Visual cortex development in the ferret. I. Genesis and migration of visual cortical neurons. J Neurosci *9*, 1242-1253.

James, D., Levine, A.J., Besser, D., and Hemmati-Brivanlou, A. (2005). TGFbeta/activin/nodal signaling is necessary for the maintenance of pluripotency in human embryonic stem cells. Development *132*, 1273-1282.

James, D., Noggle, S.A., Swigut, T., and Brivanlou, A.H. (2006). Contribution of human embryonic stem cells to mouse blastocysts. Dev Biol *295*, 90-102.

Johnson, M.B., Kawasawa, Y.I., Mason, C.E., Krsnik, Z., Coppola, G., Bogdanovic, D., Geschwind, D.H., Mane, S.M., State, M.W., and Sestan, N. (2009). Functional and evolutionary insights into human brain development through global transcriptome analysis. Neuron *62*, 494-509.

Jones-Villeneuve, E.M., McBurney, M.W., Rogers, K.A., and Kalnins, V.I. (1982). Retinoic acid induces embryonal carcinoma cells to differentiate into neurons and glial cells. J Cell Biol *94*, 253-262.

Jung, S.M., Lee, J.H., Park, J., Oh, Y.S., Lee, S.K., Park, J.S., Lee, Y.S., Kim, J.H., Lee, J.Y., Bae, Y.S*., et al.* (2013). Smad6 inhibits non-canonical TGF-beta1 signalling by recruiting the deubiquitinase A20 to TRAF6. Nature communications *4*, 2562.

Kadoshima, T., Sakaguchi, H., Nakano, T., Soen, M., Ando, S., Eiraku, M., and Sasai, Y. (2013). Self-organization of axial polarity, inside-out layer pattern, and species-specific progenitor dynamics in human ES cell-derived neocortex. Proceedings of the National Academy of Sciences of the United States of America *110*, 20284-20289.

Kamiya, D., Banno, S., Sasai, N., Ohgushi, M., Inomata, H., Watanabe, K., Kawada, M., Yakura, R., Kiyonari, H., Nakao, K.*, et al.* (2011). Intrinsic transition of embryonic stem-cell differentiation into neural progenitors. Nature *470*, 503-509.

Kang, L., Wang, J., Zhang, Y., Kou, Z., and Gao, S. (2009). iPS cells can support full-term development of tetraploid blastocyst-complemented embryos. Cell stem cell *5*, 135-138.

Kelava, I., Reillo, I., Murayama, A.Y., Kalinka, A.T., Stenzel, D., Tomancak, P., Matsuzaki, F., Lebrand, C., Sasaki, E., Schwamborn, J.C.*, et al.* (2012). Abundant occurrence of basal radial glia in the subventricular zone of embryonic neocortex of a lissencephalic primate, the common marmoset Callithrix jacchus. Cereb Cortex *22*, 469-481.

Ken-ichi, M., Keejung, Y., Louis, D., Akinori, T., and Nicholas, G. (2007). Differential Notch signalling distinguishes neural stem cells from intermediate progenitors. Nature *449*, 351-355.

Kepecs, A., and Fishell, G. (2014). Interneuron cell types are fit to function. Nature *505*, 318-326.

Khokha, M.K., Yeh, J., Grammer, T.C., and Harland, R.M. (2005). Depletion of three BMP antagonists from Spemann's organizer leads to a catastrophic loss of dorsal structures. Dev Cell *8*, 401-411.

Kimura, J., Suda, Y., Kurokawa, D., Hossain, Z.M., Nakamura, M., Takahashi, M., Hara, A., and Aizawa, S. (2005). Emx2 and Pax6 function in cooperation with Otx2 and Otx1 to develop caudal forebrain primordium that includes future archipallium. J Neurosci *25*, 5097-5108.

Kintner, C. (1988). Effects of altered expression of the neural cell adhesion molecule, N-CAM, on early neural development in Xenopus embryos. Neuron *1*, 545-555.

Kirkeby, A., Grealish, S., Wolf, D.A., Nelander, J., Wood, J., Lundblad, M., Lindvall, O., and Parmar, M. (2012). Generation of regionally specified neural progenitors and functional neurons from human embryonic stem cells under defined conditions. Cell Rep *1*, 703-714.

Koehler, K.R., Mikosz, A.M., Molosh, A.I., Patel, D., and Hashino, E. (2013). Generation of inner ear sensory epithelia from pluripotent stem cells in 3D culture. Nature *500*, 217-221.

Kornack, D.R., and Rakic, P. (1998). Changes in cell-cycle kinetics during the development and evolution of primate neocortex. Proceedings of the National Academy of Sciences of the United States of America *95*, 1242-1246.

Kriegstein, A., and Alvarez-Buylla, A. (2009). The glial nature of embryonic and adult neural stem cells. Annual review of neuroscience *32*, 149-184.

Kriegstein, A., Noctor, S., and Martinez-Cerdeno, V. (2006). Patterns of neural stem and progenitor cell division may underlie evolutionary cortical expansion. Nat Rev Neurosci *7*, 883-890.

Kriks, S., Shim, J.W., Piao, J., Ganat, Y.M., Wakeman, D.R., Xie, Z., Carrillo-Reid, L., Auyeung, G., Antonacci, C., Buch, A.*, et al.* (2011). Dopamine neurons derived from human ES cells efficiently engraft in animal models of Parkinson's disease. Nature *480*, 547-551.

Kuan, C.Y., Elliott, E.A., Flavell, R.A., and Rakic, P. (1997). Restrictive clonal allocation in the chimeric mouse brain. Proceedings of the National Academy of Sciences of the United States of America *94*, 3374-3379.

Kumamoto, T., and Hanashima, C. (2014). Neuronal subtype specification in establishing mammalian neocortical circuits. Neurosci Res *86*, 37-49.

Kunath, T., Saba-El-Leil, M.K., Almousailleakh, M., Wray, J., Meloche, S., and Smith, A. (2007). FGF stimulation of the Erk1/2 signalling cascade triggers transition of pluripotent embryonic stem cells from self-renewal to lineage commitment. Development *134*, 2895-2902.

Kuo, D.H., and Weisblat, D.A. (2011). A new molecular logic for BMP-mediated dorsoventral patterning in the leech Helobdella. Current biology : CB *21*, 1282-1288.

Kurth, T., Meissner, S., Schackel, S., and Steinbeisser, H. (2005). Establishment of mesodermal gene expression patterns in early Xenopus embryos: the role of repression. Dev Dyn *233*, 418-429.

Kwan, K.Y., Sestan, N., and Anton, E.S. (2012). Transcriptional co-regulation of neuronal migration and laminar identity in the neocortex. Development *139*, 1535-1546.

Lacoste, A., Berenshteyn, F., and Brivanlou, A.H. (2009). An efficient and reversible transposable system for gene delivery and lineage-specific differentiation in human embryonic stem cells. Cell stem cell *5*, 332-342.

LaMonica, B.E., Lui, J.H., Hansen, D.V., and Kriegstein, A.R. (2013). Mitotic spindle orientation predicts outer radial glial cell generation in human neocortex. Nature communications *4*, 1665.

Lancaster, M.A., Renner, M., Martin, C.A., Wenzel, D., Bicknell, L.S., Hurles, M.E., Homfray, T., Penninger, J.M., Jackson, A.P., and Knoblich, J.A. (2013). Cerebral organoids model human brain development and microcephaly. Nature *501*, 373-379.

Lange, C., Huttner, W.B., and Calegari, F. (2009). Cdk4/cyclinD1 overexpression in neural stem cells shortens G1, delays neurogenesis, and promotes the generation and expansion of basal progenitors. Cell stem cell *5*, 320-331.

LaVaute, T.M., Yoo, Y.D., Pankratz, M.T., Weick, J.P., Gerstner, J.R., and Zhang, S.C. (2009). Regulation of neural specification from human embryonic stem cells by BMP and FGF. Stem Cells *27*, 1741-1749.

Lee, D.R., Yoo, J.E., Lee, J.S., Park, S., Lee, J., Park, C.Y., Ji, E., Kim, H.S., Hwang, D.Y., Kim, D.S.*, et al.* (2015). PSA-NCAM-Negative Neural Crest Cells Emerging during Neural Induction of Pluripotent Stem Cells Cause Mesodermal Tumors and Unwanted Grafts. Stem Cell Reports *4*, 821-834.

Lee, S.J., Ralston, H.J., Drey, E.A., Partridge, J.C., and Rosen, M.A. (2005). Fetal pain: a systematic multidisciplinary review of the evidence. JAMA *294*, 947-954.

Lehtinen, M.K., Zappaterra, M.W., Chen, X., Yang, Y.J., Hill, A.D., Lun, M., Maynard, T., Gonzalez, D., Kim, S., Ye, P.*, et al.* (2011). The cerebrospinal fluid provides a proliferative niche for neural progenitor cells. Neuron *69*, 893-905.

Levine, A.J., and Brivanlou, A.H. (2007). Proposal of a model of mammalian neural induction. Dev Biol *308*, 247-256.

Li, H.S., Wang, D., Shen, Q., Schonemann, M.D., Gorski, J.A., Jones, K.R., Temple, S., Jan, L.Y., and Jan, Y.N. (2003). Inactivation of Numb and Numblike in embryonic dorsal forebrain impairs neurogenesis and disrupts cortical morphogenesis. Neuron *40*, 1105-1118.

Li, W., Sun, W., Zhang, Y., Wei, W., Ambasudhan, R., Xia, P., Talantova, M., Lin, T., Kim, J., Wang, X.*, et al.* (2011). Rapid induction and long-term self-renewal of primitive neural precursors from human embryonic stem cells by small molecule inhibitors. Proceedings of the National Academy of Sciences of the United States of America *108*, 8299-8304.

Li, X.J., Du, Z.W., Zarnowska, E.D., Pankratz, M., Hansen, L.O., Pearce, R.A., and Zhang, S.C. (2005). Specification of motoneurons from human embryonic stem cells. Nature biotechnology *23*, 215-221.

Li, Y., Lu, H., Cheng, P.L., Ge, S., Xu, H., Shi, S.H., and Dan, Y. (2012). Clonally related visual cortical neurons show similar stimulus feature selectivity. Nature *486*, 118-121.

Liguori, G.L., Echevarria, D., Improta, R., Signore, M., Adamson, E., Martinez, S., and Persico, M.G. (2003). Anterior neural plate regionalization in cripto null mutant mouse embryos in the absence of node and primitive streak. Dev Biol *264*, 537-549.

Linker, C., and Stern, C.D. (2004). Neural induction requires BMP inhibition only as a late step, and involves signals other than FGF and Wnt antagonists. Development *131*, 5671-5681.

Liu, A., and Niswander, L.A. (2005). Bone morphogenetic protein signalling and vertebrate nervous system development. Nat Rev Neurosci *6*, 945-954.

Liu, H., Zhu, F., Yong, J., Zhang, P., Hou, P., Li, H., Jiang, W., Cai, J., Liu, M., Cui, K.*, et al.* (2008). Generation of induced pluripotent stem cells from adult rhesus monkey fibroblasts. Cell stem cell *3*, 587-590.

Lopez-Bendito, G., and Molnar, Z. (2003). Thalamocortical development: how are we going to get there? Nat Rev Neurosci *4*, 276-289.

Lou, C.H., Shao, A., Shum, E.Y., Espinoza, J.L., Huang, L., Karam, R., and Wilkinson, M.F. (2014). Posttranscriptional control of the stem cell and neurogenic programs by the nonsense-mediated RNA decay pathway. Cell Rep *6*, 748-764.

Loulier, K., Barry, R., Mahou, P., Le Franc, Y., Supatto, W., Matho, K.S., Ieng, S., Fouquet, S., Dupin, E., Benosman, R.*, et al.* (2014). Multiplex cell and lineage tracking with combinatorial labels. Neuron *81*, 505-520.

Lowe, C.J., Terasaki, M., Wu, M., Freeman, R.M., Jr., Runft, L., Kwan, K., Haigo, S., Aronowicz, J., Lander, E., Gruber, C.*, et al.* (2006). Dorsoventral patterning in hemichordates: insights into early chordate evolution. PLoS Biol *4*, e291.

Lui, J.H., Hansen, D.V., and Kriegstein, A.R. (2011). Development and evolution of the human neocortex. Cell *146*, 18-36.

Lui, J.H., Nowakowski, T.J., Pollen, A.A., Javaherian, A., Kriegstein, A.R., and Oldham, M.C. (2014). Radial glia require PDGFD-PDGFRbeta signalling in human but not mouse neocortex. Nature *515*, 264-268.

Lukaszewicz, A., Savatier, P., Cortay, V., Giroud, P., Huissoud, C., Berland, M., Kennedy, H., and Dehay, C. (2005). G1 phase regulation, area-specific cell cycle control, and cytoarchitectonics in the primate cortex. Neuron *47*, 353-364.

Lupo, G., Novorol, C., Smith, J.R., Vallier, L., Miranda, E., Alexander, M., Biagioni, S., Pedersen, R.A., and Harris, W.A. (2013). Multiple roles of Activin/Nodal, bone morphogenetic protein, fibroblast growth factor and Wnt/beta-catenin signalling in the anterior neural patterning of adherent human embryonic stem cell cultures. Open biology *3*, 120167.

Luskin, M.B., Pearlman, A.L., and Sanes, J.R. (1988). Cell lineage in the cerebral cortex of the mouse studied in vivo and in vitro with a recombinant retrovirus. Neuron *1*, 635-647.

Ma, T., Wang, C., Wang, L., Zhou, X., Tian, M., Zhang, Q., Zhang, Y., Li, J., Liu, Z., Cai, Y.*, et al.* (2013). Subcortical origins of human and monkey neocortical interneurons. Nature neuroscience *16*, 1588-1597.

Marion, B., Veronique, C., Dorothée, P., Sabina, P., Elodie, G., Angèle, B.-M., Marielle, A., Cyril, H., Rodney, J.D., Henry, K.*, et al.* (2013). Precursor Diversity and Complexity of Lineage Relationships in the Outer Subventricular Zone of the Primate. Neuron.

Maroof, A.M., Brown, K., Shi, S.H., Studer, L., and Anderson, S.A. (2010). Prospective isolation of cortical interneuron precursors from mouse embryonic stem cells. J Neurosci *30*, 4667-4675.

Maroof, A.M., Keros, S., Tyson, J.A., Ying, S.W., Ganat, Y.M., Merkle, F.T., Liu, B., Goulburn, A., Stanley, E.G., Elefanty, A.G.*, et al.* (2013). Directed differentiation and functional maturation of cortical interneurons from human embryonic stem cells. Cell stem cell *12*, 559-572.

Martin, G.R. (1981). Isolation of a pluripotent cell line from early mouse embryos cultured in medium conditioned by teratocarcinoma stem cells. Proceedings of the National Academy of Sciences of the United States of America *78*, 7634-7638.

Mathews, L.S., and Vale, W.W. (1991). Expression cloning of an activin receptor, a predicted transmembrane serine kinase. Cell *65*, 973-982.

Maury, Y., Come, J., Piskorowski, R.A., Salah-Mohellibi, N., Chevaleyre, V., Peschanski, M., Martinat, C., and Nedelec, S. (2015). Combinatorial analysis of developmental cues efficiently converts human pluripotent stem cells into multiple neuronal subtypes. Nature biotechnology *33*, 89-96.

McCarthy, S.E., Gillis, J., Kramer, M., Lihm, J., Yoon, S., Berstein, Y., Mistry, M., Pavlidis, P., Solomon, R., Ghiban, E.*, et al.* (2014). De novo mutations in schizophrenia implicate chromatin remodeling and support a genetic overlap with autism and intellectual disability. Mol Psychiatry *19*, 652-658.

McConnell, S.K. (1988). Fates of visual cortical neurons in the ferret after isochronic and heterochronic transplantation. J Neurosci *8*, 945-974.

McConnell, S.K., and Kaznowski, C.E. (1991). Cell cycle dependence of laminar determination in developing neocortex. Science *254*, 282-285.

McMahon, J.A., Takada, S., Zimmerman, L.B., Fan, C.M., Harland, R.M., and McMahon, A.P. (1998). Noggin-mediated antagonism of BMP signaling is required for growth and patterning of the neural tube and somite. Genes Dev *12*, 1438-1452.

Menendez, L., Yatskievych, T.A., Antin, P.B., and Dalton, S. (2011). Wnt signaling and a Smad pathway blockade direct the differentiation of human pluripotent stem cells to multipotent neural crest cells. Proceedings of the National Academy of Sciences of the United States of America *108*, 19240-19245.

Meno, C., Ito, Y., Saijoh, Y., Matsuda, Y., Tashiro, K., Kuhara, S., and Hamada, H. (1997). Two closely-related left-right asymmetrically expressed genes, lefty-1 and lefty-2: their distinct expression domains, chromosomal linkage and direct neuralizing activity in Xenopus embryos. Genes to cells : devoted to molecular & cellular mechanisms *2*, 513-524.

Metallo, C.M., Ji, L., de Pablo, J.J., and Palecek, S.P. (2008). Retinoic acid and bone morphogenetic protein signaling synergize to efficiently direct epithelial differentiation of human embryonic stem cells. Stem Cells *26*, 372-380.

Miller, J.A., Ding, S.L., Sunkin, S.M., Smith, K.A., Ng, L., Szafer, A., Ebbert, A., Riley, Z.L., Royall, J.J., Aiona, K.*, et al.* (2014). Transcriptional landscape of the prenatal human brain. Nature *508*, 199-206.

Miya, T., Morita, K., Suzuki, A., Ueno, N., and Satoh, N. (1997). Functional analysis of an ascidian homologue of vertebrate Bmp-2/Bmp-4 suggests its role in the inhibition of neural fate specification. Development *124*, 5149-5159.

Miyoshi, G., and Fishell, G. (2012). Dynamic FoxG1 expression coordinates the integration of multipolar pyramidal neuron precursors into the cortical plate. Neuron *74*, 1045-1058.

Mizutani, C.M., and Bier, E. (2008). EvoD/Vo: the origins of BMP signalling in the neuroectoderm. Nat Rev Genet *9*, 663-677.

Mizutani, C.M., Nie, Q., Wan, F.Y., Zhang, Y.T., Vilmos, P., Sousa-Neves, R., Bier, E., Marsh, J.L., and Lander, A.D. (2005). Formation of the BMP activity gradient in the Drosophila embryo. Dev Cell *8*, 915-924.

Molnar, Z., and Butt, S.J. (2013). Best-laid schemes for interneuron origin of mice and men. Nature neuroscience *16*, 1512-1514.

Molyneaux, B.J., Arlotta, P., Menezes, J.R., and Macklis, J.D. (2007). Neuronal subtype specification in the cerebral cortex. Nat Rev Neurosci *8*, 427-437.

Muguruma, K., Nishiyama, A., Kawakami, H., Hashimoto, K., and Sasai, Y. (2015). Self-Organization of Polarized Cerebellar Tissue in 3D Culture of Human Pluripotent Stem Cells. Cell Rep.

Muguruma, K., and Sasai, Y. (2012). In vitro recapitulation of neural development using embryonic stem cells: from neurogenesis to histogenesis. Dev Growth Differ *54*, 349-357.

Munji, R.N., Choe, Y., Li, G., Siegenthaler, J.A., and Pleasure, S.J. (2011). Wnt signaling regulates neuronal differentiation of cortical intermediate progenitors. J Neurosci *31*, 1676-1687.

Muotri, A.R., Marchetto, M.C., Coufal, N.G., Oefner, R., Yeo, G., Nakashima, K., and Gage, F.H. (2010). L1 retrotransposition in neurons is modulated by MeCP2. Nature *468*, 443-446.

Murielle, R., Joshua, G.C., and Gord, F. (2002). Parsing the prosencephalon. Nature Reviews Neuroscience *3*, 943-951.

Mutch, C.A., Funatsu, N., Monuki, E.S., and Chenn, A. (2009). Beta-catenin signaling levels in progenitors influence the laminar cell fates of projection neurons. J Neurosci *29*, 13710-13719.

Muzio, L., and Mallamaci, A. (2005). Foxg1 confines Cajal-Retzius neuronogenesis and hippocampal morphogenesis to the dorsomedial pallium. J Neurosci *25*, 4435-4441.

Nagy, A., Rossant, J., Nagy, R., Abramow-Newerly, W., and Roder, J.C. (1993). Derivation of completely cell culture-derived mice from early-passage embryonic stem cells. Proceedings of the National Academy of Sciences of the United States of America *90*, 8424-8428.

Najm, F.J., Chenoweth, J.G., Anderson, P.D., Nadeau, J.H., Redline, R.W., McKay, R.D., and Tesar, P.J. (2011). Isolation of epiblast stem cells from preimplantation mouse embryos. Cell stem cell *8*, 318-325.

Naka, H., Nakamura, S., Shimazaki, T., and Okano, H. (2008). Requirement for COUP-TFI and II in the temporal specification of neural stem cells in CNS development. Nature neuroscience *11*, 1014-1023.

Nakagawa, M., Koyanagi, M., Tanabe, K., Takahashi, K., Ichisaka, T., Aoi, T., Okita, K., Mochiduki, Y., Takizawa, N., and Yamanaka, S. (2008). Generation of induced pluripotent stem cells without Myc from mouse and human fibroblasts. Nature biotechnology *26*, 101-106.

Nakano, T., Ando, S., Takata, N., Kawada, M., Muguruma, K., Sekiguchi, K., Saito, K., Yonemura, S., Eiraku, M., and Sasai, Y. (2012). Self-formation of optic cups and storable stratified neural retina from human ESCs. Cell stem cell *10*, 771-785.

Nakao, A., Afrakhte, M., Moren, A., Nakayama, T., Christian, J.L., Heuchel, R., Itoh, S., Kawabata, M., Heldin, N.E., Heldin, C.H.*, et al.* (1997). Identification of Smad7, a TGFbeta-inducible antagonist of TGF-beta signalling. Nature *389*, 631-635.

Namihira, M., Kohyama, J., Semi, K., Sanosaka, T., Deneen, B., Taga, T., and Nakashima, K. (2009). Committed neuronal precursors confer astrocytic potential on residual neural precursor cells. Dev Cell *16*, 245-255.

Nicholas, C.R., Chen, J., Tang, Y., Southwell, D.G., Chalmers, N., Vogt, D., Arnold, C.M., Chen, Y.J., Stanley, E.G., Elefanty, A.G.*, et al.* (2013). Functional maturation of hPSC-derived forebrain interneurons requires an extended timeline and mimics human neural development. Cell stem cell *12*, 573-586.

Nieto, M., Monuki, E.S., Tang, H., Imitola, J., Haubst, N., Khoury, S.J., Cunningham, J., Gotz, M., and Walsh, C.A. (2004). Expression of Cux-1 and Cux-2 in the subventricular zone and upper layers II-IV of the cerebral cortex. J Comp Neurol *479*, 168-180.

Nieuwkoop, P.D. (1951). New Experiments on the Activation and Organization of the Central Nervous System in Amphibians. Anatomical Record *111*, 453-454.

Nieuwkoop, P.D., and Nigtevecht, G.V. (1954). Neural Activation and Transformation in Explants of Competent Ectoderm under the Influence of Fragments of Anterior Notochord in Urodeles. Journal of Embryology and Experimental Morphology *2*, 175-193.

Noctor, S.C., Flint, A.C., Weissman, T.A., Dammerman, R.S., and Kriegstein, A.R. (2001). Neurons derived from radial glial cells establish radial units in neocortex. Nature *409*, 714-720.

Noctor, S.C., Martinez-Cerdeno, V., Ivic, L., and Kriegstein, A.R. (2004). Cortical neurons arise in symmetric and asymmetric division zones and migrate through specific phases. Nature neuroscience *7*, 136-144.

Nonaka-Kinoshita, M., Reillo, I., Artegiani, B., Martinez-Martinez, M.A., Nelson, M., Borrell, V., and Calegari, F. (2013). Regulation of cerebral cortex size and folding by expansion of basal progenitors. EMBO J *32*, 1817-1828.

O'Leary, D.D., Chou, S.J., and Sahara, S. (2007). Area patterning of the mammalian cortex. Neuron *56*, 252-269.

O'Leary, D.D.M. (1989). Do cortical areas emerge from a protocortex? Trends in Neurosciences *12*, 400-406.

Okada, Y., Matsumoto, A., Shimazaki, T., Enoki, R., Koizumi, A., Ishii, S., Itoyama, Y., Sobue, G., and Okano, H. (2008). Spatiotemporal recapitulation of central nervous system development by murine embryonic stem cell-derived neural stem/progenitor cells. Stem Cells *26*, 3086-3098.

Ono, T., Suzuki, Y., Kato, Y., Fujita, R., Araki, T., Yamashita, T., Kato, H., Torii, R., and Sato, N. (2014). A single-cell and feeder-free culture system for monkey embryonic stem cells. PloS one *9*, e88346.

Onorati, M., Castiglioni, V., Biasci, D., Cesana, E., Menon, R., Vuono, R., Talpo, F., Goya, R.L., Lyons, P.A., Bulfamante, G.P.*, et al.* (2014). Molecular and functional definition of the developing human striatum. Nature neuroscience *17*, 1804-1815.

Oppenheimer, J.M. (1936). Transplantation experiments on developing teleosts (Fundulus and Perca). Journal of Experimental Zoology *72*, 409-437.

Oppenheimer, J.M. (1953). The Development of Transplanted Fragments of Fundulus Gastrulae. Proc Natl Acad Sci U S A *39*, 1149-1152.

Ozair, M.Z., Kintner, C., and Brivanlou, A.H. (2013). Neural induction and early patterning in vertebrates. Wiley interdisciplinary reviews Developmental biology *2*, 479-498.

Pankratz, M.T., Li, X.J., Lavaute, T.M., Lyons, E.A., Chen, X., and Zhang, S.C. (2007). Directed neural differentiation of human embryonic stem cells via an obligated primitive anterior stage. Stem Cells *25*, 1511-1520.

Park, I.H., Zhao, R., West, J.A., Yabuuchi, A., Huo, H., Ince, T.A., Lerou, P.H., Lensch, M.W., and Daley, G.Q. (2008). Reprogramming of human somatic cells to pluripotency with defined factors. Nature *451*, 141-146.

Parthasarathy, S., Srivatsa, S., Nityanandam, A., and Tarabykin, V. (2014). Ntf3 acts downstream of Sip1 in cortical postmitotic neurons to control progenitor cell fate through feedback signaling. Development *141*, 3324-3330.

Pasko, R. (1974). Neurons in rhesus monkey visual cortex: systematic relation between time of origin and eventual disposition. Science *183*, 425-427.

Patani, R., Compston, A., Puddifoot, C.A., Wyllie, D.J., Hardingham, G.E., Allen, N.D., and Chandran, S. (2009). Activin/Nodal inhibition alone accelerates highly efficient neural conversion from human embryonic stem cells and imposes a caudal positional identity. PloS one *4*, e7327.

Pera, E.M., Ikeda, A., Eivers, E., and De Robertis, E.M. (2003). Integration of IGF, FGF, and anti-BMP signals via Smad1 phosphorylation in neural induction. Genes Dev *17*, 3023-3028.

Perea-Gomez, A., Vella, F.D., Shawlot, W., Oulad-Abdelghani, M., Chazaud, C., Meno, C., Pfister, V., Chen, L., Robertson, E., Hamada, H.*, et al.* (2002). Nodal antagonists in the anterior visceral endoderm prevent the formation of multiple primitive streaks. Dev Cell *3*, 745-756.

Pfaffl, M.W., Horgan, G.W., and Dempfle, L. (2002). Relative expression software tool (REST) for group-wise comparison and statistical analysis of relative expression results in real-time PCR. Nucleic Acids Res *30*, e36.

Piccolo, S., Agius, E., Leyns, L., Bhattacharyya, S., Grunz, H., Bouwmeester, T., and De Robertis, E.M. (1999). The head inducer Cerberus is a multifunctional antagonist of Nodal, BMP and Wnt signals. Nature *397*, 707-710.

Piccolo, S., Sasai, Y., Lu, B., and De Robertis, E.M. (1996). Dorsoventral patterning in Xenopus: inhibition of ventral signals by direct binding of chordin to BMP-4. Cell *86*, 589-598.

Pilaz, L.J., Patti, D., Marcy, G., Ollier, E., Pfister, S., Douglas, R.J., Betizeau, M., Gautier, E., Cortay, V., Doerflinger, N*., et al.* (2009). Forced G1-phase reduction alters mode of division, neuron number, and laminar phenotype in the cerebral cortex. Proceedings of the National Academy of Sciences of the United States of America *106*, 21924-21929.

Pilz, G.A., Shitamukai, A., Reillo, I., Pacary, E., Schwausch, J., Stahl, R., Ninkovic, J., Snippert, H.J., Clevers, H., Godinho, L*., et al.* (2013). Amplification of progenitors in the mammalian telencephalon includes a new radial glial cell type. Nature communications *4*, 2125.

Pollard, K.S., Salama, S.R., Lambert, N., Lambot, M.A., Coppens, S., Pedersen, J.S., Katzman, S., King, B., Onodera, C., Siepel, A*., et al.* (2006). An RNA gene expressed during cortical development evolved rapidly in humans. Nature *443*, 167-172.

Pollen, A.A., Nowakowski, T.J., Shuga, J., Wang, X., Leyrat, A.A., Lui, J.H., Li, N., Szpankowski, L., Fowler, B., Chen, P*., et al.* (2014). Low-coverage single-cell mRNA sequencing reveals cellular heterogeneity and activated signaling pathways in developing cerebral cortex. Nature biotechnology *32*, 1053-1058.

Poorgholi Belverdi, M., Krause, C., Guzman, A., and Knaus, P. (2012). Comprehensive analysis of TGF-beta and BMP receptor interactomes. Eur J Cell Biol *91*, 287-293.

Pouchelon, G., Gambino, F., Bellone, C., Telley, L., Vitali, I., Luscher, C., Holtmaat, A., and Jabaudon, D. (2014). Modality-specific thalamocortical inputs instruct the identity of postsynaptic L4 neurons. Nature *511*, 471-474.

Purves, D. (2012). Neuroscience, 5th edn (Sunderland, Mass.: Sinauer Associates).

Radonjic, N.V., Ayoub, A.E., Memi, F., Yu, X., Maroof, A., Jakovcevski, I., Anderson, S.A., Rakic, P., and Zecevic, N. (2014). Diversity of cortical interneurons in primates: the role of the dorsal proliferative niche. Cell Rep *9*, 2139-2151.

Rakic, P. (1974). Neurons in Rhesus-Monkey Visual-Cortex - Systematic Relation between Time of Origin and Eventual Disposition. Science *183*, 425-427.

Rakic, P. (1988). Specification of cerebral cortical areas. Science *241*, 170-176.

Rallu, M., Corbin, J.G., and Fishell, G. (2002). Parsing the prosencephalon. Nat Rev Neurosci *3*, 943-951.

Ran, F.A., Hsu, P.D., Wright, J., Agarwala, V., Scott, D.A., and Zhang, F. (2013). Genome engineering using the CRISPR-Cas9 system. Nat Protoc *8*, 2281-2308.

Reid, C.B., Liang, I., and Walsh, C. (1995). Systematic widespread clonal organization in cerebral cortex. Neuron *15*, 299-310.

Reillo, I., de Juan Romero, C., Garcia-Cabezas, M.A., and Borrell, V. (2011). A role for intermediate radial glia in the tangential expansion of the mammalian cerebral cortex. Cereb Cortex *21*, 1674-1694.

Ronan, J.L., Wu, W., and Crabtree, G.R. (2013). From neural development to cognition: unexpected roles for chromatin. Nat Rev Genet *14*, 347-359.

Rosa, A., and Brivanlou, A.H. (2009). MicroRNAs in early vertebrate development. Cell Cycle *8*, 3513-3520.

Rosa, A., and Brivanlou, A.H. (2011). A regulatory circuitry comprised of miR-302 and the transcription factors OCT4 and NR2F2 regulates human embryonic stem cell differentiation. EMBO J *30*, 237-248.

Sakaue-Sawano, A., Kurokawa, H., Morimura, T., Hanyu, A., Hama, H., Osawa, H., Kashiwagi, S., Fukami, K., Miyata, T., Miyoshi, H.*, et al.* (2008). Visualizing spatiotemporal dynamics of multicellular cell-cycle progression. Cell *132*, 487-498.

Sanes, D.H., Reh, T.A., and Harris, W.A. (2012). Development of the nervous system, 3rd edn (Amsterdam ; Boston

Burlington, MA: Elsevier ;

Academic Press).

Sanjana, N.E., Cong, L., Zhou, Y., Cunniff, M.M., Feng, G., and Zhang, F. (2012). A transcription activator-like effector toolbox for genome engineering. Nat Protoc *7*, 171-192.

Sansom, S.N., and Livesey, F.J. (2009). Gradients in the brain: the control of the development of form and function in the cerebral cortex. Cold Spring Harb Perspect Biol *1*, a002519.

Sasai, Y., Lu, B., Steinbeisser, H., and De Robertis, E.M. (1995). Regulation of neural induction by the Chd and Bmp-4 antagonistic patterning signals in Xenopus. Nature *377*, 757.

Sasai, Y., Lu, B., Steinbeisser, H., Geissert, D., Gont, L.K., and De Robertis, E.M. (1994). Xenopus chordin: a novel dorsalizing factor activated by organizer-specific homeobox genes. Cell *79*, 779-790.

Sato, S.M., and Sargent, T.D. (1989). Development of neural inducing capacity in dissociated Xenopus embryos. Dev Biol *134*, 263-266.

Scerbo, P., Girardot, F., Vivien, C., Markov, G.V., Luxardi, G., Demeneix, B., Kodjabachian, L., and Coen, L. (2012). Ventx factors function as Nanog-like guardians of developmental potential in Xenopus. PLoS One *7*, e36855.

Schier, A.F. (2009). Nodal morphogens. Cold Spring Harb Perspect Biol *1*, a003459.

Schindelin, J., Arganda-Carreras, I., Frise, E., Kaynig, V., Longair, M., Pietzsch, T., Preibisch, S., Rueden, C., Saalfeld, S., Schmid, B.*, et al.* (2012). Fiji: an open-source platform for biological-image analysis. Nat Methods *9*, 676-682.

Schmidt, J.E., Suzuki, A., Ueno, N., and Kimelman, D. (1995). Localized BMP-4 mediates dorsal/ventral patterning in the early Xenopus embryo. Dev Biol *169*, 37-50.

Schulte-Merker, S., Lee, K.J., McMahon, A.P., and Hammerschmidt, M. (1997). The zebrafish organizer requires chordino. Nature *387*, 862-863.

Sebastian, J.A., Guo-Jen, H., Amanda, F.P.C., Takumi, E., Shin-Ichi, N., Elizabeth, K.B., Zoltán, M., Elizabeth, J.R., and Matthias, G. (2008). The T-box transcription factor Eomes/Tbr2 regulates neurogenesis in the cortical subventricular zone. Genes Dev.

Sessa, A., Mao, C.A., Hadjantonakis, A.K., Klein, W.H., and Broccoli, V. (2008). Tbr2 directs conversion of radial glia into basal precursors and guides neuronal amplification by indirect neurogenesis in the developing neocortex. Neuron *60*, 56-69.

Seuntjens, E., Nityanandam, A., Miquelajauregui, A., Debruyn, J., Stryjewska, A., Goebbels, S., Nave, K.A., Huylebroeck, D., and Tarabykin, V. (2009). Sip1 regulates sequential fate decisions by feedback signaling from postmitotic neurons to progenitors. Nature neuroscience *12*, 1373-1380.

Shen, M.M. (2007). Nodal signaling: developmental roles and regulation. Development *134*, 1023-1034.

Shen, Q., Wang, Y., Dimos, J.T., Fasano, C.A., Phoenix, T.N., Lemischka, I.R., Ivanova, N.B., Stifani, S., Morrisey, E.E., and Temple, S. (2006). The timing of cortical neurogenesis is encoded within lineages of individual progenitor cells. Nature neuroscience *9*, 743-751.

Sheng, G., dos Reis, M., and Stern, C.D. (2003). Churchill, a zinc finger transcriptional activator, regulates the transition between gastrulation and neurulation. Cell *115*, 603-613.

Shi, Y., Kirwan, P., Smith, J., Robinson, H.P., and Livesey, F.J. (2012). Human cerebral cortex development from pluripotent stem cells to functional excitatory synapses. Nature neuroscience *15*, 477-486, S471.

Shim, S., Kwan, K.Y., Li, M., Lefebvre, V., and Sestan, N. (2012). Cis-regulatory control of corticospinal system development and evolution. Nature *486*, 74-79.

Siegenthaler, J.A., Ashique, A.M., Zarbalis, K., Patterson, K.P., Hecht, J.H., Kane, M.A., Folias, A.E., Choe, Y., May, S.R., Kume, T.*, et al.* (2009). Retinoic acid from the meninges regulates cortical neuron generation. Cell *139*, 597-609.

Silva, A.C., Filipe, M., Kuerner, K.M., Steinbeisser, H., and Belo, J.A. (2003). Endogenous Cerberus activity is required for anterior head specification in Xenopus. Development *130*, 4943-4953.

Simone, A.F., Robert, L., Holger, B., Martin, K., Nikolay, S., Roland, S., Naharajan, L., Ian, H., Johannes, V., Axel, R.*, et al.* (2012). Transcriptomes of germinal zones of human and mouse fetal neocortex suggest a role of extracellular matrix in progenitor self-renewal. Proceedings of the National Academy of Sciences.

Singh, A.M., Reynolds, D., Cliff, T., Ohtsuka, S., Mattheyses, A.L., Sun, Y., Menendez, L., Kulik, M., and Dalton, S. (2012). Signaling network crosstalk in human pluripotent cells: a Smad2/3-regulated switch that controls the balance between self-renewal and differentiation. Cell stem cell *10*, 312-326.

Slack, J.M., and Forman, D. (1980). An interaction between dorsal and ventral regions of the marginal zone in early amphibian embryos. J Embryol Exp Morphol *56*, 283-299.

Smith, J.R., Vallier, L., Lupo, G., Alexander, M., Harris, W.A., and Pedersen, R.A. (2008). Inhibition of Activin/Nodal signaling promotes specification of human embryonic stem cells into neuroectoderm. Dev Biol *313*, 107-117.

Smith, W.C., and Harland, R.M. (1992). Expression cloning of noggin, a new dorsalizing factor localized to the Spemann organizer in Xenopus embryos. Cell *70*, 829-840.

Soriano, E., and Del Rio, J.A. (2005). The cells of cajal-retzius: still a mystery one century after. Neuron *46*, 389-394.

Soriano, E., Dumesnil, N., Auladell, C., Cohen-Tannoudji, M., and Sotelo, C. (1995). Molecular heterogeneity of progenitors and radial migration in the developing cerebral cortex revealed by transgene expression. Proceedings of the National Academy of Sciences of the United States of America *92*, 11676-11680.

Spemann, H., and Mangold, H. (1924). The induction of embryonic predispositions by implantation of organizers foreign to the species. Archiv Fur Mikroskopische Anatomie Und Entwicklungsmechanik *100*, 599-638.

Srinivasan, K., Leone, D.P., Bateson, R.K., Dobreva, G., Kohwi, Y., Kohwi-Shigematsu, T., Grosschedl, R., and McConnell, S.K. (2012). A network of genetic repression and derepression specifies projection fates in the developing neocortex. Proceedings of the National Academy of Sciences of the United States of America *109*, 19071-19078.

Srivatsa, S., Parthasarathy, S., Britanova, O., Bormuth, I., Donahoo, A.L., Ackerman, S.L., Richards, L.J., and Tarabykin, V. (2014). Unc5C and DCC act downstream of Ctip2 and Satb2 and contribute to corpus callosum formation. Nature communications *5*, 3708.

Stahl, R., Walcher, T., De Juan Romero, C., Pilz, G.A., Cappello, S., Irmler, M., Sanz-Aquela, J.M., Beckers, J., Blum, R., Borrell, V.*, et al.* (2013). Trnp1 regulates expansion and folding of the mammalian cerebral cortex by control of radial glial fate. Cell *153*, 535-549.

Stavridis, M.P., Collins, B.J., and Storey, K.G. (2010). Retinoic acid orchestrates fibroblast growth factor signalling to drive embryonic stem cell differentiation. Development *137*, 881-890.

Stavridis, M.P., Lunn, J.S., Collins, B.J., and Storey, K.G. (2007). A discrete period of FGF-induced Erk1/2 signalling is required for vertebrate neural specification. Development *134*, 2889-2894.

Stern, C.D. (2005). Neural induction: old problem, new findings, yet more questions. Development *132*, 2007-2021.

Sterneckert, J., Stehling, M., Bernemann, C., Arauzo-Bravo, M.J., Greber, B., Gentile, L., Ortmeier, C., Sinn, M., Wu, G., Ruau, D*., et al.* (2010). Neural induction intermediates exhibit distinct roles of Fgf signaling. Stem Cells *28*, 1772-1781.

Stoner, R., Chow, M.L., Boyle, M.P., Sunkin, S.M., Mouton, P.R., Roy, S., Wynshaw-Boris, A., Colamarino, S.A., Lein, E.S., and Courchesne, E. (2014). Patches of disorganization in the neocortex of children with autism. N Engl J Med *370*, 1209-1219.

Streit, A., Lee, K.J., Woo, I., Roberts, C., Jessell, T.M., and Stern, C.D. (1998). Chordin regulates primitive streak development and the stability of induced neural cells, but is not sufficient for neural induction in the chick embryo. Development *125*, 507-519.

Strubing, C., Ahnert-Hilger, G., Shan, J., Wiedenmann, B., Hescheler, J., and Wobus, A.M. (1995). Differentiation of pluripotent embryonic stem cells into the neuronal lineage in vitro gives rise to mature inhibitory and excitatory neurons. Mech Dev *53*, 275-287.

Su Myung, J., Ji-Hyung, L., Jinyoung, P., Young Sun, O., Sung Kyun, L., Jin Seok, P., Youn Sook, L., Jun Hwan, K., Jae Young, L., Yoe-Sik, B*., et al.* (2013). Smad6 inhibits non-canonical TGF-β1 signalling by recruiting the deubiquitinase A20 to TRAF6. Nature communications.

Suarez-Farinas, M., Noggle, S., Heke, M., Hemmati-Brivanlou, A., and Magnasco, M.O. (2005). Comparing independent microarray studies: the case of human embryonic stem cells. BMC Genomics *6*, 99.

Subramanian, A., Tamayo, P., Mootha, V.K., Mukherjee, S., Ebert, B.L., Gillette, M.A., Paulovich, A., Pomeroy, S.L., Golub, T.R., Lander, E.S*., et al.* (2005). Gene set enrichment analysis: a knowledge-based approach for interpreting genome-wide expression profiles. Proceedings of the National Academy of Sciences of the United States of America *102*, 15545-15550.

Suga, H., Kadoshima, T., Minaguchi, M., Ohgushi, M., Soen, M., Nakano, T., Takata, N., Wataya, T., Muguruma, K., Miyoshi, H*., et al.* (2011). Self-formation of functional adenohypophysis in three-dimensional culture. Nature *480*, 57-62.

Sun, T., and Hevner, R.F. (2014). Growth and folding of the mammalian cerebral cortex: from molecules to malformations. Nat Rev Neurosci *15*, 217-232.

Suzuki, A., Kaneko, E., Ueno, N., and Hemmati-Brivanlou, A. (1997). Regulation of epidermal induction by BMP2 and BMP7 signaling. Dev Biol *189*, 112-122.

Taisuke, K., Hideya, S., Tokushige, N., Mika, S., Satoshi, A., Mototsugu, E., and Yoshiki, S. (2013). Self-organization of axial polarity, inside-out layer pattern, and species-specific progenitor dynamics in human ES cell-derived neocortex. Proceedings of the National Academy of Sciences of the United States of America.

Takahashi, K., Tanabe, K., Ohnuki, M., Narita, M., Ichisaka, T., Tomoda, K., and Yamanaka, S. (2007). Induction of pluripotent stem cells from adult human fibroblasts by defined factors. Cell *131*, 861-872.

Takahashi, K., and Yamanaka, S. (2006). Induction of pluripotent stem cells from mouse embryonic and adult fibroblast cultures by defined factors. Cell *126*, 663-676.

Tamplin, O.J., Kinzel, D., Cox, B.J., Bell, C.E., Rossant, J., and Lickert, H. (2008). Microarray analysis of Foxa2 mutant mouse embryos reveals novel gene expression and inductive roles for the gastrula organizer and its derivatives. BMC Genomics *9*, 511.

Tan, S.S., and Breen, S. (1993). Radial mosaicism and tangential cell dispersion both contribute to mouse neocortical development. Nature *362*, 638-640.

Tan, S.S., Kalloniatis, M., Sturm, K., Tam, P.P., Reese, B.E., and Faulkner-Jones, B. (1998). Separate progenitors for radial and tangential cell dispersion during development of the cerebral neocortex. Neuron *21*, 295-304.

Tanegashima, K., Haramoto, Y., Yokota, C., Takahashi, S., and Asashima, M. (2004). Xantivin suppresses the activity of EGF-CFC genes to regulate nodal signaling. Int J Dev Biol *48*, 275-283.

Taverna, E., Gotz, M., and Huttner, W.B. (2014). The cell biology of neurogenesis: toward an understanding of the development and evolution of the neocortex. Annu Rev Cell Dev Biol *30*, 465-502.

Taylor, I.W., and Wrana, J.L. (2008). SnapShot: The TGFbeta pathway interactome. Cell *133*, 378 e371.

ten Berge, D., Kurek, D., Blauwkamp, T., Koole, W., Maas, A., Eroglu, E., Siu, R.K., and Nusse, R. (2011). Embryonic stem cells require Wnt proteins to prevent differentiation to epiblast stem cells. Nature cell biology *13*, 1070-1075.

Theil, T., Aydin, S., Koch, S., Grotewold, L., and Ruther, U. (2002). Wnt and Bmp signalling cooperatively regulate graded Emx2 expression in the dorsal telencephalon. Development *129*, 3045-3054.

Theunissen, T.W., Costa, Y., Radzisheuskaya, A., van Oosten, A.L., Lavial, F., Pain, B., Castro, L.F., and Silva, J.C. (2011). Reprogramming capacity of Nanog is functionally conserved in vertebrates and resides in a unique homeodomain. Development *138*, 4853-4865.

Theunissen, T.W., Powell, B.E., Wang, H., Mitalipova, M., Faddah, D.A., Reddy, J., Fan, Z.P., Maetzel, D., Ganz, K., Shi, L.*, et al.* (2014). Systematic identification of culture conditions for induction and maintenance of naive human pluripotency. Cell stem cell *15*, 471-487.

Thomson, J.A., Itskovitz-Eldor, J., Shapiro, S.S., Waknitz, M.A., Swiergiel, J.J., Marshall, V.S., and Jones, J.M. (1998). Embryonic stem cell lines derived from human blastocysts. Science *282*, 1145-1147.

Thomson, R.E., Kind, P.C., Graham, N.A., Etherson, M.L., Kennedy, J., Fernandes, A.C., Marques, C.S., Hevner, R.F., and Iwata, T. (2009). Fgf receptor 3 activation promotes selective growth and expansion of occipitotemporal cortex. Neural Dev *4*, 4.

Toma, K., Kumamoto, T., and Hanashima, C. (2014). The timing of upper-layer neurogenesis is conferred by sequential derepression and negative feedback from deep-layer neurons. J Neurosci *34*, 13259-13276.

Torii, M., Hashimoto-Torii, K., Levitt, P., and Rakic, P. (2009). Integration of neuronal clones in the radial cortical columns by EphA and ephrin-A signalling. Nature *461*, 524-528.

Tropepe, V., Hitoshi, S., Sirard, C., Mak, T.W., Rossant, J., and van der Kooy, D. (2001). Direct neural fate specification from embryonic stem cells: a primitive mammalian neural stem cell stage acquired through a default mechanism. Neuron *30*, 65-78.

Vallier, L., Alexander, M., and Pedersen, R.A. (2005). Activin/Nodal and FGF pathways cooperate to maintain pluripotency of human embryonic stem cells. Journal of cell science *118*, 4495-4509.

Vallier, L., Mendjan, S., Brown, S., Chng, Z., Teo, A., Smithers, L.E., Trotter, M.W., Cho, C.H., Martinez, A., Rugg-Gunn, P.*, et al.* (2009a). Activin/Nodal signalling maintains pluripotency by controlling Nanog expression. Development *136*, 1339-1349.

Vallier, L., Rugg-Gunn, P.J., Bouhon, I.A., Andersson, F.K., Sadler, A.J., and Pedersen, R.A. (2004). Enhancing and diminishing gene function in human embryonic stem cells. Stem Cells *22*, 2-11.

Vallier, L., Touboul, T., Brown, S., Cho, C., Bilican, B., Alexander, M., Cedervall, J., Chandran, S., Ahrlund-Richter, L., Weber, A.*, et al.* (2009b). Signaling pathways controlling pluripotency and early cell fate decisions of human induced pluripotent stem cells. Stem Cells *27*, 2655-2666.

Vallier, L., Touboul, T., Chng, Z., Brimpari, M., Hannan, N., Millan, E., Smithers, L.E., Trotter, M., Rugg-Gunn, P., Weber, A.*, et al.* (2009c). Early cell fate decisions of human embryonic stem cells and mouse epiblast stem cells are controlled by the same signalling pathways. PloS one *4*, e6082.

Vasistha, N.A., Garcia-Moreno, F., Arora, S., Cheung, A.F., Arnold, S.J., Robertson, E.J., and Molnar, Z. (2014). Cortical and Clonal Contribution of Tbr2 Expressing Progenitors in the Developing Mouse Brain. Cereb Cortex.

Waddington, C.H. (1952). The Epigenetics of Brids. Cambridge: Cambridge University Press.

Walsh, C., and Cepko, C.L. (1988). Clonally Related Cortical-Cells Show Several Migration Patterns. Science *241*, 1342-1345.

Wang, W.Z., Hoerder-Suabedissen, A., Oeschger, F.M., Bayatti, N., Ip, B.K., Lindsay, S., Supramaniam, V., Srinivasan, L., Rutherford, M., Mollgard, K.*, et al.* (2010). Subplate in the developing cortex of mouse and human. J Anat *217*, 368-380.

Wang, X., Wang, J., Huang, V., Place, R.F., and Li, L.C. (2012a). Induction of NANOG expression by targeting promoter sequence with small activating RNA antagonizes retinoic acid-induced differentiation. The Biochemical journal *443*, 821-828.

Wang, Z., Oron, E., Nelson, B., Razis, S., and Ivanova, N. (2012b). Distinct lineage specification roles for NANOG, OCT4, and SOX2 in human embryonic stem cells. Cell stem cell *10*, 440-454.

Ware, C.B., Nelson, A.M., Mecham, B., Hesson, J., Zhou, W., Jonlin, E.C., Jimenez-Caliani, A.J., Deng, X., Cavanaugh, C., Cook, S.*, et al.* (2014). Derivation of naive human embryonic stem cells. Proceedings of the National Academy of Sciences of the United States of America *111*, 4484-4489.

Warmflash, A., Sorre, B., Etoc, F., Siggia, E.D., and Brivanlou, A.H. (2014). A method to recapitulate early embryonic spatial patterning in human embryonic stem cells. Nat Methods *11*, 847-854.

Watanabe, K., Kamiya, D., Nishiyama, A., Katayama, T., Nozaki, S., Kawasaki, H., Watanabe, Y., Mizuseki, K., and Sasai, Y. (2005). Directed differentiation of telencephalic precursors from embryonic stem cells. Nature neuroscience *8*, 288-296.

Watanabe, K., Ueno, M., Kamiya, D., Nishiyama, A., Matsumura, M., Wataya, T., Takahashi, J.B., Nishikawa, S., Nishikawa, S., Muguruma, K.*, et al.* (2007). A ROCK inhibitor permits survival of dissociated human embryonic stem cells. Nature biotechnology *25*, 681-686.

Whalley, K. (2013). Neural development: Tracing interneuron roots. Nat Rev Neurosci *14*, 818-819.

Wichterle, H., Lieberam, I., Porter, J.A., and Jessell, T.M. (2002). Directed differentiation of embryonic stem cells into motor neurons. Cell *110*, 385-397.

Wills, A.E., Choi, V.M., Bennett, M.J., Khokha, M.K., and Harland, R.M. (2010). BMP antagonists and FGF signaling contribute to different domains of the neural plate in Xenopus. Dev Biol *337*, 335-350.

Wilson, P.A., and Hemmati-Brivanlou, A. (1995). Induction of epidermis and inhibition of neural fate by Bmp-4. Nature *376*, 331-333.

Wilson, S.I., Graziano, E., Harland, R., Jessell, T.M., and Edlund, T. (2000). An early requirement for FGF signalling in the acquisition of neural cell fate in the chick embryo. Current biology : CB *10*, 421-429.

Wilson, S.I., Rydstrom, A., Trimborn, T., Willert, K., Nusse, R., Jessell, T.M., and Edlund, T. (2001). The status of Wnt signalling regulates neural and epidermal fates in the chick embryo. Nature *411*, 325-330.

Xu, R.H., Kim, J., Taira, M., Zhan, S., Sredni, D., and Kung, H.F. (1995). A dominant negative bone morphogenetic protein 4 receptor causes neuralization in Xenopus ectoderm. Biochemical and biophysical research communications *212*, 212-219.

Xu, R.H., Peck, R.M., Li, D.S., Feng, X., Ludwig, T., and Thomson, J.A. (2005). Basic FGF and suppression of BMP signaling sustain undifferentiated proliferation of human ES cells. Nat Methods *2*, 185-190.

Yamamizu, K., Piao, Y., Sharov, A.A., Zsiros, V., Yu, H., Nakazawa, K., Schlessinger, D., and Ko, M.S. (2013). Identification of transcription factors for lineage-specific ESC differentiation. Stem Cell Reports *1*, 545-559.

Yan, X., Liu, Z., and Chen, Y. (2009). Regulation of TGF-beta signaling by Smad7. Acta Biochim Biophys Sin (Shanghai) *41*, 263-272.

Yao, S., Chen, S., Clark, J., Hao, E., Beattie, G.M., Hayek, A., and Ding, S. (2006). Long-term self-renewal and directed differentiation of human embryonic stem cells in chemically defined conditions. Proceedings of the National Academy of Sciences of the United States of America *103*, 6907-6912.

Yeo, C., and Whitman, M. (2001). Nodal signals to Smads through Cripto-dependent and Cripto-independent mechanisms. Mol Cell *7*, 949-957.

Yichen, S., Peter, K., James, S., Hugh, P.C.R., and Frederick, J.L. (2012). Human cerebral cortex development from pluripotent stem cells to functional excitatory synapses. Nature neuroscience *15*, 477.

Ying, Q.L., Stavridis, M., Griffiths, D., Li, M., and Smith, A. (2003). Conversion of embryonic stem cells into neuroectodermal precursors in adherent monoculture. Nature biotechnology *21*, 183-186.

Ying, Q.L., Wray, J., Nichols, J., Batlle-Morera, L., Doble, B., Woodgett, J., Cohen, P., and Smith, A. (2008). The ground state of embryonic stem cell self-renewal. Nature *453*, 519-523.

Yoo, Y.D., Huang, C.T., Zhang, X., Lavaute, T.M., and Zhang, S.C. (2011). Fibroblast growth factor regulates human neuroectoderm specification through ERK1/2-PARP-1 pathway. Stem Cells *29*, 1975-1982.

Yoon, K.J., Koo, B.K., Im, S.K., Jeong, H.W., Ghim, J., Kwon, M.C., Moon, J.S., Miyata, T., and Kong, Y.Y. (2008). Mind bomb 1-expressing intermediate progenitors generate notch signaling to maintain radial glial cells. Neuron *58*, 519-531.

Yu, J., Vodyanik, M.A., Smuga-Otto, K., Antosiewicz-Bourget, J., Frane, J.L., Tian, S., Nie, J., Jonsdottir, G.A., Ruotti, V., Stewart, R*., et al.* (2007a). Induced pluripotent stem cell lines derived from human somatic cells. Science *318*, 1917-1920.

Yu, J.K., Satou, Y., Holland, N.D., Shin, I.T., Kohara, Y., Satoh, N., Bronner-Fraser, M., and Holland, L.Z. (2007b). Axial patterning in cephalochordates and the evolution of the organizer. Nature *445*, 613-617.

Yu, P., Pan, G., Yu, J., and Thomson, J.A. (2011). FGF2 sustains NANOG and switches the outcome of BMP4-induced human embryonic stem cell differentiation. Cell stem cell *8*, 326-334.

Yu, Y.C., He, S., Chen, S., Fu, Y., Brown, K.N., Yao, X.H., Ma, J., Gao, K.P., Sosinsky, G.E., Huang, K*., et al.* (2012). Preferential electrical coupling regulates neocortical lineage-dependent microcircuit assembly. Nature *486*, 113-117.

Zeng, H., Guo, M., Martins-Taylor, K., Wang, X., Zhang, Z., Park, J.W., Zhan, S., Kronenberg, M.S., Lichtler, A., Liu, H.X*., et al.* (2010). Specification of region-specific neurons including forebrain glutamatergic neurons from human induced pluripotent stem cells. PloS one *5*, e11853.

Zeng, H., Shen, E.H., Hohmann, J.G., Oh, S.W., Bernard, A., Royall, J.J., Glattfelder, K.J., Sunkin, S.M., Morris, J.A., Guillozet-Bongaarts, A.L*., et al.* (2012). Large-scale cellular-resolution gene profiling in human neocortex reveals species-specific molecular signatures. Cell *149*, 483-496.

Zhang, L., Huang, H., Zhou, F., Schimmel, J., Pardo, C.G., Zhang, T., Barakat, T.S., Sheppard, K.A., Mickanin, C., Porter, J.A*., et al.* (2012). RNF12 controls embryonic stem cell fate and morphogenesis in zebrafish embryos by targeting Smad7 for degradation. Mol Cell *46*, 650-661.

Zhang, S.C., Wernig, M., Duncan, I.D., Brustle, O., and Thomson, J.A. (2001). In vitro differentiation of transplantable neural precursors from human embryonic stem cells. Nature biotechnology *19*, 1129-1133.

Zhang, X., Huang, C.T., Chen, J., Pankratz, M.T., Xi, J., Li, J., Yang, Y., Lavaute, T.M., Li, X.J., Ayala, M*., et al.* (2010). Pax6 is a human neuroectoderm cell fate determinant. Cell stem cell *7*, 90-100.

Zhou, C.J., Borello, U., Rubenstein, J.L., and Pleasure, S.J. (2006). Neuronal production and precursor proliferation defects in the neocortex of mice with loss of function in the canonical Wnt signaling pathway. Neuroscience *142*, 1119-1131.

Zhou, W., Choi, M., Margineantu, D., Margaretha, L., Hesson, J., Cavanaugh, C., Blau, C.A., Horwitz, M.S., Hockenbery, D., Ware, C*., et al.* (2012). HIF1alpha induced switch from

bivalent to exclusively glycolytic metabolism during ESC-to-EpiSC/hESC transition. EMBO J *31*, 2103-2116.

Zhu, Q., Song, L., Peng, G., Sun, N., Chen, J., Zhang, T., Sheng, N., Tang, W., Qian, C., Qiao, Y.*, et al.* (2014). The transcription factor Pou3f1 promotes neural fate commitment via activation of neural lineage genes and inhibition of external signaling pathways. Elife *3*.

Zimmerman, C.M., and Mathews, L.S. (1996). Activin receptors: cellular signalling by receptor serine kinases. Biochemical Society symposium *62*, 25-38.

Zusman, S.B., Sweeton, D., and Wieschaus, E.F. (1988). short gastrulation, a mutation causing delays in stage-specific cell shape changes during gastrulation in Drosophila melanogaster. Dev Biol *129*, 417-427.